AD NUMBER

AD-518 002

CLASSIFICATION CHANGES

TO **UNCLASSIFIED**

FROM **CONFIDENTIAL**

AUTHORITY

AFAL Ltr; Apr 11, 1978

AD NUMBER

AD-518 002

NEW LIMITATION CHANGE

TO

DISTRIBUTION STATEMENT: A

Approved for public release; Distribution is unlimited.

LIMITATION CODE: 1

FROM **No Prior DoD Distr Scty Cntrl St'mt Assgn'd**

AUTHORITY

AFAL Ltr; Apr 11, 1978

[redacted]

AFAPL-TR-69-92
VOLUME VI

(UNCLASSIFIED TITLE)
INVESTIGATION OF A HIGHLY LOADED TWO-STAGE FAN-DRIVE TURBINE

VOLUME VI. Final Technical Report

H. Welna and D. E. Dahlberg
Pratt & Whitney Aircraft
Division of United Aircraft Corporation

Technical Report
AFAPL-TR-69-92 Volume VI
November, 1971

AIR FORCE AERO PROPULSION LABORATORY
AIR FORCE SYSTEMS COMMAND
WRIGHT-PATTERSON AIR FORCE BASE, OHIO

[redacted]

SECURITY MARKING

The classified or limited status of this report applies to each page, unless otherwise marked.
Separate page printouts MUST be marked accordingly.

THIS DOCUMENT CONTAINS INFORMATION AFFECTING THE NATIONAL DEFENSE OF THE UNITED STATES WITHIN THE MEANING OF THE ESPIONAGE LAWS, TITLE 18, U.S.C., SECTIONS 793 AND 794. THE TRANSMISSION OR THE REVELATION OF ITS CONTENTS IN ANY MANNER TO AN UNAUTHORIZED PERSON IS PROHIBITED BY LAW.

NOTICE: When government or other drawings, specifications or other data are used for any purpose other than in connection with a definitely related government procurement operation, the U.S. Government thereby incurs no responsibility, nor any obligation whatsoever; and the fact that the Government may have formulated, furnished, or in any way supplied the said drawings, specifications, or other data is not to be regarded by implication or otherwise as in any manner licensing the holder or any other person or corporation, or conveying any rights or permission to manufacture, use or sell any patented invention that may in any way be related thereto.

[redacted]

NOTICE

WHEN GOVERNMENT DRAWINGS, SPECIFICATIONS, OR OTHER DATA ARE USED FOR ANY PURPOSE OTHER THAN IN CONNECTION WITH A DEFINITELY RELATED GOVERNMENT PROCUREMENT OPERATION, THE UNITED STATES GOVERNMENT THEREBY INCURS NO RESPONSIBILITY OR ANY OBLIGATION WHATSOEVER, AND THE FACT THAT THE GOVERNMENT MAY HAVE FORMULATED, FURNISHED, OR IN ANY WAY SUPPLIED THE SAID DRAWINGS, SPECIFICATIONS, OR OTHER DATA, IS NOT TO BE REGARDED BY IMPLICATION OR OTHERWISE, OR IN ANY MANNER LICENSING THE HOLDER OR ANY OTHER PERSON OR CORPORATION, OR CONVEYING ANY RIGHTS OR PERMISSION TO MANUFACTURE, USE, OR SELL ANY PATENTED INVENTION THAT MAY IN ANY WAY BE RELATED THERETO.

COPIES OF THIS REPORT SHOULD NOT BE RETURNED UNLESS RETURN IS REQUIRED BY SECURITY CONSIDERATIONS, CONTRACTUAL OBLIGATIONS, OR NOTICE ON A SPECIFIC DOCUMENT.

[redacted]

[redacted]

NOFORN

(UNCLASSIFIED TITLE)
INVESTIGATION OF A HIGHLY LOADED TWO-STAGE FAN-DRIVE TURBINE

VOLUME VI. Final Technical Report

H. Welna and D. E. Dahlberg
Pratt & Whitney Aircraft
Division of United Aircraft Corporation

Downgraded at 3 Year Intervals;
Declassified after 12 Years,
DOD DIR. 5200.10

SPECIAL HANDLING REQUIRED
NOT RELEASABLE TO FOREIGN NATIONALS
The information contained in this document will not be disclosed to foreign nationals or their representatives.

This document contains information affecting the national defense of the United States within the meaning of the Espionage Laws. Its transmission or the revelation of its contents in any manner to an unauthorized person is prohibited by law.

NOFORN

[redacted]

FOREWORD

(U) This Final Technical Report (Contractor's Reference No. PWA-4291) was prepared by Pratt & Whitney Aircraft Division of United Aircraft Corporation, East Hartford, Connecticut, as the sixth and final Report under United States Air Force Contract F33615-68-C-1208, Project No. 3066, Task No. 306606. This report was submitted by the Contractor on 1 November 1971, and covers the Contract period from 1 January 1968 to 1 November 1971.

(U) The data presented in the Interim Technical Reports (AFAPL-TR-69-92, Volumes I through V) are considered by the Contractor to be accurate and final.

(U) The Air Force Program Monitor is Mr. Wayne Tall, TBC, Air Force Aero Propulsion Laboratory, Wright-Patterson Air Force Base, Ohio 45433.

(U) This report contains no Classified information extracted from other Classified documents.

(U) This technical report has been reviewed and is accepted.

E. Clifford Simpson
Director, Turbine Engine Division
Air Force Aero Propulsion Laboratory
Wright-Patterson Air Force Base, Ohio, 45433.

(This page is Unclassified)

UNCLASSIFIED ABSTRACT

(U) An exploratory research program was conducted to develop turbine aerodynamic methods and design procedures for efficient high work, low pressure turbines. This program consisted of various phases, including analyses of promising increased loading concepts, and experimental cascade testing to verify and extend the turbine aerodynamic techniques and design procedures. Based on these findings, a two-stage turbine was designed and evaluated in a rotating cold flow rig in order to demonstrate the effectiveness of the techniques.

(U) The results of the efforts leading to the design and evaluation of the demonstrator turbine have been reported in detail in previously published Interim Technical Reports (AFAPL-TR-69-92, Volumes 1 through 5). This final Technical report (AFAPL-TR-69-92, Volume 6) summarizes that work and presents in its entirety the design and results of the investigation of the demonstrator turbine builds.

(The reverse of this page is blank)

TABLE OF CONTENTS

TABLE OF CONTENTS (Cont'd)

LIST OF ILLUSTRATIONS

LIST OF ILLUSTRATIONS (Cont'd)

LIST OF ILLUSTRATIONS (Cont'd)

LIST OF ILLUSTRATIONS (Cont'd)

LIST OF ILLUSTRATIONS (Cont'd)

LIST OF ILLUSTRATIONS (Cont'd)

LIST OF ILLUSTRATIONS (Cont'd)

LIST OF ILLUSTRATIONS (Cont'd)

LIST OF ILLUSTRATIONS (Cont'd)

LIST OF ILLUSTRATIONS (Cont'd)

LIST OF ILLUSTRATIONS (Cont'd)

LIST OF ILLUSTRATIONS (Cont'd)

LIST OF ILLUSTRATIONS (Cont'd)

LIST OF ILLUSTRATIONS (Cont'd)

LIST OF TABLES

LIST OF SYMBOLS

A	–	area, square inches
AR	–	aspect ratio, h/B
b	–	chord, inches
B	–	axial chord, inches
C_L	–	load coefficient, $\Delta V_u/U$
D	–	diameter, inches
D_f	–	diffusion factor
E	–	diffusion parameter
h	–	airfoil average height, inches
Δh	–	work, Btu-per-pound
k	–	ratio of specific heats
L	–	airfoil height, inches
M	–	Mach number
m	–	mass rate of flow, lb-m/sec
N	–	number of airfoils; or rotating speed, rpm
p	–	absolute pressure, psia
P	–	total pressure, psia
P_R	–	pressure ratio
ΔP	–	pressure rise from minimum to exit value on suction surface
Q	–	exit dynamic head
R	–	radius, inches
R_C	–	radius of curvature, inches
T	–	temperature, °R
u	–	tangential velocity, feet-per-second
V	–	velocity, feet-per-second
W	–	airflow rate, lb/sec
X	–	axial distance, inches
Y	–	tangential distance, inches
Z	–	loss parameter
α	–	absolute gas angle, degrees
β	–	relative gas angle, measured from axial direction, degrees
η	–	turbine total-to-total efficiency
ρ	–	density
σ	–	solidity ratio, b/τ

LIST OF SYMBOLS (Cont'd)

τ	–	airfoil spacing, inches
$\overline{\omega}$	–	loss parameter
$\Delta p_o/p_o$	–	loss parameter

Subscripts

o	–	inlet to first vane
1	–	inlet to first blade
2	–	exit from stage or airfoil section
e	–	exit plane of EGV
el	–	end loss related quantity
i	–	inlet plane of EGV
m	–	mean section
o	–	stagnation or total condition
p	–	profile loss related quantity
r	–	root section
s	–	static conditions
t	–	tip section
x	–	axial direction
θ	–	tangential direction

Superscripts

*	–	Metal Dimension

(The reverse of this page is blank)

SECTION I

INTRODUCTION

SECTION I

INTRODUCTION

(U) The design analysis and optimization of aircraft jet engines has always involved a trade between increasing turbine efficiency and reducing turbine size and weight. The bypass turbofan engine has become an attractive propulsion system for future multi-mission aircraft. The specific fuel consumption of bypass engines generally decreases with increasing bypass ratio, and it is, therefore, essential to achieve advances in bypass flow. However, increased bypass ratios require increased fan power supplied by the low pressure turbine. The objective, then, is to increase fan-drive turbine power, or loading, while maintaining or improving the turbine aerodynamic efficiency.

(U) The turbine designer is constrained by certain unique requirements when designing fan-drive turbines. The rotational speed of the low pressure turbine must be limited in order that the fan tip Mach number does not exceed the limit for reasonable losses. This problem becomes more critical as the bypass ratio and fan diameter increase. Applying conventional aerodynamics, when faced with a limiting rotational speed, the designer usually increases the diameter of the low pressure turbine stages or increases the number of stages in order to obtain more work and still maintain turbine efficiency. Conversely, the reduction of turbine diameter or solidity results in a lighter turbine, but with a sacrifice in efficiency due to losses associated with increased loading. Considerable gains can be realized by an engine if the size and weight reduction can be made with no loss in efficiency. Furthermore, because of the time required between the evolution of new concepts and engine production, turbine technology must be improved so that the desired level of turbofan engine performance can be achieved for aircraft which will be operational in the 1975-1980 time period.

(U) The objective of the work done under this Contract was to analyze and test concepts which would increase the low pressure turbine loading and maintain or increase current turbine efficiency levels. The goals of this program were to develop turbine aerodynamic techniques and design procedures for efficient, high work, low pressure turbines by means of analytical studies and cascade testing, and to demonstrate the effectiveness of the techniques by designing and testing a two-stage turbine that met or exceeded the Contract stage-work and efficiency goals.

(U) The program was conducted in four phases. Phase I defined the basic turbine design, and promising increased loading concepts were analyzed. Phases II and III consisted of cascade testing to verify and extend the turbine aerodynamic techniques and design procedures for high loading levels. Phase IV subjected the aerodynamic techniques and design procedures to a two-stage rotating rig test. An investigation of end wall configurations was also made as part of an add-on to the Contract.

(U) The results of the work performed in the first three phases of the Contract were reported in detail in the Interim Technical Reports (References 1 through 5) and are briefly summarized in Section II of this report. In this Final Technical Report, a description of the Phase IV demonstrator turbine design, and the results of the turbine rotating rig test and data analysis are presented.

(The reverse of this page is blank)

SECTION II

BACKGROUND

SECTION II

BACKGROUND

1. INTRODUCTION

(U) The results of the first three Phases of this Contract have been reported in detail in References 1 through 5. The pertinent results of this work will be summarized in this Section, mainly for convenience but also as verification that the data presented in the referenced Interim Technical Reports are considered to be accurate and final.

2. DISCUSSION

(U) The first Phase effort was directed toward defining a turbine design with the highest resistance to boundary layer separation, and to select boundary layer control techniques that are best suited for extending the loading limits of the basic design.

(U) The turbine design parameters which were defined in the Contract are those shown in Table I. Based on these parameters, a parametric study was made where variations in work distribution, levels of reaction, solidity and flow path were considered. The inlet and exit conditions were those which represented current engine cycles. The flowpath assumed a fixed inlet as would normally be the case for a real engine, sized to close-couple with a high pressure turbine. A constant inside diameter was chosen in order to provide the greatest possible blade speeds. The exit was sized for reasonable exit guide vane diffusion.

TABLE I

TURBINE DESIGN PARAMETERS

Number of Stages	2
Average Load Coefficient, C_L	2.2
First Blade Tip Wheel Speed	1000 FPS
First Blade Inlet Hub-Tip Diameter Ratio	≤ 0.8
Average Turbine Gas Inlet Angle	65°
Exit Swirl Angle - without Exit Guide Vane	$< 20°$
- with Exit Guide Vane	0°
Turbine Inlet Temperature	1450°F
Airflow [redacted]	$\geq$ 50 lb/sec
Overall Efficiency	91%
Life	10,000 hrs
Increase Work Level Over Free Vortex Design Capability	> 50%

(U) Figure 1 shows the predicted turbine efficiency where the exit area, reaction level and stage work split were varied. Mean diameter static pressure reaction was varied from 25 to 55 percent, while the work split was evaluated at 50, 55 and 60 percent to the first stage. For tne range of exit areas investigated, the variation in efficiency was fairly insensitive. The exit area chosen was defined by the exit Mach number which had to be held to a value acceptable for afterburner operation (see Figure 2), and by exit guide vane considerations (see Figure 3) where excessive swirl would present large exit guide vane losses. Based on these considerations, the exit area was fixed at 264 inches^2.

(U) Reaction levels were studied at levels of 25, 30 and 45 percent for the mean diameter of the first-stage, and 25, 40 and 55 percent for the second stage. Based on the calculations of inlet and exit conditions, the spanwise inlet and exit Mach number distributions were determined at these various reaction levels and are shown in Figures 4 through 8. The highest reaction was eliminated from consideration due to the high exit Mach number which would result in a large exit guide vane turning requirement, high solidity and the possibility of choked root in the exit guide vane, all of which would increase the exit guide vane turning losses.

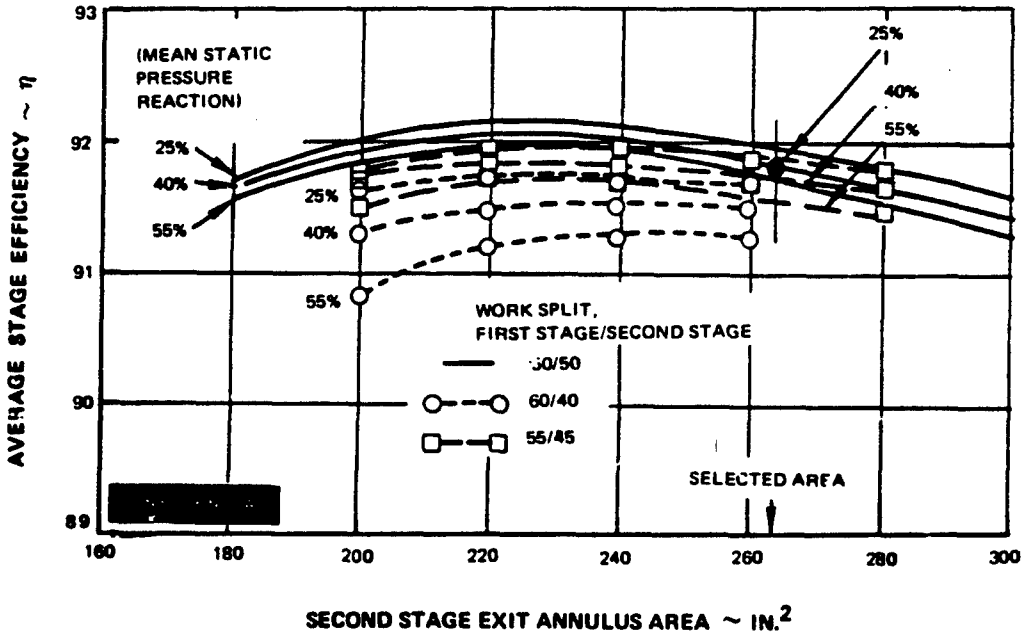

Figure 1 Turbine Parametric Study

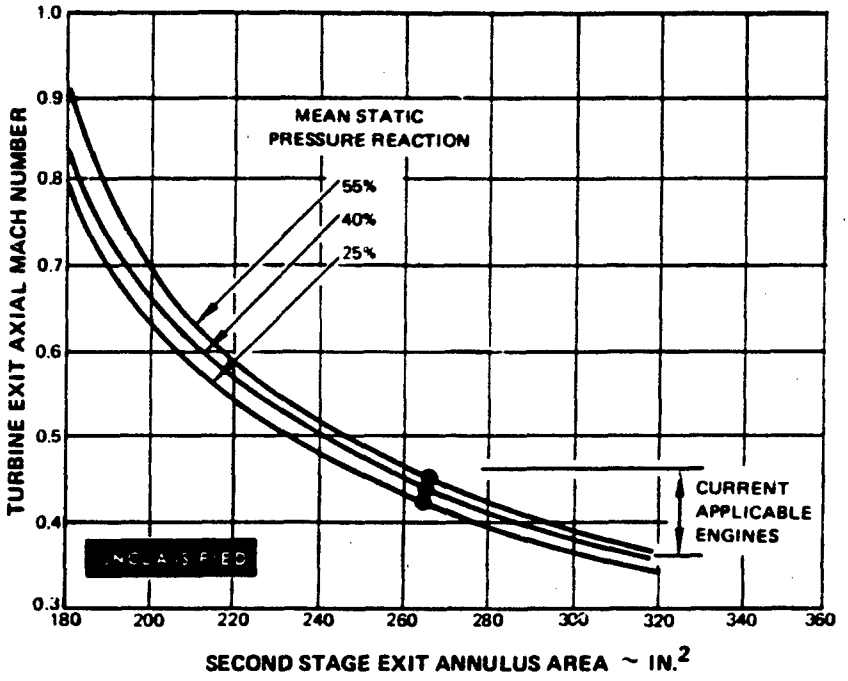

Figure 2 Variation of Turbine Exit Axial Mach Number With Exit Area at Various Reaction Levels

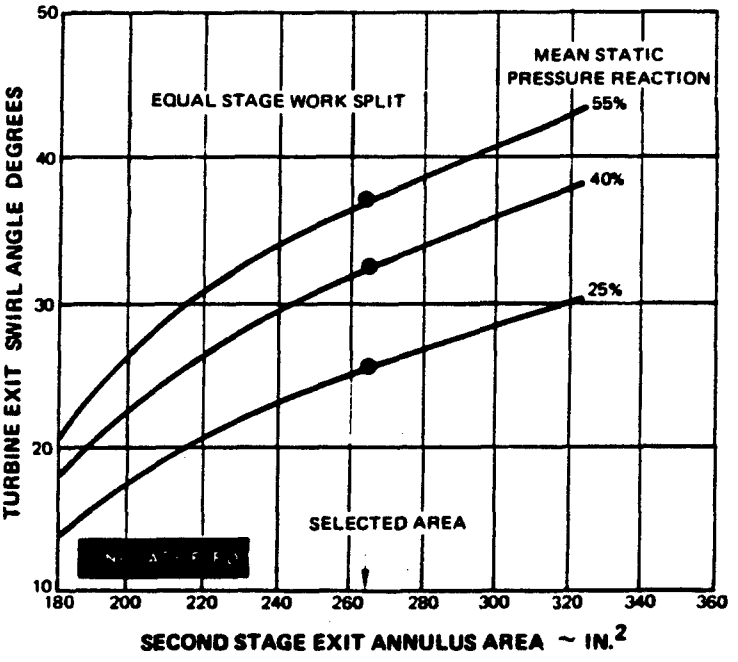

Figure 3 Variation of Turbine Exit Swirl Angle With Exit Area At Various Reaction Levels

(This page is Unclassified)

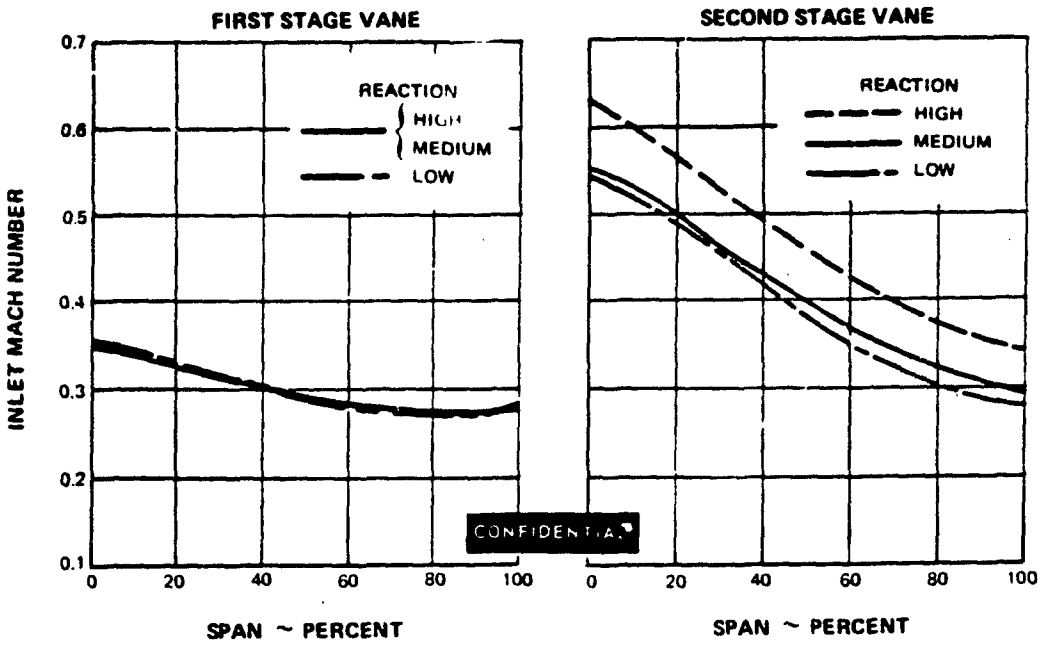

Figure 4 Variation of Inlet Mach Number with Span at Various Reaction Levels

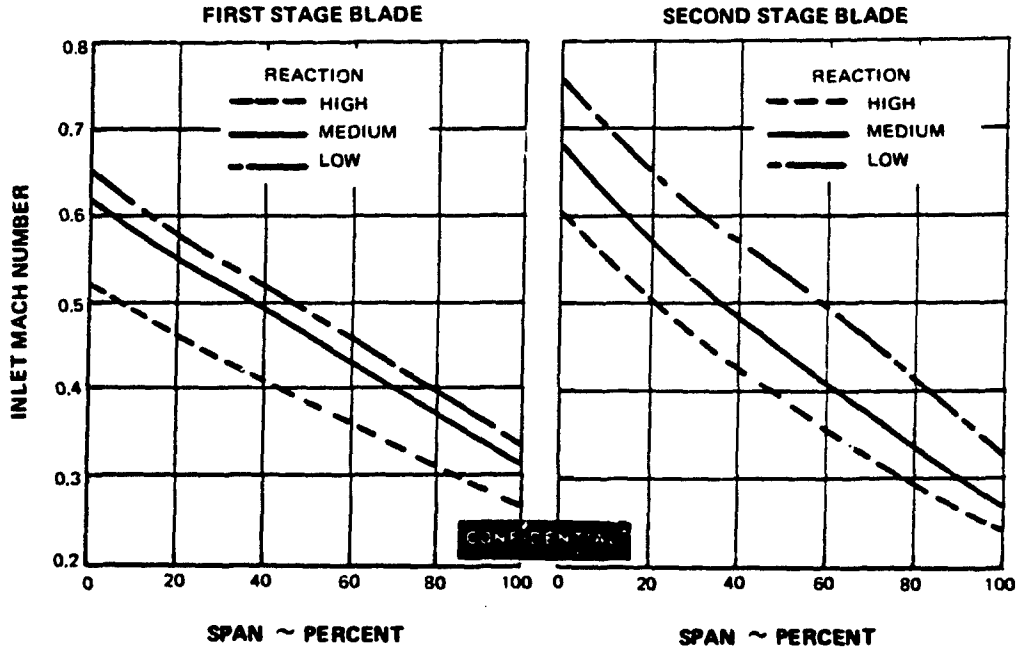

Figure 5 Variation of Inlet Mach Number With Span at Various Reaction Levels

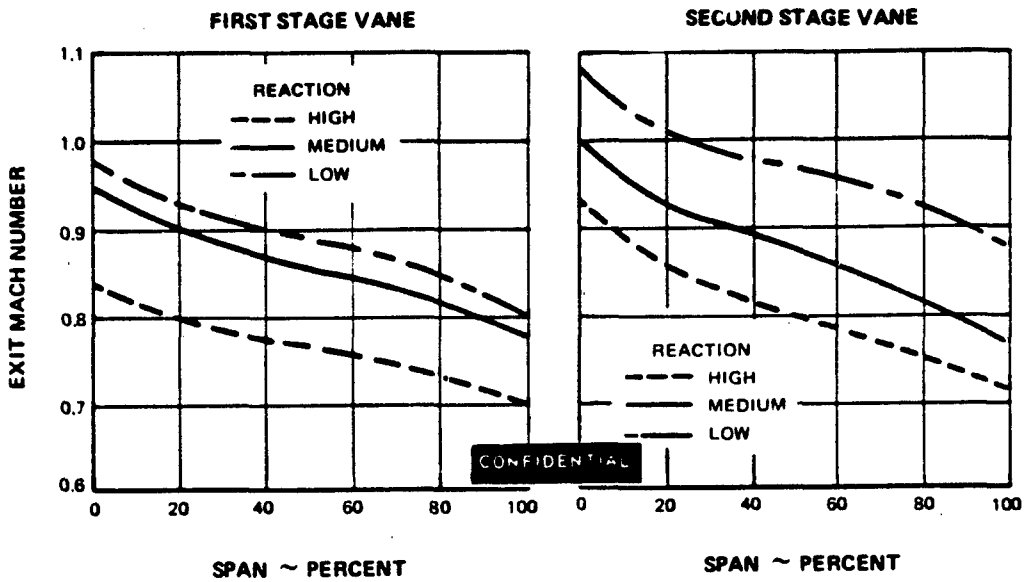

Figure 6 Variation of Exit Mach Number With Span at Various Reaction Levels

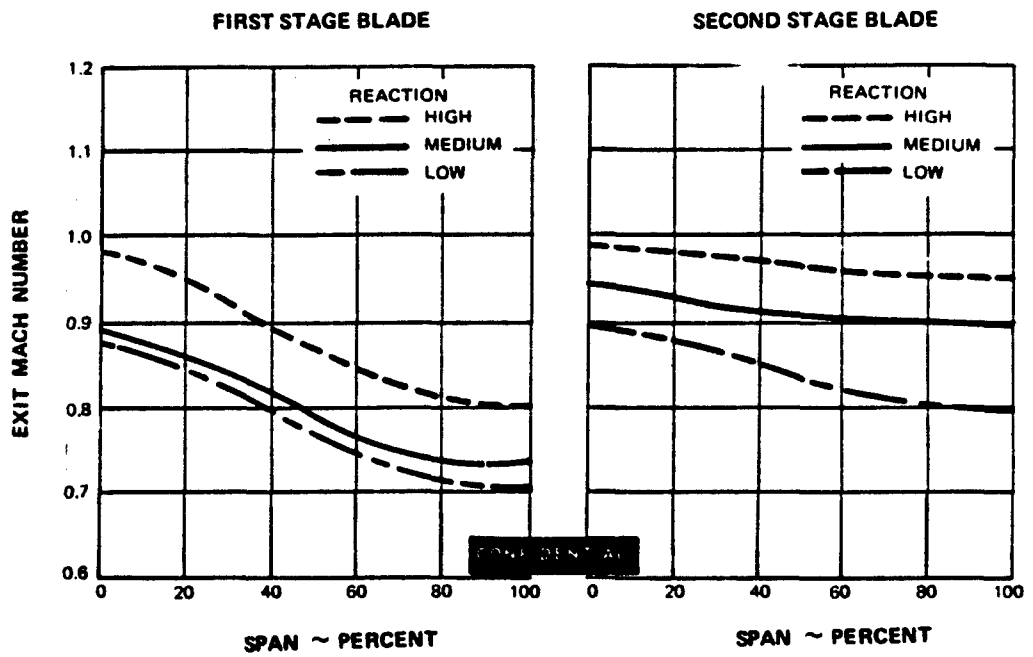

Figure 7 Variation of Exit Mach Number With Span at Various Reaction Levels

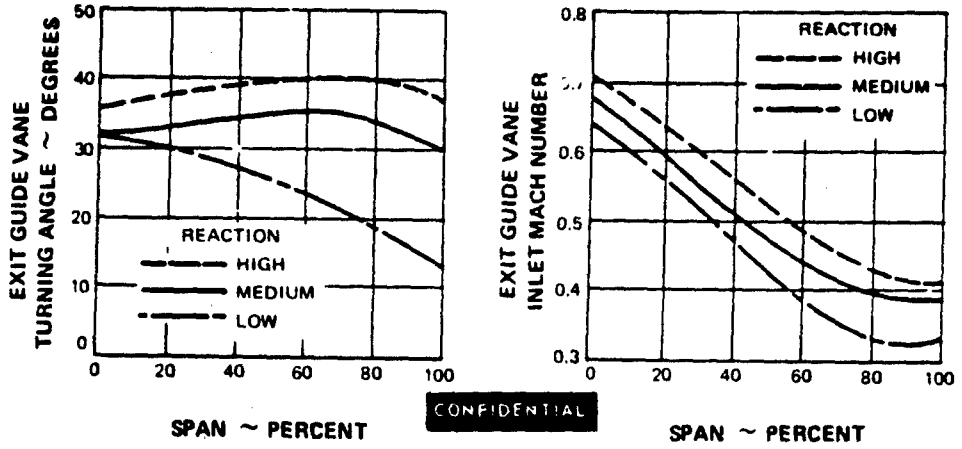

Figure 8 Variation of Exit Guide Vane Turning Angle and Inlet Mach Number With Span at Various Reaction Levels

(U) Solidity was considered next, and three levels were considered at the medium reaction level and four solidities at the low reaction level. Preliminary airfoils were designed based on airfoil surface pressure distribution, loading coefficient, pressure rise coefficient and maximum surface Mach number. Due to the high loading, the turbine had a higher-than-normal surface Mach number and lower-than-normal airfoil convergence, especially at the root section. This was predominant for the low reaction levels, which would lead to large shock losses. A very low suction surface pressure appeared near the leading edge, and almost a continuous deceleration over the entire length of the airfoil. This resulted also in a high pressure rise coefficient for the low reaction designs and led to the elimination of the low reaction from further consideration. This, therefore, narrowed the study to the 50/50 stage work distribution and the medium reaction level arrived at by elimination of the high reaction configurations which had an impractical exit guide vane design, and low reaction configurations which had potentially a high loss blade root airfoil section.

(U) Detailed airfoil designs were now undertaken, with detailed studies of airfoil surface pressure distributions, suction surface radius of curvature, passage convergence, and airfoil cross-sections. The goal was to design for the highest resistance to flow separation. Two-dimensional preliminary airfoil boundary layer calculations to evaluate boundary layer characteristics of each airfoil were made to assist in selecting the practical lower solidity limit. Two types of boundary layer calculations were made. The first assumed no transition and the calculation continued until either laminar separation was indicated, or the end of the airfoil was reached. The criterion for separation was a drag coefficient of 0.001 or less. The second method assumed transition to turbulent flow at the first minimum on suction side pressure distribution. However, these calculations do not take into account the three-dimensional flow phenomena which cause separation in the suction surface corners prior to separation on the airfoil contour. Therefore, a drag coefficient of 0.002 was used as the cut-off point. Using this criterion (Ref. 1), the normal solidity was chosen for preliminary cascade evaluations.

(U) A boundary layer control literature survey was conducted of possible boundary layer control methods that would be effective for reducing secondary flow. Secondary flow losses are defined as all losses not accounted for by the skin-friction losses on the airfoils and annulus walls. The boundary layer control methods considered had to be applicable to high aspect ratio, uncooled turbines with no external fluid source or sink available, feasible to manufacture and of acceptable structural integrity. The ranking of the methods selected was grouped into two classes, depending on whether separation occurred or if large corner losses occurred without separation. This ranking is shown in Table II.

TABLE II

CATEGORIZATION OF BOUNDARY LAYER CONTROL METHODS

Unseparated corner Boundary Layer

- Local Recontouring at Root and Tip
- End Wall Contouring at Root and Tip
- Local Uncambering at Root and Tip

Separated Corner Boundary Layer

- End Wall Contouring
- Local Uncambering
- Corner Slots
- Fillets

(U) The second Phase of the total program was to determine the location and severity of losses due to airfoil and/or corner boundary layer separation. This was accomplished by fabricating and testing a part-annular cascade for each of the baseline airfoils shown in Figures 9 and 10. A photograph of a typical annular cascade assembly is shown in Figure 11, with a cross-sectional view shown in Figure 12. Inlet guide vanes were used to turn the flow to the desired inlet angle. Traverses were made behind the inlet guide vane to assure that the angle requirements were met. The central airfoil in each cascade had root, mean and tip surface static pressure taps installed. Exit traverses were made to measure exit angle and flow losses, and define regions of separation, if any. Boundary layer bleeds at the entrance to the cascade were used to give a two-dimensional flow characteristic. Flow visualization of airfoil and endwalls was also made on each airfoil.

(U) Each cascade was tested at the design Reynolds number, design incidence, and at three Mach numbers around the design point. The objectives of these tests were met by measuring all important aerodynamic properties at cascade inlet and exit planes, by reconstruction of the entire exit plane loss distribution and exit flow pattern, by measurements of airfoil surface static pressure distributions at three radial locations and by flow visualization of airfoils and endwalls. A summary of the design point loss distribution is shown in Figure 13. The performance of the baseline airfoils was very similar; no corner boundary layer separation was observed in any of the baseline cascades.

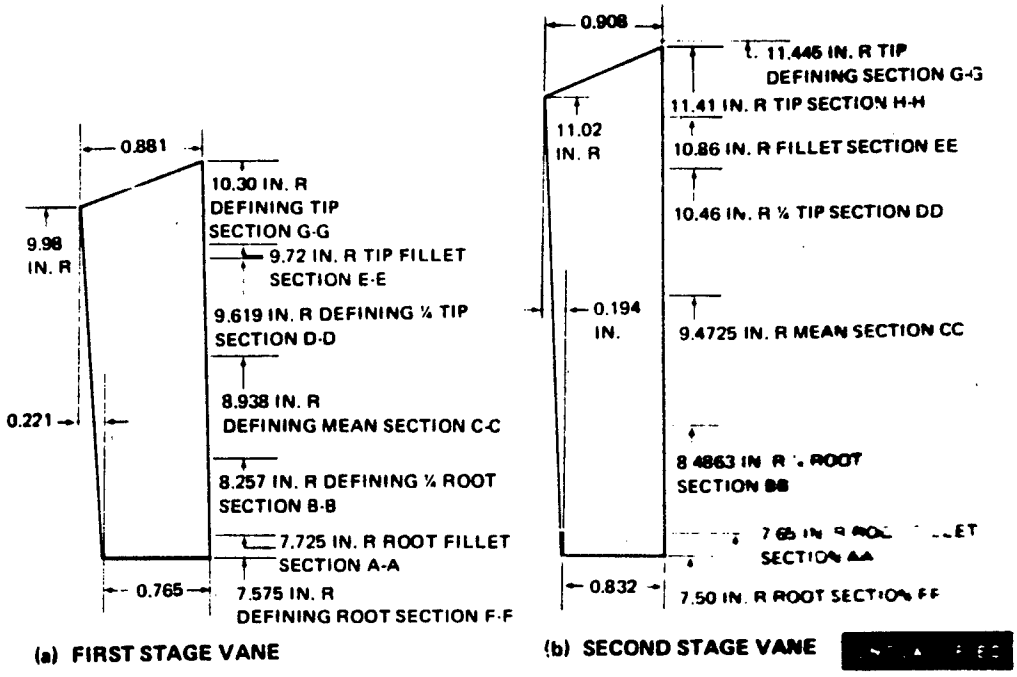

Figure 9 Turbine Test Airfoil Elevations

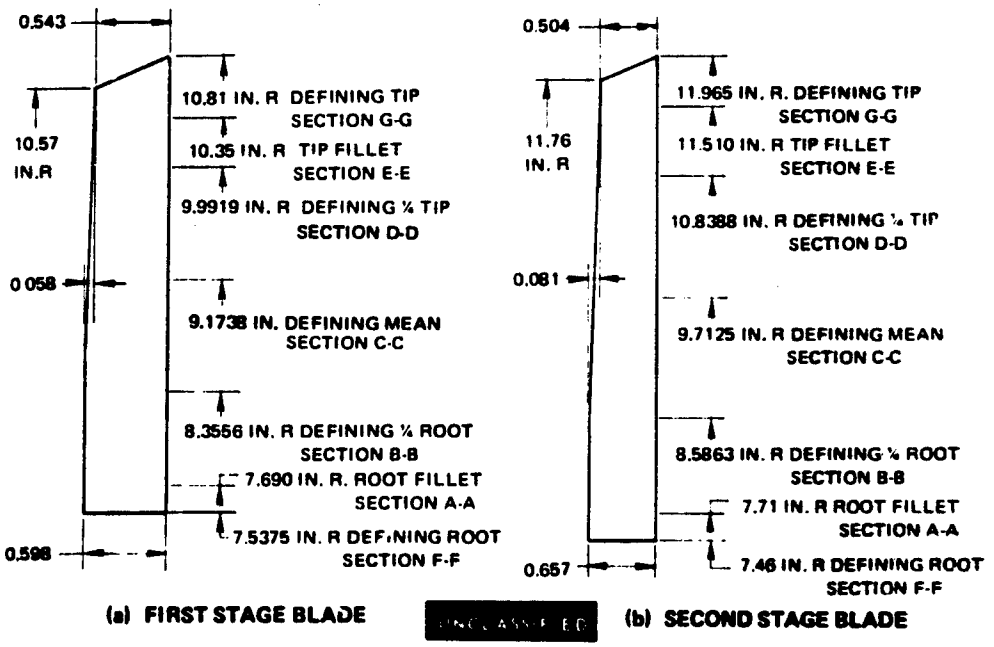

Figure 10 Turbine Test Airfoil Elevations

Figure 11 First-Stage Blade Cascade Assembly With Static Pressure Connections

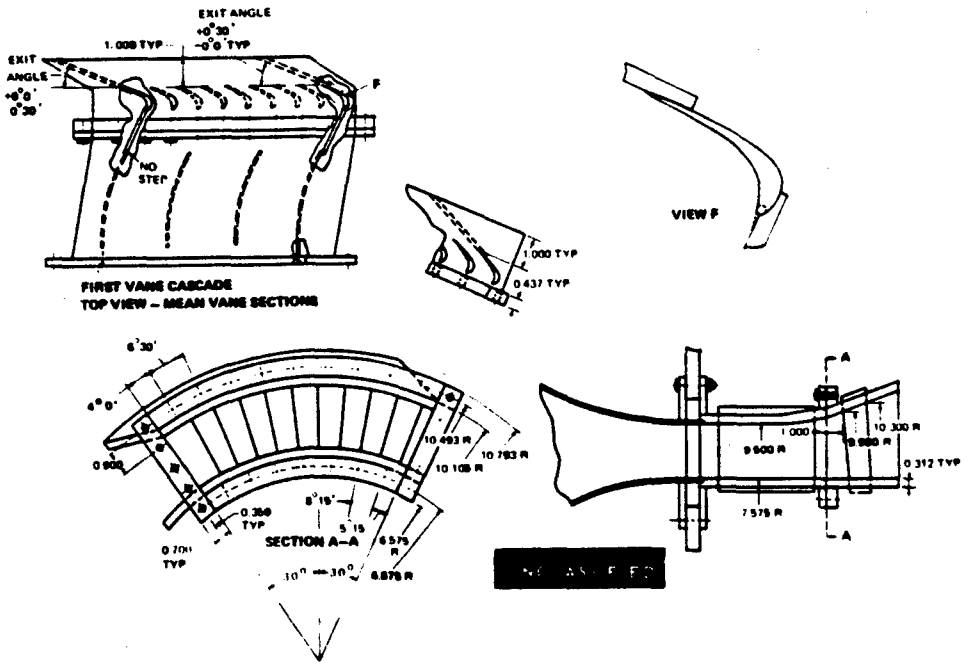

Figure 12 Assembly of First-Stage Vane Cascade

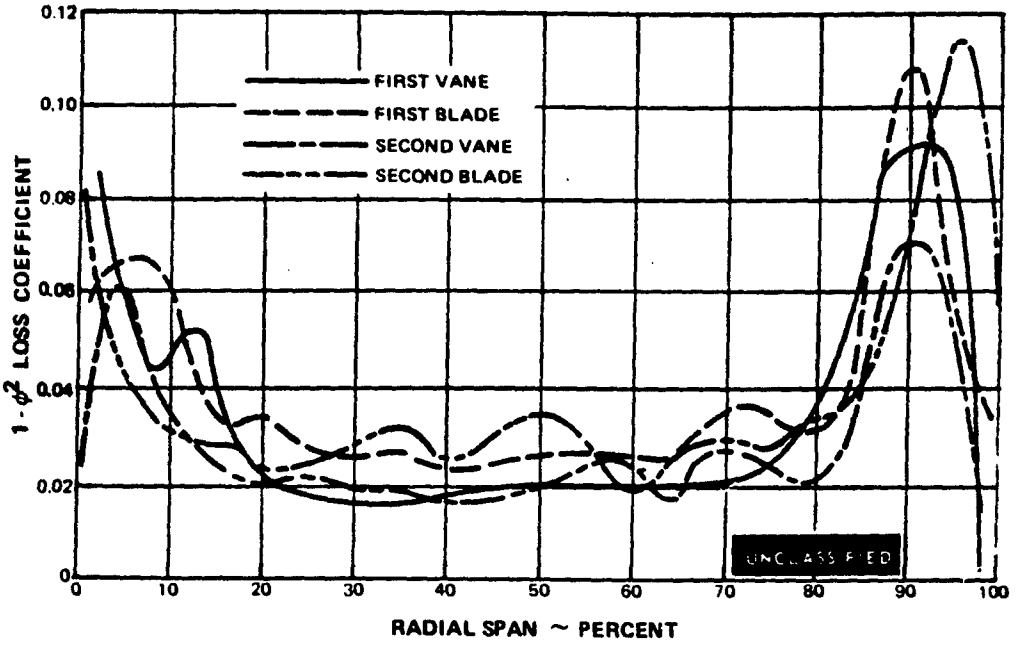

Figure 13 Loss Coefficient Versus Percent Span – Baseline Airfoils

(U) In order to compare the midspan losses with those measured in the annular cascade, and to verify the accuracy of the two-dimensional prediction procedure, plane cascade tests of the mean sections of each airfoil were also made. These, in addition to root sections of the second vane and blade, were tested in the facility shown in Figure 14. A typical plane cascade pack is shown in Figure 15. During these tests both the inlet and exit pressures were independently controlled, as well as the inlet temperature level, allowing correct simulation of inlet and exit Mach number and Reynolds number. A comparison of the resulting measured losses is shown in Table III. The midspan section loss coefficients for the first vane, first blade, second vane and second blade measured in the plane cascade were consistent with the mean values measured in the annular segment cascade.

(U) The second vane was selected for investigating various boundary layer control techniques. Because the corner boundary layer remained attached, only the first group of boundary layer control methods was applicable. These methods were intended to minimize secondary flow losses at the root and tip regions. The principal techniques selected were: (1) local recontouring of the airfoil, (2) local recambering of the airfoil, and (3) endwall contouring.

(U) The second vane was recontoured as indicated in Figures 16 and 17. The surface static pressure gradient at the leading edge portion was reduced in order to decrease the loading toward the airfoil leading edge, while keeping the overall loading constant. These changes were intended to delay the onset of strong secondary flow in the upstream portion of the channel, and thereby to reduce the total accumulation of secondary flows near the airfoil suction corners.

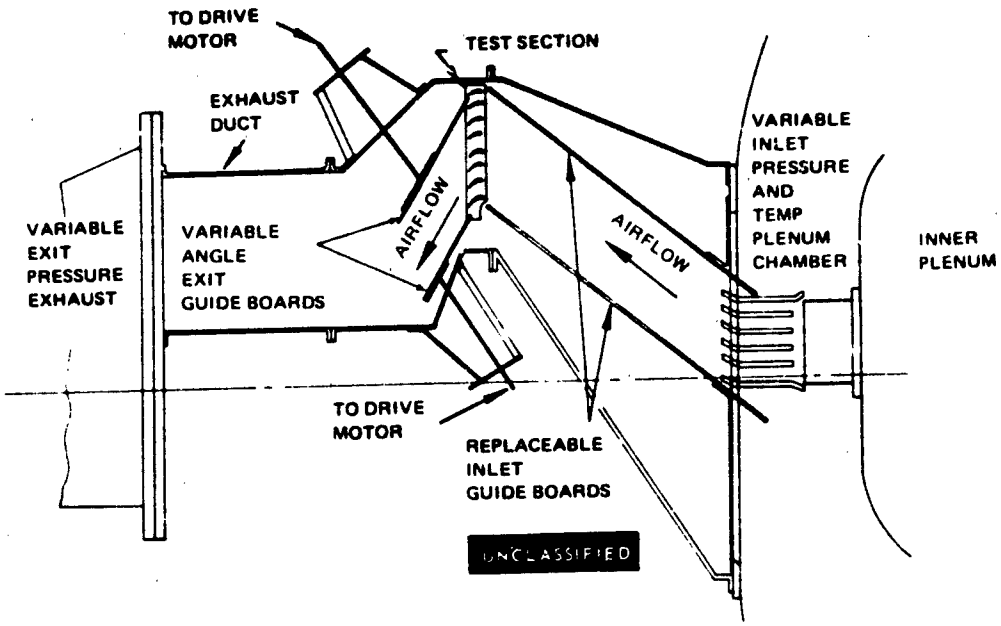

Figure 14 Schematic of Plane Cascade Test Rig

Figure 15 First-Stage Vane Mean Plane Cascade Pack – Leading Edge

TABLE III

MEASURED PLANE CASCADE LOSS COMPARISON
WITH MEASURED MIDSPAN ANNULAR CASCADE LOSS
AND PREDICTED LOSS AT DESIGN REYNOLDS NUMBERS

Midspan Section	Exit Mach Number	Loss Coefficient Measured, $1-\phi^2$		Loss Coefficient Predicted, $1-\phi^2$	
		Plane Cascade	Annular Cascade	Global Correlation	Fully Turbulent Boundary Layer
First Vane	0.852	0.025	0.017 0.023*	0.031	0.031
First Blade	0.788	0.025	0.027	0.036	0.049
Second Vane	0.870	0.024	0.021 0.028*	0.036	0.034
Second Blade	0.904	0.023	0.028	0.030	0.040

*With inlet turbulence screen

UNCLASSIFIED

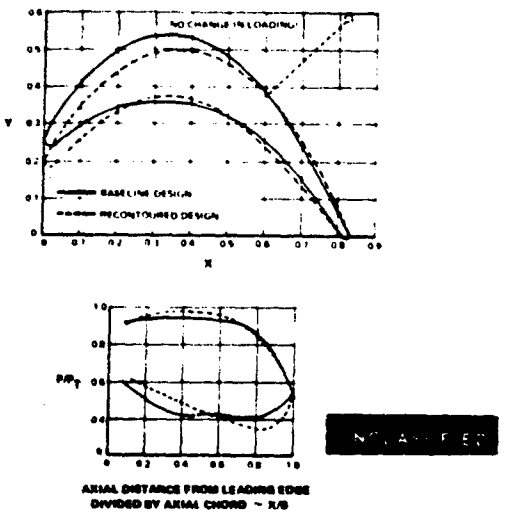

UNCLASSIFIED

Figure 16 Second-Stage Vane Baseline Airfoil Recontouring, Root Section Static Pressure Redistribution

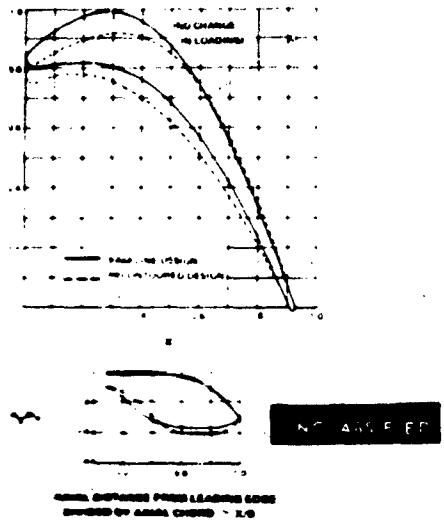

Figure 17 Second-Stage Vane Baseline Airfoil Recontouring, Tip Section Static Pressure Redistribution

(U) A locally recambered second vane was also evaluated where the tip exit angle was reduced (closed 5°) while the root was increased (opened 5°). These were then faired into the 25 and 75 percent span sections. These changes are shown in Figures 18 and 19. Such changes were believed to have a tendency to reduce the root overturning and tip underturning. Tip loading was increased, but the increase in passage convergence shifted the loading toward the trailing edge. This reduces the pressure difference between suction and pressure sides of the channel at the forward end and will tend to delay the onset of strong secondary flow.

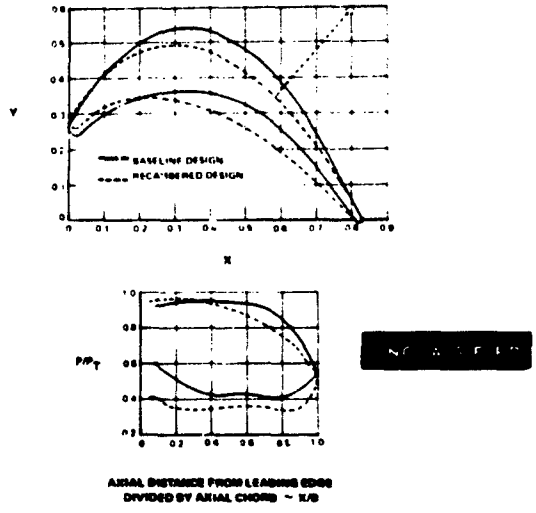

Figure 18 Second-Stage Vane Root Section Recambering

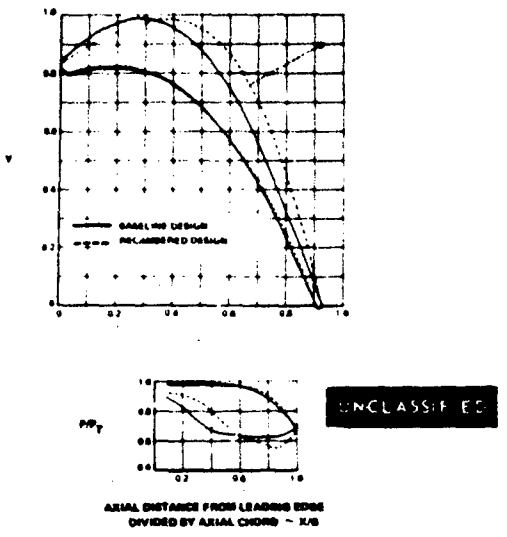

Figure 19 Second-Stage Vane Tip Section Recambering

(U) Endwall contouring was another method which held promise of reducing the local airfoil loading, and therefore the secondary flow losses, without causing any appreciable disturbance to the flow at the other sections of the airfoil. The goal was to achieve a reduction in strength of the secondary flow field in order to reduce the tangential pressure difference near the endwall. Two computer programs were used to design the wall contours. The first calculated the pressure distribution around an airfoil of the desired profile on a cylindrical surface. This program allows stream tube height variations, but cannot account for radial pressure gradients. The second program performs axisymmetric intrablade calculations. The requirements were such that the contour must decrease the local airfoil loading, and not cause flow separation on the endwalls. The best contour was analyzed to be one with a sinusoidal inlet and exit wall height distribution, with leading and trailing edges intersecting at inflection points as shown in Figure 20.

(U) The spanwise profile loss distributions are shown in Figure 21 for the various treatments. For the recontoured airfoil, there was a slightly lower loss at both the inside and outside diameter walls, with only a slight change to overall loss. Exit angles were almost identical to baseline values (see Figure 22) with some increase in underturning at the tip section. No separation was indicated in the flow visualization tests.

(U) Endwall contouring indicated a negligible increase in loss level at the root section and a large increase in loss coefficients at the tip section when compared to the baseline results. The exit angle measurements indicated a large underturning at the root and tip sections.

(U) The recambered airfoil root loss measurements showed a significant reduction, with only a slight increase at the tip, when compared with baseline values. The angle measurements indicated attached flow and only a slight underturning from the design values. The root section had a slightly increased underturning from baseline design with no separation indicated by flow visualization. A summary of the integrated losses for the various endwall treatments is shown in Table IV.

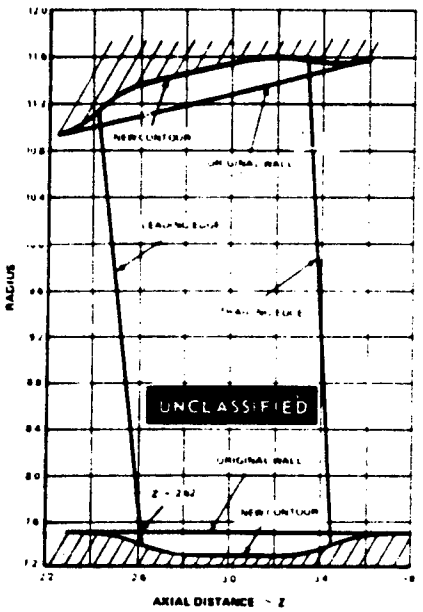

Figure 20 End-Wall Contouring, Second-Stage Vane

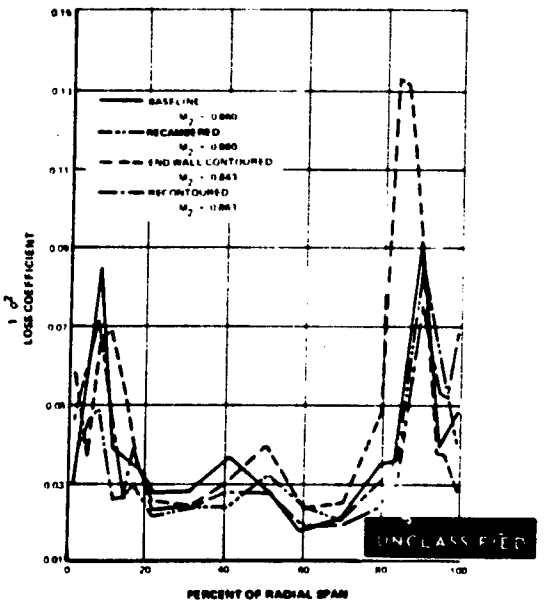

Figure 21 Comparison of Baseline Loss Coefficients With Those of Various Boundary Layer Control Methods

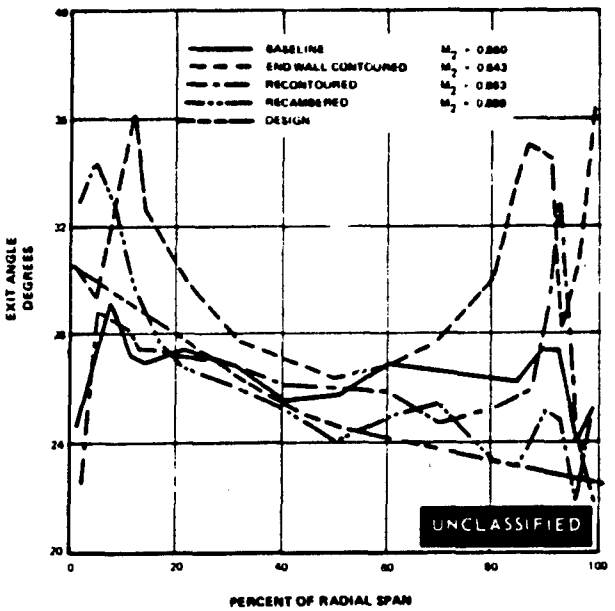

Figure 22 Comparison of Baseline Exit Flow Angles With Those of Various Boundary Layer Control Methods

TABLE IV

INTEGRATED AVERAGE PROFILE COEFFICIENTS
SECOND VANE CASCADE

	Midspan Mach No.	Loss Coefficient ($1-\phi^2$) Overall	Midspan To I.D.	Midspan To O.D.
Baseline	0.860	0.0349	0.0353	0.0345
Recontoured Airfoil	0.863	0.0336	0.0338	0.0334
End Wall Contoured	0.843	0.0428	0.0374	0.0482
Recambered Airfoil	0.880	0.0329	0.0286	0.0372

(U) Based on these results, the recambering at the root and tip appeared to have the best promise of reducing the endwall losses. Additional geometric variations of the recambered design were next investigated. These changes are shown in Figure 23. The results of this evaluation are summarized in Table V. The performance of Recambering Design A agreed well with that of the first recambered design. It had a slightly increased root section loss coefficient and a decreased mean-to-tip section value. The overall loss had a slight increase compared to the first recambering and midspan losses were close to the baseline airfoil values. Recambering Design B showed a peak loss almost identical to the baseline measurements at the root even though the root exit angle was increased by approximately 8.5°. Integrated root-to-midspan loss was about the same as for the baseline airfoil, and the midspan-to-tip loss was slightly lower than the baseline, even though the tip exit angle was increased by 10°. Recambering Design C had the root exit angle increased by 13.5° and the tip by 15°. The losses at the root for this design were the largest for all the recambered designs and this is also true for the overall losses. All measured angles agreed well with the design, with some underturning indicated at the tip for recambering Design A, as was the case for the baseline design. This was not observed for Recambering Design B and C. In general, the exit flow angles behaved in a predictable manner, indicating that such local uncambering can be a potentially useful technique for improving the entrance flow conditions in the following row. In most cases the midspan losses increased with increasing amount of midspan overcambering applied to the cascades to maintain constant overall work for each design.

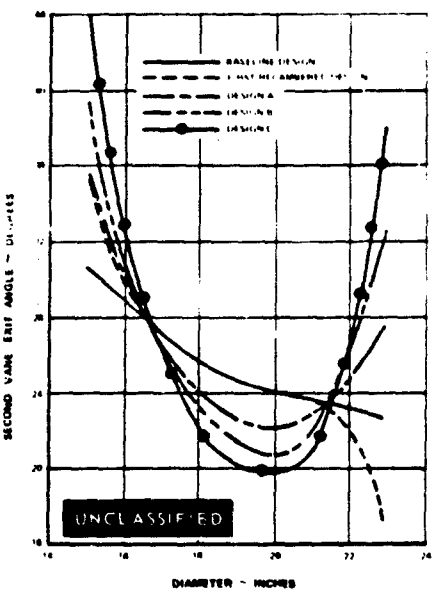

Figure 23 Second-Stage Vane Recambering Design Comparison

TABLE V

COMPARISON OF LOSS COEFFICIENTS FOR SECOND VANE RECAMBERING CORRECTED TO DESIGN POINT

Mach Number = 0.869, Zero Incidence

	Measured Loss Coefficient, $1-\phi^2$		
Airfoil	Midspan-to-Root	Midspan-to-Tip	Overall
Baseline	0.035	0.035	0.035
First Recambering	0.029	0.038	0.033
Recambering Design A	0.036	0.035	0.036
Recambering Design B	0.031	0.033	0.032
Recambering Design C	0.044	0.034	0.038

(U) Off-design performance of the baseline and three of the four recambered designs was also evaluated in the annular segment cascade. The initial goal was to test at ±10° of incidence but, due to the problems with the inlet design, only 6° could be attained in the negative direction. Results of these tests are shown in Table VI. The first recambering design had an increase in loss at the root for the +10° incidence, and about the same level for -6° incidence. Little change was noted in the tip section for this design. The overall loss was larger for the +10° incidence, and slightly larger for the -6° incidence.

TABLE VI

SECOND VANE RECAMBERING LOSS COEFFICIENTS CORRECTED TO DESIGN POINT MACH NO. = 0.869

	Midspan-to-Root			Midspan-to-Tip			Overall		
Incidence, Degrees	+10	0	-6	+10	0	-6	+10	0	-6
Baseline	0.039	0.035	0.029	0.035	0.035	0.029	0.038	0.035	0.029
First Recambering	0.047	0.029	0.031	0.040	0.038	0.042	0.043	0.033	0.036
Recambering Design A	0.043	0.036	0.034	0.051	0.035	0.031	0.048	0.036	0.033
Recambering Design B	–	0.031	–	–	0.033	–	–	0.032	–
Recambering Design C	0.038	0.044	0.038	0.042	C.034	0.035	0.040	0.038	0.036

(U) Recambering Design A had a large loss in the root section at +10° incidence and no difference at -6° incidence when compared to baseline values. For +10° of incidence, the loss was much larger in the tip region than baseline, and only slightly larger at the -6° level. The overall loss was greater at +10° incidence and less than baseline at -6° incidence.

(U) The losses with recambering Design C were slightly lower at +10° and -6° incidence at the root, greater at +10° incidence level and the same at -6° incidence at the tip section. Overall, the positive incidence loss was slightly higher and the negative incidence lower than the baseline values.

(U) Angle measurements were in close agreement with predicted values. No separation on the airfoils was indicated by flow visualization. In general, the results of the Phase III off design evaluation indicated an increase in loss coefficient with positive incidence and a decrease in loss coefficient with negative incidence for the tested airfoils. None of the airfoils were sensitive to angle of attack, and the flow patterns did not change significantly with incidence. These results, therefore, verified that the design procedure used was sound.

(U) The next Phase of the program was to design the two-stage demonstrator turbine. This Phase IV effort will be described in Sections III and IV of this report.

(The reverse of this page is blank)

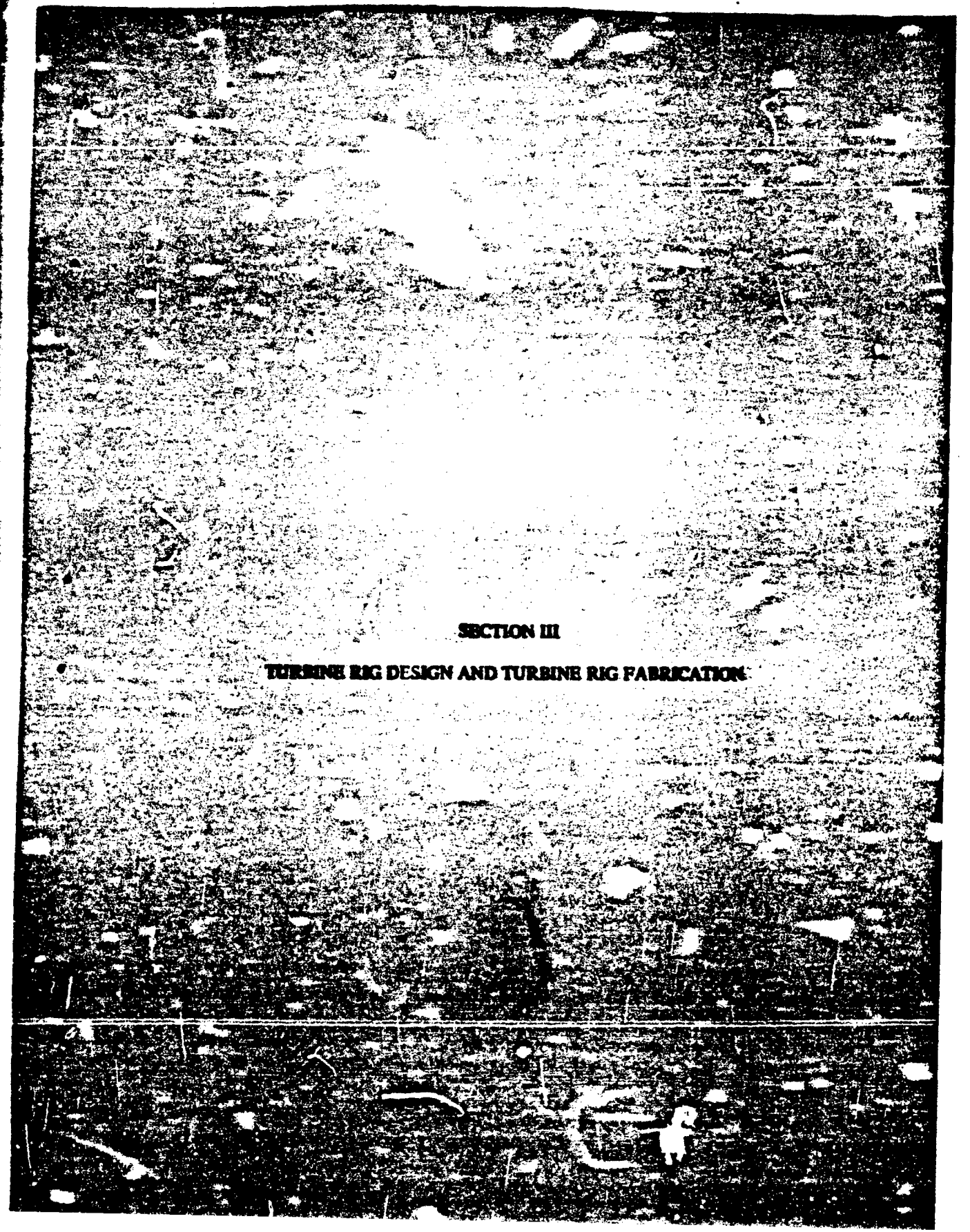

SECTION III

TURBINE RIG DESIGN AND TURBINE RIG FABRICATION

SECTION III

TURBINE RIG DESIGN AND TURBINE RIG FABRICATION (TASKS IVa AND b)

1. RFP OBJECTIVE

(U) Using the design procedures established in Phase III, design and fabricate a two-stage turbine that met the RFP performance objectives.

2. TASK OBJECTIVE

(U) The available turbine design system, as modified by the experimental results of Phase II and Phase III were used to design a turbine having the characteristics summarized in Table I. The turbine flowpath was defined by calculating inlet and exit flow areas and selecting reasonable inner- and outer-wall divergence angles based on experience. Using the results of previous Phases of this program, the reaction levels and spanwise work distributions were selected. Velocity diagrams were generated for each vane and blade by the Streamline Analysis Deck. Airfoil contours were defined for at least five radial stations making use of the Pressure Distribution Boundary Layer Program, and Airfoil Design Program. The airfoil sections were used to define airfoil center of gravity, principal stresses, gas bending loads, centrifugal loads and total stresses. The Airfoil Fairing Programs were applied to define vane and blade coordinates. The final turbine layout and detailed drawings were then completed. Careful consideration was given to such characteristics of the resulting turbine as strength, weight, life, maintainability, cost, low cycle fatigue and high frequency fatigue.

(U) Upon receiving approval of the turbine design by the Air Force Contracting Officer, the turbine parts and necessary modifications to the turbine rig were fabricated, inspected and assembled. Instrumentation designed for the selected flowpath were fabricated and installed.

3. INTRODUCTION

(U) Upon completion of the plane and annular cascade evaluations of the preliminary (Phase I) airfoils and the design and off-design tests of the various boundary layer control techniques (Phases II and III), the two-stage demonstrator turbine was designed incorporating aerodynamic features shown to be beneficial from cascade testing. This section includes a description of the design and fabrication of the demonstrator turbine.

4. DESIGN

(U) The basic turbine design followed the preliminary design described in Reference 1. The final flowpath was modified slightly from the Phase I version in order to increase the inlet Mach number to 0.35 from 0.29. The higher inlet Mach number is more consistent with high pressure turbine exit conditions and thus represents a more realistic engine design. The turbine stage exit Mach number remains relatively unchanged at 0.457. Again, this level is consistent with engine design procedures where the turbine discharge Mach number is set at a

low enough level to allow a margin for rematching of the engine for development purposes by modifying the jet nozzle area. A moderate Mach number level is also beneficial for an afterburning engine since a low Mach number is required for burning and a moderate turbine discharge Mach number enables the use of a short and light-weight diffuser between the turbine and afterburner. Figure 24 illustrates the turbine elevation that was used in the aerodynamic design. Figure 25 shows the turbine flowpath, depicting the structural components of the test rig.

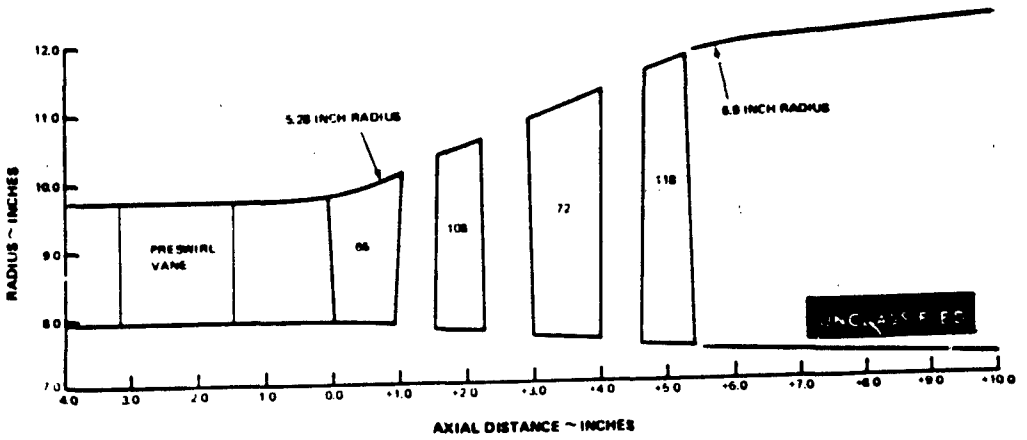

Figure 24 Turbine Elevation Final Flowpath

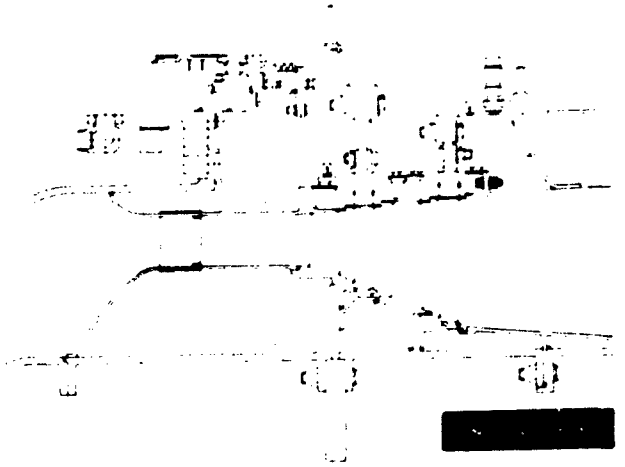

Figure 25 Cross-Section of Test Rig

(U) Analysis of the results of the cascade testing performed in Phases II and III indicated that reducing the work at the endwalls by uncambering the airfoils can increase turbine efficiency. This increase in efficiency results from lower secondary flow losses created by uncambering the airfoil endwall regions. The final turbine design had the airfoil endwall angles opened by approximately 4°, which appeared to be close to optimum in the cascade testing.

(U) An equal stage-work split was chosen in order that relatively uniform vane and blade Mach numbers and stage pressure ratios could be achieved. This work split also provides greater work potential than a turbine with the last stage more highly loaded. An additional benefit of an equal stage-work distribution, as opposed to say 45 percent in the first-stage and 55 percent in the second-stage, is the reduced level of gas turning required by the exit guide vane. Blade mean static pressure reaction levels of 40 percent were selected for both stages, based on the Phase I design study.

(U) The turbine velocity triangles were defined using the three design parameters, namely radial work profile, stage-work split and reaction level, along with a radial loss profile which was incorporated in the Turbine Streamline Computer Program. The final first- and second-stage radial work distribution is shown in Figure 26. The reaction levels are shown for each stage in Figures 27 and 28. The radial loss profile was determined by summing the airfoil penalties for the profile losses, trailing edge losses and the endwall losses for each airfoil. The profile and endloss distributions for each airfoil are shown in Figure 29 where the integrated loss values are also tabulated. The resulting velocity diagrams for this turbine (Table VII) are listed in Table VIII.

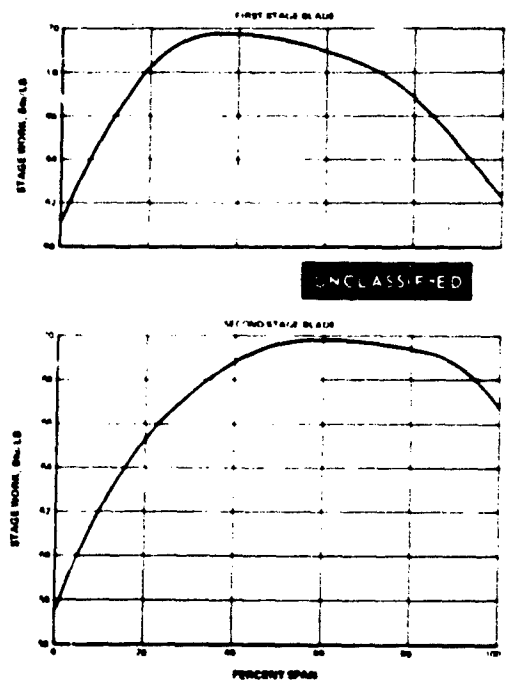

Figure 26 Stage Work Versus Percent Span, First- and Second-Stage Blade

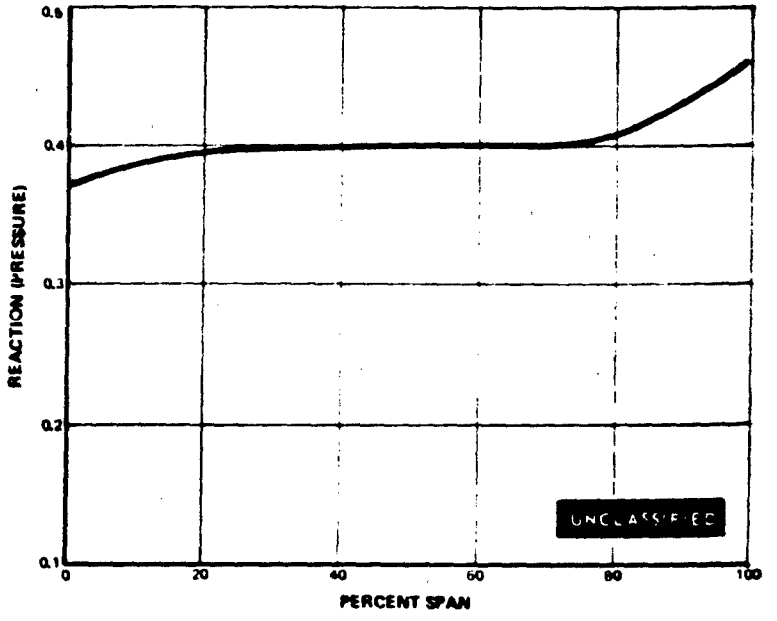

Figure 27 First-Stage Blade Reaction Versus Percent Span

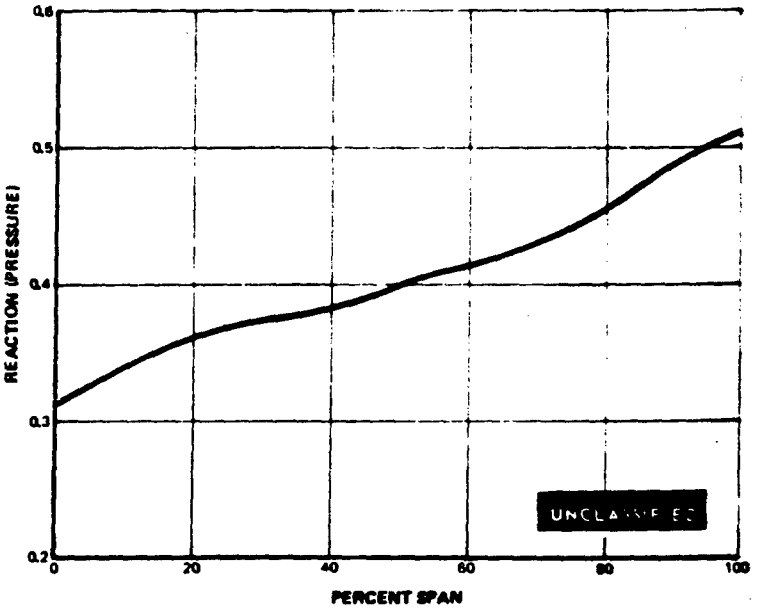

Figure 28 Second-Stage Blade Reaction Versus Percent Span

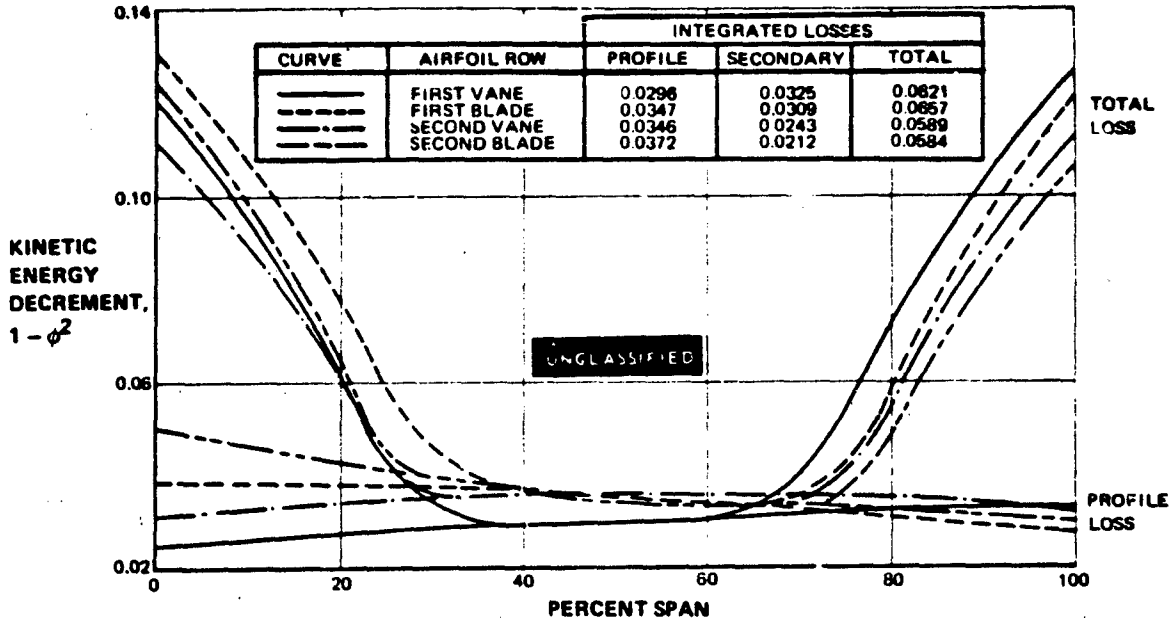

Figure 29 Profile and End Wall Losses From the Streamline Calculation of The Final Turbine Design.

TABLE VII

TURBINE AERODYNAMIC DESIGN PARAMETERS

Number of Stages	2
Average Load Coefficient, C_L	2.2
First Blade Tip Wheel Speed	1000 fps
First Blade Inlet Hub-Tip Ratio	0.75
Exit Swirl Angle At Exit Guide Vane	0°
Turbine Inlet Temperature	1450°F
Airflow	67.7 lbs/sec
Turbine Work	134.5 Btu/lb
Average Stage Work Parameter, $\Delta h/T$	0.0352
Mean Velocity Ratio	0.478
Rim Velocity Ratio	0.389
Turbine Pressure Ratio	3.723
Average Stage Pressure Ratio	1.930
Inlet Flow Parameter	0.1937
Inlet Axial Mach Number	0.35
Exit Axial Mach Number	0.457
Rotor Speed	10,680 rpm
Exit Swirl From Last Blade	30.7°

TABLE VIII

VECTOR DIAGRAM SUMMARY

	Stage 1			Stage 2		
Radial Station	Root	Mean	Tip	Root	Mean	Tip
R_0 (Vane Inlet)	7.940	8.936	9.820	7.712	9.383	10.912
R_1 (Vane Exit)	7.900	8.988	10.13	7.625	9.511	11.31
$R_{1.5}$ (Blade Inlet)	7.815	8.029	10.390	7.575	9.547	11.59
R_2 (Blade Exit)	7.785	9.279	10.629	7.520	9.693	11.815
U_2 Wheel Speed	726.0	865.0	991.0	701.0	903.0	1101.0
Δh	61.07	69.45	62.34	57.54	69.72	66.73
Vel. Ratio	0.415	0.464	0.561	0.413	0.484	0.602
α_0	66.	62.71	81.24	48.68	46.68	61.42
α_1	37. 2	27.00	26.05	35.70	25.63	27.04
θ_v	77.55	90.29	72.71	95.62	107.69	91.54
$\beta_{1.5}$	52.85	45.98	60.15	53.25	47.01	74.23
β_2	31.88	25.97	28.97	42.13	30.09	26.93
θ_B	95.27	108.19	90.88	84.62	102.9	78.84
α_2	50.97	72	64.72	63.95	59.37	66.15
Reaction T_S	0.435	0.531	0.530	0.382/	0.479/	0.601/
P_S	0.370	0.488	0.460	0.311	0.401	0.509
$(P_S/P_S)_V$	1.503	1.439	1.350	1.597	1.490	1.372
$(P_S/P_S)_B$	1.463	1.426	1.475	1.343	1.460	1.591
$(C_L)_V$	0.959	0.850	0.757	0.948	0.854	0.910
$(C_L)_B$	0.835	0.894	1.010	0.839	0.925	0.934
$(M_R)_{B\,INLET}$	0.549	0.453	0.317	0.732	0.486	0.315
$(M_R)_{B\,EXIT}$	0.903	0.866	0.806	0.960	0.910	0.898
$(M_A)_{V\,INLET}$	0.395	0.358	0.371	0.591	0.458	0.389
$(M_A)_{V\,EXIT}$	0.857	0.831	0.737	1.011	0.910	0.770
C_{X1} / C_{X2}	863.0/ 910.0	638.0/ 717.0	520.0/ 743.0	1064.0/ 1136.0	647.0/ 797.0	532.0/ 721.0

(U) Cascade testing indicated that the normal solidity airfoils performed more efficiently than those of the medium solidity design. Based on the loss data and on the exit gas angle distributions reported previously (Ref. 5), it can be concluded that normal solidity designs are sufficiently superior to the medium solidity designs, when compared under annular segment cascade conditions, to justify their choice in the final turbine design. Furthermore, a deviation criterion which has been successfully used on other turbine designs was used to assure that a correct flow parameter and reaction level was attained. Three degrees of negative incidence was designed into the airfoils with the exception of the endwall region, since cascade testing indicated that overturning may occur. Figures 30, 31 and 32 show the design gas and metal inlet angles, and the gas angles which would result from using measured cascade losses for the first blade, second vane and second blade. The outside diameter endwall metal angles of the first blade, second vane and second blade were designed with 7° negative incidence (relative to the design gas angles) to insure that some negative incidence should still exist if cascade-type end losses were achieved. The second blade root was designed with 3° of positive incidence so that channel convergence could be increased from 0.5 to 5.0 percent. This results in an airfoil with a better pressure distribution and with improved separation resistance. The final airfoil geometry is tabulated in Tables IX and X. The details of the final airfoil designs, including the profiles and their pertinent parameters, the airfoil pressure distributions convergence ratios, diffusion factors and stress values are presented in Appendices I through IV.

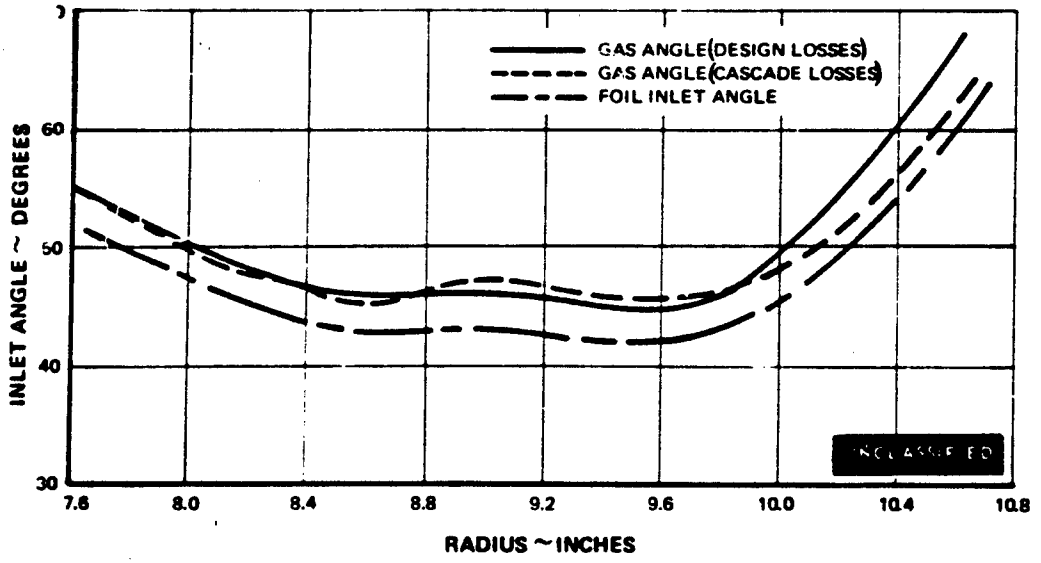

Figure 30 First-Stage Blade Inlet Angle Versus Radius

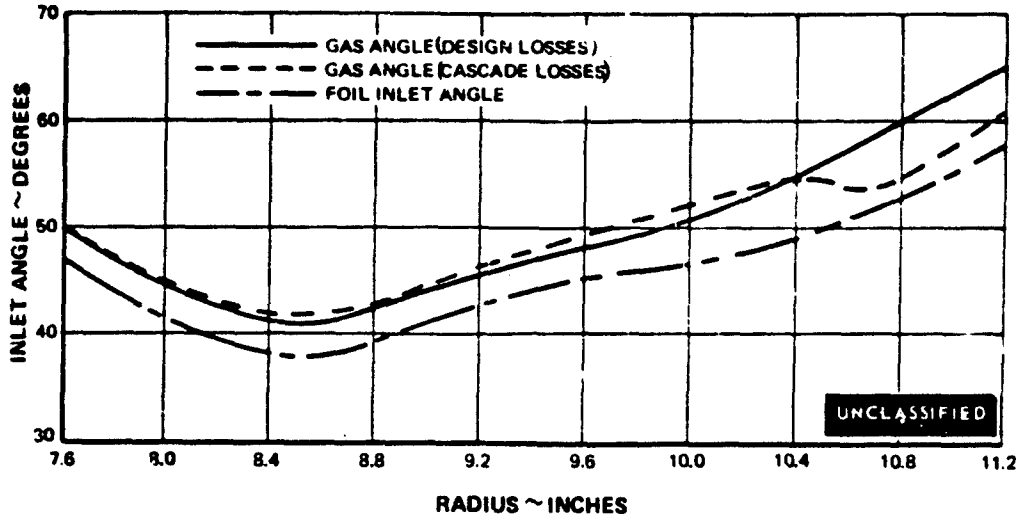

Figure 31 Second-Stage Vane Inlet Angle Versus Radius

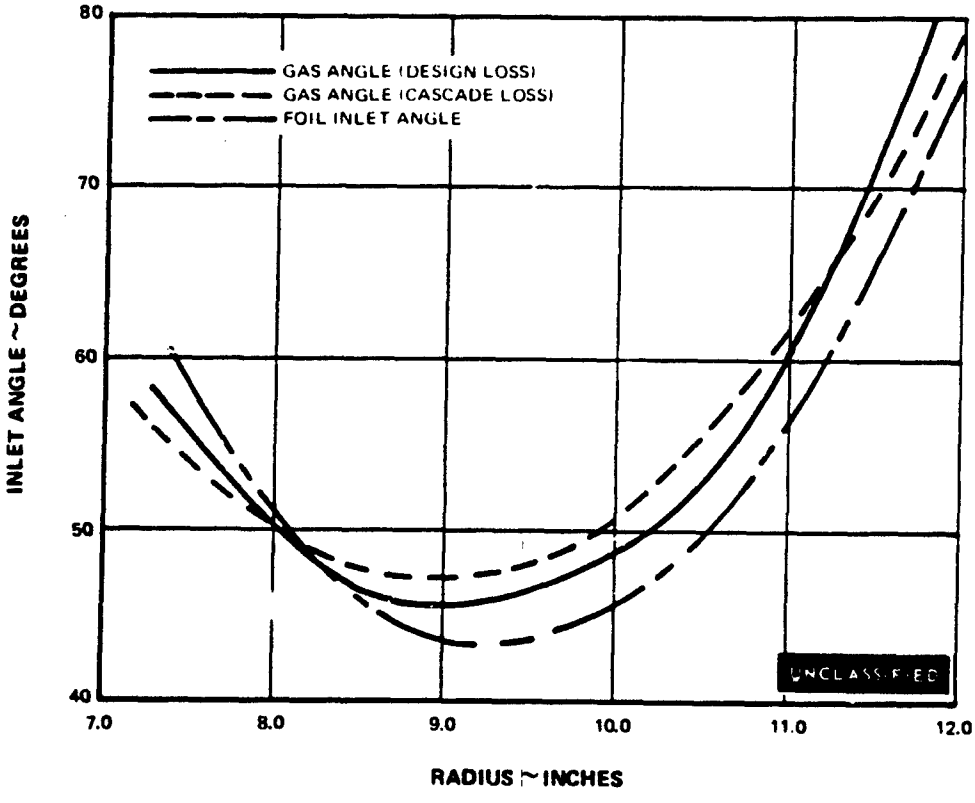

Figure 32 Second-Stage Blade Inlet Gas Angle Versus Radius

TABLE IX

STAGE ONE AIRFOIL GEOMETRY

Radial Station	Root	Mean	Tip
Vane Defining Radius	7.90	9.015	10.13
No. of Vanes	66		
Axial Chord	0.918	1.005	1.092
Taper Ratio (b_R/b_T)	0.840		
Aspect Ratio (L/b_T)	2.04		
Foil Weight	0.0889		
Gap Chord	0.819	0.854	0.883
(Hub/Tip Ratio) Average	0.794		
Average Length (L)	2.055		
α_0 *	64.9	60.5	90.0
α_1 (Gaging Angle)/α_1 *	35.08/35.7	26.98/26.93	26.7/26.05
ϕ - Camber ($180 - \alpha_0 * - \alpha_1 *$)	79.4	92.57	63.95
Gas Bending Stress	0	3900	15.000
Material			
Material Density lb/in^3	0.297		
Uncooled Metal Temperature °F			

TABLE IX (Cont'd)

STAGE ONE AIRFOIL GEOMETRY

Radial Station	Root	Mean	Tip
Blade Defining Radius	7.78	9.1975	10.615
No. of Blades	106.		
Axial Chord	0.7176	0.6816	0.6456
Taper Ratio (b_T/b_R)	0.900		
Aspect Ratio (L/b_R)	3.950		
Foil and Shroud - Weight	0.0633		
Gap Chord	0.643	0.800	0.975
(Hub/Tip Ratio) Average	0.742		
Average Length (L)	2.702		
β_1 *	50.1	42.6	60.5
β_2 (Gaging Angle)/β_2 *	32.97/31.97	26.3, 25.95	27.65/28.88
ϕ - Camber ($180 - \beta_1^* - \beta_2^*$)	97.93	111.45	90.62
P/A Stress	12,800	7600	2900
Gas Bending (Untilted)	29,200	6500	0
Shroud Misalign Stress	1500	1700	3700
Material			
Material Density lb/in^3	0.286		
Uncooled Metal Temperature °F			UNCLASSIFIED

TABLE X

STAGE TWO AIRFOIL GEOMETRY

Radial Station	Root	Mean	Tip
Vane Defining Radius	7.63	9.465	11.3
No. of Vanes	72		
Axial Chord	0.998	1.057	1.116
Taper Ratio (b_R/b_T)	0.895		
Aspect Ratio (L/b_T)	3.29		
Foil Weight	0.1481		
Gap Chord	0.667	0.781	0.884
(Hub/Tip Ratio) Average	0.690		
Average Length (L)	3.442		
α_0 *	46.0	44.2	60.75
α_1 (Gaging Angle)/α_1 *	36.03/35.49	25.95/25.49	26.85/26.85
ϕ - Camber ($180 - \alpha_0$ * - α_1 *)	97.61	110.31	92.4
Gas Bending Stress	0	5,500	24,400
Material			
Material Density lb/in^3	0.297		
Uncooled Metal Temperature °F			[redacted]

TABLE X (Cont'd)

STAGE TWO AIRFOIL GEOMETRY

Radial Station	Root	Mean	Tip
Blade Defining Radius	7.515	9.655	11.795
No. of Blades	118		
Axial Chord	0.788	0.694	0.600
Taper Ratio (b_T/b_R)	0.762		
Aspect Ratio (L/b_R)	5.43		
Foil and Shroud Weight	0.0727		
Gap Chord	0.508	0.741	1.047
(Hub/Tip Ratio) Average	0.643		
Average Length (L)	4.161		
β_1 *	58.3	44.0	71.6
β_2 (Gaging Angle)/β_2 *	43.6/42.08	30.31/30.22	26.72/26.72
ϕ - Camber ($180 - \beta_1 * - \beta_2 *$)	79.62	105.78	81.68
P/A Stress	17,000	11,100	3100
Gas Bending (Untilted)	52,800	13,100	0
Shroud Misalign Stress	2000	2300	5100
Material			
Material Density lb/in^3	0.286		
Uncooled Metal Temperature °F			[redacted]

5. PREDICTION OF THE OVERALL TURBINE EFFICIENCY

(U) The prediction process by which the overall efficiency was obtained consisted of three major steps: a Meanline Deck Calculation, a Streamline Deck Calculation and an Exit Guide Vane Loss Calculation. Each of these procedures will be described below.

Meanline Deck Calculation

(U) Initial calculations were made using the Turbine Off-Design Meanline Computer Program which provided the necessary input information to insure that the best possible estimate of turbine efficiency was obtained from the Turbine Streamline Analysis Computer Program.

(U) The Turbine Off-Design Deck is such that the spanwise integrated value of profile loss could be specified for each row. The local profile losses, from which these integrated values were calculated were determined at five radial locations from considerations of pressure distribution, boundary layer friction (fully turbulent), form drag and wake mixing. This method of calculation takes all cascade geometric properties (e.g. solidity and trailing-edge thickness) and flow properties (e.g. Mach number, Reynolds number and flow angle) into proper account. The integrated end-loss for each airfoil row was iteratively calculated using an empirical end-loss correlation. This correlation, which is based on engine data, predicts the combined effects of channel cross-flow, cavity recirculation and some leakage airflows. Leakage flow around the rotor tip shroud was calculated using an updated Egli calculation. This method was modified based on the results of labyrinth seal tests conducted by the Contractor.

Streamline Analysis

(U) The spanwise distribution of profile loss coefficient was determined as in the meanline calculations. The integrated end-loss coefficients and rotor tip shroud leakage efficiencies were taken directly from the meanline calculation results. The end-losses were distributed in the spanwise direction using empirical correlations.

(U) The output of this analysis was a total-to-total efficiency based on mass-averaged total pressures and temperatures. The inlet station for this efficiency was between the inlet guide vane and first-stage vane and the exit station was between the second-stage rotor and the exit guide vane. This efficiency corresponds to what will be measured in the rig and must be decreased by the inclusion of a theoretical exit guide vane penalty. The method of computing the exit guide vane loss will be discussed in the following paragraph.

Exit Guide Vane (EGV) Selection

A. Geometry

(U) An analytical model of an EGV was established which is theoretically capable of removing the swirl distribution present in the turbine rig exit measuring plane (designated EGV inlet plane). Since this EGV must be able to accept any distribution of inlet Mach number and

inlet swirl angle, it was impractical to do a detailed analysis of each combination. For this reason, the EGV was examined for feasibility under its nominal operating conditions, which are listed below:

	β_i	M_i
Root	28°	0.70
Mean	33°	0.49
Tip	24°	0.43

(U) Based on existing EGV designs, a maximum thickness of 0.70 inch was selected as being sufficient to allow oil lines to be passed radially through the airfoil. In order to keep the maximum thickness to actual chord ratio less than 15 percent, an axial chord of 4.6 inches was chosen. For simplicity, this axial chord was kept at a constant spanwise value. The pitch was varied, by varying the number of vanes, until a reasonable spanwise loss level distribution was obtained, but not without due regard being given to choking margin. With these constraints imposed, the number of airfoils turned out to be sixteen. Figure 33 summarizes the resulting pertinent EGV geometric parameters.

(U) An examination of this EGV, under nominal operating conditions, reveals that:

1. The airfoils are thin (< 15 percent thick).

2. The approach Mach numbers are subcritical, thus avoiding the possibility of transonic drag rise.

3. The Reynolds number is greater than critical ($> 2.5 \times 10^5$) and because of the turbine upstream the free stream will be very turbulent (~ 4 percent). These two factors combine to all but completely exclude the possibility of any laminar separation.

Items one, two and three allow the analysis of Reference (6) to be used.

4. The airfoils are thick enough to accommodate oil lines.

5. The airfoils have sufficient overall choking margin, as is shown in Figure 34. Even though the EGV has local root choking, the major portion of the span has a large choking margin. Therefore, were the EGV actually placed in this nominal flow field, the fluid would undergo a readjustment which would alleviate this situation. The choking margin study was done using a Pratt & Whitney Compressor Cascade Deck which, incidentally, agrees well in loss level with the NASA method at low values of diffusion factor, but predicts a much slower increase of loss with diffusion factor.

This information, which defines the EGV in a global sense, shows that the nominal EGV could be made into a functional piece of hardware.

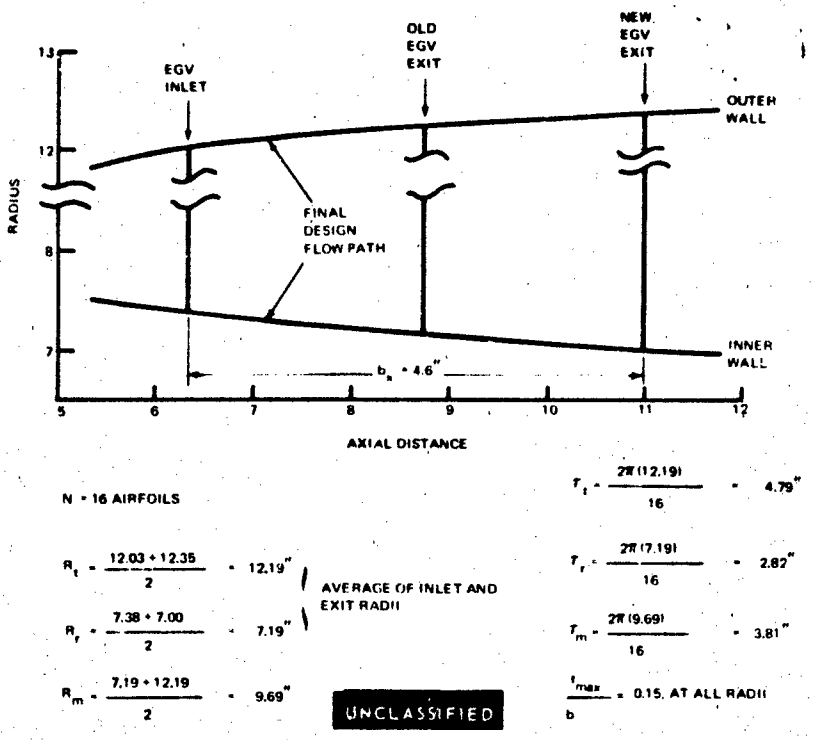

Figure 33 Pertinent Exit Guide Vane Geometry

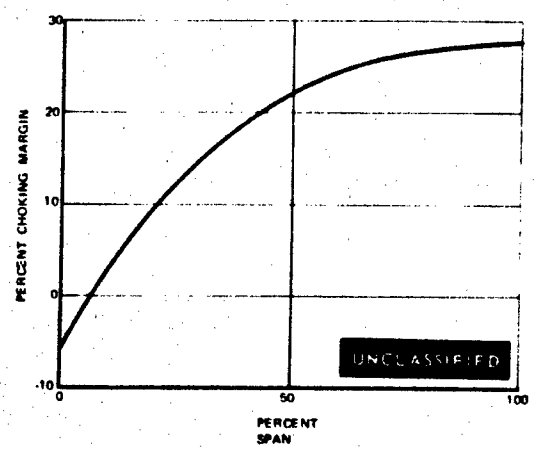

Figure 34 Exit Guide Vane Choking Margin

B. Interpretation and Extension of the NASA Compressor Cascade Loss System

(U) This section of the report is only meant to serve as an outline of the development of the pertinent equations. For the sake of completeness, detailed discussions of the derivations of many of the following equations are included in the appendix at the end of this report.

(U) Using the geometry shown in Figure 33, and by following the method of calculation given in Reference (6), with some minor modifications, the loss associated with the EGV and its effect on turbine efficiency will be determined.

The compressible diffusion factor, D_f, is defined as

$$D_f = \left(1 - \frac{V_e}{V_i}\right) + \frac{\Delta V_\theta}{2\sigma V_i} \tag{1}$$

on page 203 of Reference (6). This is the parameter that NASA chose to correlate their data. Using the equation developed in Appendix V(a), M_e and therefore V_e/V_i may be determined since

$$\frac{V_e}{V_i} = \sqrt{\frac{M_e^2\left(1 + \frac{k-1}{2} M_i^2\right)}{M_i^2\left(1 + \frac{k-1}{2} M_e^2\right)}}$$

for an adiabatic cascade. Furthermore, using the information given in Appendix V(b) and Figure 33, the solidity ratio (σ) can be determined. Finally, because $V_{e\theta} = 0$,

$$\frac{\Delta V_\theta}{V_i} = \frac{V_{\theta i}}{V_i} = \sin\beta_i \ .$$

With this information, the diffusion factor defined by Equation (1) can be evaluated.

(U) The next task is to determine the profile-loss coefficient

$$Z_p = \text{function}\,(D_f). \tag{2}$$

The method by which this is accomplished is explained in Appendix V(c).

Having Z_p, it is desirable to change this to a stagnation pressure-loss coefficient $(\Delta p_o/p_o)_p$

$$\left(\frac{\Delta p_o}{p_o}\right)_p = 2Z_p\,\sigma\cos^2\beta_i \left[\frac{\left(1 + \frac{k-1}{2} M_i^2\right)^{\frac{k}{k-1}} - 1}{\left(1 + \frac{k-1}{2} M_i^2\right)^{\frac{k}{k-1}}}\right] . \tag{3}$$

The above expression is derived in detail in Appendix V(d).

(U) The stagnation pressure loss given by Equation (3) only accounts for the profile loss. In Appendix V(e) a method for accounting for the end-wall loss is derived and the result is that

$$\frac{\Delta p_o}{p_o} = \left(\frac{\Delta p_o}{p_o}\right)_p \left(1 + \frac{1}{\sigma\, AR}\right),$$

or, by substituting the expression for $(\Delta p_o/p_o)_p$ given by Equation (3) we further find that

$$\frac{\Delta p_o}{p_o} = 2Z_p \cos^2\beta_i \left[\frac{\left(1 + \frac{k-1}{2} M_i^2\right)^{\frac{k}{k-1}} - 1}{\left(1 + \frac{k-1}{2} M_i^2\right)^{\frac{k}{k-1}}}\right] \left(\sigma + \frac{1}{AR}\right) \qquad (4)$$

(U) Finally, the measured turbine efficiency must be debited by this stagnation pressure loss. To this end, Appendix V(f) contains the derivation of the following equation

$$\frac{\eta}{\eta_{\text{MEASURED}}} = \frac{P_R^{\frac{k-1}{k}} - 1}{P_R^{\frac{k-1}{k}} - \left(1 - \frac{\Delta p_o}{p_o}\right)^{\frac{k-1}{k}}} \qquad (5)$$

where $\frac{\Delta p_o}{p_o}$ is given by Equation (4). This is the final working form of the equation whose use will be described in the following section.

C. Application of the Modified NASA Loss System to the Contract EGV

(U) Figure 35 shows the results of calculating $\frac{\Delta p_o}{p_o}$, for the root, mean, and tip section, using Equation (4) which was developed in the previous section. This figure shows that the root and tip sections are relatively insensitive to β_i and M_i variations. The mean section, although insensitive to M_i changes, is very sensitive to β_i variations and is therefore, the section that is most likely to fail.

A mass-averaged total pressure loss, $\left(\frac{\Delta p_o}{p_o}\right)_{avg}$, may be defined by

$$\left(\frac{\Delta p_o}{p_o}\right)_{avg} \int_{r_r}^{r_t} 2\pi\rho V r dr = \int_{r_r}^{r_t} \frac{\Delta p_o}{p_o} 2\pi\rho V r dr \qquad (6)$$

(U) Assuming that the flow is uniform (i.e. ρV is not a function of radius) leaving the exit guide vane, Equation (6) reduces to

$$\left(\frac{\Delta p_o}{p_o}\right)_{avg} \left(\frac{r_t + r_r}{2}\right)\left(r_t - r_r\right) = \int_{r_r}^{r_t} \frac{\Delta p_o}{p_o}\, r dr ,$$

or,

$$\left(\frac{\Delta p_o}{p_o}\right)_{avg} r_m h = \int_{r_r}^{r_t} \frac{\Delta p_o}{p_o}\, r dr ,$$

or finally,

$$\left(\frac{\Delta p_o}{p_o}\right)_{avg} = \int_{r_r}^{r_t} \frac{\Delta p_o}{p_o}\, \frac{r}{r_m}\, \frac{dr}{h} \qquad (7)$$

Introducing a dummy variable

$$\psi_{(r)} \equiv \frac{r - r_r}{h}$$

which has the properties

$$d\psi = \frac{dr}{h} ,$$

$$\psi_{(r_r)} = 0 ,$$

$$\psi_{(r_t)} = 1 .$$

Using ψ, Equation (7) may be rewritten as

$$\left(\frac{\Delta p_o}{p_o}\right)_{avg} = \int_{o}^{1} \frac{\Delta p_o}{p_o} \left(\frac{h\psi + r_r}{r_m}\right) d\psi .$$

(U) A plot of $\frac{\Delta p_o}{p_o}\left(\frac{h\psi + r_r}{r_m}\right)$ versus ψ is shown in Figure 35. A comparison of the midspan value (0.0076) with the value obtained from a trapezoidal rule integration (0.0080) shows that the mean section gives an accurate estimate of the mass-averaged total pressure loss. Because of this, and since the mean section is the only one at all sensitive to changing flow conditions, it is recommended that the loss calculation only be done at the midspan section. Furthermore, Figure 36, which is a plot of the results derived from applying Equation (5) to the mean EGV section, shows that relatively large changes in EGV inlet conditions will have a small effect on efficiency, so that their accurate knowledge is not imperative.

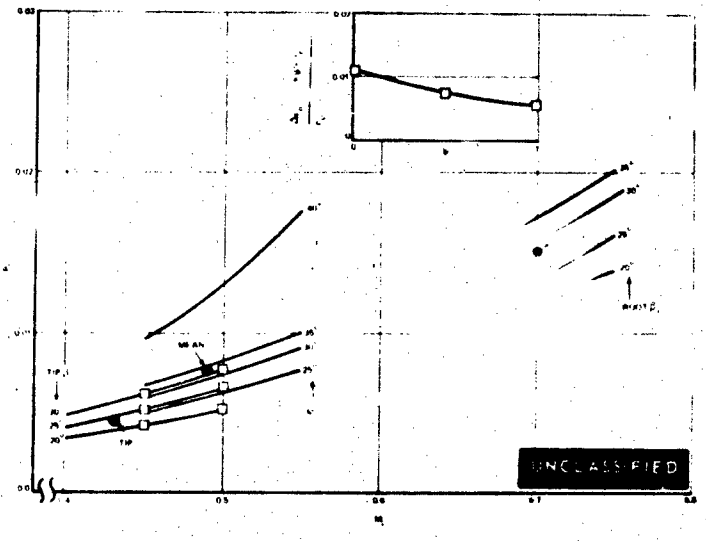

Figure 35 Root, Mean and Tip Exit Guide Vane Total Pressure Losses

(U) Figure 36 is used by knowing the EGV midspan M_i and β_i to obtain the ratio of the adjusted demonstrated overall total-to-total turbine efficiency to the demonstrated overall total-to-total turbine efficiency, $\eta/\eta_{MEASURED}$. For example, based on the conditions shown before for the mean section (β_i 33°, M_i = 0.49), $\eta/\eta_{MEASURED}$ would equal about 0.995, hence the measured efficiency would be reduced by about one-half of one point.

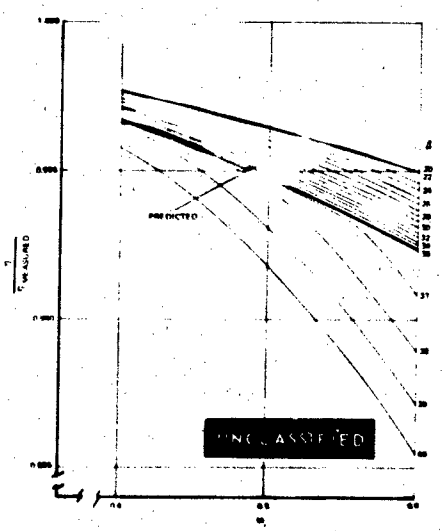

Figure 36 EGV Stagnation Efficiency Penalty, Based on a Mean-Pitus Calculation

EGV Conclusions

- (U) The loss calculation presented herein should be used to determine the exit guide vane losses.
- (U) The EGV, although never designed in detail, was shown to be realistic and practical. Furthermore, the method of loss evaluation presented in Reference (6) is shown to be applicable to the EGV in its predicted environment.
- (U) The loss calculation should be done at the mean radius, only, as the mean section yields an answer that is an accurate representation of the integrated spanwise average loss (See Figure 35).
- (U) The graphical results obtained from doing the mean radius calculation are shown in Figure 36. As shown in this figure, the ratio of the adjusted demonstrated overall total-to-total efficiency to the demonstrated overall total-to-total efficiency is shown versus the mean radius EGV approach Mach number for a variety of mean radius approach swirl angles.

Prediction

(C) The result of the calculation described in this section was a predicted turbine efficiency of 90.7 percent and an exit guide vane penalty of 0.5 percent based on the calculated second blade mean exit absolute Mach number and exit swirl angle of 0.51 and 34.5 degrees, respectively. These calculations were made at the design pressure ratio and velocity ratio which will be set when operating in the cold flow test rig. Since the end-loss correlation was believed to be conservative, based on the results of applying this correlation to other turbine designs, there is confidence that this turbine will meet the efficiency goal (91 percent) of the Contract.

6. FABRICATION

(U) A two-stage turbine was designed to demonstrate performance improvements that can be realized from the application of boundary layer control techniques investigated during Phases II and III of the Contract. This turbine was fabricated and a schematic drawing of the initial build was shown in Figure 25. The turbine was of rig-type mechanical construction, designed to accurately measure low pressure turbine efficiency. It used rig-type inlet turbine and exhaust cases, rotor shafting and instrumentation.

(U) There were a total of four builds during the course of the Contract, including the Add-on. These test configurations are shown in Figures 37, 38 and 39. Build I was the basic configuration. Build II had the root cavity volumes decreased by filler rings. The platforms remained the same as for Build I. Builds III and IV were a repeat of Builds II and I, respectively, with the platforms cut off to the airfoil fillets.

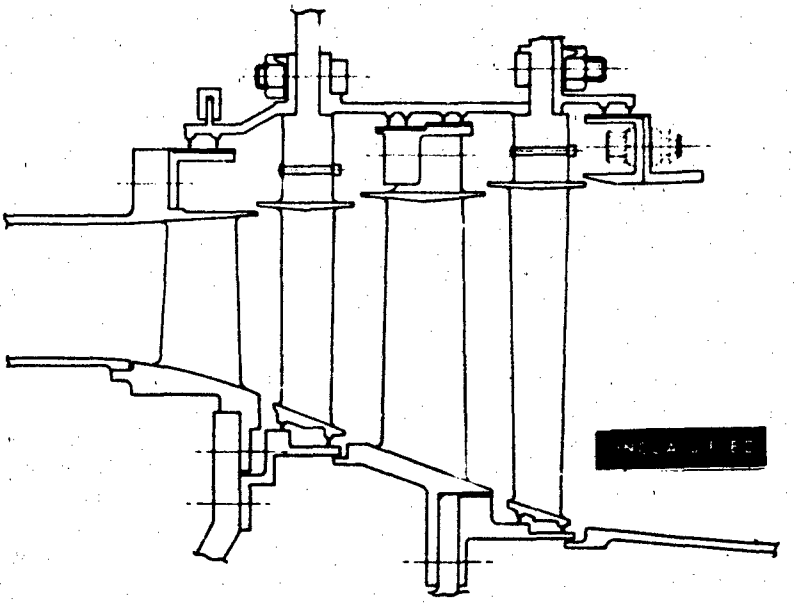

Figure 37 Test Configuration Build I – Basic Configuration

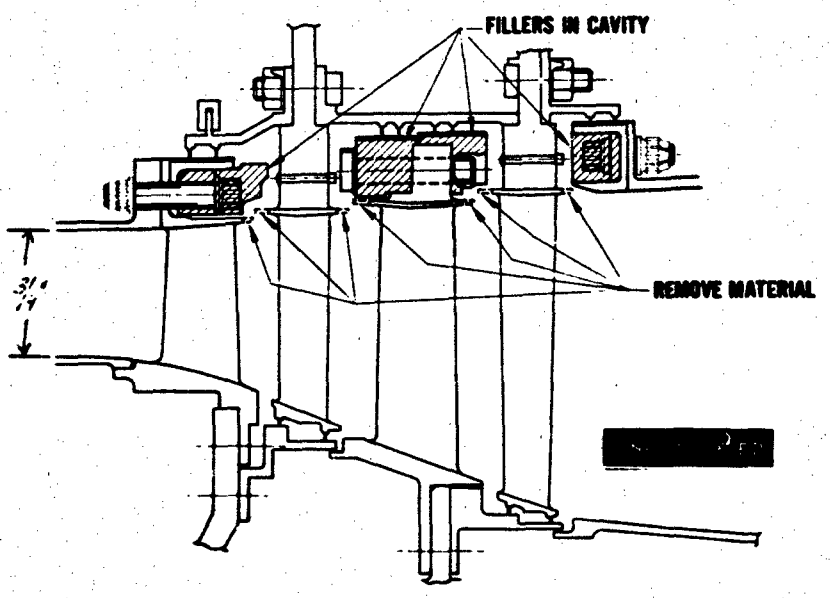

Figure 38 Test Configuration; Build II – Fillers Installed, Build III – Platforms Removed

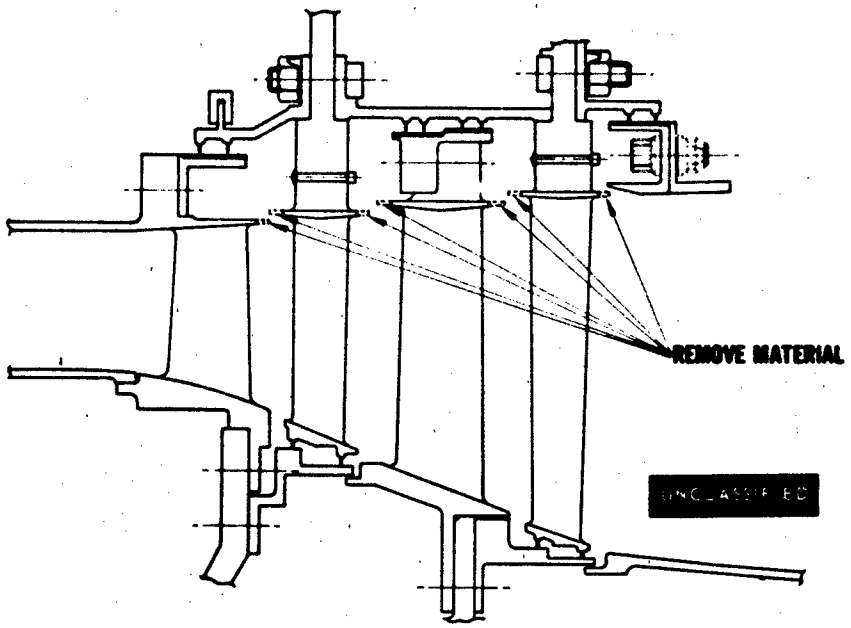

Figure 39 Test Configuration Build IV – Platforms Removed and No Filler

(U) The details of the Build I hardware are presented in the following photographs. Airfoils were machined from stainless steel and are shown in Figures 40 and 41. The inlet guide vane was designed to simulate exit conditions from a high pressure turbine. Assembly of the inlet guide vane case is shown in Figures 42 and 43. The first vane assembly is shown in Figures 44 and 45. The first blade rotor front view is shown in Figure 46, the rear view in Figure 47 and the installed rotor in Figure 48. The second vane assembly is presented in Figures 49 and 50. A close-up view of the Kiel heads on the second vane to show details of the thermocouples and total pressure taps is shown in Figures 51 and 52. The second blade rotor assembly is presented in Figures 53 and 54.

(U) The amount of cut-back on the platforms of the airfoils is shown in the following photographs, as tested in Builds III and IV. The first vane is shown in Figures 55 and 56. The leading edge view of the vane shows the installation of the trip wires wnich were necessary to assure that engine-type turbulence levels were attained during the performance calibration. Figures 57 and 58 show the amount of platform cut-back on the first rotor. Second vane cut-back and tripwire installation is shown in Figures 59 and 60. Finally, similar photographs of the second blade are presented in Figures 61 and 62.

(U) The inspection measurements of the various build assemblies are shown in Figures 63 through 66.

(U) The location and amount of instrumentation is shown in Figure 67. This instrumentation was common to all builds of the turbine rig with some modification of static pressure taps around the cavity fillers.

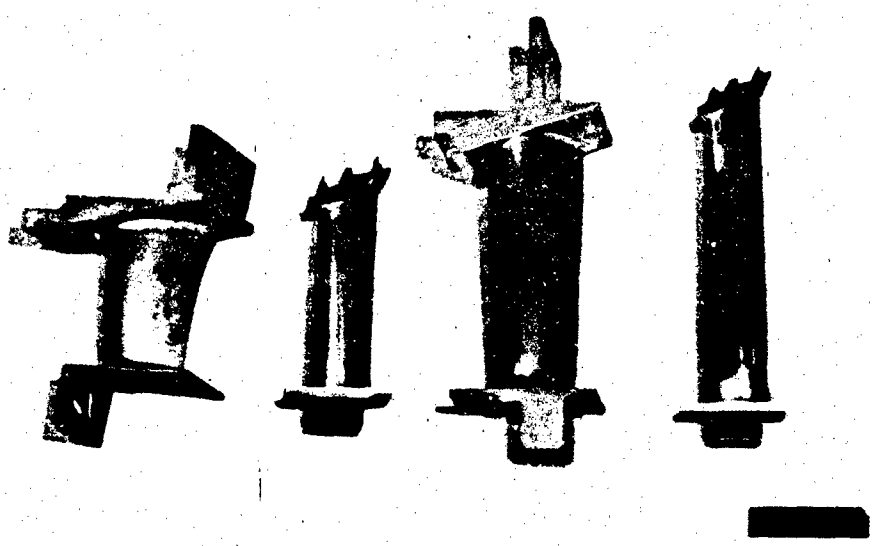

Figure 40 Build No. 1, Close-up View of Rig Airfoils Showing Vane Trip Wires (XPN 18909)

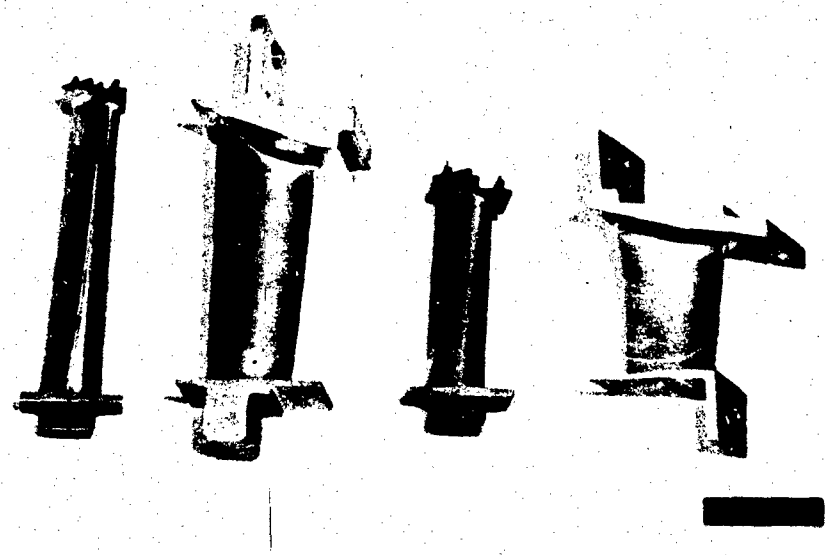

Figure 41 Build No. 1, Close-Up View of Rig Airfoils Showing Blade Trip Wires (XPN 18910)

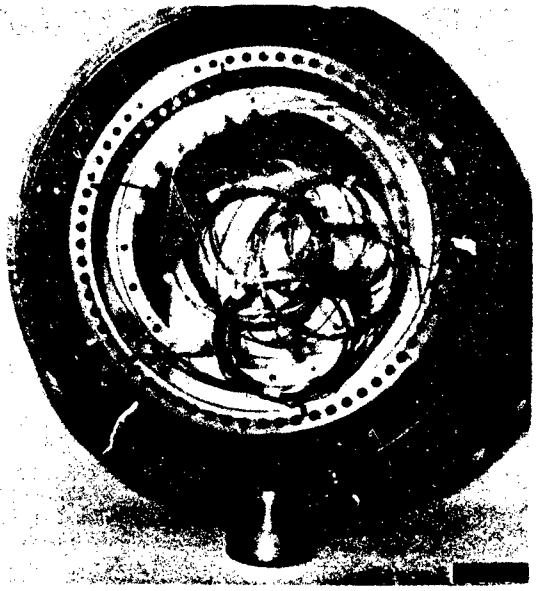

Figure 42 Build I, Full Rear View of Inlet Guide Vane Case (XPN-18124)

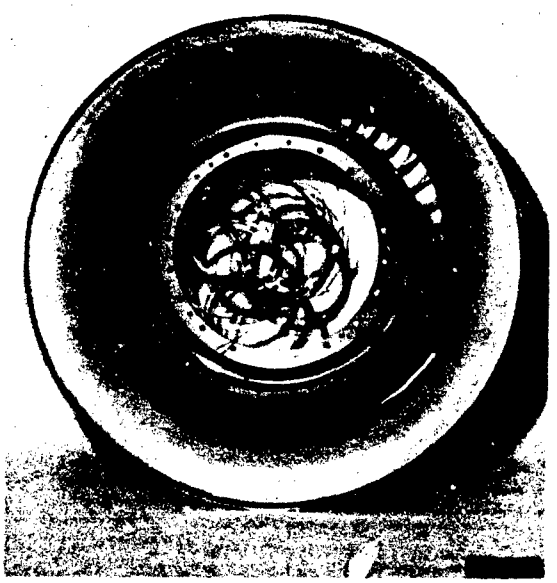

Figure 43 Build I, Full Front View of Inlet Guide Vane Case (XPN-18125)

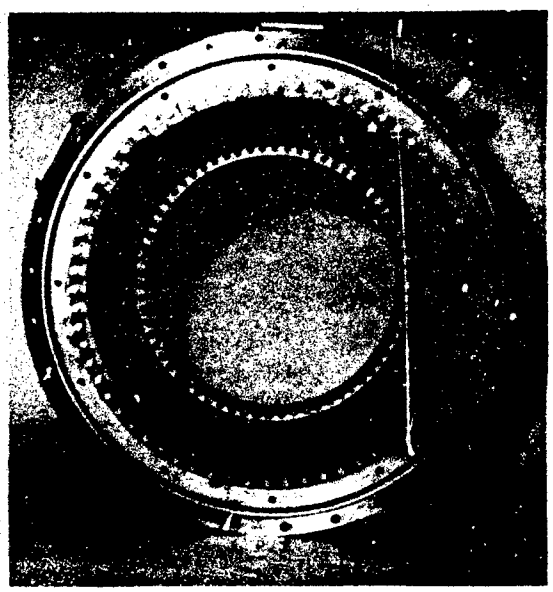

Figure 44 Build I, Full Rear View of First Nozzle Assembly (XPN-18126)

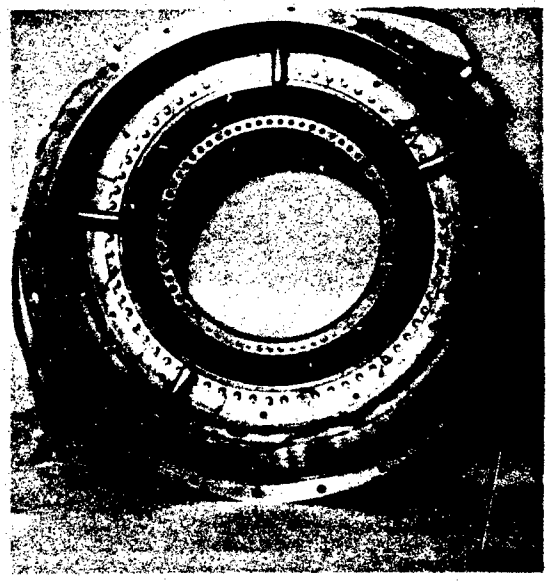

Figure 45 Build I, Full Front View of First Nozzle Assembly (XPN-18127)

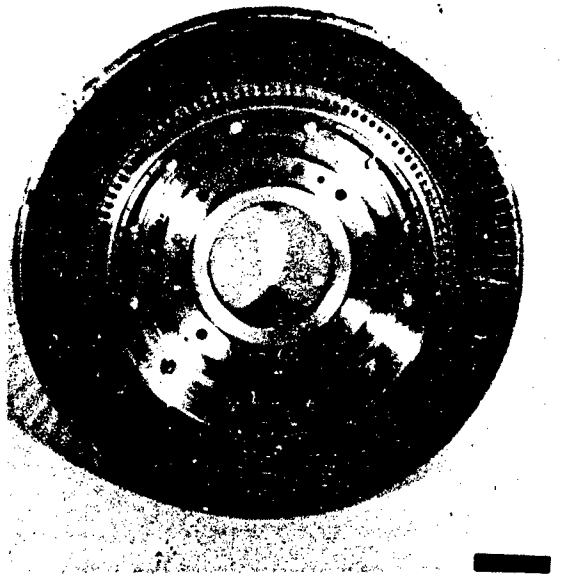

Figure 46 Build I, Full Front View of First Rotor Assembly (XPN-18905)

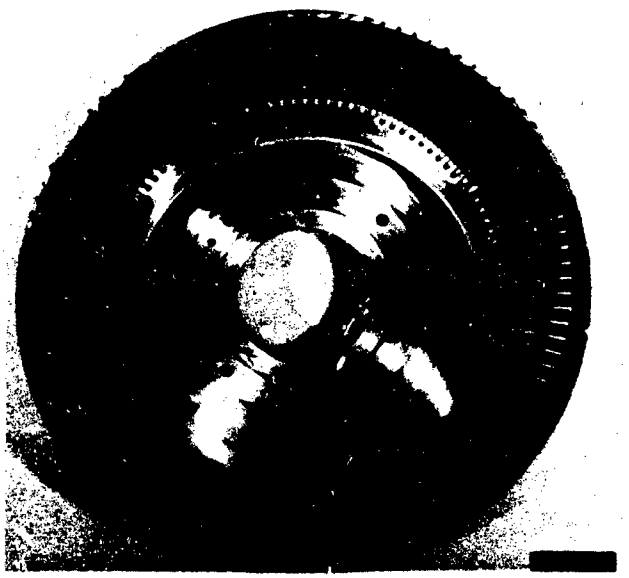

Figure 47 Build I, Full Rear View of First Rotor Assembly (XPN-18906)

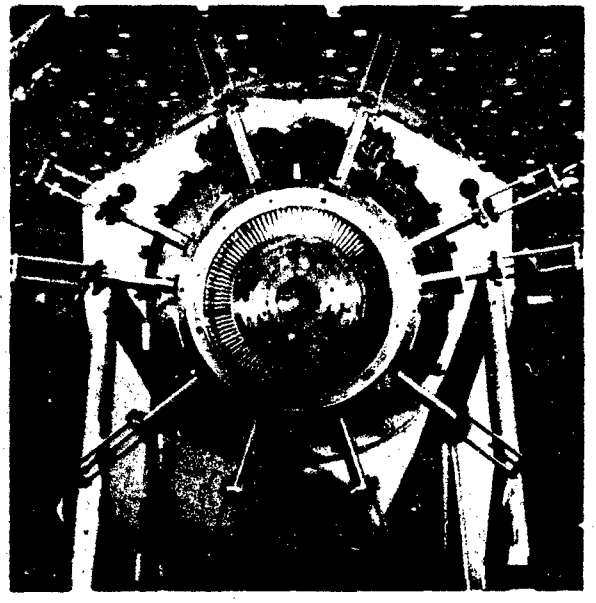

Figure 48 Build I, Full Rear View of Rig With First Rotor Installed (XPN-18622)

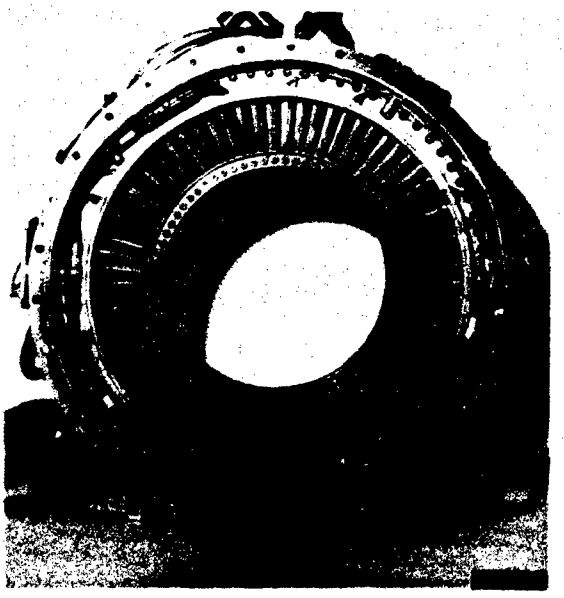

Figure 49 Build I, Full Front View of Second Assembly (XPN-18129)

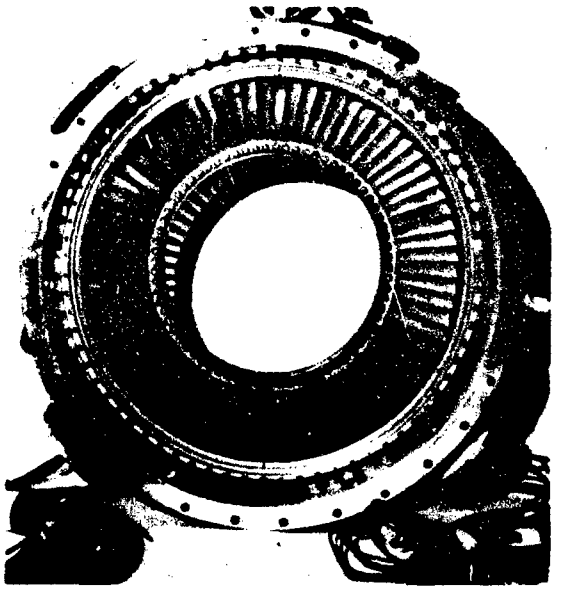

Figure 50 Build I, Full Rear View of Second Nozzle Assembly (XPN-18128)

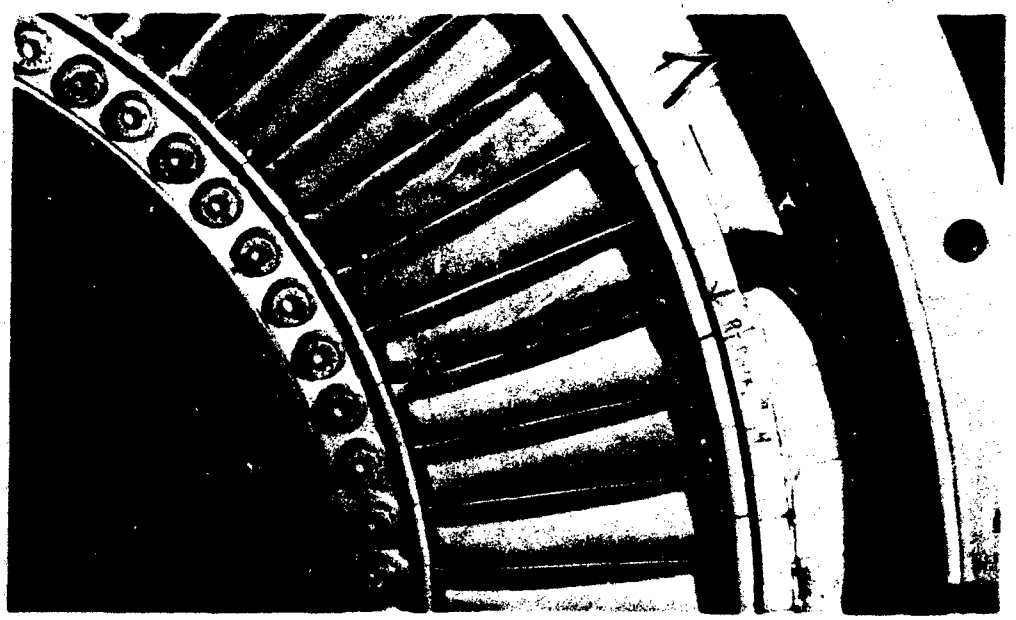

Figure 51 Build I, Close-Up View of Second-Stage Vane Leading Edge Temperature Kiel Heads (XPN-18911)

Figure 52 Build I, Close-Up View of Second-Stage Vane Leading Edge Pressure Kiel Heads (XPN-18912)

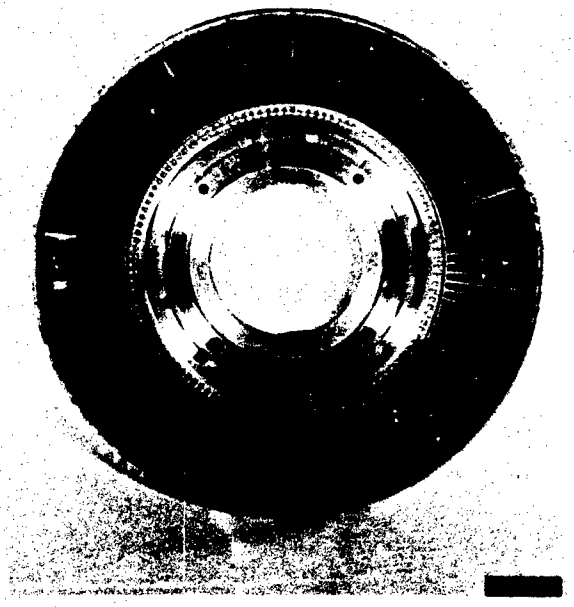

Figure 53 Build I, Full Front View of Second Rotor Assembly (XPN-18907)

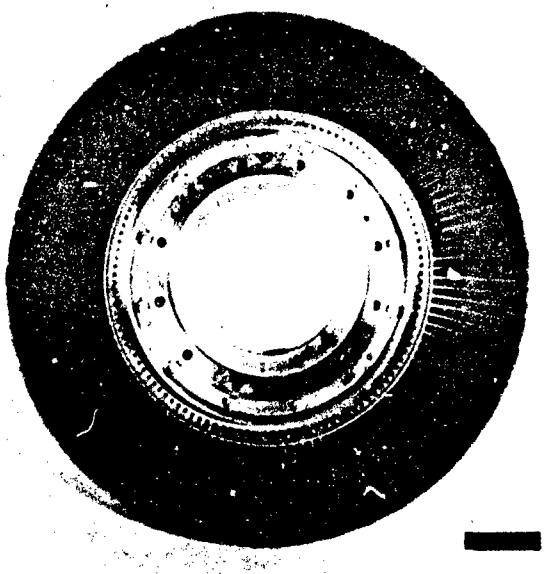

Figure 54 Build I, Full Rear View of Second Rotor Assembly (XPN-18908)

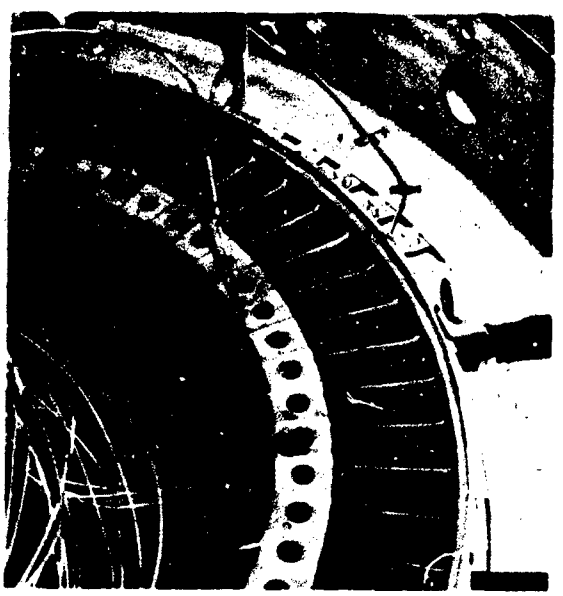

Figure 55 Build IV Showing Leading Edge of The First Nozzle Vane Assembly. Nozzle Vanes Have Section Wall Trip Wires Installed (XPN-23438)

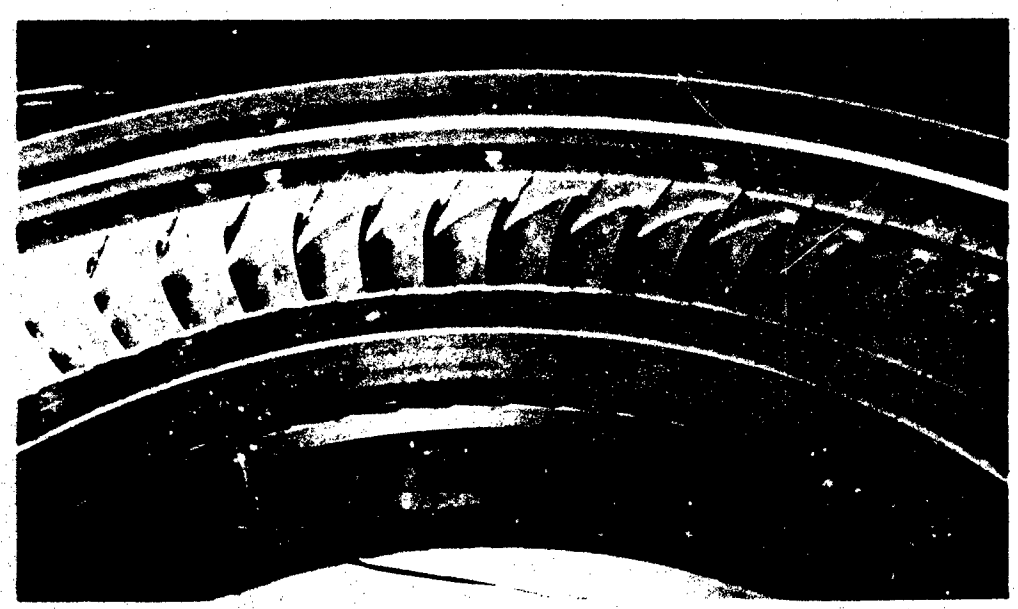

Figure 56 Build IV, First Nozzle Vanes, Trailing Edge Showing Cut-Back Inside Diameter Platforms (XPN-23419)

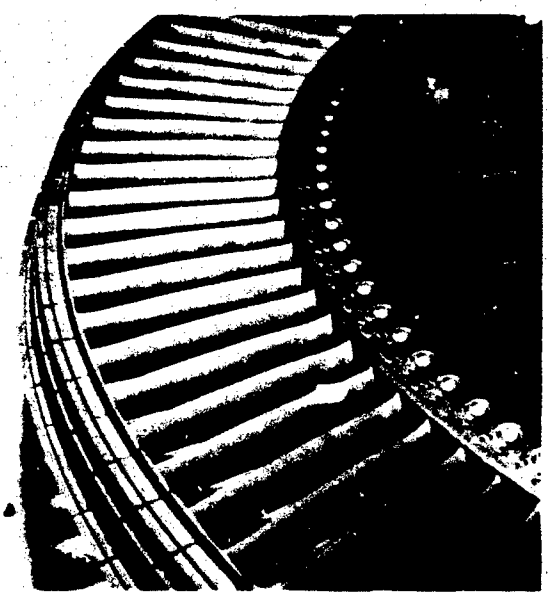

Figure 57 Build IV, First Rotor, Leading Edge Showing Cut-Back Inside Diameter Platforms and Tripwires (XPN-23417)

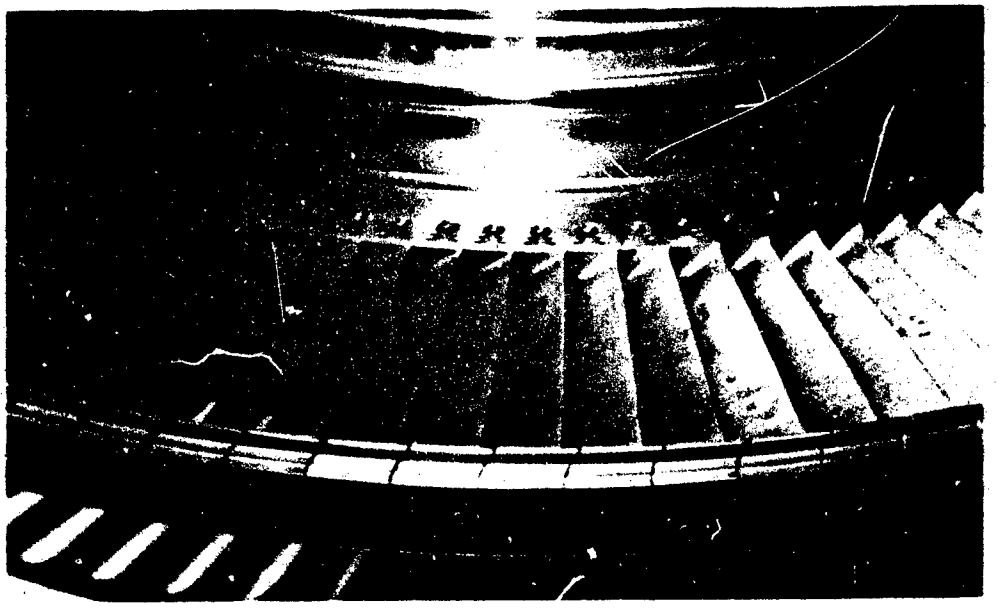

Figure 58 Build IV, First Rotor, Trailing Edge Showing Cut-Back Inside Diameter Platforms (XPN-23418)

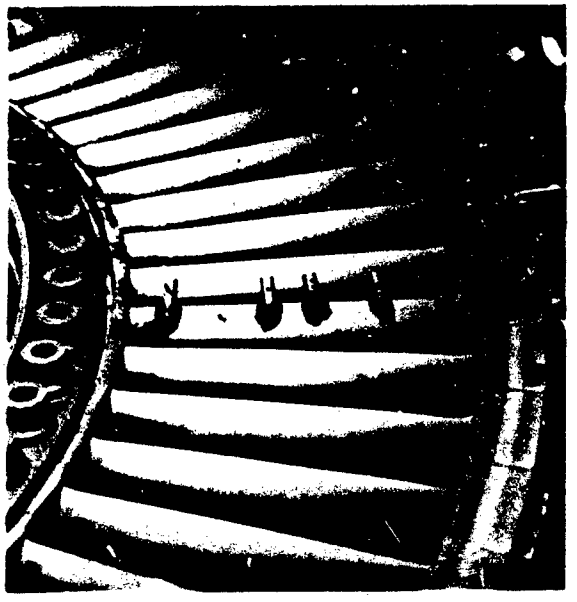

Figure 59 Build IV, Second Nozzle Vanes, Leading Edge Showing Cut-Back Inside Diameter Platforms and Tripwires (XPN-23421)

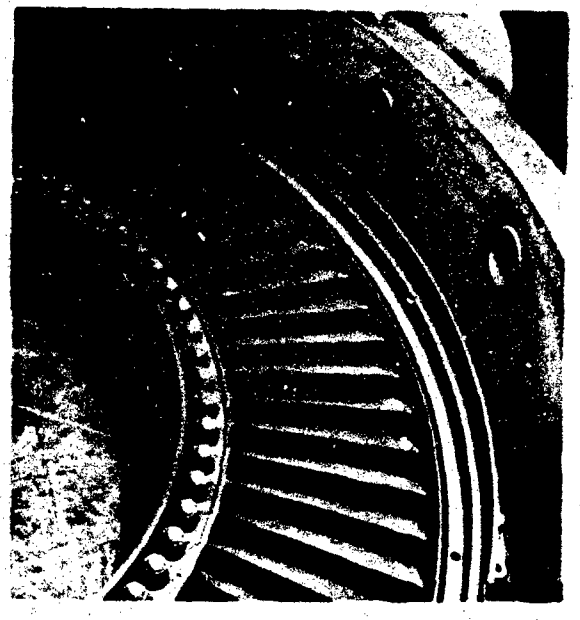

Figure 60 Build IV, Second Nozzle Vanes, Trailing Edge Showing Cut-Back Inside Diameter Platforms (XPN-23423)

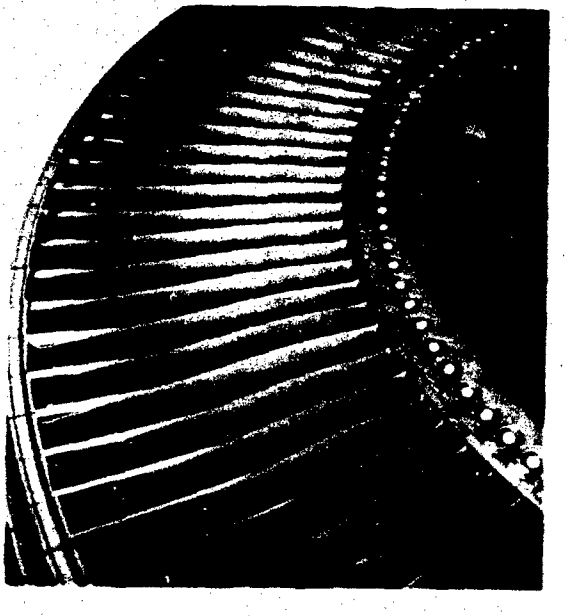

Figure 61 Build IV, Secton Rotor, Leading Edge Showing Cut-Back Inside Diameter Platforms and Tripwires (XPN-23416)

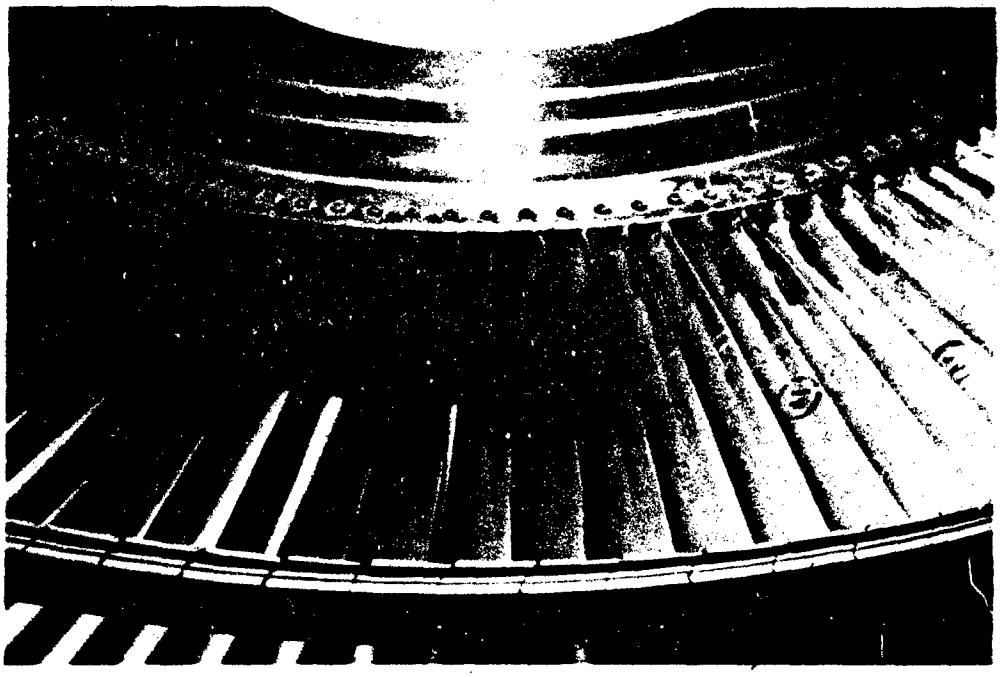

Figure 62 Build IV, Second Rotor, Trailing Edge Showing Cut-Back Inside Diameter Platforms (XPN-23415)

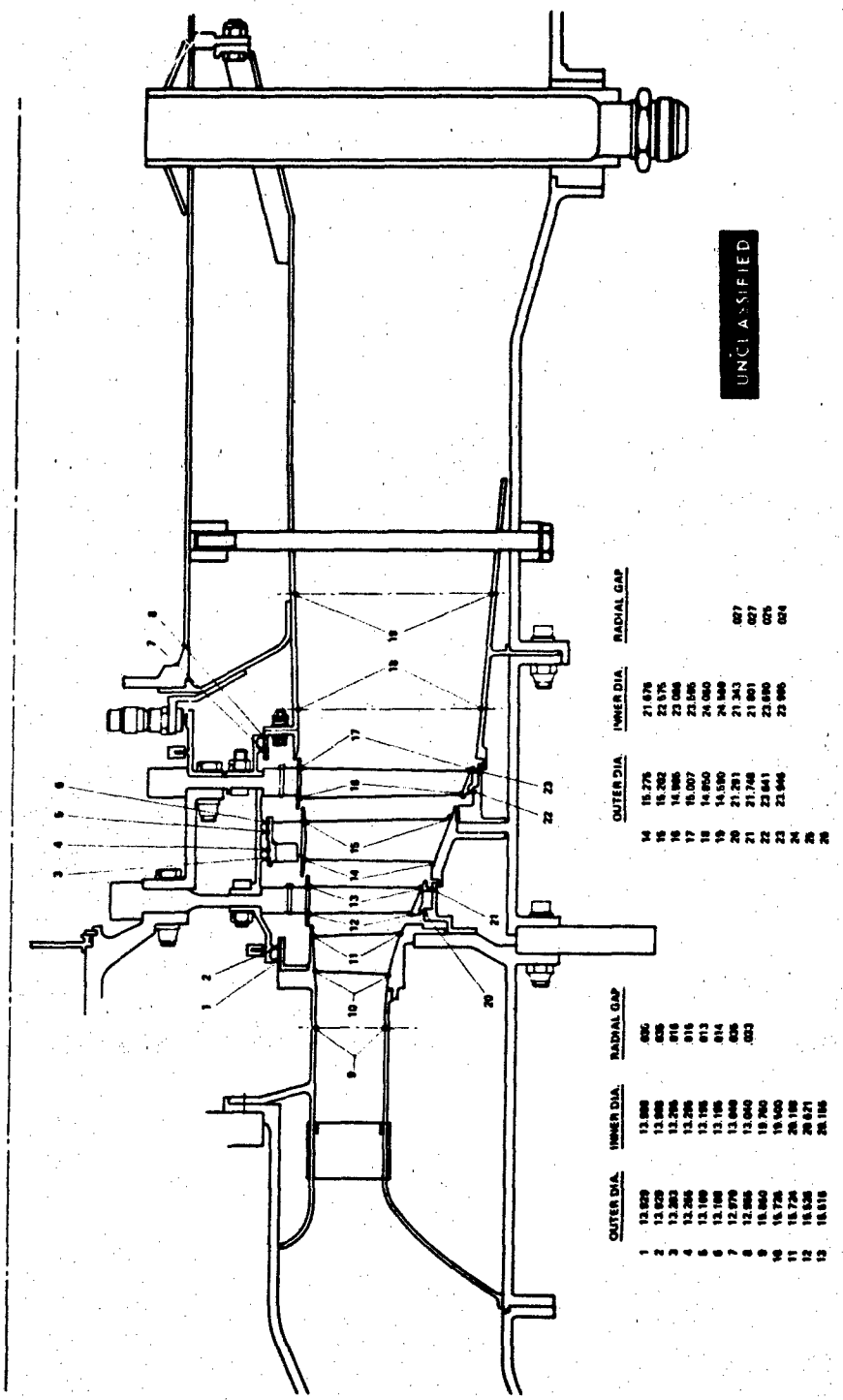

Figure 63 Build 1 Assembly Measurements

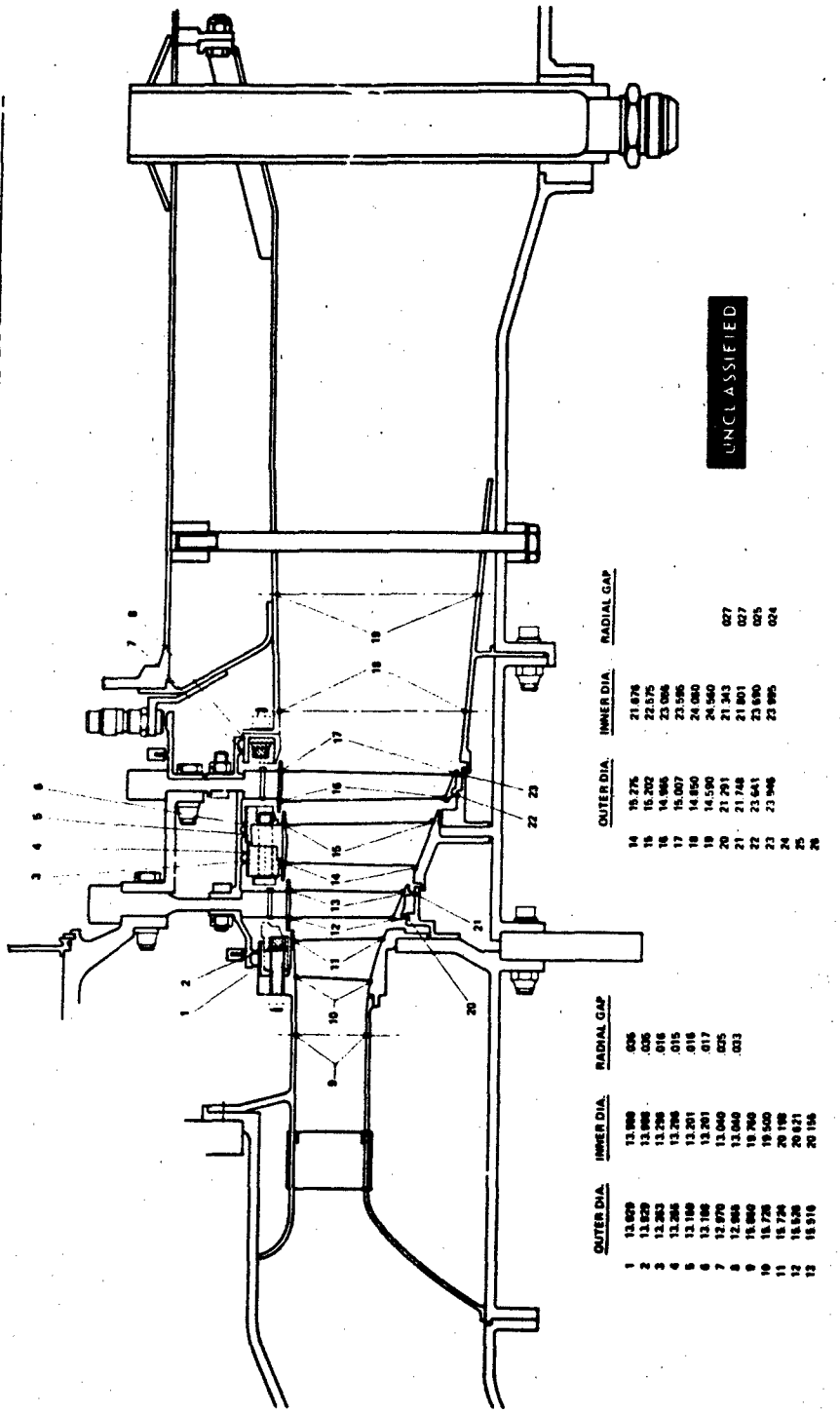

Figure 64 Build II Assembly Measurements

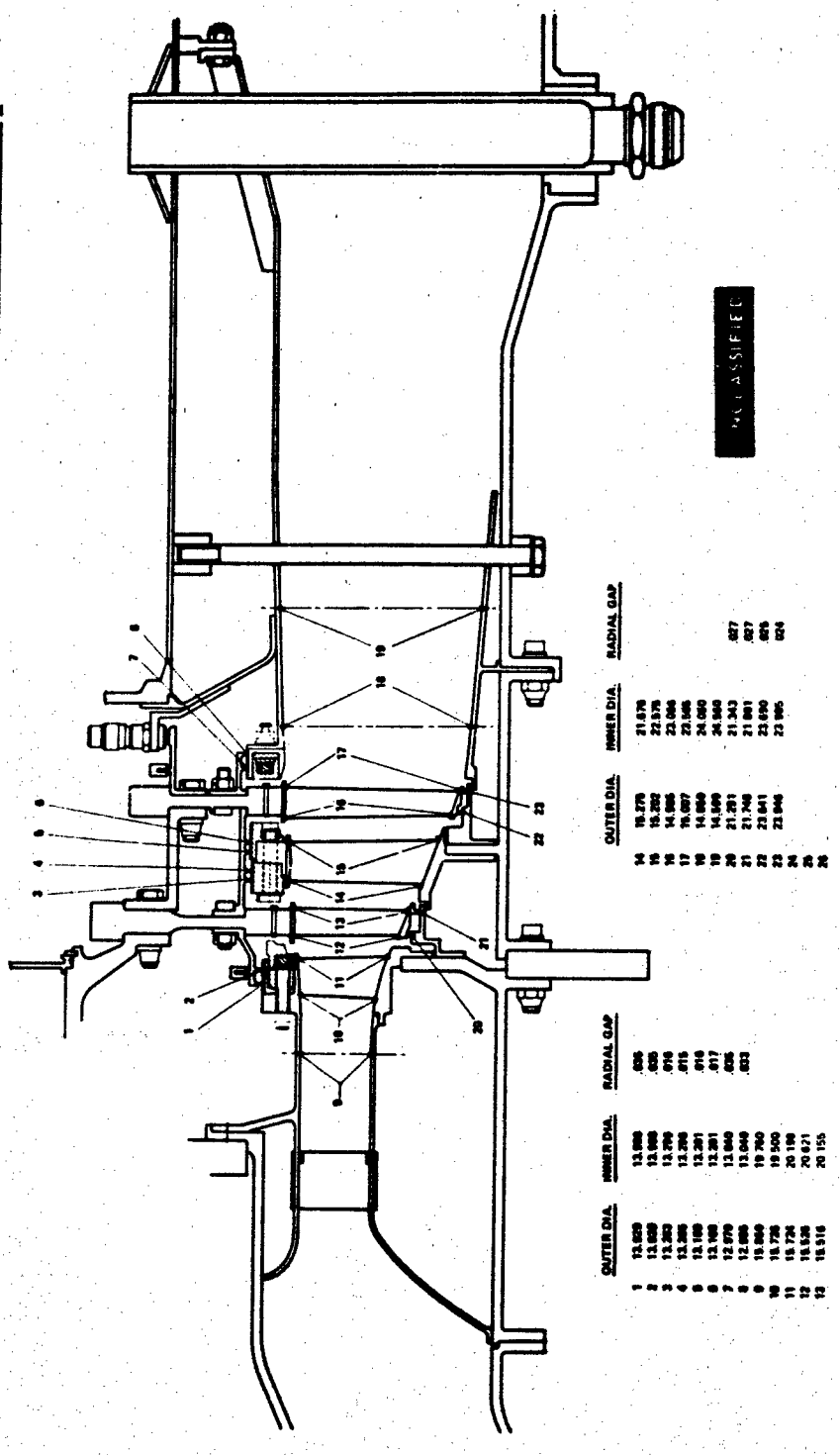

Figure 65 Build III Assembly Measurements

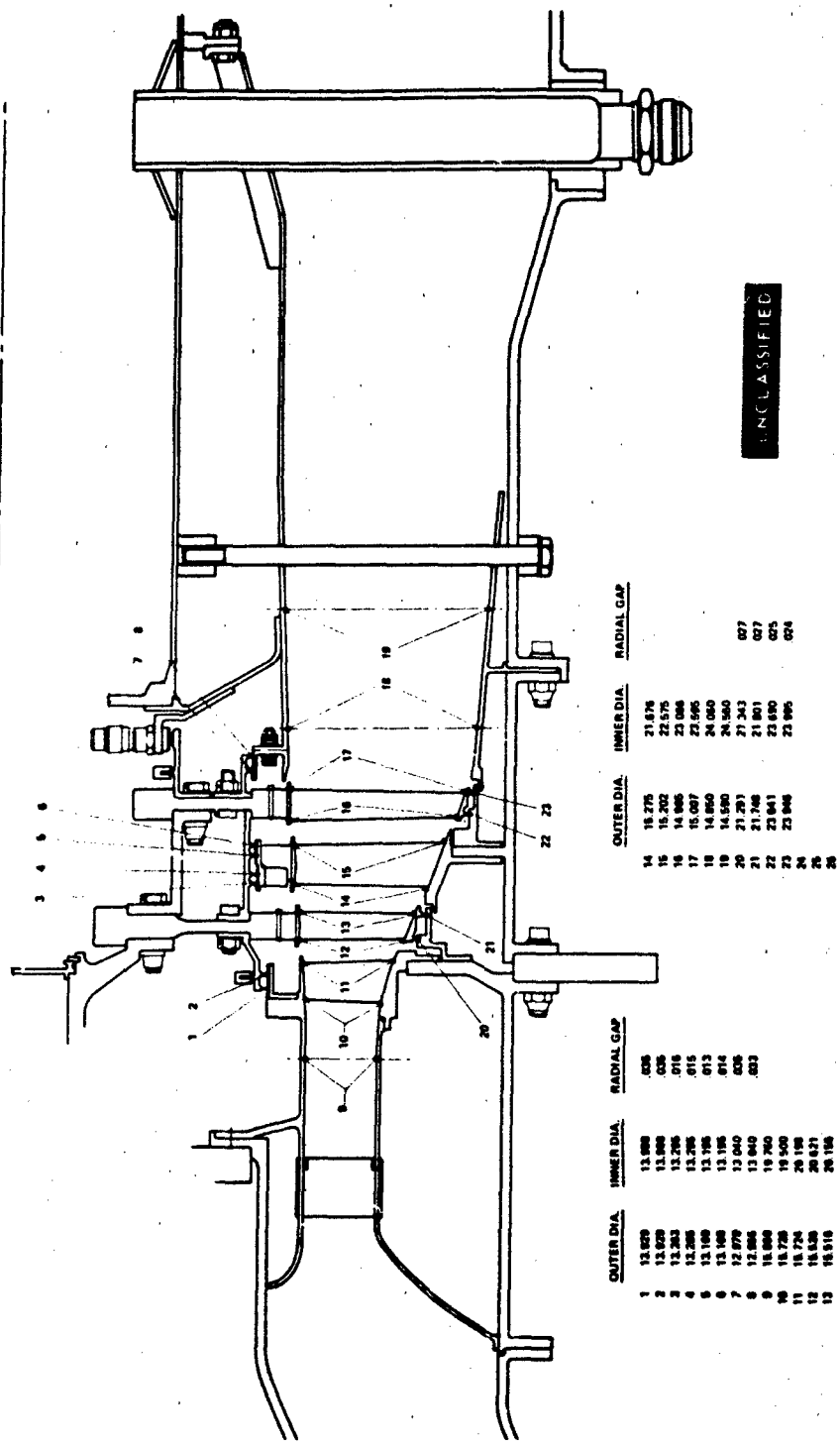

Figure 66 Build IV Assembly Measurements

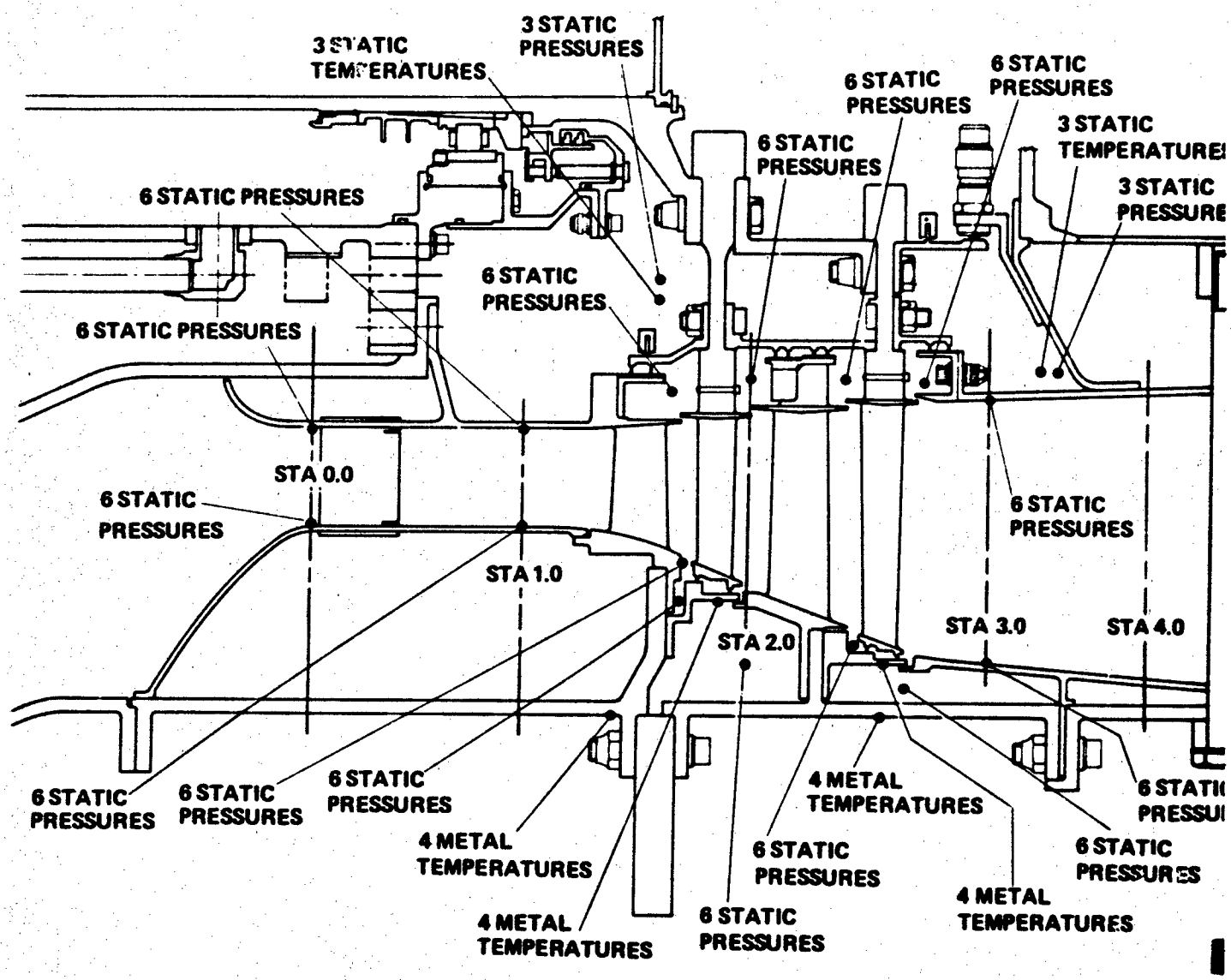
3 STATIC TEMPERATURES
3 STATIC PRESSURES
6 STATIC PRESSURES
6 STATIC PRESSURES
3 STATIC TEMPERATURE
3 STATIC PRESSURE
6 STATIC PRESSURES
6 STATIC PRESSURES
6 STATIC PRESSURES
6 STATIC PRESSURES
STA 0.0
6 STATIC PRESSURES
STA 1.0
6 STATIC PRESSURES
STA 3.0
STA 4.0
STA 2.0
6 STATIC PRESSURES
6 STATIC PRESSURES
6 STATIC PRESSURES
4 METAL TEMPERATURES
4 METAL TEMPERATURES
6 STATIC PRESSURES
4 METAL TEMPERATURES
6 STATIC PRESSURES
6 STATIC PRESSURES
4 METAL TEMPERATURES
6 STATIC PRESSURES

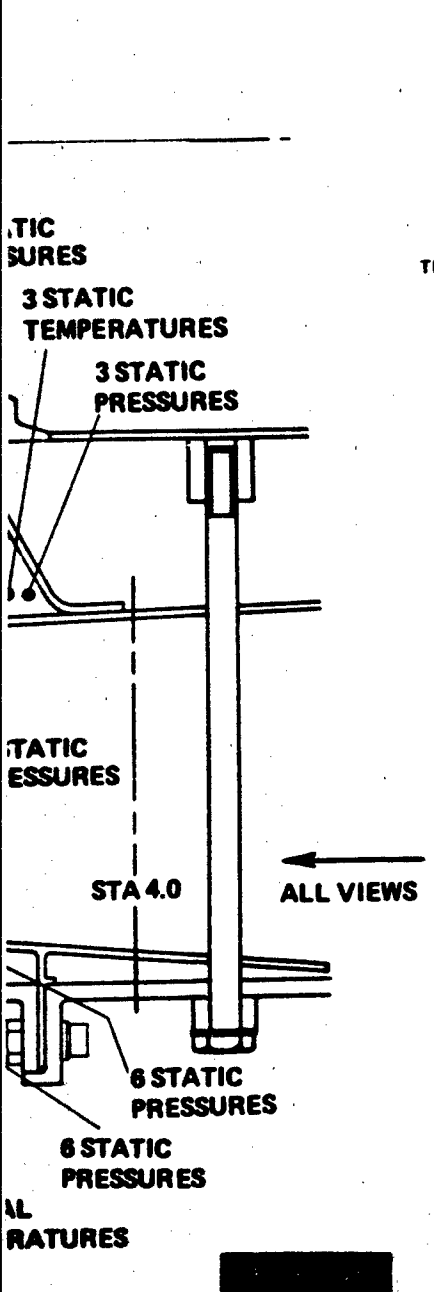

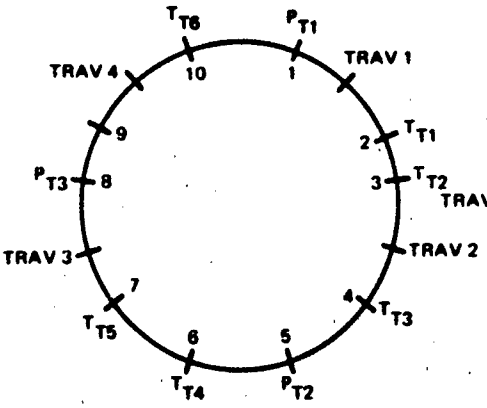

STATION 1.0

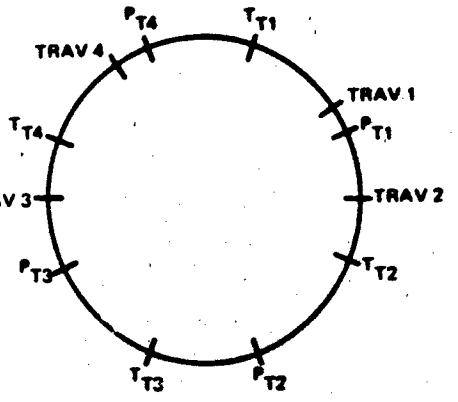

STATION 2.0

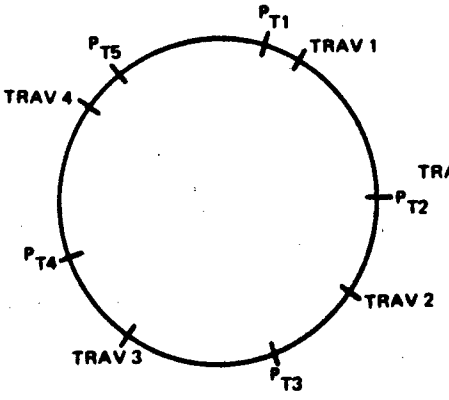

STATION 3.0

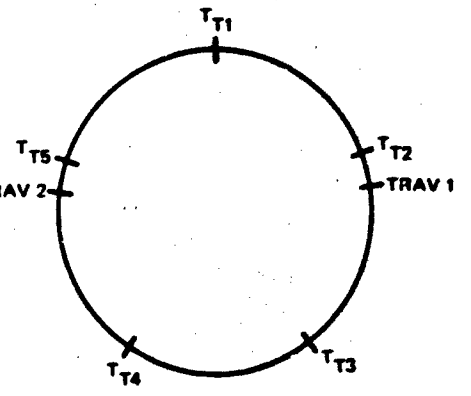

STATION 4.0

ALL VIEWS

LOCATION OF
STATIC TAPS

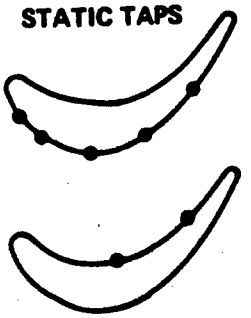

FIRST-STAGE VANE
MID-STREAM STATICS

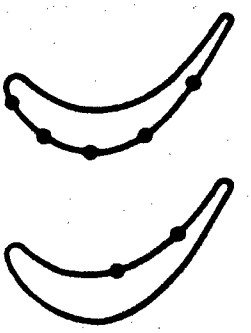

SECOND-STAGE VANE
MID-STREAM STATICS

Figure 67 Instrumentation

(The reverse of this page is blank.)

SECTION IV

DEMONSTRATOR TURBINE PERFORMANCE

SECTION IV

DEMONSTRATOR TURBINE PERFORMANCE

1. RFP OBJECTIVE

(U) Determine the performance of the demonstrator turbine and demonstrate the turbine performance goals and the accuracy of the design procedures.

2. TASK OBJECTIVE

(U) The two-stage demonstrator turbine will be installed in the test rig and tested over a range of operating conditions, including the design point, in order to establish a complete performance map. Inlet, inter-stage, and exit data will be obtained from fixed and traversing instrumentation. The spanwise variation in efficiency, blade exit angles and reaction will be determined for both stages. Mass-averaged values for these parameters and the overall turbine efficiency will be computed for each operating condition. Performance maps will be plotted for each stage, and for the complete turbine. Test results will be used to verify the design system predictions.

The rotating rig test results will be used to demonstrate that this turbine has at least 50 percent higher work level than an equivalent free-vortex machine which operates at the same efficiency.

3. BUILD 1 BASELINE TESTS OF THE DEMONSTRATOR TURBINE

(a) Design Point Operation

(U) The baseline testing of the initial build of the two-stage demonstrator turbine was accomplished in Build 1. During this test, as well as for the following builds, fixed rake and traverse data were obtained at the inlet, inter-stage and exit stations of the turbine at design and off-design operating conditions. A torquemeter was also used to measure the shaft work; however, the measured differences between thermocouple and shaft work varied from build to build to such an extent that the credibility of the torque-meter measurements was questionable.Therefore, the efficiencies based on thermocouple data will be used in this report. A summary of data for this build is shown in Table XI.

(U) Installation of the turbine into the test stand is shown in Figure 68. The inspection measurements of this build were reported in Section III. The tip clearances for the first and second stages were monitored using proximity pickups which indicated 0.021 and 0.017 inch running clearances, respectively. The location and type of instrumentation was presented in Section III.

TABLE XI

COMPARISON OF DESIGN AND BUILD I TURBINE RIG DATA

	Design	Rig
Total Pressure Ratio	3.723	3.72
Speed Parameter	244.	245.
Rim Velocity Ratio	0.389	0.395
Turbine Inlet Temperature	1910°R	~800°R
Turbine Inlet Flow Parameter	0.1937	0.1914
Overall Efficiency	90.65%	92.1%
First-Stage Efficiency	89.52%	92.2%
Second-Stage Efficiency	90.12%	90.0%
First-Stage Reaction (P_s) ~ Root	37.0%	29.0%
First-Stage Reaction (P_s) ~ Tip	46.0%	36.7%
Second-Stage Reaction (P_s) ~ Root	31.1%	37.4%
Second-Stage Reaction (P_s) ~ Tip	50.9%	44.3%
First-Stage Vane Effective Gaging Area	54.225 in^2	53.94 in^2
First-Stage Blade Effective Gaging Area	71.178 in^2	72.42 in^2
Second-Stage Vane Effective Gaging Area	96.178 in^2	96.23 in^2
Second-Stage Blade Effective Gaging Area	128.40 in^2	127.01 in^2

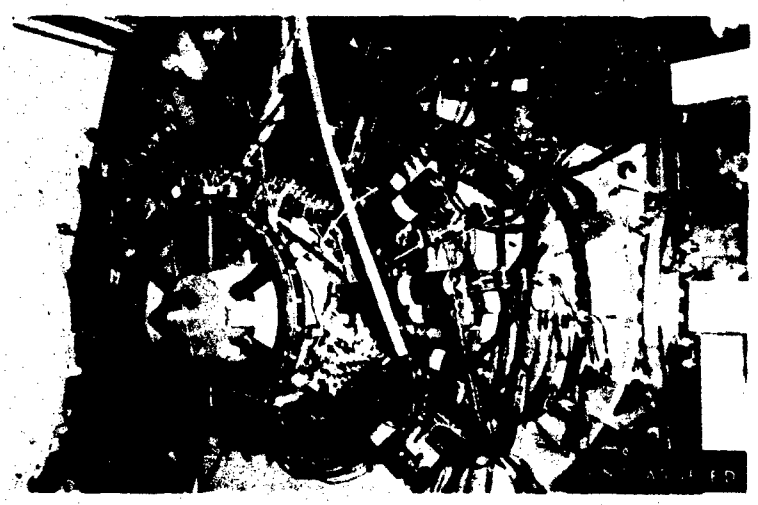

Figure 68 High Work Low Pressure Turbine Rig Mounted in X-212 Stand Collector (Rear View) X-3646

(U) As noted previously, preswirl vanes were used for this turbine rig to produce the design inlet angle into the first vane. This inlet angle is shown in Figure 69 with a comparison to the design value, and indicates that the preswirl vanes had produced an excess in negative incidence of approximately 7°. This change in incidence is believed to have a negligible effect on turbine efficiency and it did not warrant a redesign and fabrication of a new inlet guide vane.

(C) The overall thermocouple efficiency was measured to be 92.1 percent with the first- and second-stage efficiencies being 92.2 and 90.0 percent, respectively. The stage efficiencies were calculated using total temperature kielhead probes on the second vane leading edge, and a total pressure calculated from the measured blade static pressure and absolute exit angle. The use of a calculated total inter-stage pressure was found necessary due to extensive data scatter from the total pressure kielheads. The resulting stage efficiencies are shown in their respective spanwise efficiency profiles in Figures 70 through 72. From these data, it is seen that the difference in stage efficiency levels is due to the presence of endlosses in the second stage, the midspan efficiency for each stage being approximately the same.

(C) The spanwise stage exit angles are presented in Figures 73 and 74. The measured flow capacity was low by 1.2 percent relative to design value, and was accompanied by first-stage root and tip reaction 8 percent below design levels. Approximately 4 percent of the reaction change is due to the flow area deviations from design nominal, but does not explain the lower flow capacity. The remainder of the reaction change and the low flow capacity seem to be the result of an effective vane area reduction of 1.8 percent. The measured second-stage reactions indicate a flow shift toward the root compared to the predicted design flow.

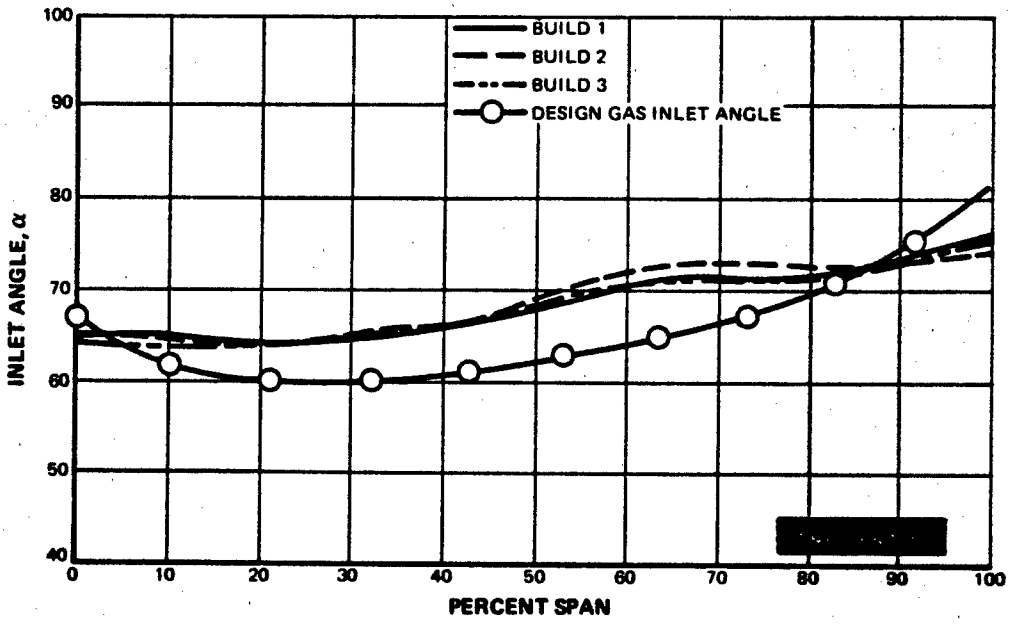

Figure 69 High Work Low Pressure Turbine - Build I, Inlet Angle Versus Percent Span

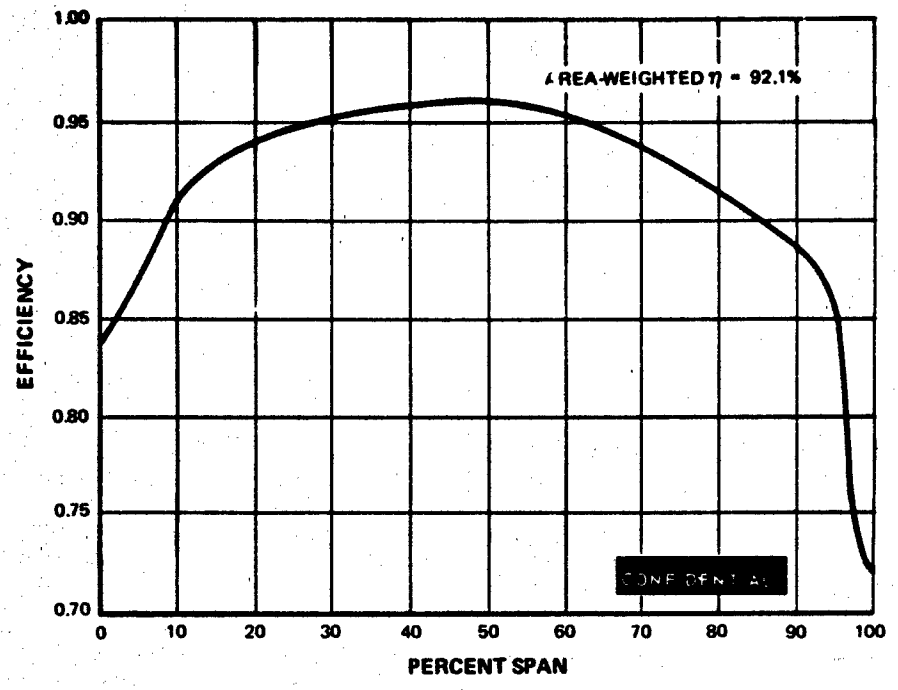

Figure 70 High Work Low Pressure Turbine - Build I, Efficiency Versus Percent Span @ 3.72 Pressure Ratio, 245 Speed Parameter

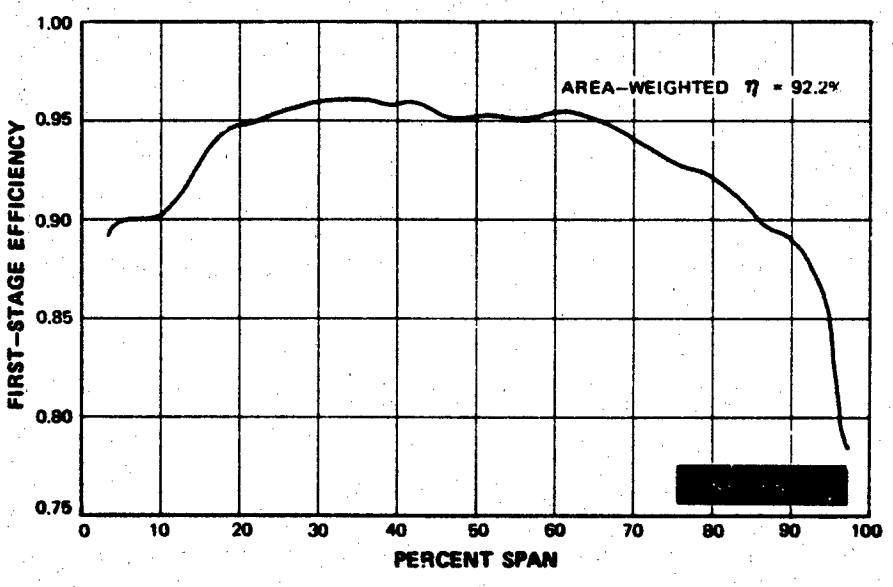

Figure 71 High Work Low Pressure Turbine - Build I, First-Stage Efficiency Versus Percent Span @ 3.72 Pressure Ratio, 245 Speed Parameter

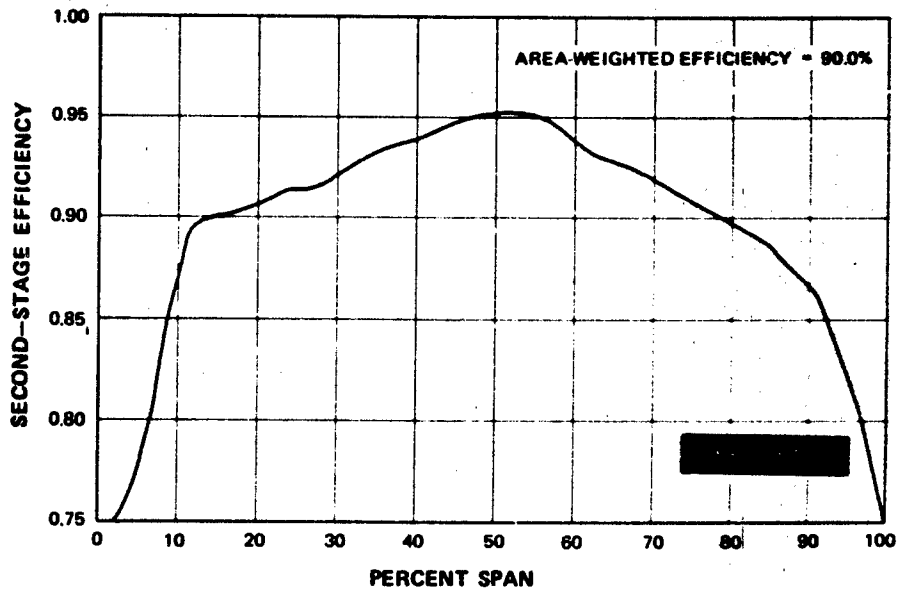

Figure 72 High Work Low Pressure Turbine - Build I, Second-Stage Efficiency Versus Percent Span @ 3.72 Pressure Ratio, 245 Speed Parameter

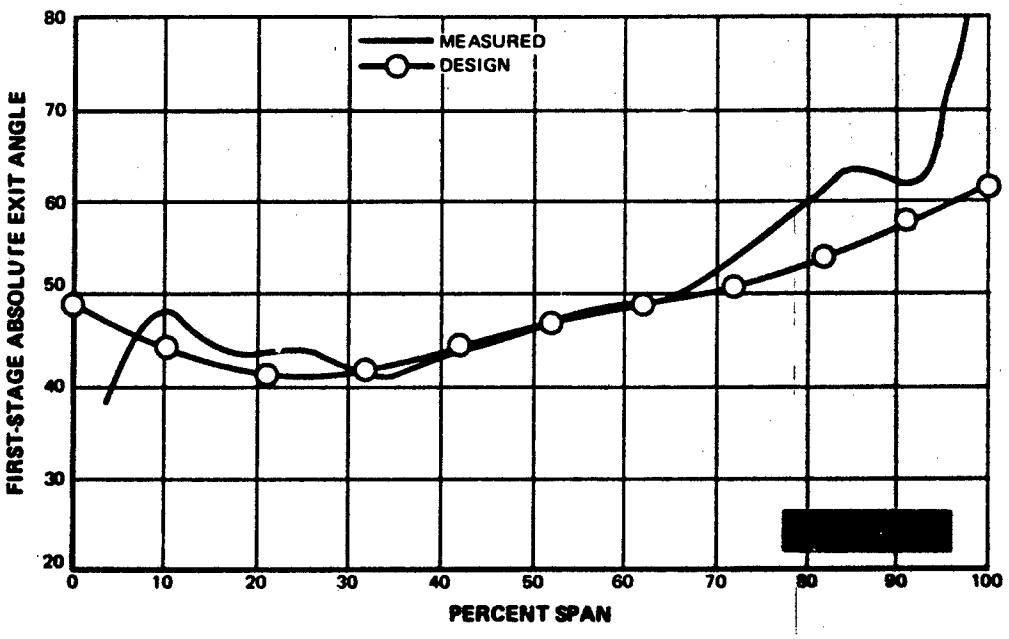

Figure 73 High Work Low Pressure Turbine - Build I, First-Stage Absolute Exit Angle Versus Percent Span

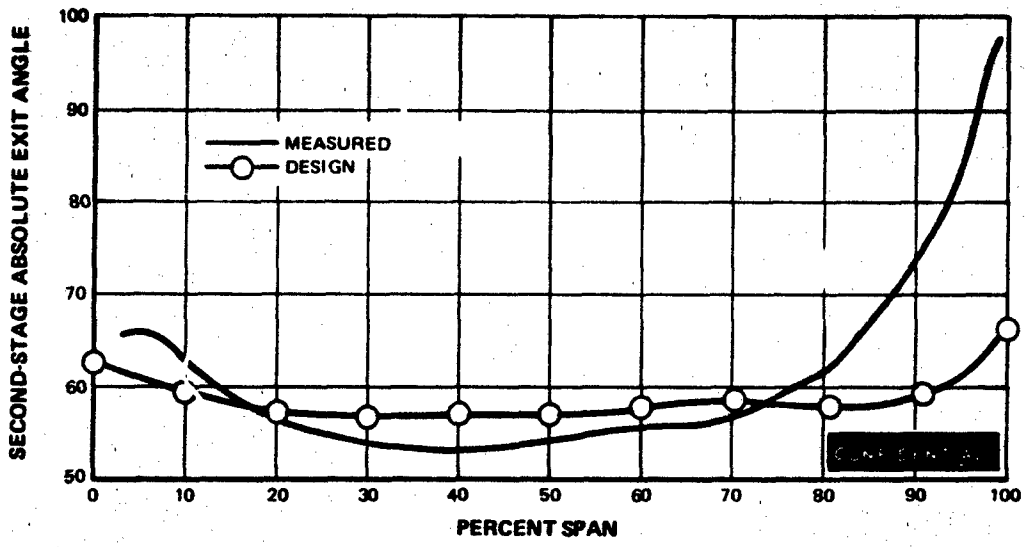

Figure 74 High Work Low Pressure Turbine - Build I, Second-Stage Absolute Exit Angle Versus Percent Span

(b) Off-Design Operation

(C) The off-design variation of the Build I overall efficiency with total pressure ratio and speed parameter are shown in Figures 75 and 76. These figures indicate that the turbine does not respond significantly to increases in total pressure ratio above the design pressure ratio of 3.72, whereas the speed parameter has a fairly strong effect on efficiency over the entire test speed range. From the spanwise efficiency curves of Figures 77 and 78, it is observed that the changes in efficiency with total pressure ratio occur primarily in the root area, whereas the changes in efficiency with speed parameter occur across the entire span. These variations in overall efficiency are found to originate in the second stage by noting in Figures 79 and 80 that the first-stage efficiency is essentially constant with changes in pressure ratio and speed parameter, while the second-stage efficiency reflects the same characteristics as the overall efficiency of Figure 75. The effect of total pressure ratio and speed parameter on the second-stage spanwise efficiency can be seen in Figures 81 and 82.

(C) The off-design variation of the turbine flow capacity is shown in Figure 83, which indicates that the turbine was essentially choked throughout most of the test program. The stage reactions are shown in Figures 84 and 85. By combining the flow parameter with the speed parameter and plotting against a work parameter defined as the specific turbine work divided by the inlet temperature, efficiency islands can be formed as shown in Figure 86. This plot indicates that little efficiency gain could be made above 92.4 percent with the present turbine through changes in total pressure ratio and speed parameter in excess of 4.2 and 265, respectively.

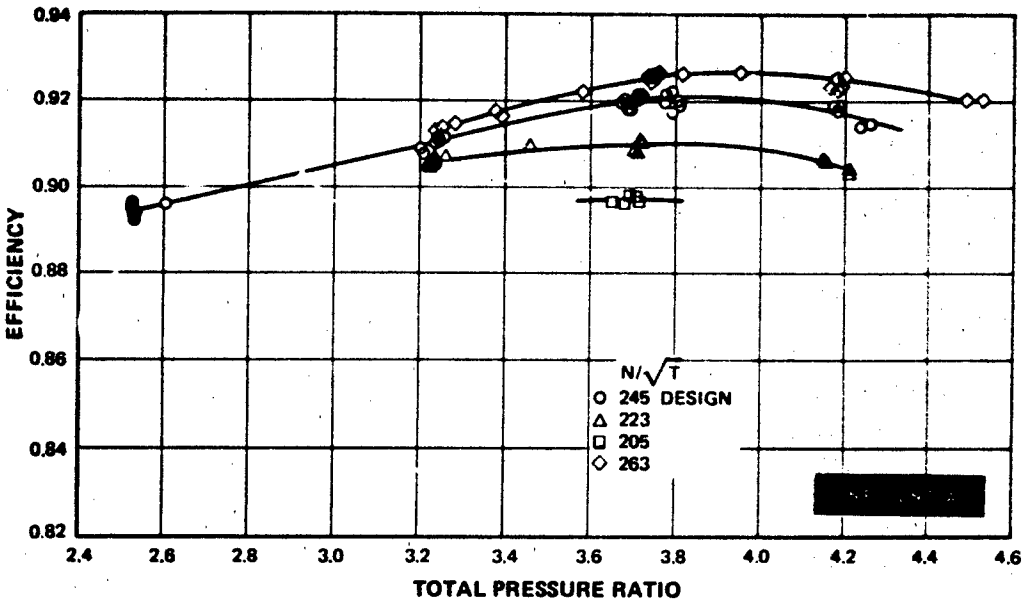

Figure 75 High Work Low Pressure Turbine - Build I, Overall Efficiency Versus Pressure Ratio

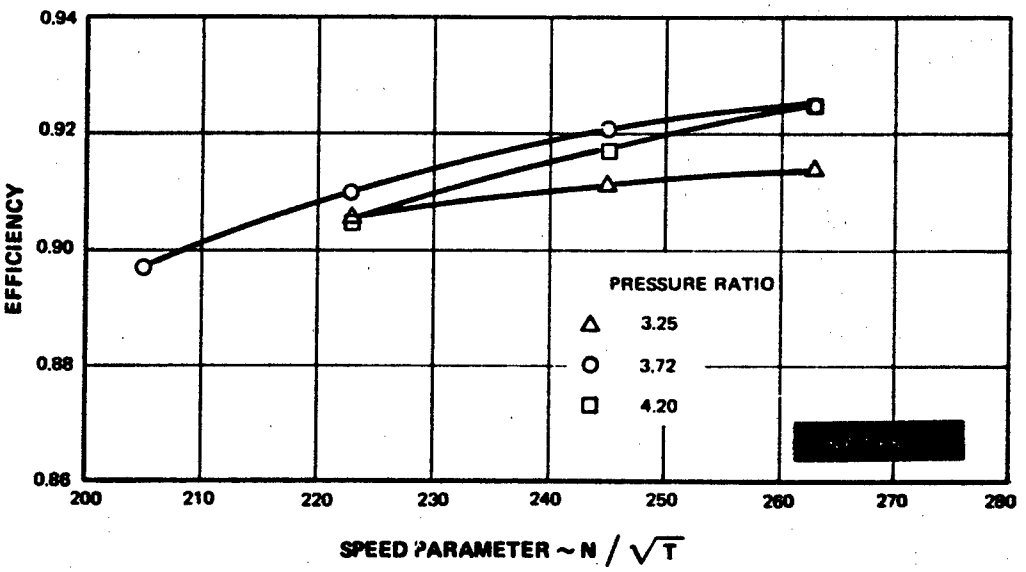

Figure 76 High Work Low Pressure Turbine - Build I, Overall Efficiency Versus Speed Parameter

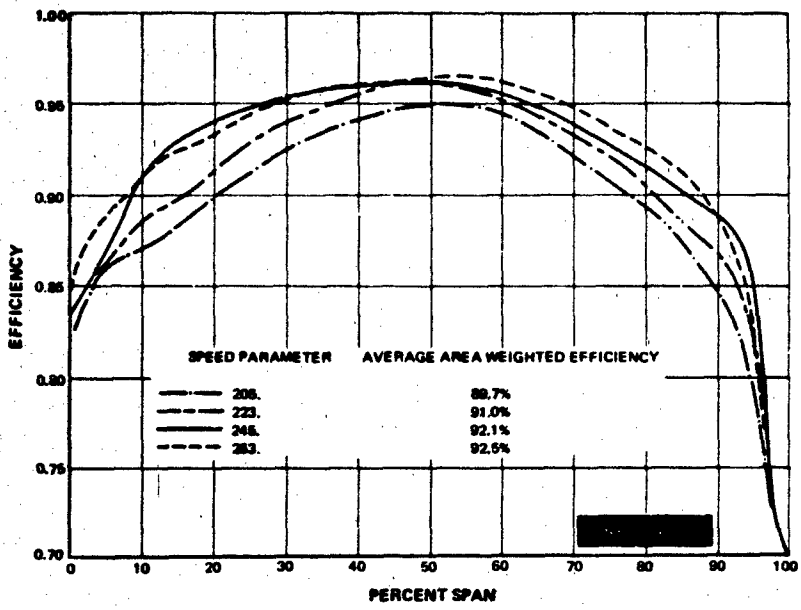

Figure 77 High Work Low Pressure Turbine - Build I, Efficiency Versus Percent Span @ 3.72 Pressure Ratio

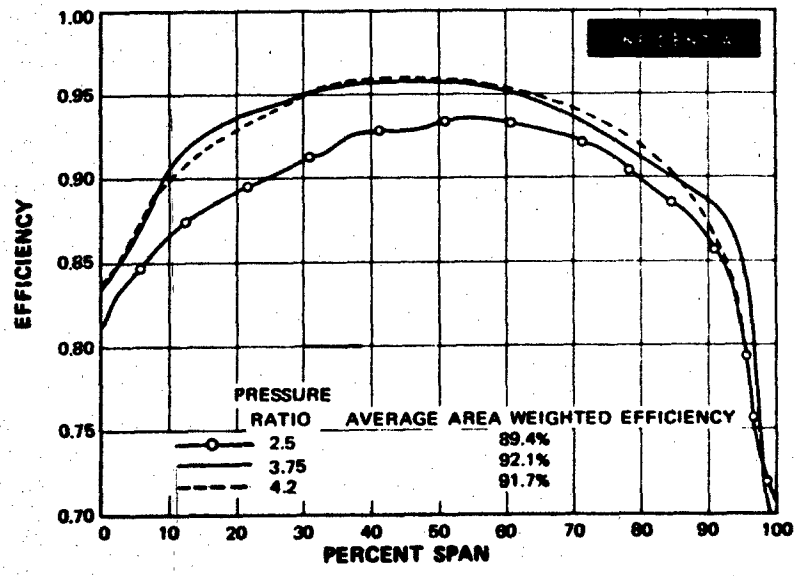

Figure 78 High Work Low Pressure Turbine - Build I, Efficiency Versus Percent Span @ 245 Speed Parameter

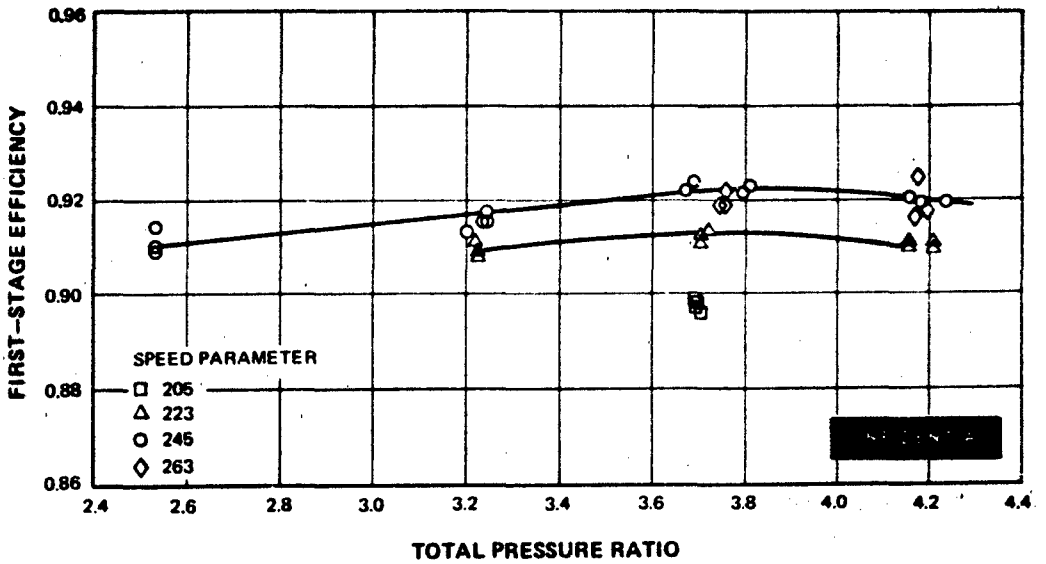

Figure 79 High Work Low Pressure Turbine - Build I, First-Stage Efficiency Versus Total Pressure Ratio

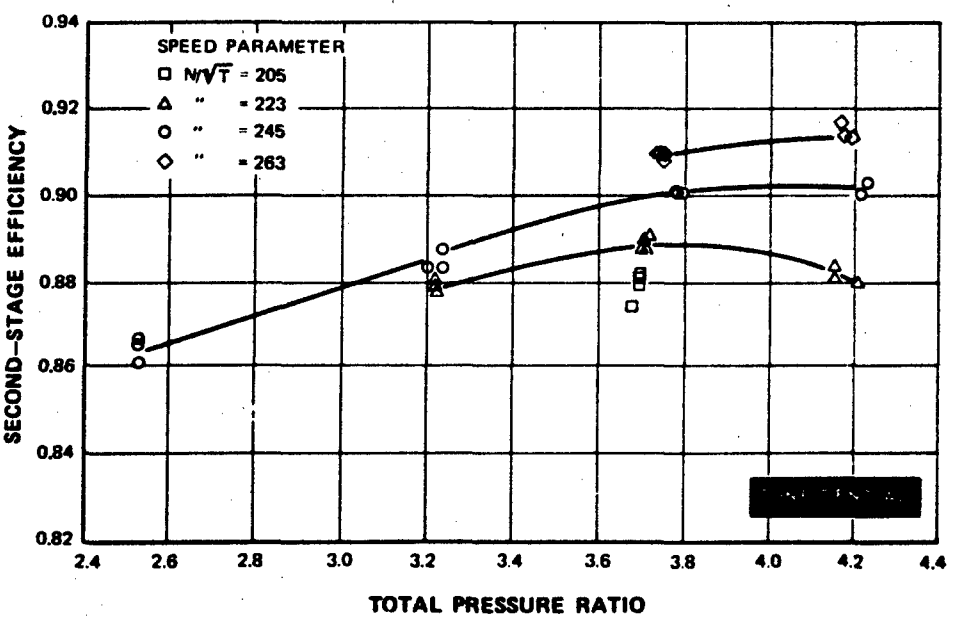

Figure 80 High Work Low Pressure Turbine - Build I, Second-Stage Efficiency Versus Total Pressure Ratio

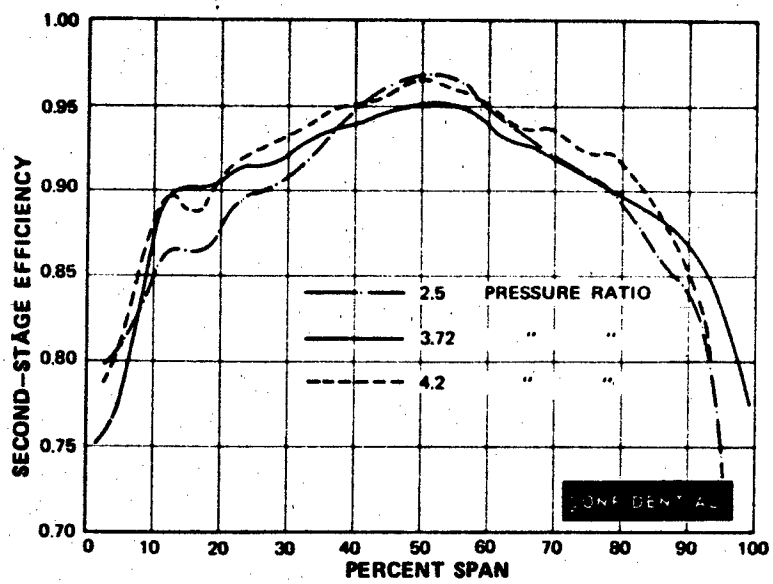

Figure 81 High Work Low Pressure Turbine - Build I, Second-Stage Efficiency Versus Percent Span @ 245 Speed Parameter

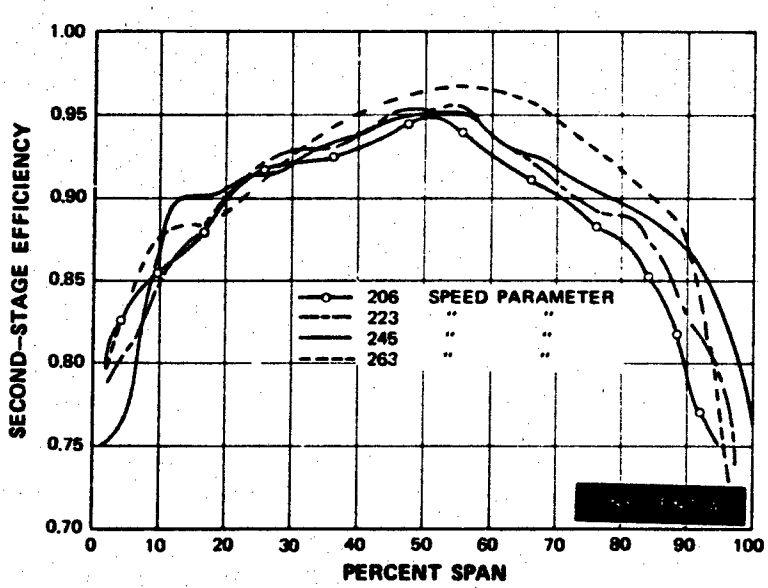

Figure 82 High Work Low Pressure Turbine - Build I, Second-Stage Efficiency Versus Percent Span @ 3.72 Pressure Ratio

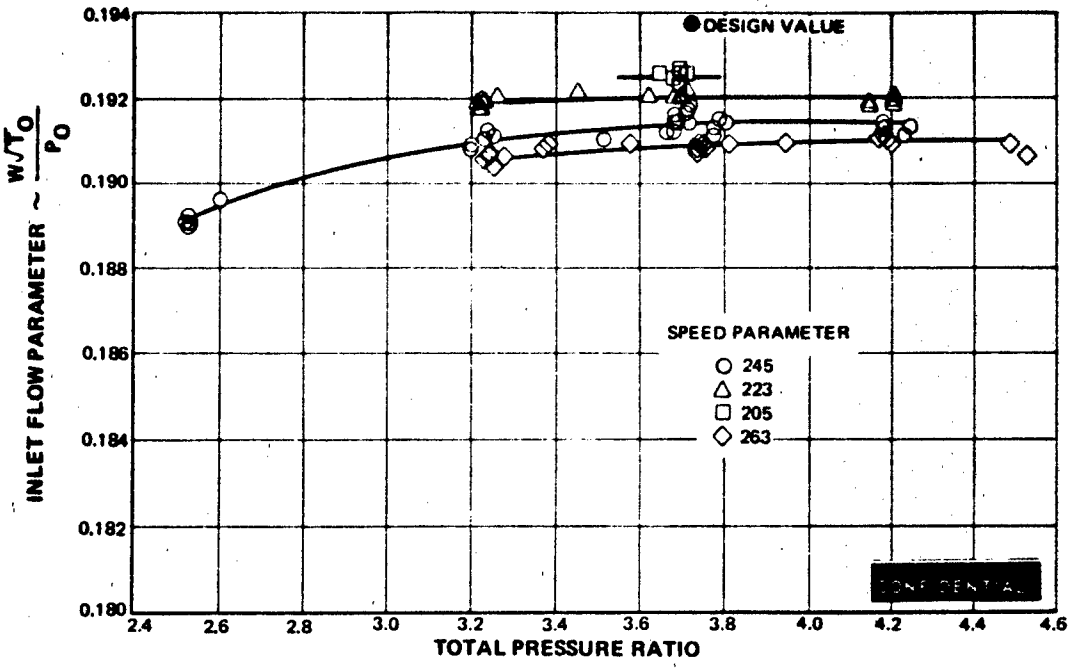

Figure 83 High Work Low Pressure Turbine - Build IV, Inlet Flow Parameter Versus Total Pressure Ratio

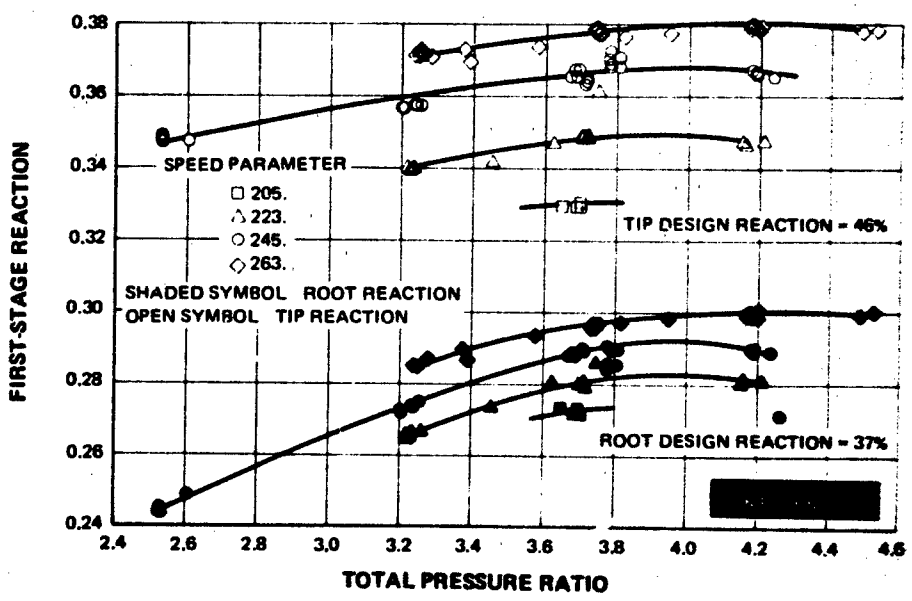

Figure 84 High Work Low Pressure Turbine - Build I, First-Stage Reaction Versus Total Pressure Ratio

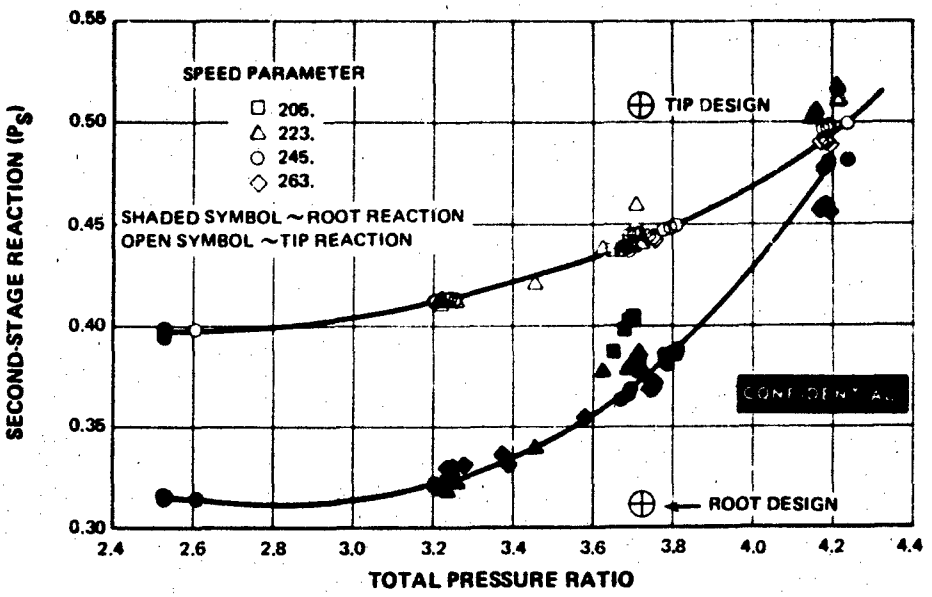

Figure 85 High Work Low Pressure Turbine - Build I, Second-Stage Reaction Versus Total Pressure Ratio

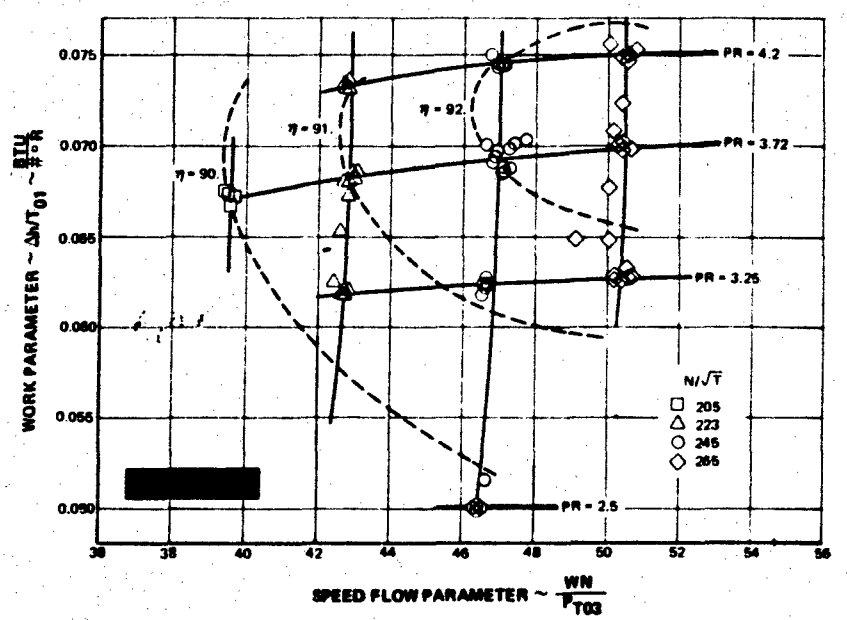

Figure 86 High Work Low Pressure Turbine - Build I, Work Parameter Versus Speed Flow Parameter

4. EVALUATION OF MODIFICATIONS TO THE BASELINE DEMONSTRATOR TURBINE

(C) Modifications were made in the root endwall regions in order to determine the effect of the local geometry on endwall losses. Three systematic modifications were made. These are referred to as Builds 2, 3 and 4, which were shown as sketches in Section III. In Build 2, solid rings of material were added to the hub diameter cavities in order to reduce the volume of these cavities. Build 3 retained these cavity fillers, but the root leading and trailing edge platforms were cut back to the airfoil fillet radius. In Build 4, the cavity filler rings were removed and the effect of large cavities with cut-back platforms was evaluated. The test results of each of these builds at design point operation are compared with Build I in Table XII. The off-design overall and stage efficiency data for Builds 2, 3 and 4 are shown in Figures 87 through 95. These results reflect the same trend as for Build I. Composite plots of the overall efficiency at design total pressure ratio and speed parameter are shown in Figures 96 and 97; composite plots of the stage absolute exit angles are shown in Figures 98 and 99.

(C) As indicated in Table XII, it is seen that when the root filler rings were installed, the overall efficiency decreased 0.4 percent relative to Build I. The stage efficiencies show this decrease to occur in the second stage only. By comparing the spanwise efficiency curves of the overall and stage efficiencies, (Figures 100, 101, and 102), it appears that the efficiency change is due to a complete spanwise shift rather than a local change in efficiency at the root. This can be seen more clearly in Figure 103 which shows that an adjustment of the Build 2 second-stage spanwise efficiency to the Build I efficiency level results in the same efficiency profile. It is concluded that the addition of the root cavity filler rings did not affect the performance of the turbine. The change in efficiency represents an unexplained baseline shift, possibly due to a combination of some slight change in the turbine rig when it was reassembled, and experimental measurement accuracy. The performance potential of root cavity filler blocks is dependent on their effectiveness in minimizing mainstream flow injection through a reduction in cavity volume without producing a substantial increase in viscous drag on the disk. It is evident from the above performance results that although the volume was reduced to the minimum for avoiding mechanical interference, this reduction was not sufficient to measurably reduce ingestion. It can therefore be concluded that, given the restriction of minimum clearance to avoid mechanical interference, the addition of root cavity fillers have no significant effect on turbine performance.

TABLE XII

PERFORMANCE COMPARISON OF BUILDS I, II, III AND IV

	Build I	Build II	Build III	Build IV
Configuration				
I.D. Solid Rings	no.	yes.	yes.	no.
Cutback Platforms	no.	no.	yes.	yes.
P_{T01}/P_{T03}	3.723	3.723	3.723	3.723
$N/\sqrt{T_{01}}$	245.	245.	245.	245.
FP5	0.1914	0.1914	0.1914	0.1914
η_{OV} T/C	92.1%	91.7%	91.0%	90.9%
η_{OV} Torque	90.8%	92.2%	90.6%	90.8%
η_1	92.2%	92.2%	91.2%	91.2%
η_2	90.0%	89.2%	88.9%	88.7%
$\Delta\eta_{OV}$ T/C	–	-0.4%	-1.1%	-1.2%

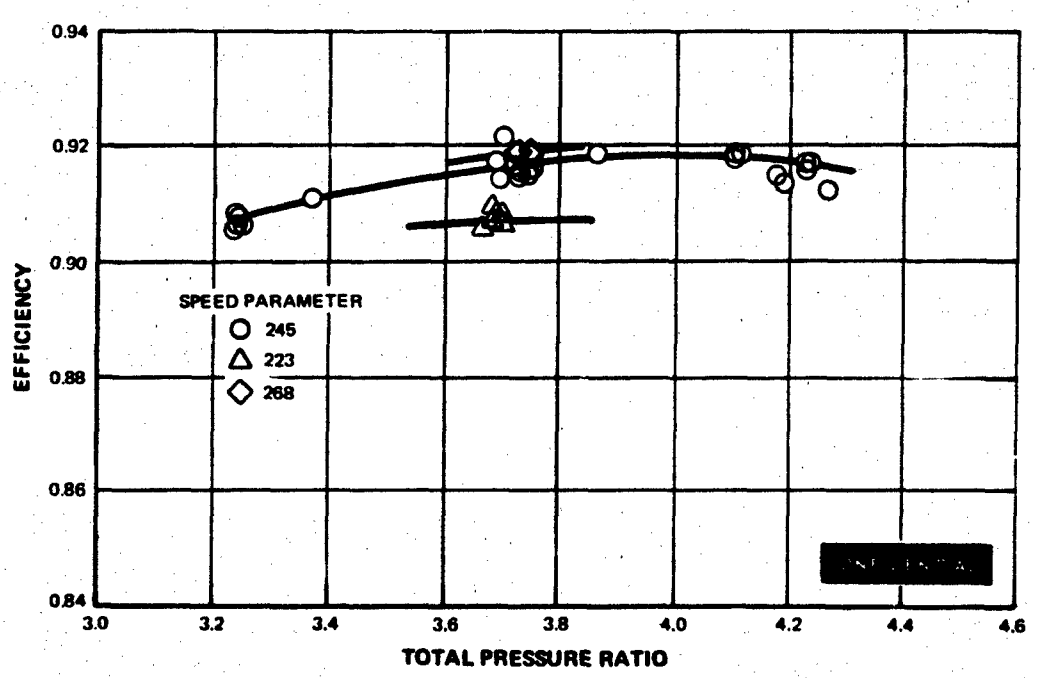

Figure 87 High Work Low Pressure Turbine - Build II; Efficiency Versus Total Pressure Ratio

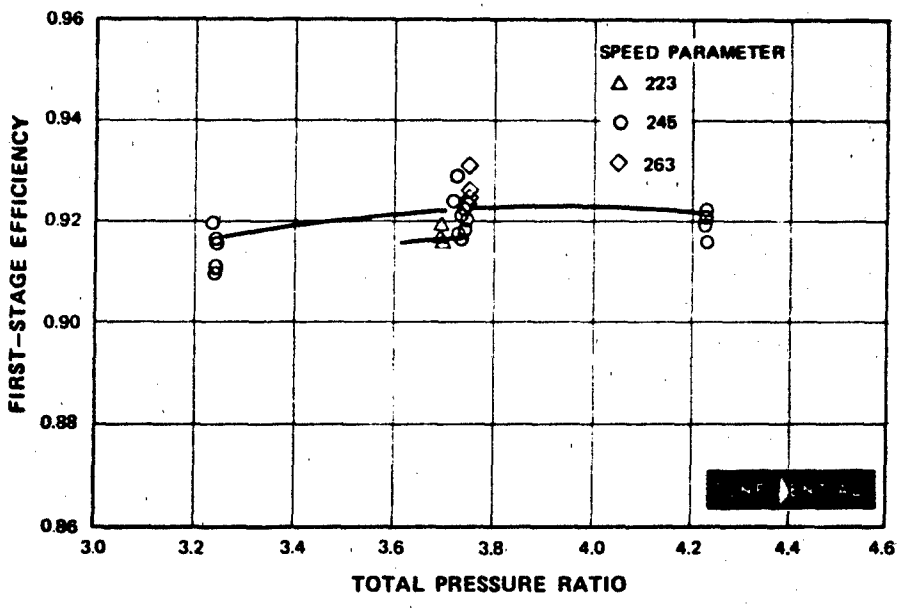

Figure 88 High Work Low Pressure Turbine - Build II, First-Stage Efficiency Versus Total Pressure Ratio

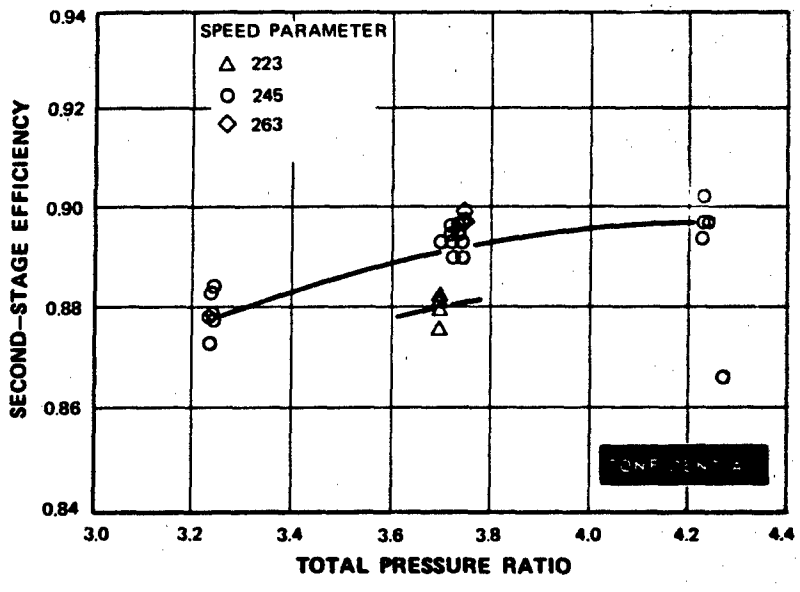

Figure 89 High Work Low Pressure Turbine - Build II, Second-Stage Efficiency Versus Total Pressure Ratio

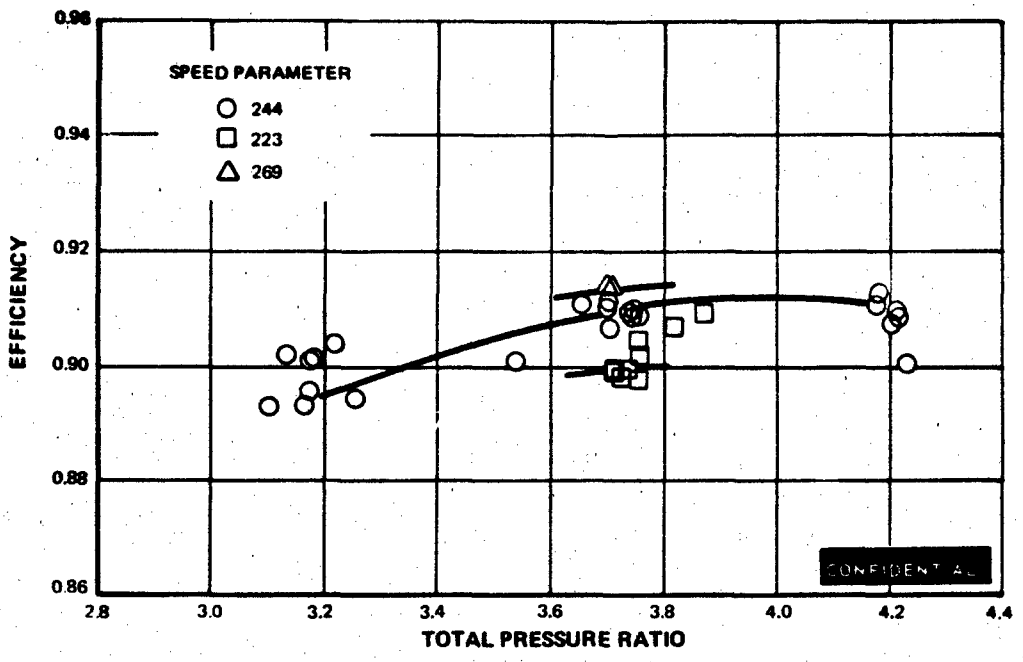

Figure 90 High Work Low Pressure Turbine - Build III, Efficiency Versus Total Pressure Ratio

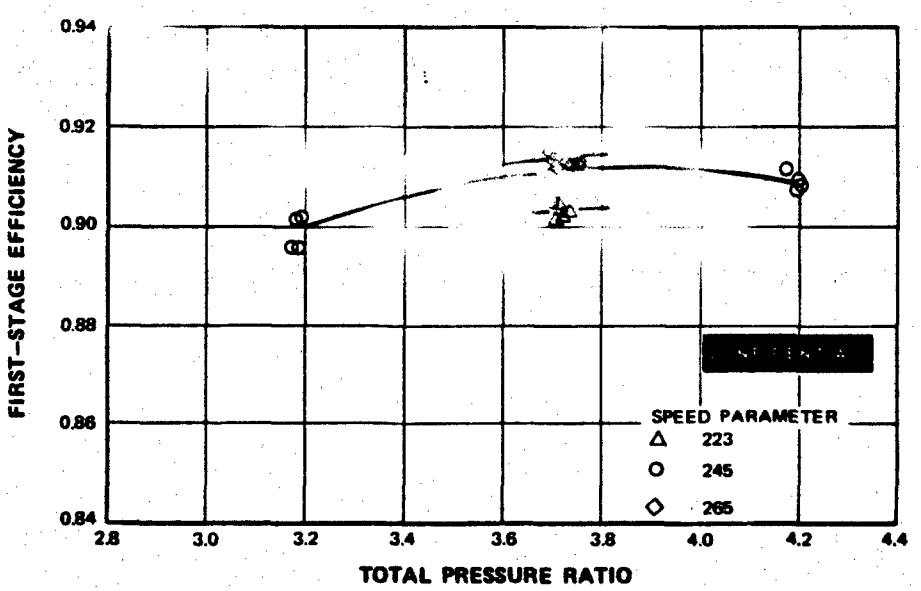

Figure 91 High Work Low Pressure Turbine - Build III, First-Stage Efficiency Versus Total Pressure Ratio

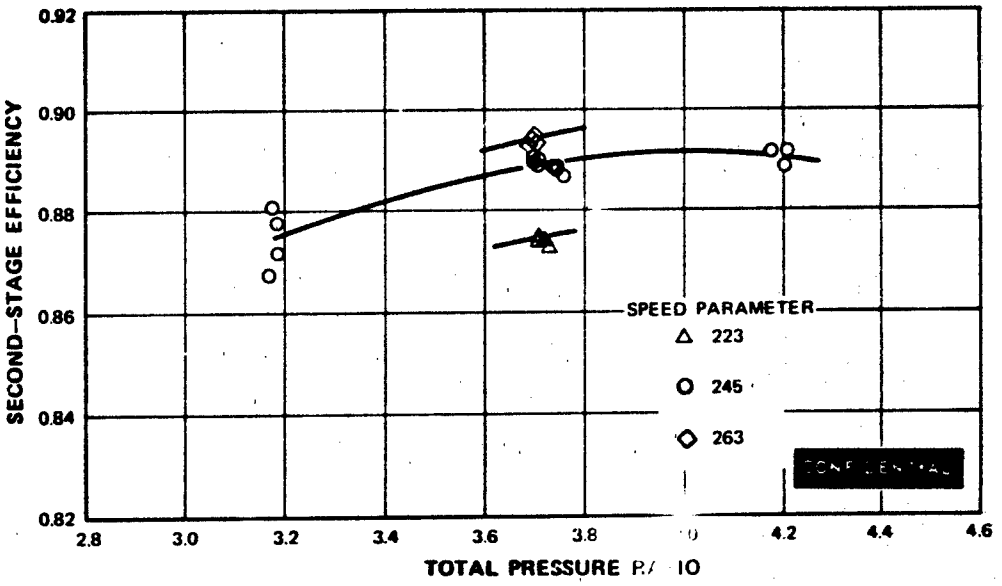

Figure 92 High Work Low Pressure Turbine - Build III. Second Stage Efficiency Versus Total Pressure Ratio

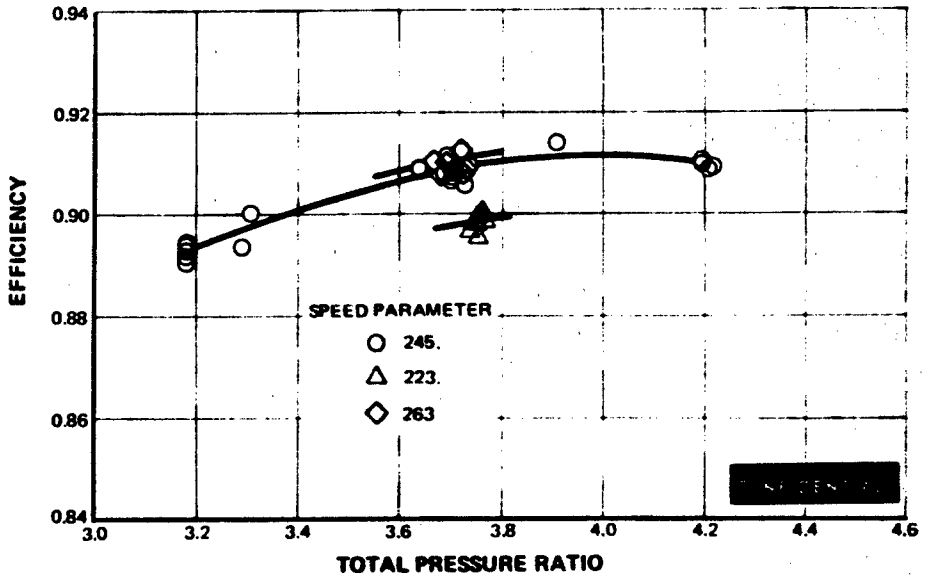

Figure 93 High Work Low Pressure Turbine - Build IV, Efficiency Versus Total Pressure Ratio

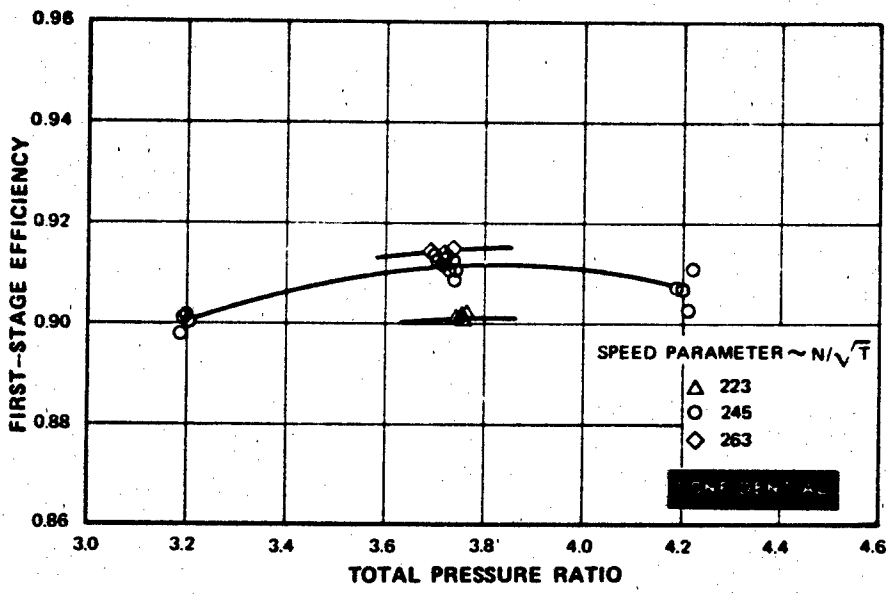

Figure 94 High Work Low Pressure Turbine - Build IV, First-Stage Efficiency Versus Total Pressure Ratio

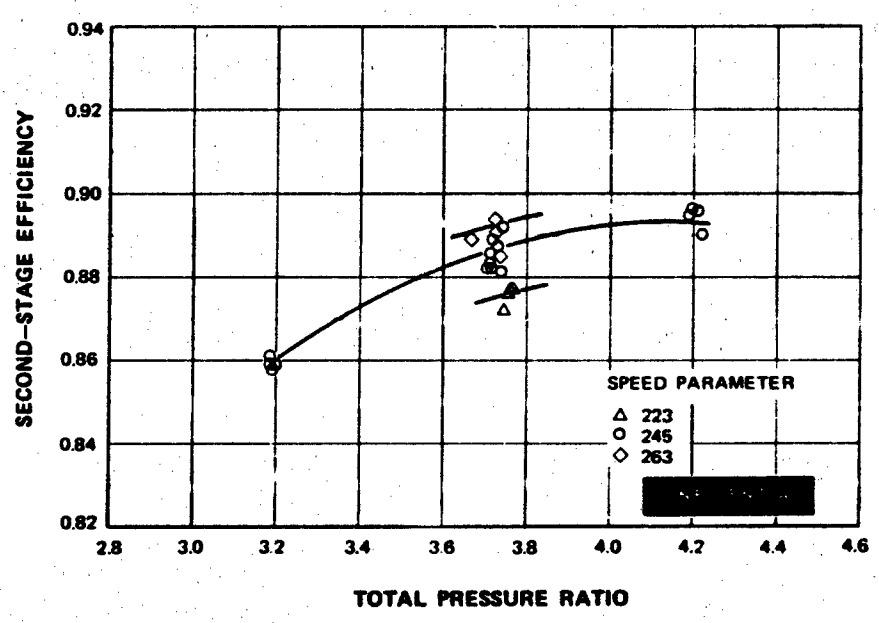

Figure 95 High Work Low Pressure Turbine - Build IV, Second-Stage Efficiency Versus Total Pressure Ratio

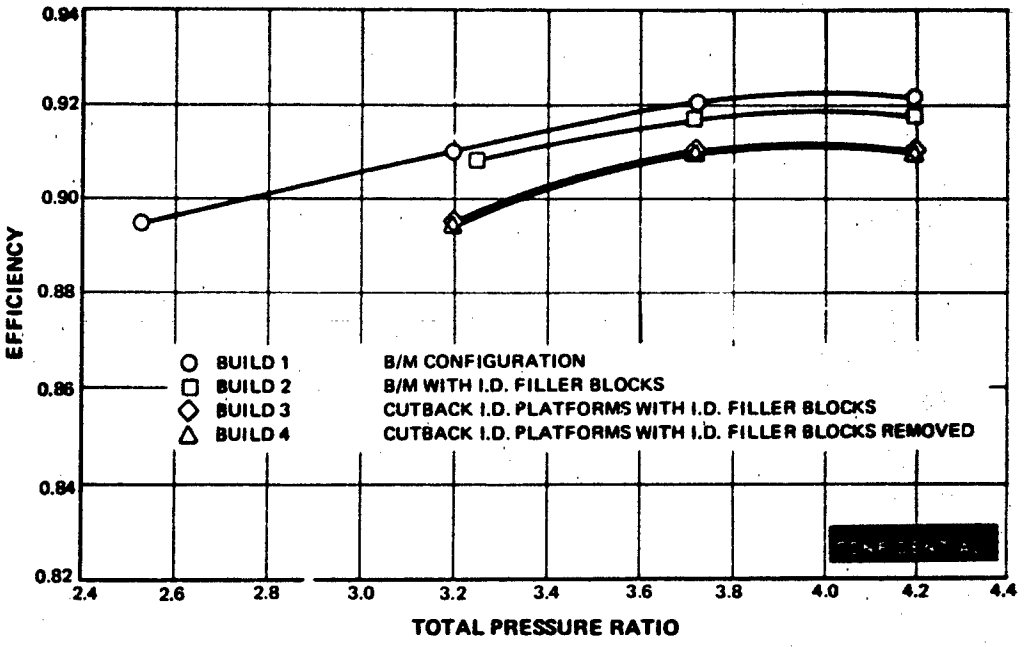

Figure 96 High Work Low Pressure Turbine Efficiency Versus Total Pressure Ratio

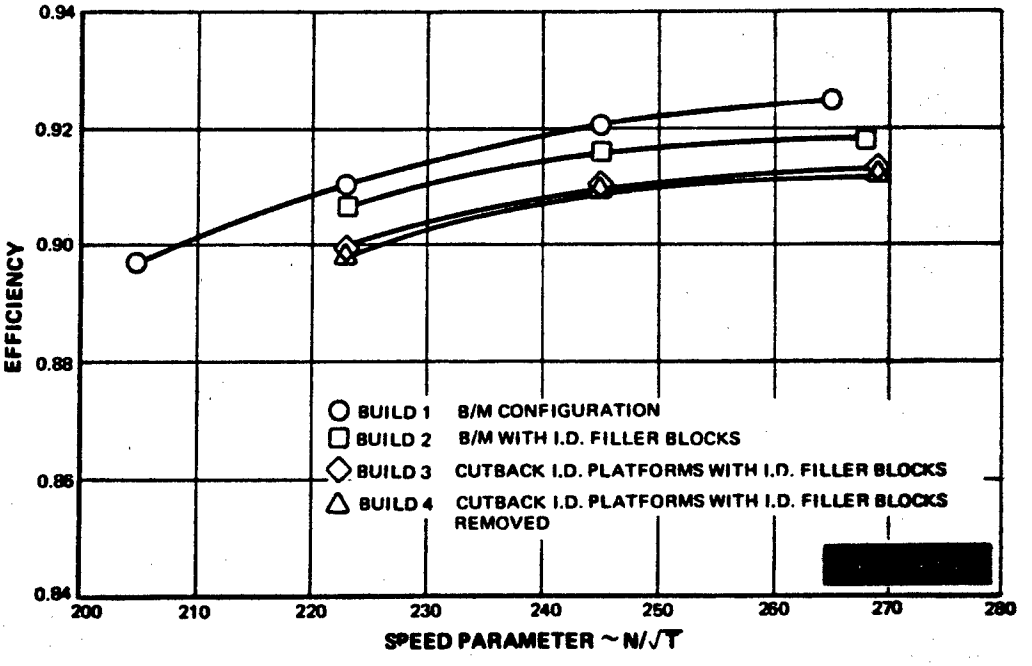

Figure 97 High Work Low Pressure Turbine, Efficiency Versus Speed Parameter @ 3.72 Pressure Ratio

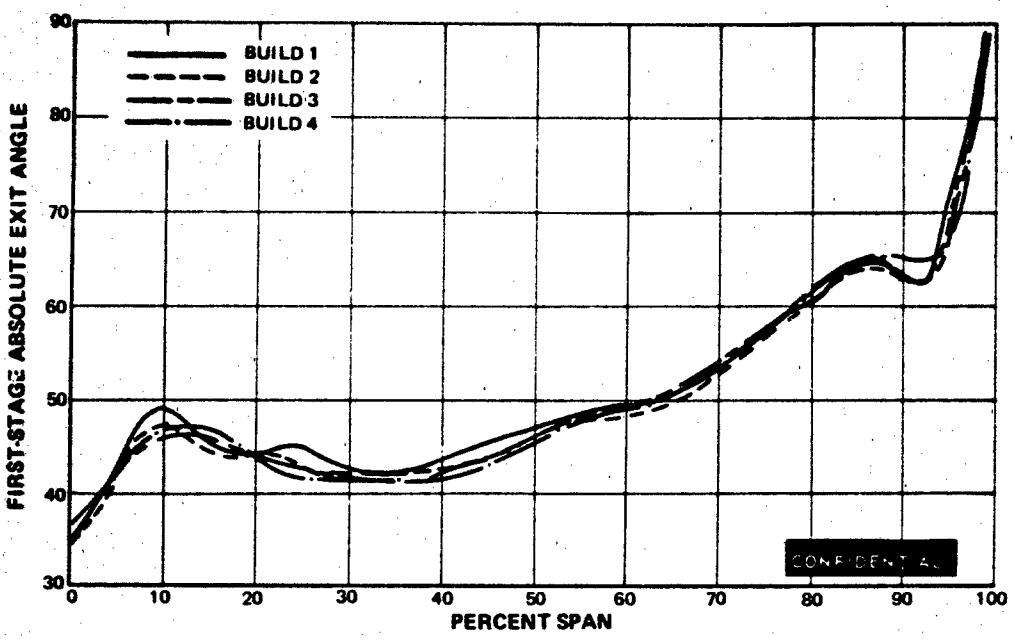

Figure 98 High Work Low Pressure Turbine, First-Stage Absolute Exit Angle Versus Percent Span @ 3.72 Pressure Ratio, 245 Speed Parameter

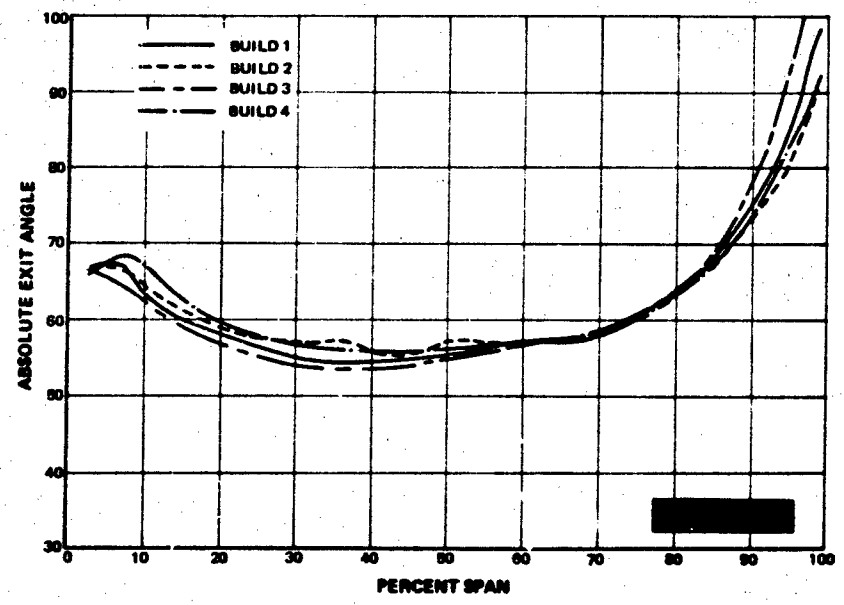

Figure 99 High Work Low Pressure Turbine, Absolute Exit Angle Versus Percent Span @ 3.72 Pressure Ratio, 245 Speed Parameter

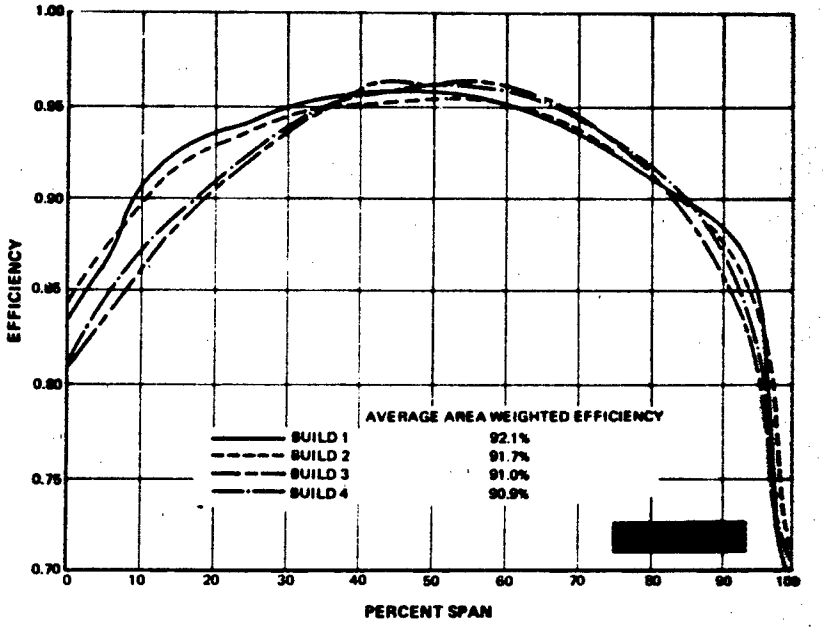

Figure 100 High Work Low Pressure Turbine, Efficiency Versus Percent Span @ 3.72 Pressure Ratio, 245 Speed Parameter

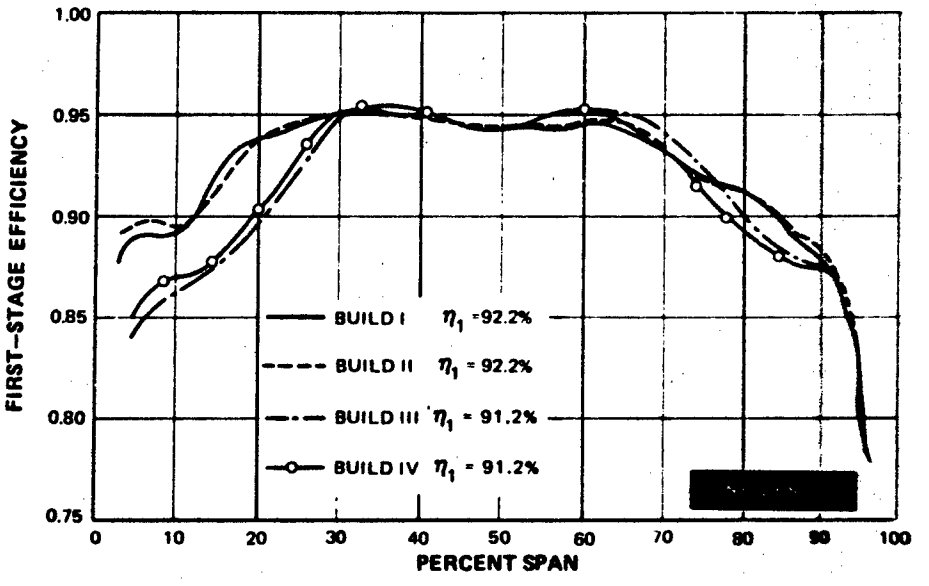

Figure 101 High Work Low Pressure Turbine, First-Stage Efficiency Versus Percent Span @ 3.72 Pressure Ratio, 245 Speed Parameter

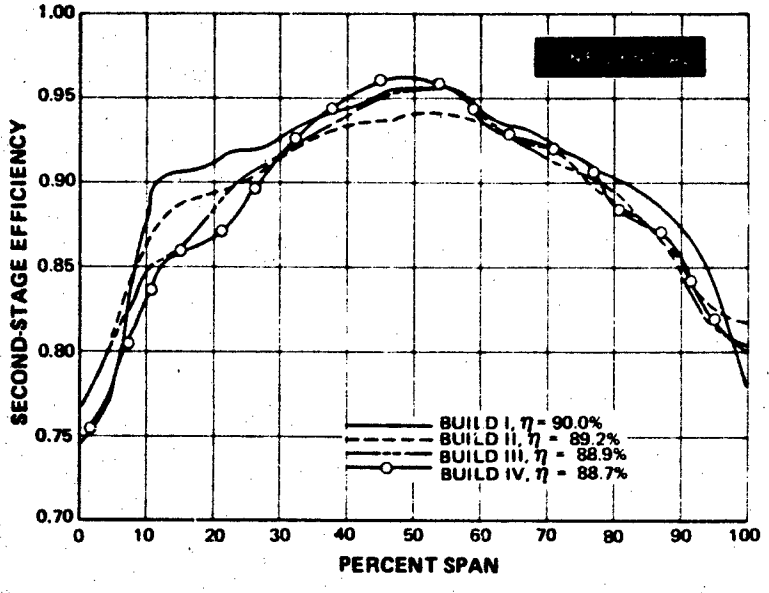

Figure 102 High Work Low Pressure Turbine, Second-Stage Efficiency Versus Percent Span @ 3.72 Pressure Ratio, 245 Speed Parameter

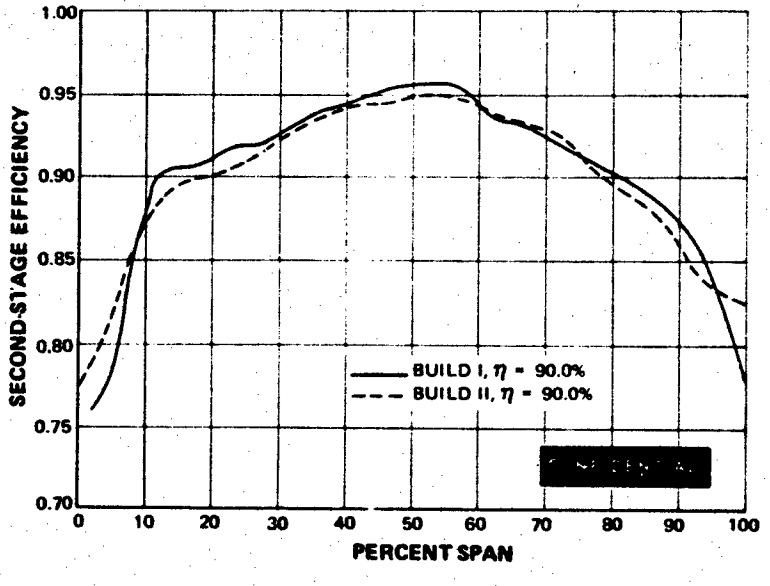

Figure 103 High Work Low Pressure Turbine, Second-Stage Efficiency Versus Percent Span @ 3.72 Pressure Ratio, 245 Speed Parameter

(C) After the airfoil root platforms were cut off in Build 3, the overall turbine efficiency was found to decrease to 91.0 percent with the first- and second-stage efficiencies being 91.2 and 88.9 percent, respectively. The loss in overall and stage efficiencies relative to Build 1 can be seen in Figures 100, 101 and 102 to occur in the root area of each stage. Build 1 is being used as the baseline test for Build 3 since the use of Build 2 would indicate a loss of only 0.3 percent in the second-stage efficiency when the spanwise efficiency profiles indicate approximately a 1 percent loss. The latter loss is in agreement with the measured efficiency change of Build 3 relative to Build 1. Therefore, the absence of root airfoil platform extensions increases the circulation and exchange of air in the root cavities with the mainstream flow which results in a 0.7 percent loss in overall efficiency with a 1.0 and 1.1 percent penalty in the first- and second-stages, respectively. The above loss in turbine efficiency of approximately 1 percent in each stage is caused by an increase in mainstream airflow ingested into the root cavities. There, it looses some of its kinetic energy and re-enters the flowpath possibly causing additional losses in the following blade or vane row. An analytical expression has been derived (see Appendix VIII) which estimates the amount of flow ingestion, and its effect on the performance, by assuming that the entire loss comes from the total dissipation of kinetic energy in the root cavities. By using the part annular cascade data to set the row losses in the referenced equation, the calculated increase in ingested airflow to produce the measured 1 percent decrease in stage efficiencies is approximately 1 percent of mainstream flow per cavity. This magnitude represents a maximum since any loss attributable to the low energy air re-entering the flowpath would have the effect of reducing the calculated change in ingested mainstream flow.

(C) For Build 4, the cavity filler rings were removed and the overall turbine efficiency was measured to be 90.9 percent, the first- and second-stage efficiencies being 91.1 and 88.7 percent, respectively. These efficiencies are essentially the same magnitude as for Build 3. The spanwise efficiency curves of Figures 100, 101 and 102 also indicate that shifts in the root efficiency did not occur upon removal of the filler rings. It is worthwhile to point out that the removal of the filler blocks in Build 4 is a more meaningful test than was their addition in Build 2. In Build 2, the airfoil platforms may have been restricting the ingestion of mainstream flow into the cavities to the point where the addition of the blocks had a negligible effect. In Build 4, however, the platforms were not present and the effect of removing the blocks should have been maximized. Since no change resulted from the removal of the blocks, it can be concluded that the root filler rings have no measurable effect on turbine efficiency.

5. SUMMARY OF RESULTS

(a) Build I

- (C) The two-stage turbine demonstrator efficiency is 92.1 percent at the design point total pressure ratio and rim velocity ratio of 3.723 and 0.40, respectively.

- (C) The first-and second-stage efficiencies were measured at 92.2 and 90.0 percent, respectively, at the design point pressure ratio and velocity ratio.

- (C) The design stage reactions were not realized in this turbine. The measured first-and second-stage root and tip static pressure reactions are 29.0 and 36.7 percent and 37.4 and 44.3 percent, respectively, compared to the design reactions of 37.0 and 46 percent and 31.1 and 50.9 percent.

- (C) The flow capacity was lower than design by 1.2 percent.

(b) Build 2

- (C) The Build 2 overall thermocouple efficiency is 91.7 percent at the design point total pressure ratio and velocity ratio. Running tip clearances were the same as for Build 1.

- (C) The first- and second-stage efficiencies are 92.2 and 89.2 percent at the design point total pressure ratio and velocity ratio, respectively.

- (C) The installation of the root filler blocks had no appreciable effect on turbine stage efficiency. The airfoil platform overlap minimized their effectiveness.

(c) Build 3

- (C) The Build 3 overall thermocouple efficiency is 91.0 percent at the design point total pressure ratio and velocity ratio. The running tip clearance was the same as for Builds 1 and 2.

- (C) The first-and second-stage efficiencies are 91.2 and 88.9 percent, respectively, at design point operation.

- (C) The change in overall efficiency of 0.7 percent is due to the loss in stage root efficiency caused by the platform cutbacks in each stage.

(d) Build 4

- (C) The Build 4 overall thermocouple efficiency is 90.9 percent at the design point total pressure ratio and velocity ratio. The running tip clearance was the same as for the previous three builds.

- (C) The first-and second-stage efficiencies are 91.2 and 88.7 percent, respectively.

- (C) The removal of the root filler pieces has no appreciable effect on turbine efficiency.

SECTION V

ADDITIONAL TESTS TO EVALUATE LOW SOLIDITY AIRFOILS

SECTION V

ADDITIONAL TESTS TO EVALUATE LOW SOLIDITY AIRFOILS

1. OBJECTIVE

(U) The objective of this add-on task was to evaluate the aerodynamic performance of the low solidity airfoils designed for the same velocity triangles as the baseline airfoils of Task IIb. The performance of the first vane, first blade and second vane low solidity airfoils will be reported in this Section. Also, the performance of all the airfoils of the nominal, medium and low solidities will be compared in concluding summary.

2. TASK OBJECTIVE

(U) Each of the three low solidity airfoils was evaluated in an annular segment cascade exactly as in Task IIb (Reference 3). The data has been analyzed and the task objectives were met by the following steps:

- Measurement of all important aerodynamic properties at the cascade exit plane.
- Reconstruction of the entire exit plane total pressure loss distribution.
- Reconstruction of the entire exit plane flow angle distribution.
- Measurement of airfoil surface static pressure distributions at root, mean, and tip sections.
- Careful analysis of all data and visual clues.

3. AIRFOIL SECTION DESIGN

(U) The medium-reaction, low solidity airfoils were designed to the same turbine velocity diagrams as the normal solidity airfoils. These diagrams were presented in Reference 1. A summary of the pertinent design values, the airfoil elevations, gaging distribution, airfoil sections and predicted surface pressure distributions for each of the three low solidity airfoils is presented in Appendix VI. The fabrication coordinates of each airfoil, including the airfoil angles, airfoil areas, axial chords and uncovered turnings, are presented in Appendix VII.

4. TEST FACILITY DESIGN

(U) The test section design for each of the three low solidity airfoils is identical to the medium solidity cascades described in References 4 and 5. Each test cascade was fabricated by replacing the eight medium solidity airfoils by seven of the low solidity airfoils. New, smooth inner and outer end walls were also fabricated for each cascade. The inlet guide vanes are the same as those used in the final test of the medium solidity airfoils reported in References 4 and 5.

(U) Static pressure instrumentation was installed in order to determine the static pressure distributions on the airfoil surfaces and over both the test airfoil inlet and exit end walls. The static pressure instrumentation on the airfoils was located at the mean section, and at sections 0.1 inch from the outer and inner end walls, as shown for the medium solidity airfoils in Reference 4. The axial chord locations of the pressure taps of the low solidity airfoils are listed in Tables XIII through XV. Again, great care was taken to preserve the contour and smoothness of the suction side of each instrumented airfoil. To this end, all hypodermic tube leads were placed in grooves on the pressure side, and pressure tap holes were then drilled into these tubes from the suction surface as shown in Reference 4. In each low solidity cascade the instrumented airfoil was located next to the airfoil at the center of the cascade. The endwall static pressure taps were located in the exit plane of the inlet guide vanes and 0.1 inch axially downstream from the test airfoils. There were three static taps on each inlet endwall and thirteen taps on each exit endwall as shown in Reference 4. Due to the change in solidity, the exit static pressure taps are not aligned with the airfoils as they were in the medium solidity cascades.

(U) Four inlet static pressure taps and four total temperature probes were located before and after the inlet plenum screen. Four pressure taps, located in the exit plenum, measured the exit static pressure. A study of these plenum configurations showed the static pressures were equal to the total pressures; therefore, the static taps were used for the plenum total pressure readings. One of these inlet plenum total pressure measurements after the screen was used as the upstream total pressure reference of the traversing probe. This permitted making a differential loss measurement free of error due to inlet pressure fluctuations.

(U) The axial location of the exit traverse plane, the traversing mechanism, the annular sector traversed, and the percent of span of the total pressure loss and flow direction traverse probe measurements were identical to those of the medium solidity cascades. No traverses were made of the inlet plane in the low solidity tests, since the inlet guide vanes had been tested previously as part of the medium solidity test program.

(U) The traversing probe used to measure the exit total pressure and flow direction was a modified, extended tip, yaw angle - seeking cobra probe. This probe has low blockage, operates well at high Mach numbers and is ideally suited for the traversing mechanisms used in this rig. The modification to the standard cobra probe shown in Reference 4 gives the probe zero pitch angle error over a range of 90-to-110 degrees. Hence, in the low solidity tests it was unnecessary to measure the exit flow pitch angle or make any corrections to the cobra probe total pressure measurements due to pitch angle error.

(U) The results of the annular cascade tests on the nominal and medium solidity airfoils strongly indicated that a laminar boundary layer might be present over a large portion of these airfoil suction surfaces, presumably because of the cascade rigs low inlet turbulence. The very low profile losses due to the low skin friction of the laminar boundary layer or the high losses due to laminar boundary separation are, however, uncharacteristic of airfoil performance in operating turbines. In operating turbines, boundary layers are generally fully turbulent, except at very low Reynolds numbers. To promote the turbulent boundary layer in the low solidity cascade tests, trip wires of 0.005 inch diameter were placed at the 20 percent axial chord location from root-to-tip on each airfoil.

TABLE XIII

AIRFOIL STATIC PRESSURE INSTRUMENTATION
LOW SOLIDITY

First-Stage Vane

Section	Airfoil Side	Axial Distance From L.E.	X/bx
Root Section A-A	Suction	0.044	0.056
		0.126	0.165
		0.211	0.273
		0.324	0.419
		0.379	0.490
		0.462	0.598
		0.546	0.707
		0.630	0.816
	Pressure	0.440	0.569
		0.212	0.274
Mean Section C-C	Suction	0.084	0.100
		0.251	0.299
		0.335	0.400
		0.419	0.500
		0.482	0.575
		0.564	0.673
		0.634	0.757
		0.685	0.818
	Pressure	0.514	0.614
Tip Section G-G	Suction	0.255	0.280
		0.500	0.549
		0.555	0.609
		0.615	0.675
		0.685	0.752
		0.732	0.794
		0.792	0.870
	Pressure	0.674	0.740
		0.289	0.317

NOTE: Tip Section taps are actually located parallel to wall on section J-J.

TABLE XIV

AIRFOIL STATIC PRESSURE INSTRUMENTATION
LOW SOLIDITY

First-Stage Blade [redacted]

Section	Airfoil Side	Axial Length From L.E., X	X/bx
Root Section A-A	Suction	0.080	0.134
		0.280	0.470
		0.405	0.681
		0.458	0.769
Mean Section C-C	Suction	0.060	0.105
		0.150	0.264
		0.270	0.475
		0.360	0.633
		0.419	0.737
Tip Section G-G	Suction	0.108	0.201
		0.215	0.400
		0.323	0.600
		0.377	0.700
		0.430	0.800

NOTE: Tip section taps are actually located parallel to wall on section J-J.

TABLE XV

AIRFOIL STATIC PRESSURE INSTRUMENTATION
LOW SOLIDITY

Second-Stage Vane

Section	Airfoil Side	Axial Length From L.E., X	X/bx
Root Section A-A	Suction	0.083	0.098
		0.167	0.200
		0.250	0.300
		0.334	0.401
		0.404	0.480
		0.510	0.613
		0.585	0.703
		0.668	0.800
	Pressure	0.540	0.642
		0.180	0.214
Mean Section C-C	Suction	0.088	0.100
		0.176	0.200
		0.264	0.300
		0.371	0.421
		0.440	0.500
		0.528	0.600
		0.616	0.700
		0.705	0.800
	Pressure	0.565	0.641
		0.179	0.203
Tip Section G-G	Suction	0.056	0.060
		0.388	0.417
		0.509	0.547
		0.589	0.633
		0.640	0.688
		0.686	0.737
	Pressure	0.655	0.704

NOTE: O.D. taps are actually located parallel to wall on section J-J.

5. DISCUSSION

(U) The testing and analysis of the data on the medium-reaction, low-solidity first vane, first blade and second vane has been completed.

(U) For each of the low solidity cascades data were taken at the design Mach number and design Reynolds number. For the first and second vane cascades data were also taken at Mach numbers 0.1 above and below the design Mach number at the design Reynolds number. For the first blade data were taken at a Mach number 0.1 below the design Mach number and at the design Reynolds number.

(U) The inlet guide vanes were evaluated as part of the medium solidity test program at similar design Mach number and Reynolds number conditions as in the low solidity tests. It was therefore assumed that the inlet guide vane $\Delta P_o/P_o$ losses and exit air angles would also be similar in the corresponding low solidity test. These pressure losses and air angles were reported in References 4 and 5.

(U) The plots of the important aerodynamic quantities based on the inlet and exit plane measurements for the first vane, first blade and second vane at the test conditions nearest the design conditions are shown in Figures 104 through 133. These plots are presented in the order that they will be subsequently discussed.

(U) The first vane airfoil cascade total pressure loss contours (Figure 104), spanwise total pressure loss plot (Figure 105) and spanwise loss coefficient ($1 - \phi^2$) plot (Figure 106) indicate that the cascade is operating with low losses in the midspan area and with high localized loss areas at the endwalls. This performance is typical of an airfoil operating with attached boundary layers and strong endwall secondary flows. The integrated overall loss coefficient for this airfoil is 0.069 and the midspan loss coefficient is 0.037. The midspan loss coefficient predicted by boundary layer calculation is 0.028.

(U) The first vane gas angle contours (Figure 107) and spanwise plots (Figure 108) show close agreement with the design angles over the midspan and typical under- and over-turning at the endwalls due to secondary flow. Neither these angle plots nor the flow coefficient plot (Figure 109) give any evidence of flow separation.

(U) The first vane spanwise exit Mach number plot (Figure 110) indicates fairly good agreement with design values over the span.

(U) The surface static pressure distributions for the root, mean and tip section (Figures 111, 112 and 113) indicate that the airfoil surface pressures are lower than predicted over the first forty percent of axial chord. This may account for the higher than predicted profile losses of this airfoil.

(U) The first blade airfoil total pressure loss contours (Figure 114), spanwise total pressure loss plot (Figure 115) and spanwise loss coefficient ($1 - \phi^2$) plot (Figure 116) indicate that the cascade is operating with high losses in the midspan area, a high localized loss area at the tip and a very high loss area at the root. The integrated overall loss coefficient for this airfoil

is 0.167 and the midspan loss coeffi[illegible]. The boundary layer calculation predicted that there would be a separation on the suction side at 96 percent of the axial chord and, hence, no loss could be computed using boundary layer theory.

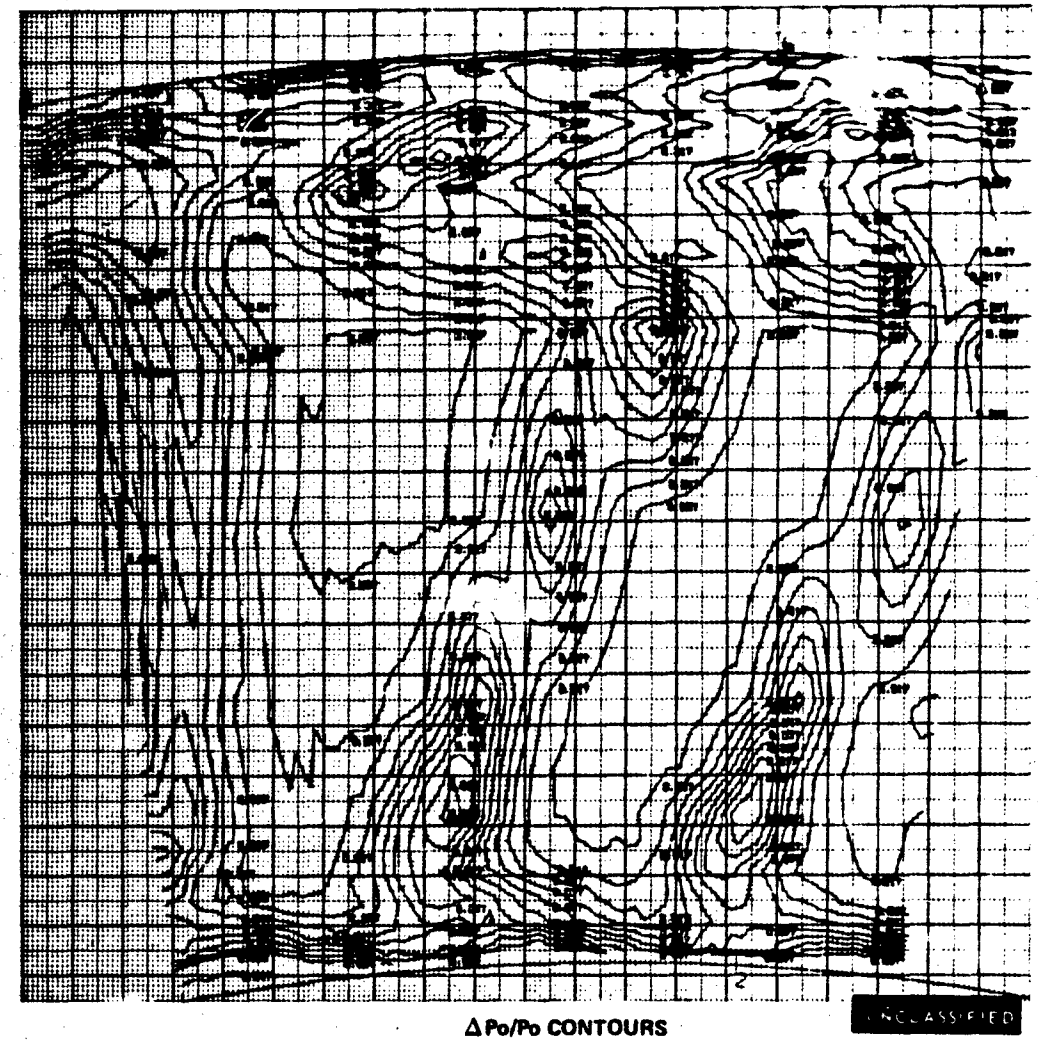

Figure 104 Pressure Loss Contours, First Vane, Low Solidity, Three Flow Passages, Midspan Exit Mach No. = 0.870

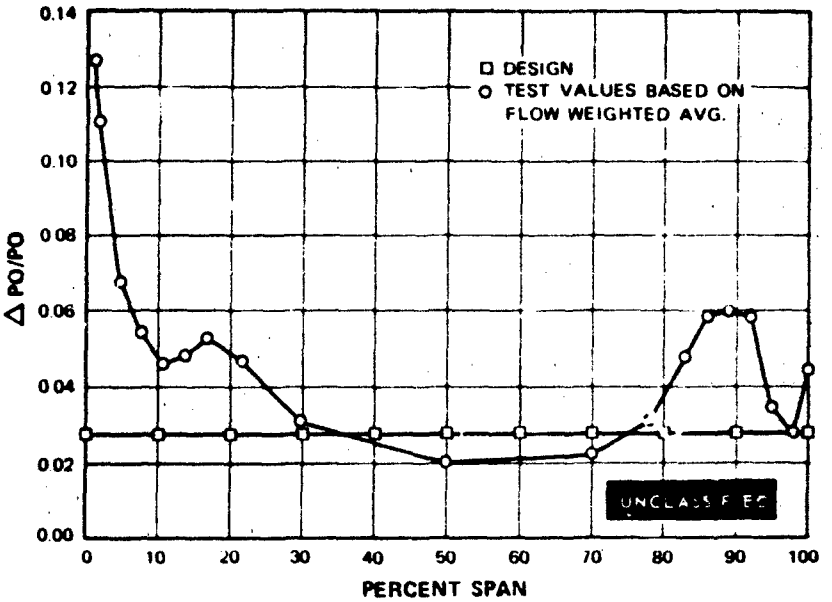

Figure 105 Spanwise Pressure Loss Distribution, First Vane, Low Solidity, Midspan Exit Mach No. = 0.870

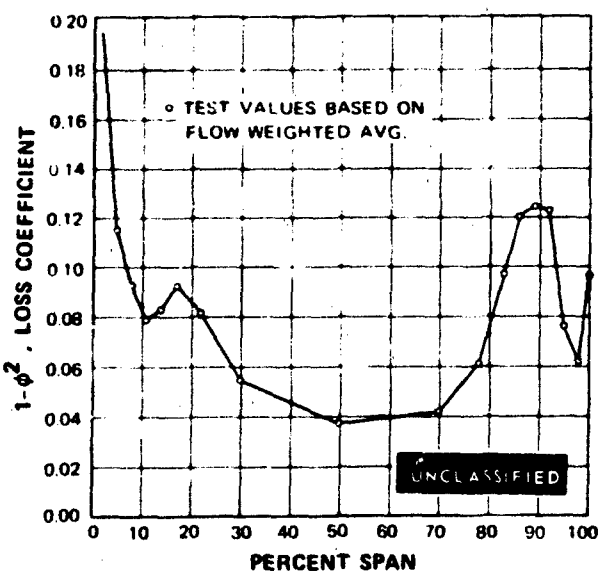

Figure 106 Spanwise Loss Coefficient Distribution, First Vane, Low Solidity, Midspan Exit Mach No. = 0.870

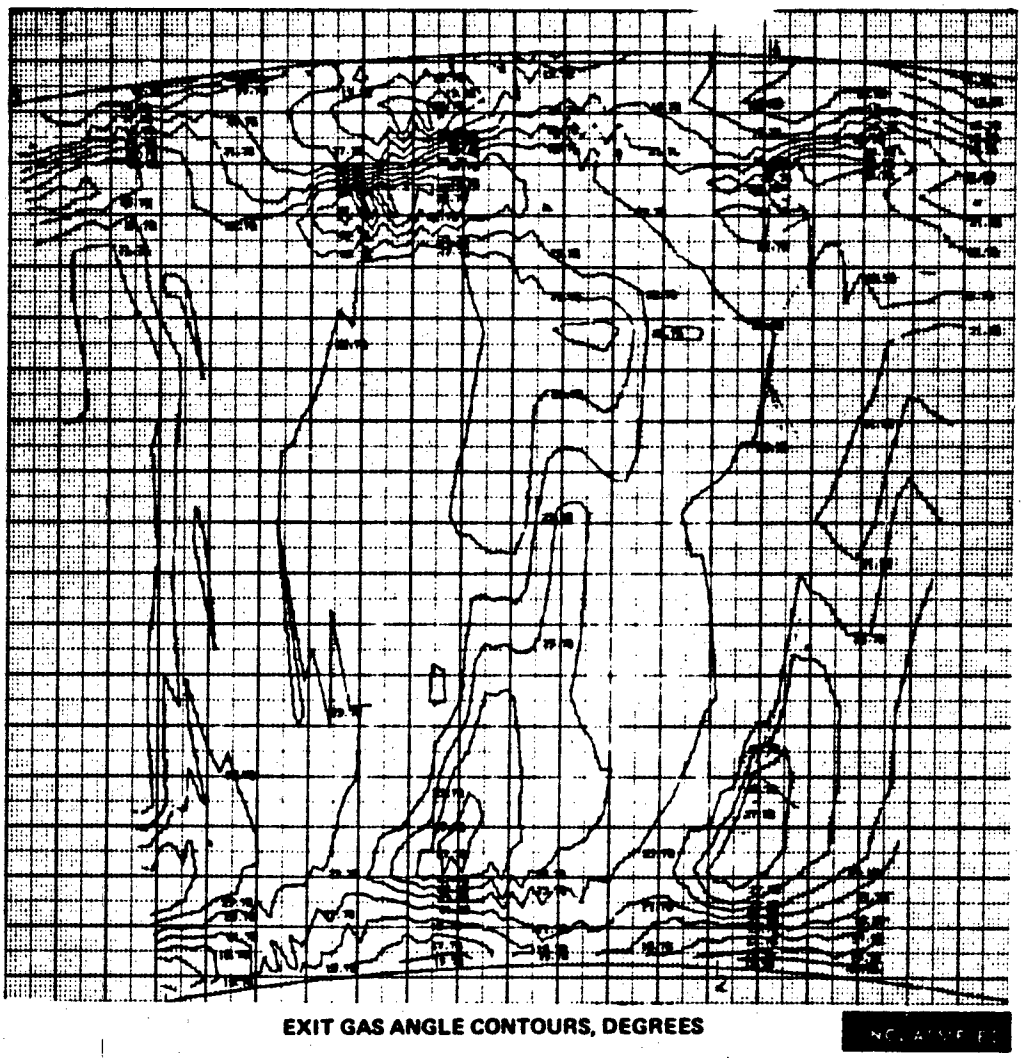

Figure 107 Exit Gas Angle Contours, First Vane, Low Solidity, Three Flow Passages, Midspan Exit Mach No. = 0.870

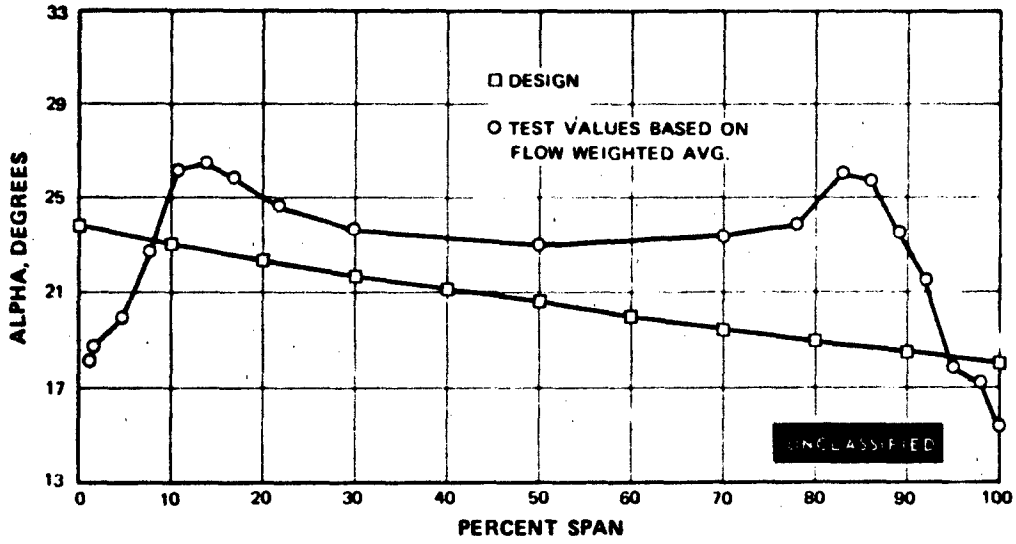

Figure 108 Spanwise Exit Gas Angle Distribution, First Vane, Low Solidity, Midspan Exit Mach No. = 0.870

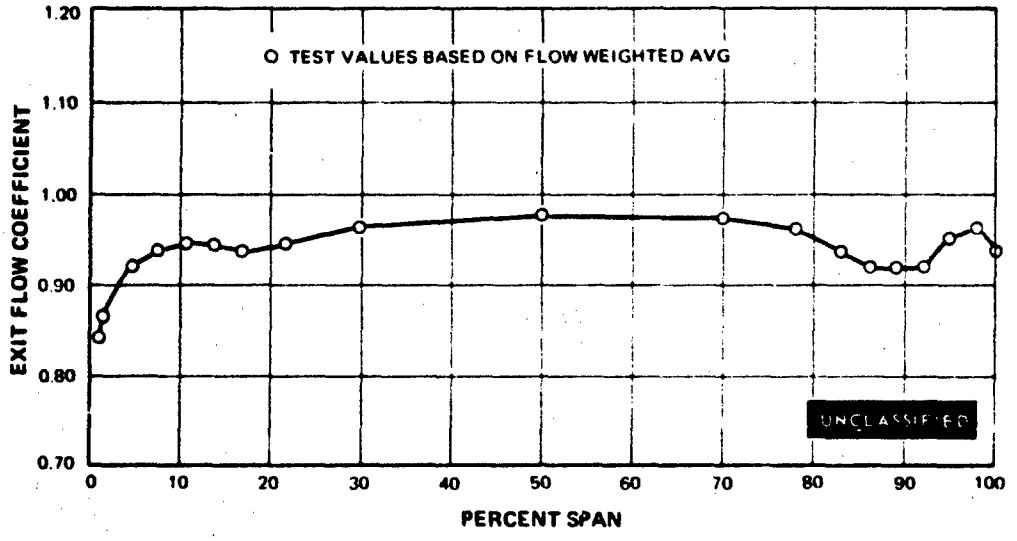

Figure 109 Spanwise Exit Flow Coefficient Distribution, First Vane, Low Solidity, Midspan Exit Mach No. = 0.870

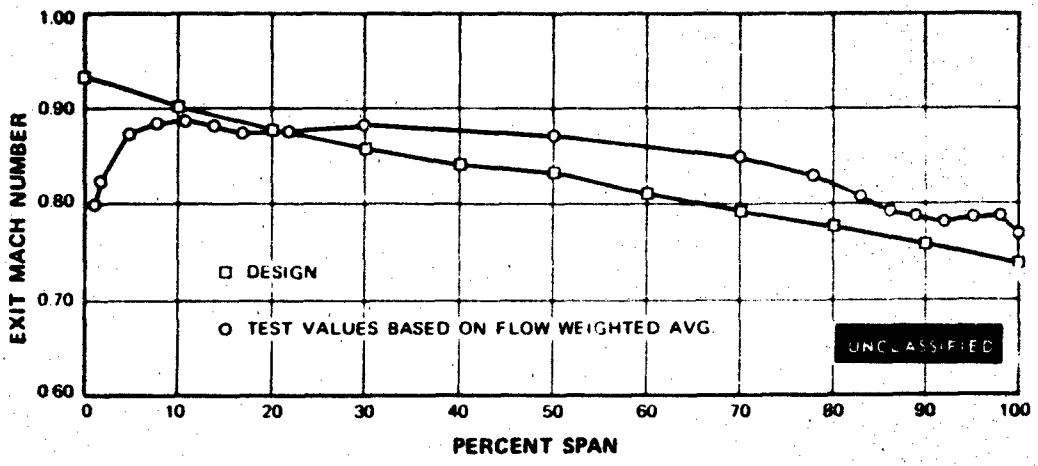

Figure 110 Spanwise Exit Mach Number Distribution, First Vane, Low Solidity, Midspan Exit Mach No. = 0.870

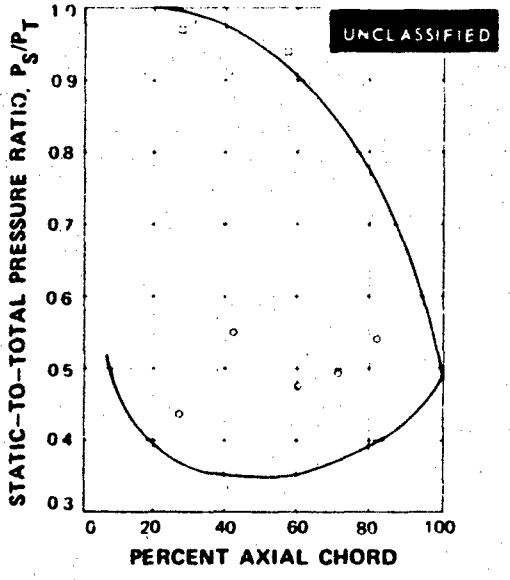

Figure 111 Static-to-Total Pressure Ratio Versus Percent Axial Chord, First Vane, Low Solidity, Root Section

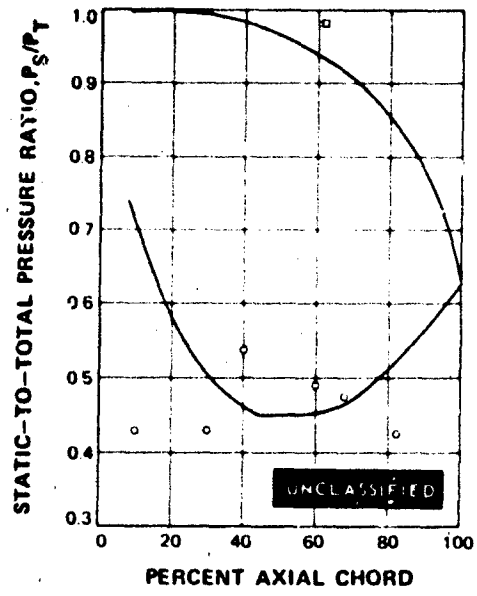

Figure 112 Static-to-Total Pressure Ratio Versus Percent Axial Chord, First Vane, Low Solidity, Mean Section

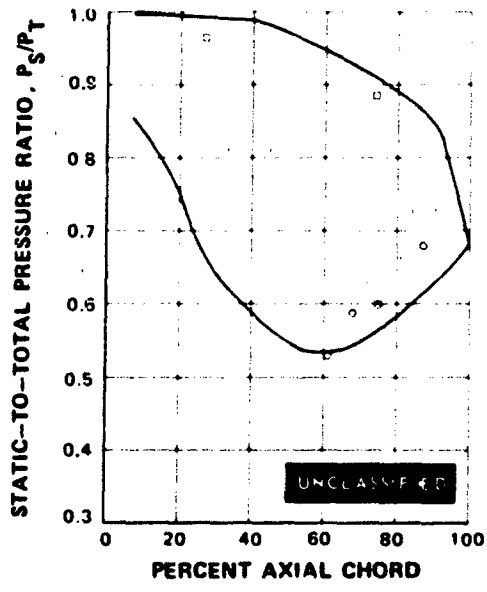

Figure 113 Static -to-Total Pressure Ratio Versus Percent Axial Chord, First Vane, Low Solidity, Tip Section

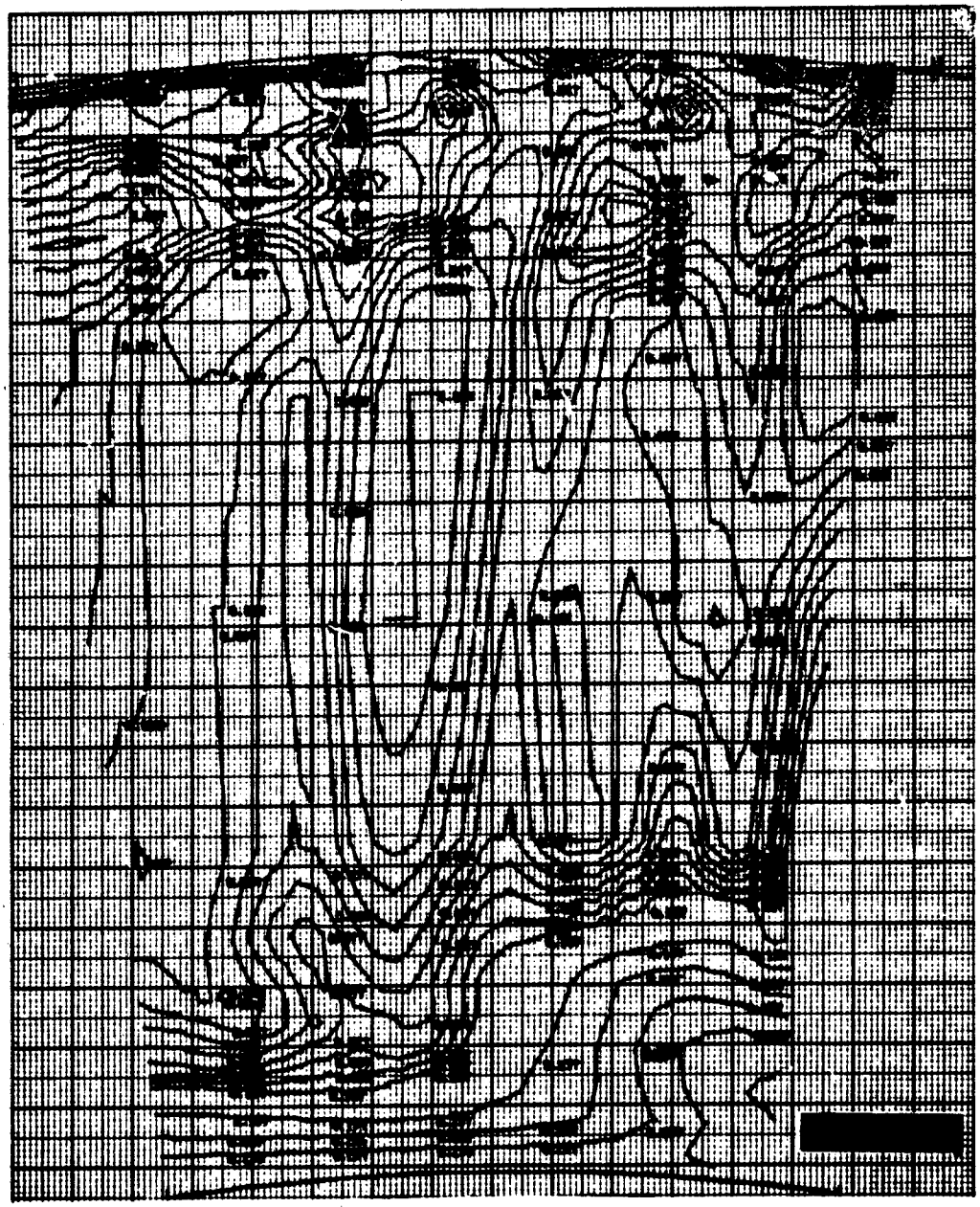

Figure 114 Pressure Loss Contours, First Blade, Low Solidity, Three Flow Passages, Midspan Exit Mach No. = 0.685

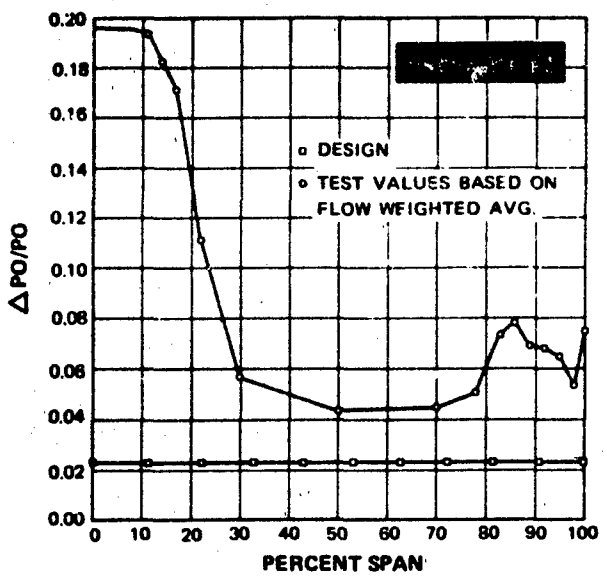

Figure 115 Spanwise Pressure Loss Distribution, First Blade, Low Solidity, Midspan Exit Mach No. = 0.685

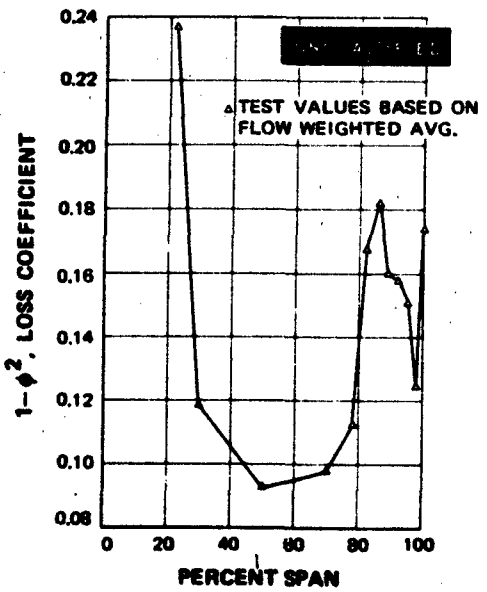

Figure 116 Spanwise Loss Coefficient Distribution, First Blade, Low Solidity, Midspan Exit Mach No. = 0.685

(U) The first blade gas angle contours (Figure 117) and spanwise plots (Figure 118) show good agreement with design values in the midspan area. In the area of the tip, the gas angles are as much as four degrees above the design values due to a typical secondary flow. From the root to about 30 percent of the span there appears to be a separated flow as well as a secondary flow causing gas angles from three-to-four degrees higher than the design values. The presence of separated flow at the root is also shown by the low values of the flow coefficient at the root shown in the flow coefficient plot (Figure 119).

(U) The first blade spanwise exit Mach number plot (Figure 120) indicates fairly good agreement with the design values from the midspan to the tip and very low values from 30 percent span to the root due to the separation.

(U) The surface static pressure distributions for the root, mean and tip sections (Figures 121, 122 and 123) indicate that the root is unloaded relative to the design values, that the mean is operating near design and that the tip is loaded more heavily than design. A similar conclusion can be reached from an examination of the Mach number plot. There is evidently a large shift in the flow from the root to the tip due to the separation.

(U) The second vane airfoil cascade total pressure loss contours (Figure 124), spanwise total pressure loss plot (Figure 125) and spanwise loss coefficient ($1 - \phi^2$) plot (Figure 126) indicate that the cascade is operating with high losses in the midspan area, a higher localized loss area at the root and a very high loss area at the tip. The integrated overall loss coefficient for this airfoil is 0.143 and the midspan loss coefficient is 0.055. The midspan loss coefficient predicted by boundary layer calculation is 0.039.

(U) The second vane gas angle contours (Figure 127) and the spanwise plot (Figure 128) show good agreement with the design values at the midspan, deviations of up to 3 degrees at the root due to secondary flow, and deviations of up to 4 degrees at the tip due to the combined effects of the separated and secondary flows. The flow coefficient plot (Figure 129) also indicates the presence of a separated region at the tip.

(U) The second vane spanwise exit Mach number plot (Figure 130) indicates good agreement with the design values from the root-to-mean sections and lower than the design Mach numbers from the mean-to-tip sections. Again, the low Mach numbers can be attributed to the separation.

(U) The surface static pressure distributions for the root, mean and tip sections (Figures 131, 132 and 133) indicate that the root is unloaded relative to the design prediction and that the mean and tip sections are operating near the design predictions. It should be noted here that the pressure distribution computation used to make the design predictions is basically a subsonic calculation. Hence, the prediction of transonic pressures in the root section may be incorrect.

(U) It is likely that the poor performance of the second vane tip section can be explained by the positive incidence from about 80-to-100 percent of the span. The inlet guide vane performance is shown in Reference 5.

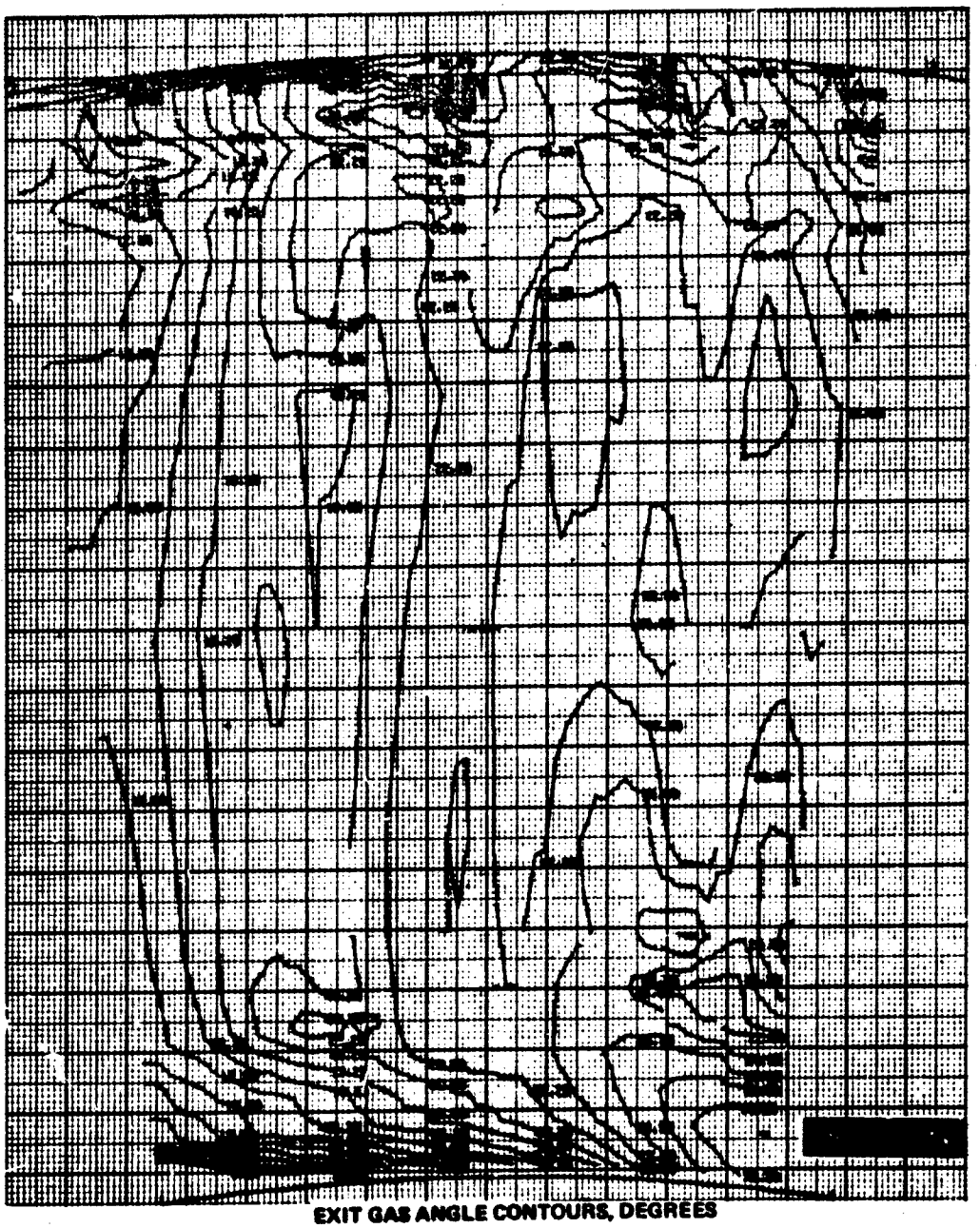

Figure 117 Exit Gas Angle Contours, First Blade, Low Solidity, Three Flow Passages, Midspan Exit Mach No. = 0.685

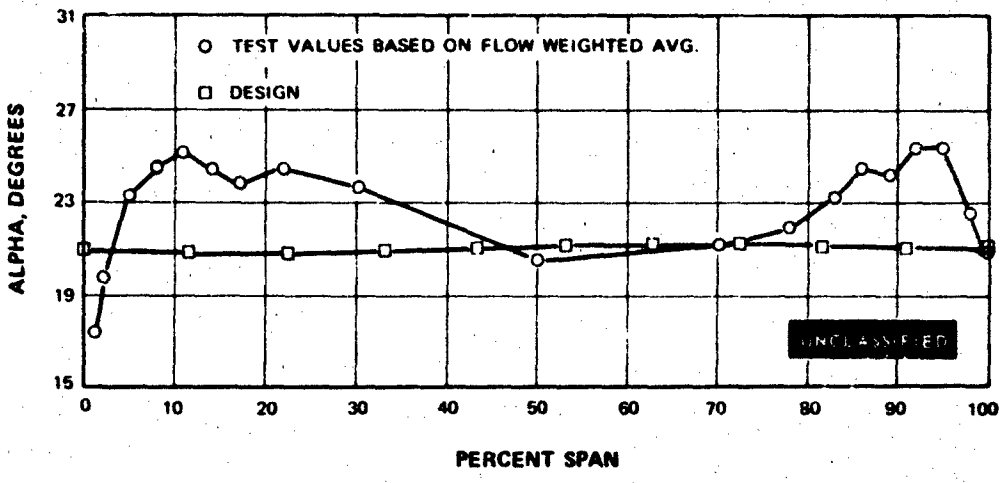

Figure 118 Spanwise Exit Gas Angle Distribution, First Blade, Low Solidity, Midspan Exit Mach No. = 0.685

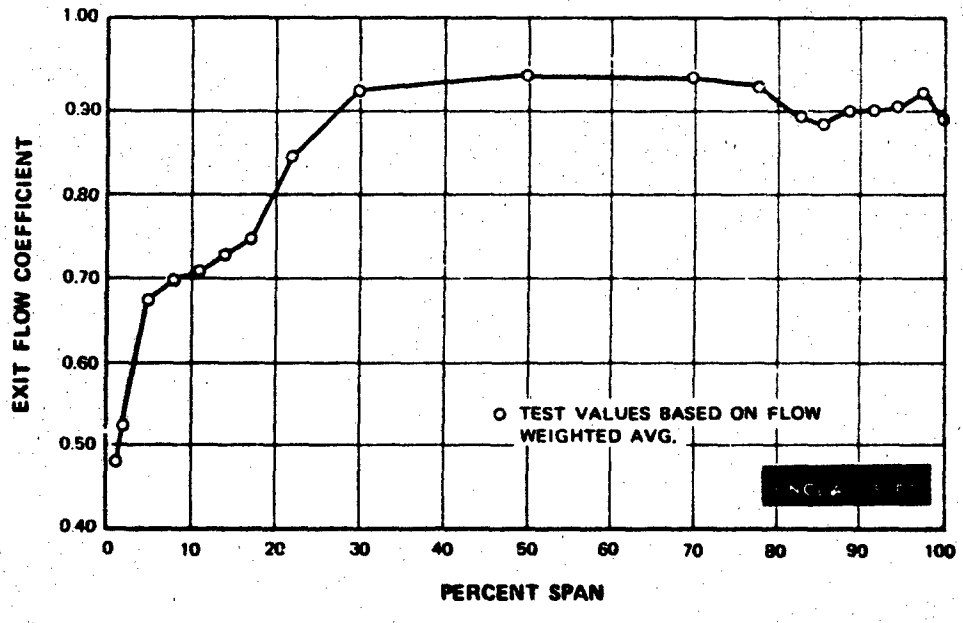

Figure 119 Spanwise Exit Flow Coefficient Distribution, First Blade, Low Solidity, Midspan Exit Mach No. = 0.685

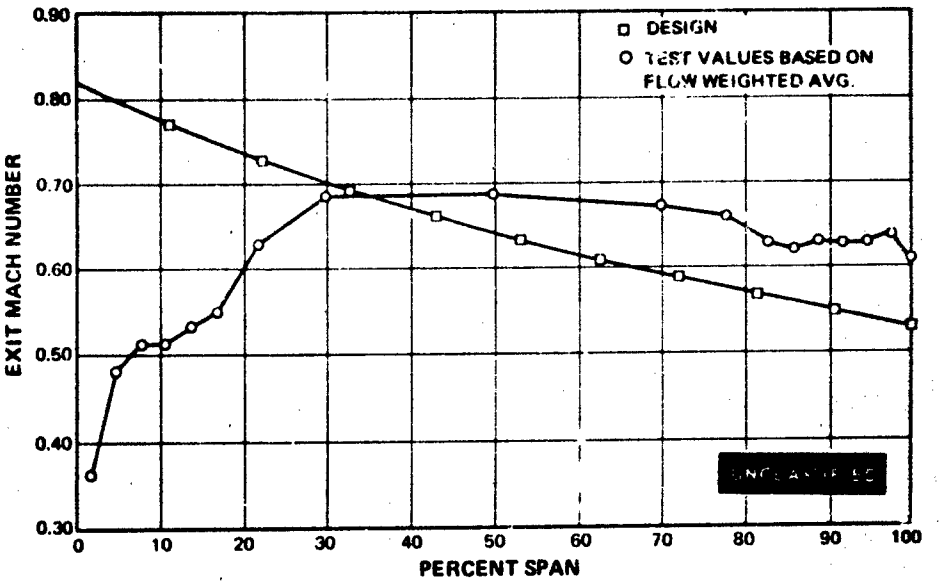

Figure 120 Spanwise Exit Mach Number Distribution, First Blade, Low Solidity, Midspan Exit Mach No. = 0.685

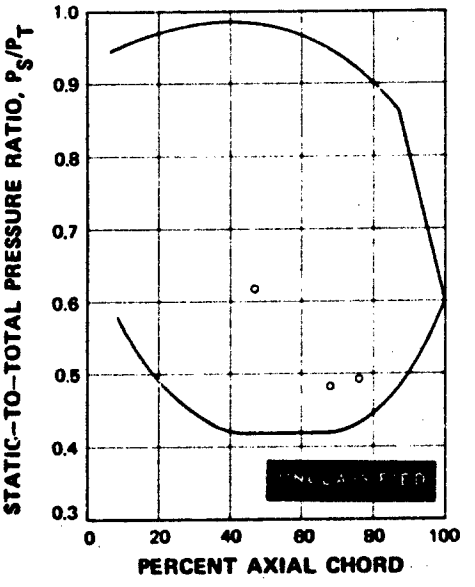

Figure 121 Static-to-Total Pressure Ratio Versus Percent Axial Chord, First Blade, Low Solidity, Root Section

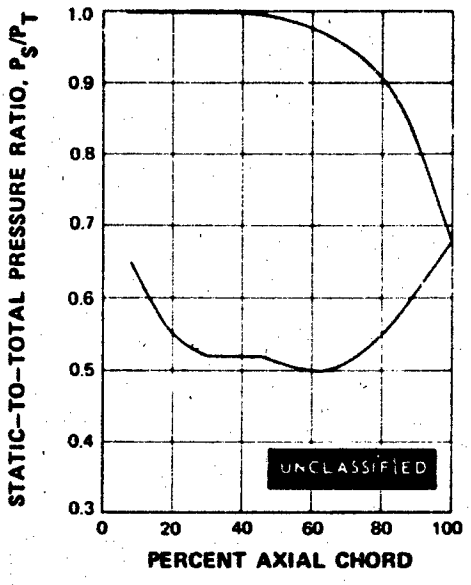

Figure 122 Static-to-Total Pressure Ratio Versus Percent Axial Chord, First Blade, Low Solidity, Mean Section

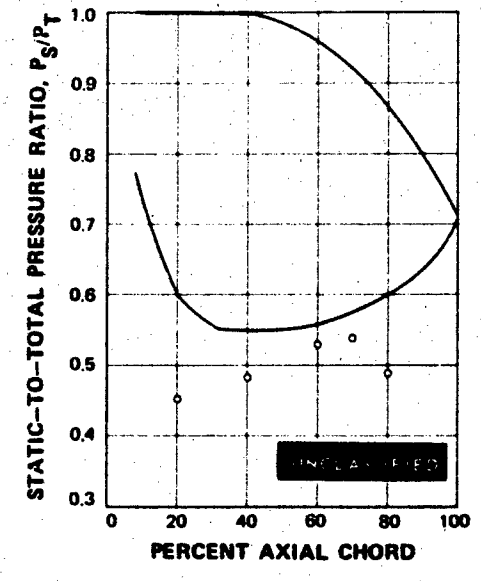

Figure 123 Static-to-Total Pressure Ratio Versus Percent Axial Chord, First Blade, Low Solidity, Tip Section

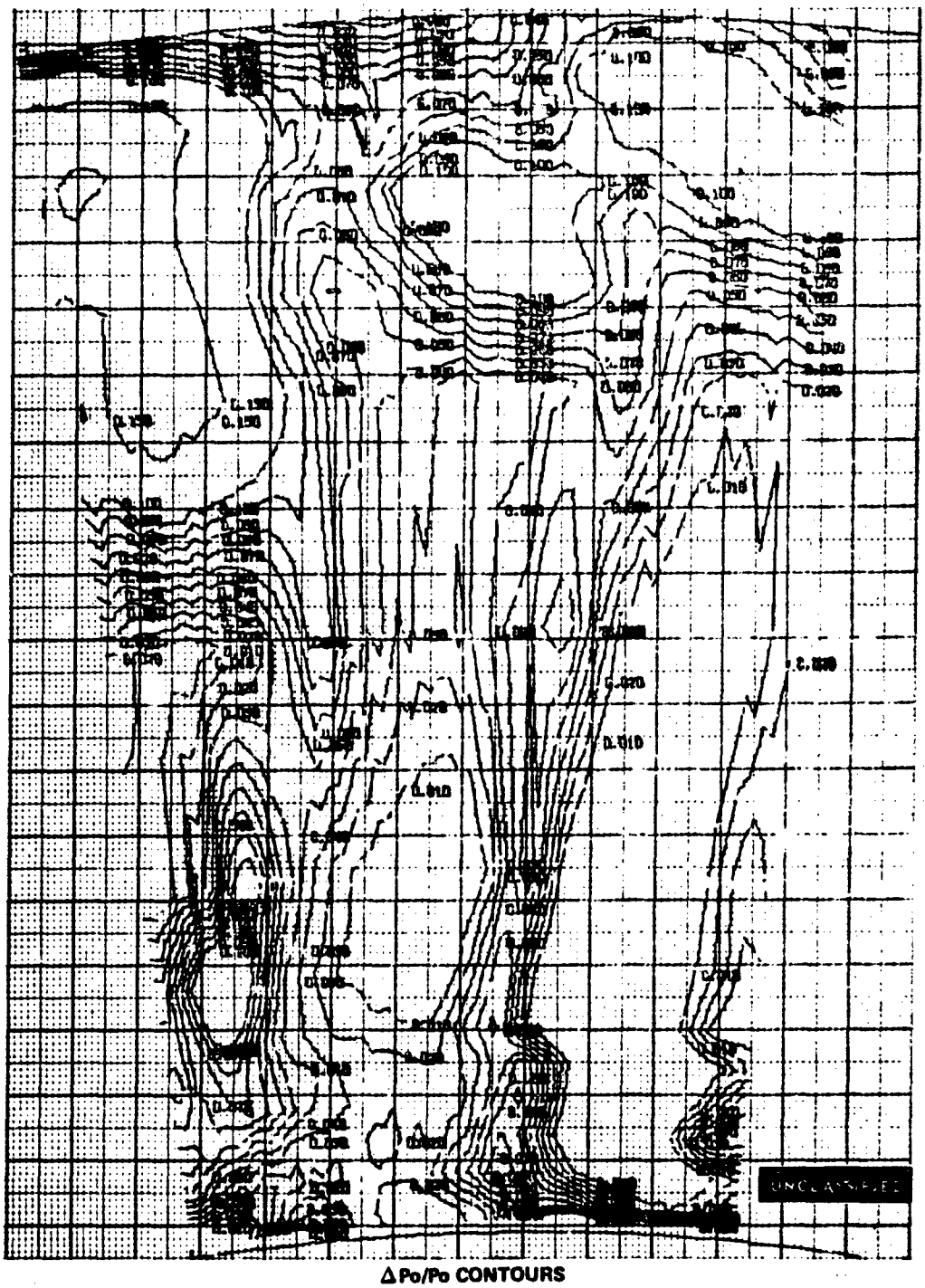

Figure 124 Pressure Loss Contours, Second Vane, Low Solidity, Three Flow Passages, Midspan Exit Mach No. = 0.870

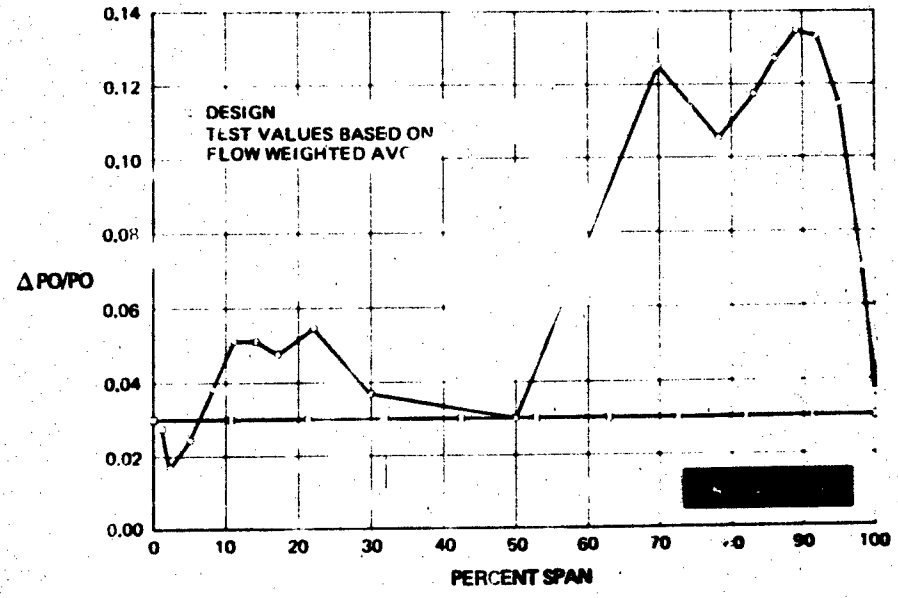

Figure 125 Spanwise Pressure Loss Distribution, Second Vane, Low Solidity, Midspan Exit Mach No. = 0.870

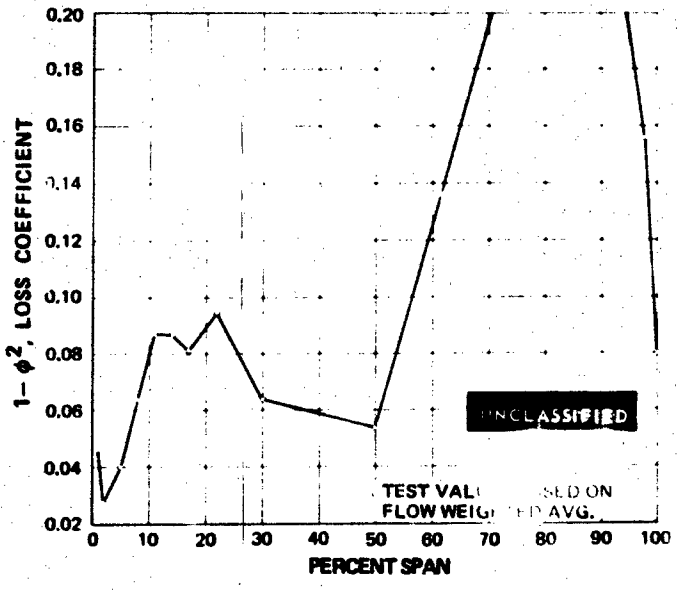

Figure 126 Spanwise Loss Coefficient Distribution, Second Vane, Low Solidity, Midspan Exit Mach No. = 0.870

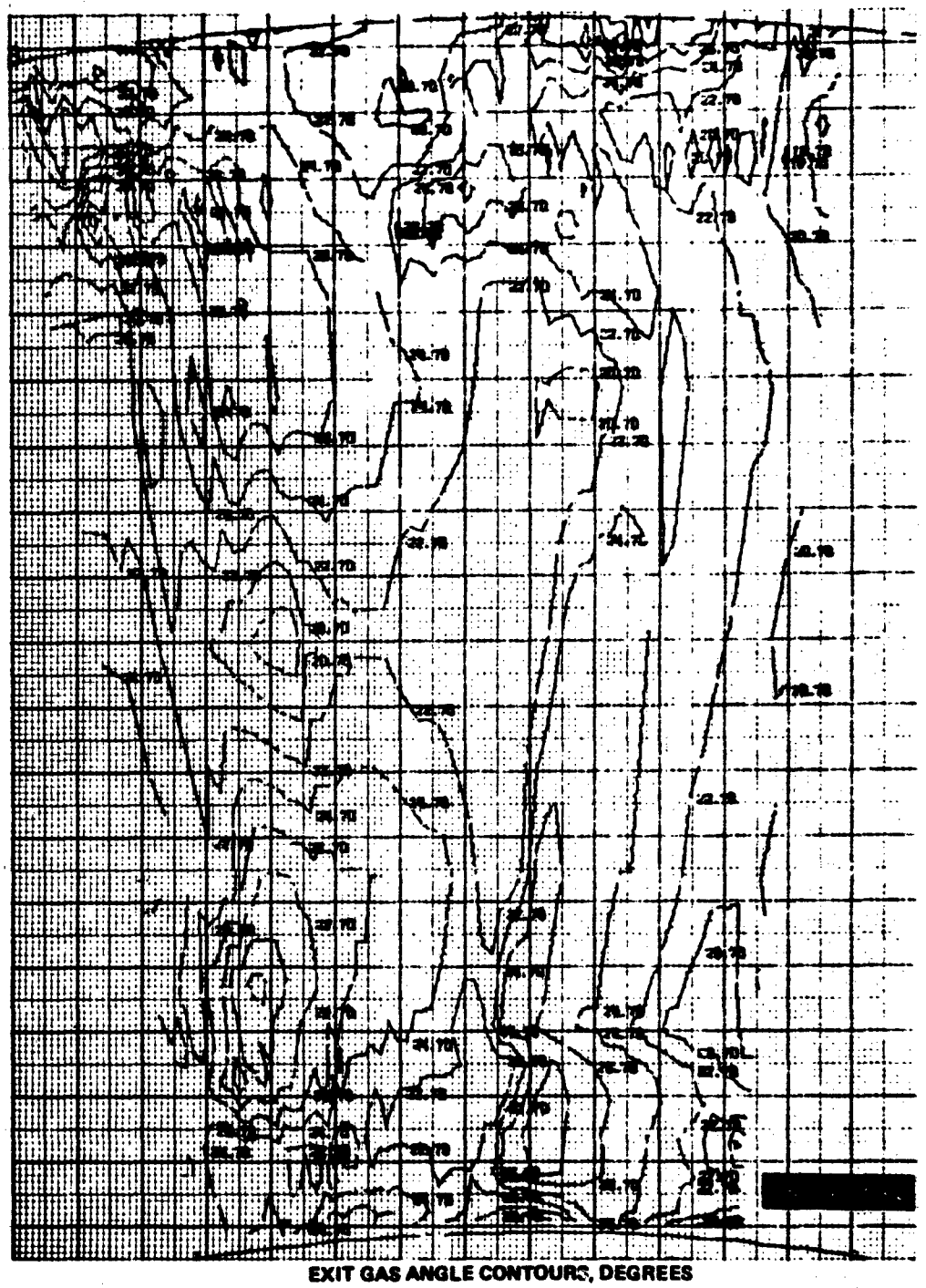

EXIT GAS ANGLE CONTOURS, DEGREES

Figure 127 Exit Gas Angle Contours, Second Vane, Low Solidity, Three Flow Passages, Midspan Exit Mach No. = 0.870

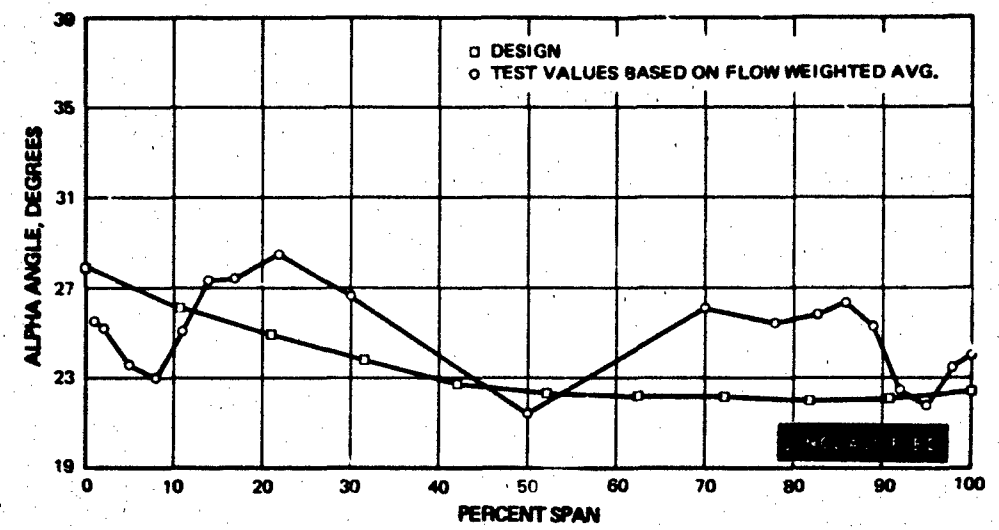

Figure 128 Spanwise Exit Gas Angle Distribution, Second Vane, Low Solidity, Midspan Exit Mach No. = 0.870

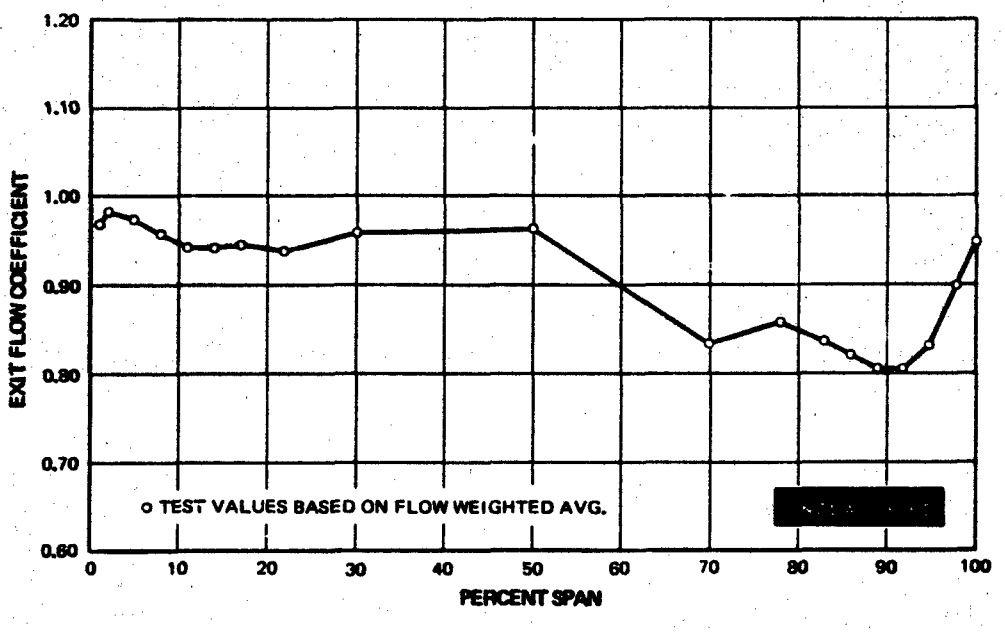

Figure 129 Spanwise Exit Flow Coefficient Distribution, Second Vane, Low Solidity, Midspan Exit Mach No. = 0.870

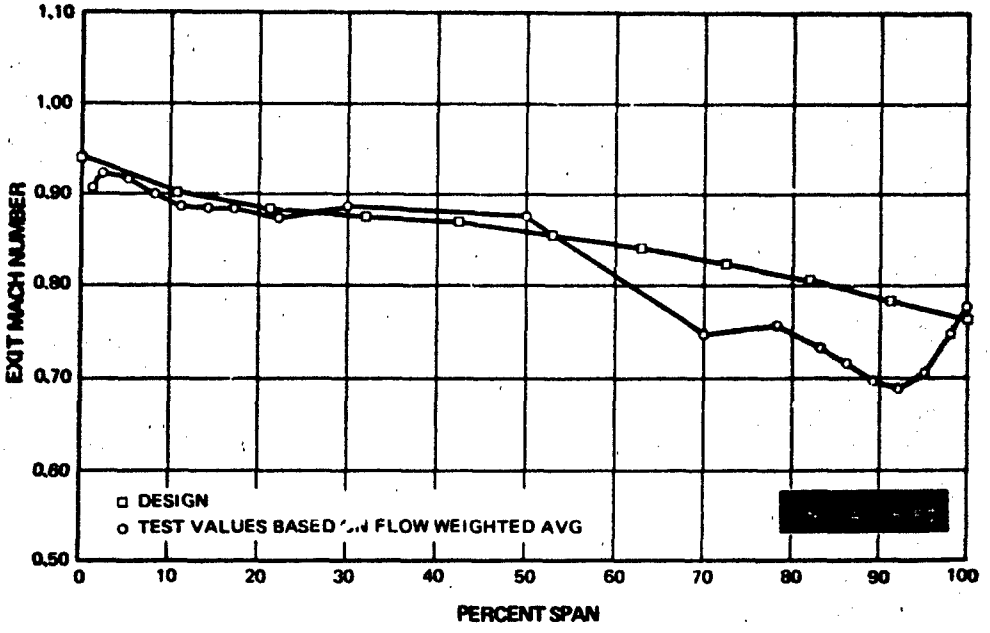

Figure 130 Spanwise Exit Mach Number Distribution, Second Vane, Low Solidity, Mid-span Exit Mach No. = 0.870

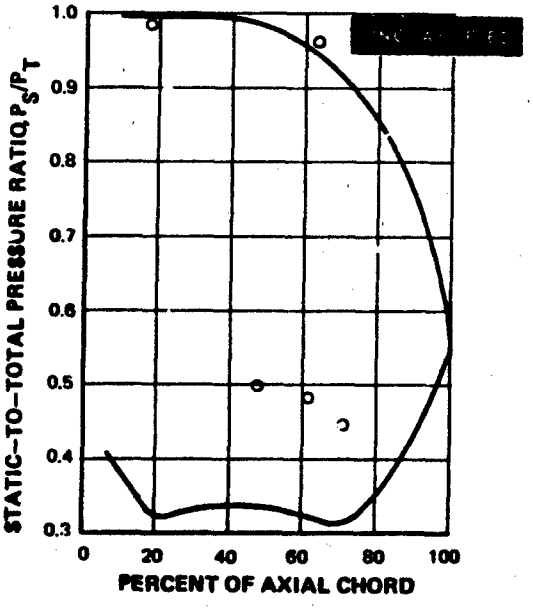

Figure 131 Static-to-Total Pressure Ratio Versus Percent Axial Chord, Second Vane, Low Solidity, Root Section

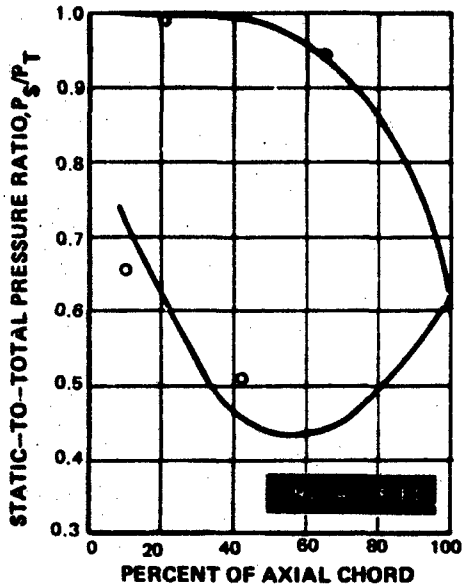

Figure 132 Static-to-Total Pressure Ratio Versus Percent Axial Chord, Second Vane, Low Solidity, Mean Section

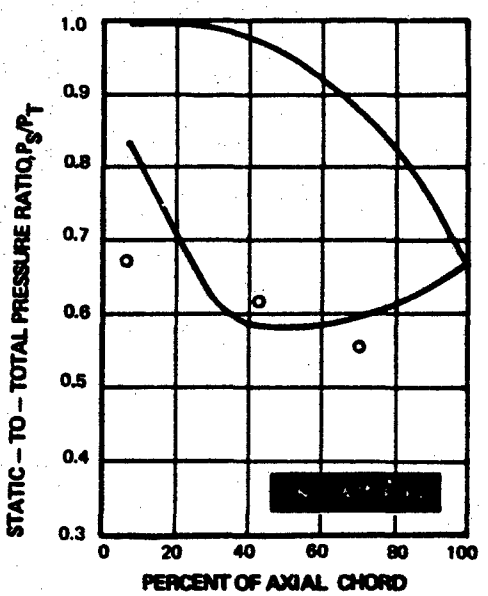

Figure 133 Static-to-Total Pressure Ratio Versus Percent Axial Chord, Second Vane, Low Solidity, Tip Section

(U) A complete summary of the loss coefficient data taken on the low solidity airfoils for the various midspan Mach numbers and design Reynolds numbers is shown in Table XVI. The data indicates that exit Mach number usually has only a small effect on the overall performance of these airfoils. However, the first vane appears to be separated at the lower Mach number with a consequent doubling of the loss. In another program the first blade was tested without the 0.005 inch trip wire installed at 20 percent of the axial chord. A comparison of the overall losses shown in Table XVI indicate no performance change occurred due to the trip wire in these tests. The midspan loss coefficients do change, but there is no consistent performance trend.

6. SUMMARY

(U) A comparison of the performance of the normal, medium and low solidity airfoils is presented in this section.

(U) The results of the low solidity annular segment cascade tests are directly comparable to the results of the normal and medium solidity tests reported in reference 5. This summary comparison is presented in Table XVII. The midspan test value presented in the table is a local value. The root-to-mean, mean-to-tip and overall test averages are the flow-weighted values computed in every instance from nineteen traverses. For completeness, the results of plane cascade tests reported in Reference 5 have been included in Table XVII. A study of the overall loss coefficients presented in Table XVII shows that the normal solidity airfoils have the best aerodynamic performance.

(U) A comparison of design parameters for all three solidities, such as pitch-to-chord ratio, load coefficient or $\Delta P/Q$, generally considered to be helpful in determining if an airfoil design will have acceptable performance, can be found in Reference 1, Section II, Table II.

TABLE XVI

SUMMARY OF DATA -- LOW SOLIDITY AIRFOILS

Airfoil	Midspan Turbine Design M_2	Midspan Test M_2	Midspan Turbine Design Reynolds No.	Midspan Test $1 - \phi^2$	Flow Weighted Averages		
					Root-To-Mean Test $1 - \phi^2$	Mean-To-Tip Test $1 - \phi^2$	Overall Test $i - \phi^2$
First Vane	0.852	0.87 0.73 0.95	4.38×10^5	0.037 0.130 0.038	0.057 0.081 0.056	0.083 0.154 0.076	0.069 0.114 0.065
First Blade	0.788	0.786 0.705	2.26×10^5	0.092 0.082	0.1[illegible] 0.191	0.163 0.174	0.167 0.184
First Blade No Trip Wire Installed	0.788	0.787 0.688 0.870	2.26×10^5	0.076 0.090 0.067	0.207 0.232 0.190	0.129 0.141 0.135	0.165 0.183 0.160
Second Vane	0.870	0.875 0.776 0.949	2.95×10^5	0.055 0.066 0.067	0.054 0.060 0.058	0.256 0.246 0.233	0.143 0.142 0.136

TABLE XVII

SUMMARY OF DESIGN POINT 1 - ϕ^2 LOSS COEFFICIENTS FOR NORMAL, MEDIUM AND LOW SOLIDITY AIRFOILS

[redacted]

	Turbine Design Midspan Exit Mach No. & Reynolds No.	Midspan		Root-To-Mean Average Test	Mean-To-Tip Average Test	Overall Average Test
		Test	Predicted For Fully Turbulent Boundary Layer			
Normal Solidity First Vane	0.854 4.38×10^5	0.017 0.023* 0.025**	0.031	0.029	0.035	0.034 0.032*
Medium Solidity First Vane	0.854 4.38×10^5	0.031	0.035	0.051	0.050	0.051
Low Solidity First Vane	0.854 4.38×10^5	0.037	0.028	0.057	0.083	0.069
Normal Solidity First Blade	0.780 2.26×10^5	0.0266 0.025**	0.049	0.0368	0.0433	0.040
Medium Solidity First Blade	0.780 2.26×10^5	0.114	0.043	0.200	0.125	0.159
Low Solidity First Blade	0.780 2.26×10^5	0.092	Separated at 96% X/bx	0.170	0.163	0.167
Normal Solidity Second Vane	0.869 2.95×10^5	0.021 0.028* 0.024**	0.034	0.0275	0.0325	0.030 0.034*
Medium Solidity Second Vane	0.869 2.95×10^5	0.123	0.034	0.085	0.214	0.157
Low Solidity Second Vane	0.869 2.95×10^5	0.055	0.039	0.054	0.256	0.143
Normal Solidity Second Blade	0.904 1.52×10^5	0.028 0.023**	0.040	0.0322	0.0438	0.038
Medium Solidity Second Blade	0.904 1.52×10^5	0.033	0.046	0.042	0.092	0.070

*Inlet Screen Installed
**Plane Cascade

SECTION VI

CONCLUSIONS AND RECOMMENDATIONS

SECTION VI

CONCLUSIONS AND RECOMMENDATIONS

1. CONCLUSIONS

(U) As part of a continuous effort to improve gas turbine engine technology, an exploratory research program was conducted to develop turbine aerodynamic methods and design procedures for efficient, high-work low pressure turbines.

(C) The turbine design parameters were chosen for the demonstrator vehicle and these were defined in the Contract (Table I, Section II). Figure 134 indicates the program goal in terms of efficiency and work level. This figure indicates the free vortex turbine experience efficiency band and work levels at the onset of this program. The goal established for this program was to maintain the peak efficiency attained with turbines of free vortex design while increasing the work level at constant wheel speed by more than 50 percent.

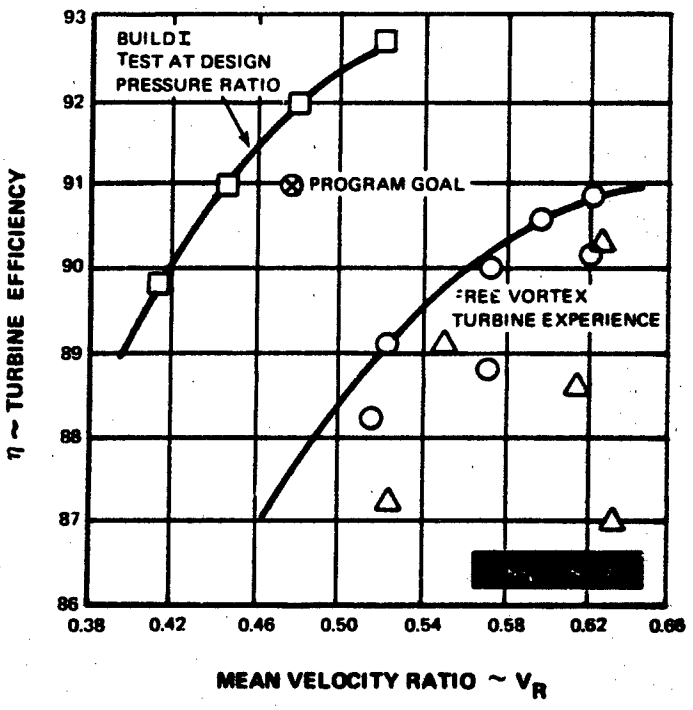

Figure 134 Program Objective - Build I, Test at Design Pressure Ratio

(U) To attain this goal, the initial guidelines were set as follows:

- Utilize sound aerodynamics.
- Develop aerodynamics in cascade tests.
- Develop the capability to synthesize these cascade aerodynamic data into the required turbine.

(U) The program was conducted in such a manner as to define a turbine design with the highest resistance to boundary layer separation. The important items learned from this program are:

- The work level can be increased by more than 50 percent over free vortex designs.
- There is no substitute for good aerodynamic contouring.
- Profile losses can be predicted from boundary layer parameters.
- Profile losses are only a part of the total loss.
- Transonic pressure distribution calculations must be used.
- A sound design can be made with radial work variations.

(C) Figure 134 shows that the efficiency goal was exceeded at the required work level, indicating that a sound design procedure was used.

2. RECOMMENDATIONS

(U) It is recommended that additional effort to further advance low pressure turbine technology be made in the following areas:

- Redesign the second stage of the demonstrator turbine in order to decrease the endwall losses measured in the present design. Data from this program indicates that the second-stage efficiency can be increased.
- Consider a turbine redesign at lower solidities to establish the upper limit of airfoil loading where a separation-free design cannot be realized.

APPENDIX I

FIRST-STAGE VANE FINAL DESIGN

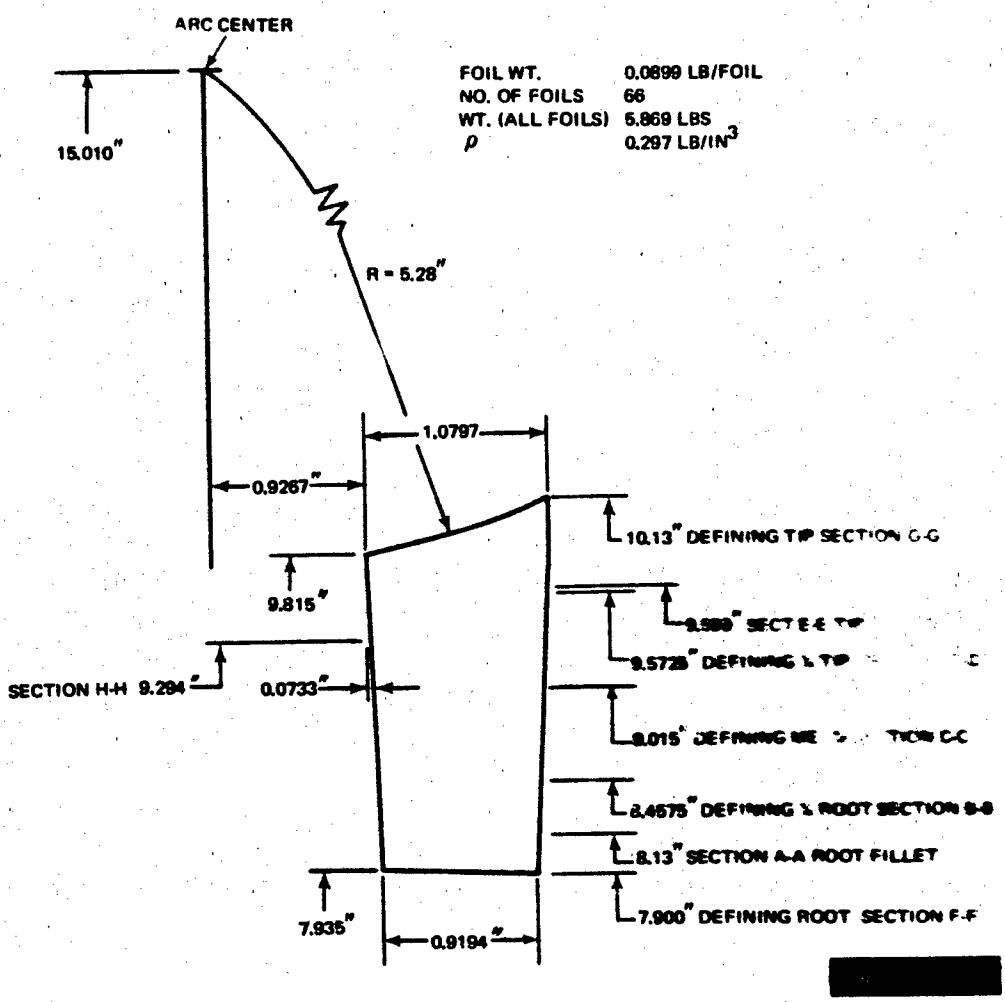

Figure 135 First-Stage Vane Elevation (not Dimensions)

L.E. RADIUS	.030	T.E. RADIUS	0.0100
FOIL INLET ANGLE	64.90	FOIL EXIT ANGLE	35.70
L.E. WEDGE ANGLE	25.03	T. E. WEDGE ANGLE	5.99
UNCOVERED TURN	11.64	GAGING ANGLE	35.08
NUMBER OF FOILS	66	DIAMETER HOT	15.800
PITCH HOT	0.7521	GAGING HOT	0.4322
AXIAL WIDTH	0.9180	METAL AREA	0.0088
RAD. REF. POINT X	0.4268	RAD. REF. POINT Y	0.4477
C.G. POINT X	0.4268	C.C. POINT Y	0.4477

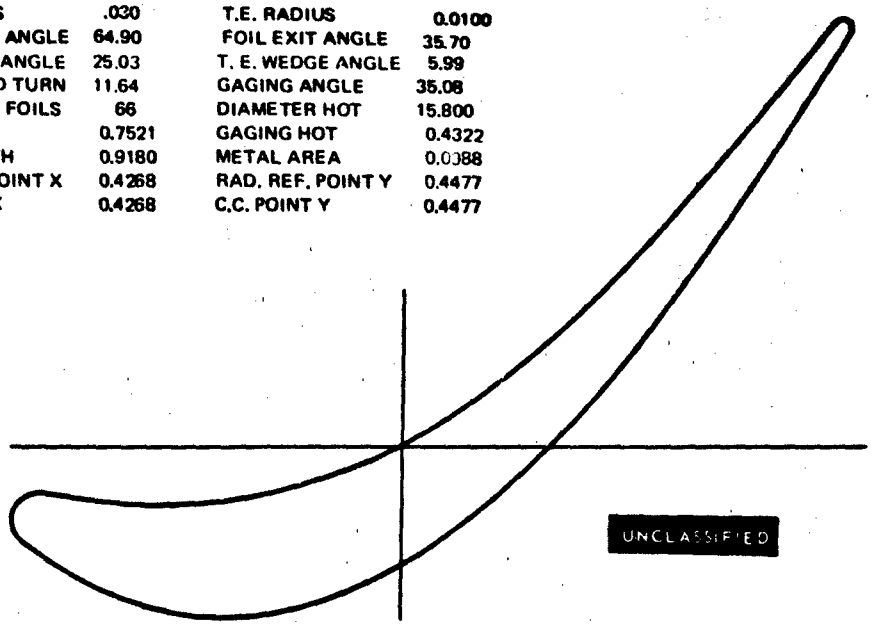

Figure 136 Section F-F, First Vane Root, Cylindrical

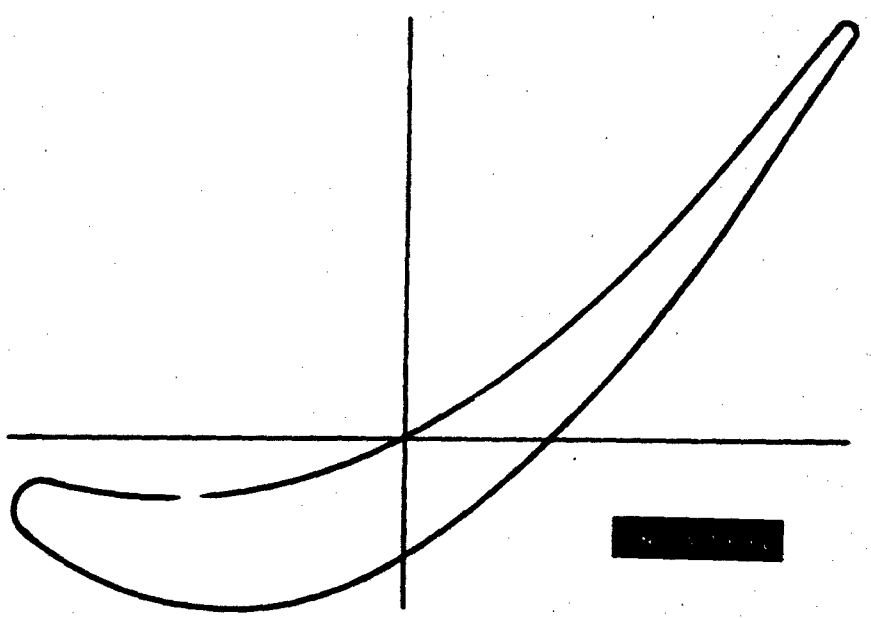

Figure 137 Section F-F, First Vane Root, Planar

L.E. RADIUS	0325	T.E. RADIUS	0.0100
FOIL INLET ANGLE	56.80	FOIL EXIT ANGLE	29.87
L.E. WEDGE ANGLE	25.09	T.E. WEDGE ANGLE	6.22
UNCOVERED TURN	18.00	GAGING ANGLE	29.08
NUMBER OF FOILS	66	DIAMETER HOT	16.915
PITCH HOT	0.8052	GAGING HOT	0.3907
AXIAL WIDTH	0.9615	METAL AREA	0.1286
RAD. REF. POINT X	0.4268	RAD. REF. POINT Y	0.4477
C.G. POINT X	0.4367	C.G. POINT Y	0.5808

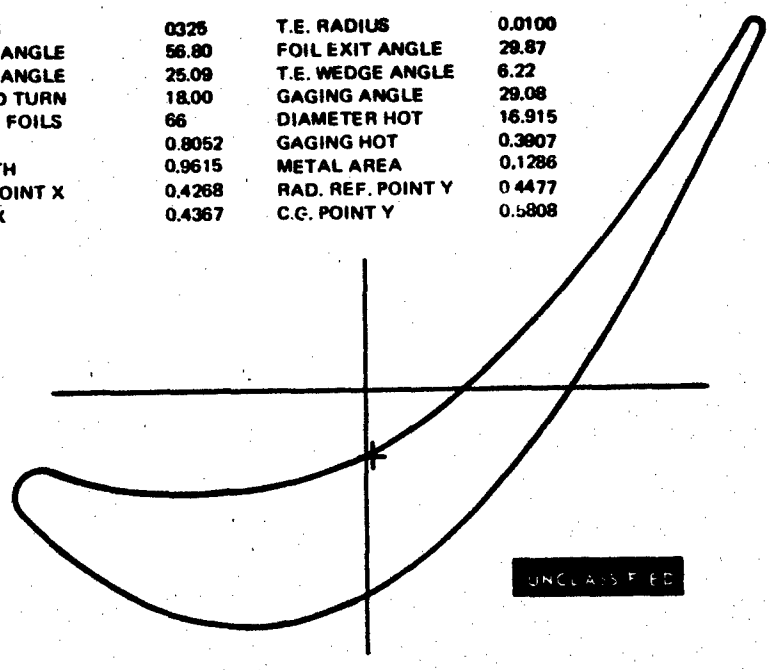

Figure 138 Section B-B, First Vane ¼ Root, Cylindrical

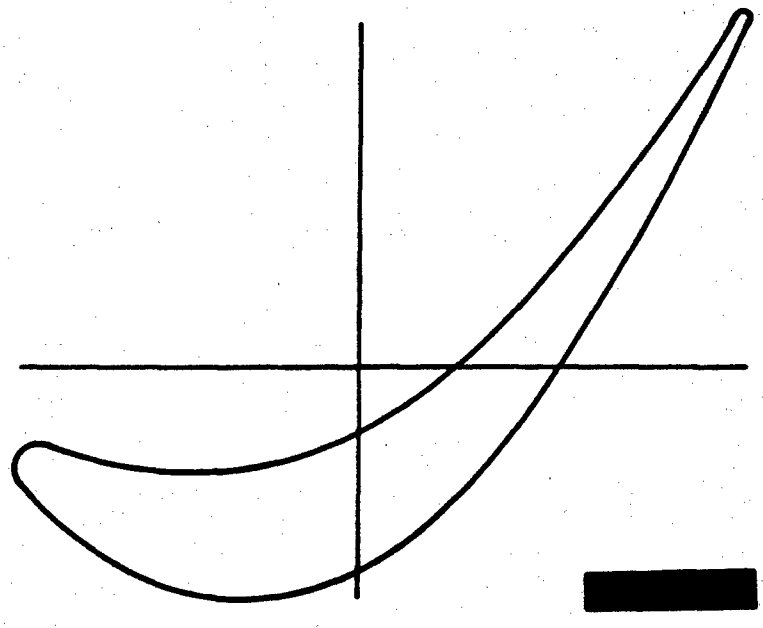

Figure 139 Section B-B, First Vane ¼ Root, Planar

L.E. RADIUS	.0360	T.E. RADIUS	0.0100
FOIL INLET ANGLE	60.48	FOIL EXIT ANGLE	26.96
L.E. WEDGE ANGLE	26.09	T.E. WEDGE ANGLE	6.48
UNCOVERED TURN	19.81	GAGING ANGLE	26.98
NUMBER OF FOILS	66	DIAMETER HOT	18.030
PITCH HOT	0.8582	GAGING HOT	0.3984
AXIAL WIDTH	1.0050	METAL AREA	0.1535
RAD. REF. POINT X	0.4268	RAD. REF. POINT Y	0.4477
C.G. POINT X	0.4482	C.G. POINT Y	0.5219

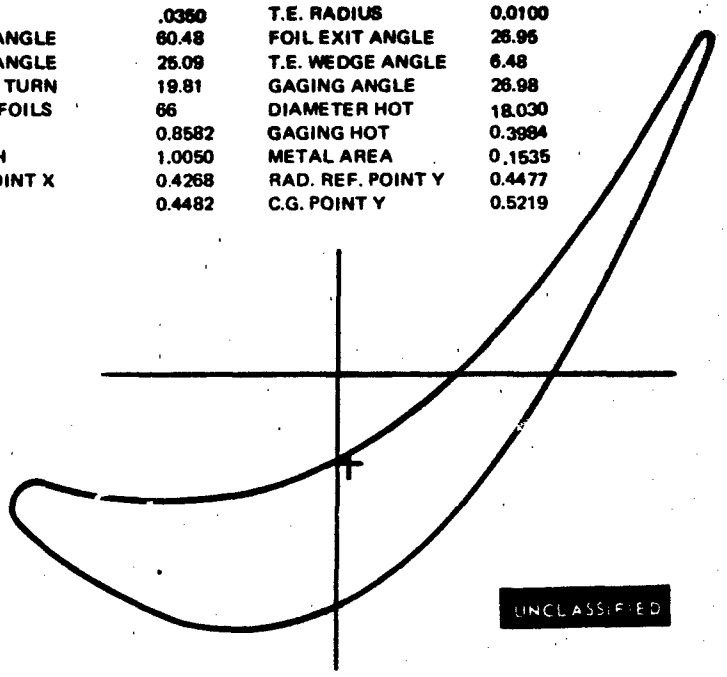

Figure 140 Section C-C, First Vane Mean, Cylindrical

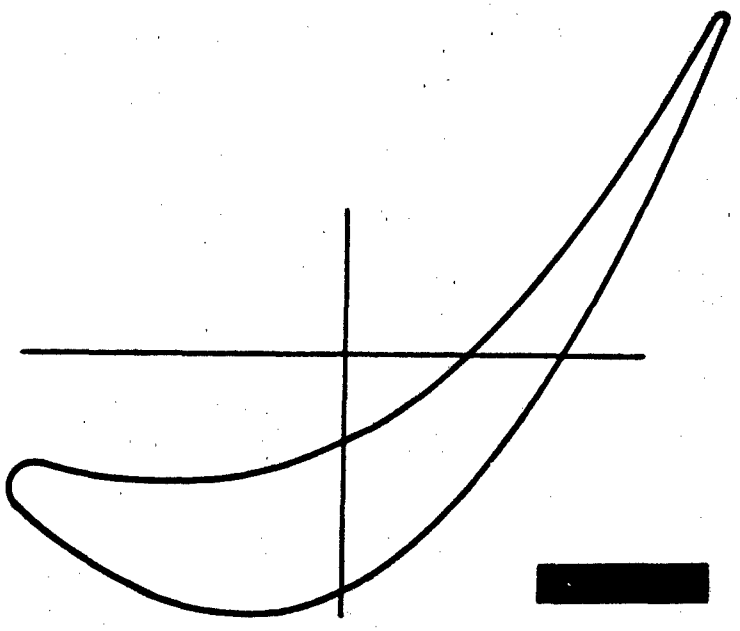

Figure 141 Section C-C, First Vane Mean, Planar

L.E. RADIUS	.0375	T.E. RADIUS	0.0100
FOIL INLET ANGLE	69.51	FOIL EXIT ANGLE	25.03
L.E. WEDGE ANGLE	24.98	T.E. WEDGE ANGLE	7.21
UNCOVERED TURN	14.31	GAGING ANGLE	25.45
NUMBER OF FOILS	88	DIAMETER HOT	19.145
PITCH HOT	0.9113	GAGING HOT	0.3916
AXIAL WIDTH	1.0485	METAL AREA	0.1657
RAD. REF. POINT X	0.4268	RAD. REF. POINT Y	0.4477
C.G. POINT X	0.4575	C.G. POINT Y	0.5500

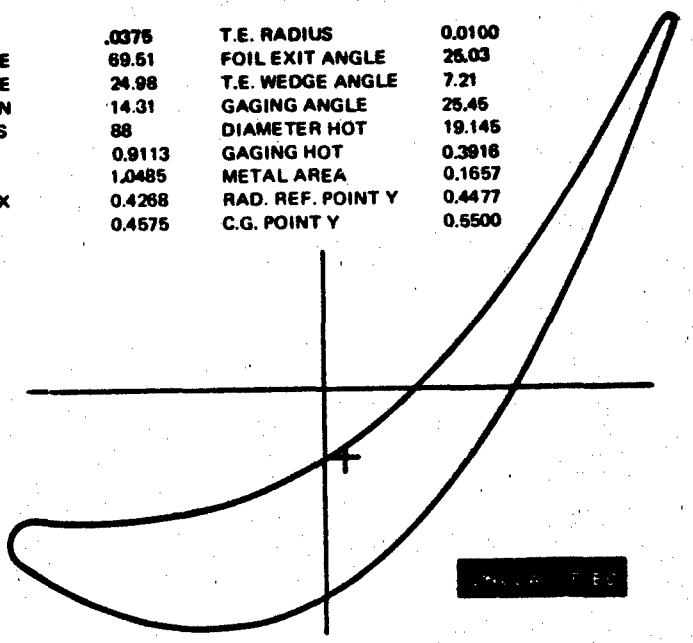

Figure 142 Section D-D, First Vane ¼ Tip, Cylindrical

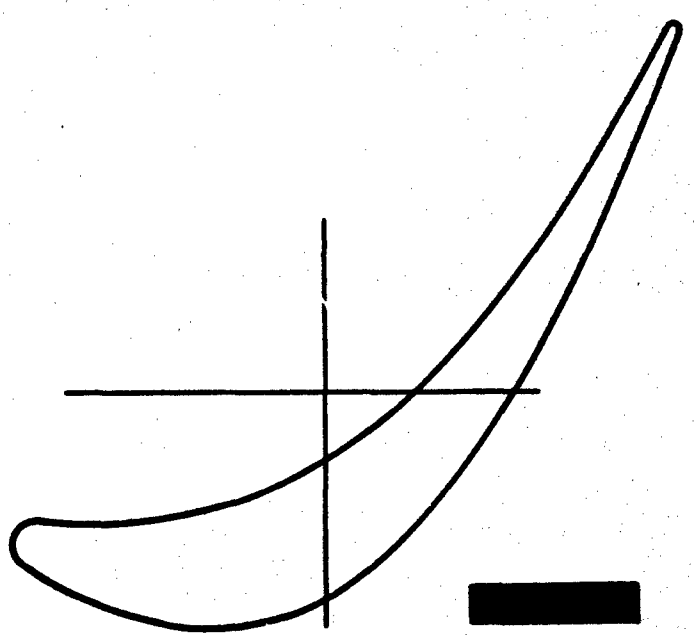

Figure 143 Section D-D, First Vane ¼ Tip, Planar

L.E. RADIUS	0.0400	T.E. RAD	0.0100
FOIL INLET ANGLE	90.00	FOIL EX GLE	26.08
L. E. WEDGE ANGLE	25.00	T. E. W D LE	7.95
UNCOVERED TURN	15.58	GAGI LE	26.70
NUMBER OF FOILS	68	DIAMETER HOT	20.260
PITCH HOT	0.9644	GAGING HOT	0.4333
AXIAL WIDTH	1.0820	METAL AREA	0.1705
RAD. REF. POINT X	0.4268	RAD. REF. POINT Y	0.4477
C.G. POINT X	0.4621	C.G. POINT Y	0.4709

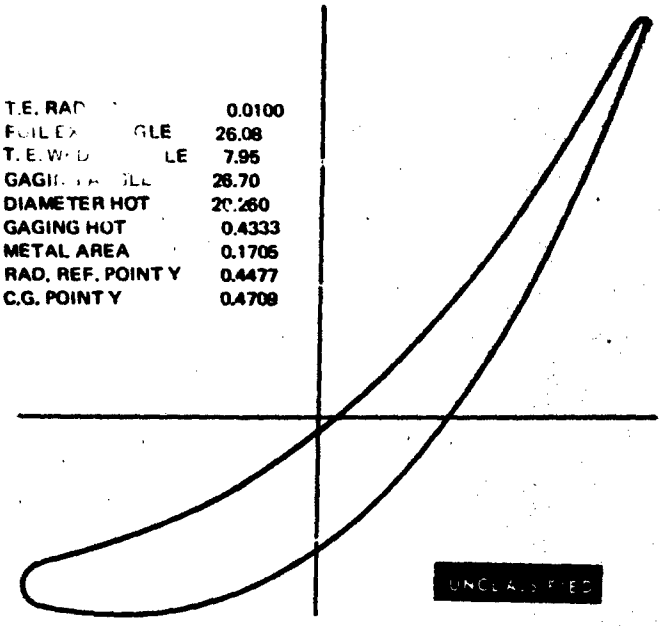

Figure 144 Section G-G, First Vane Tip, Cylindrical

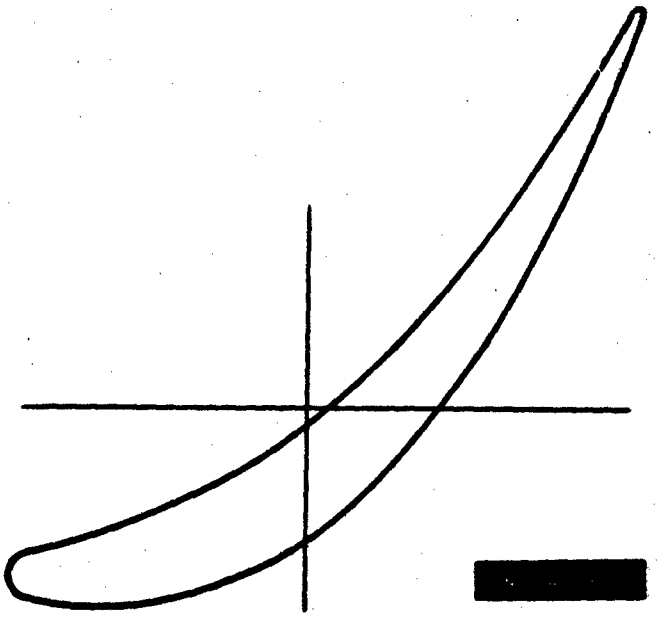

Figure 145 Section G-G, First Vane Tip, Planar

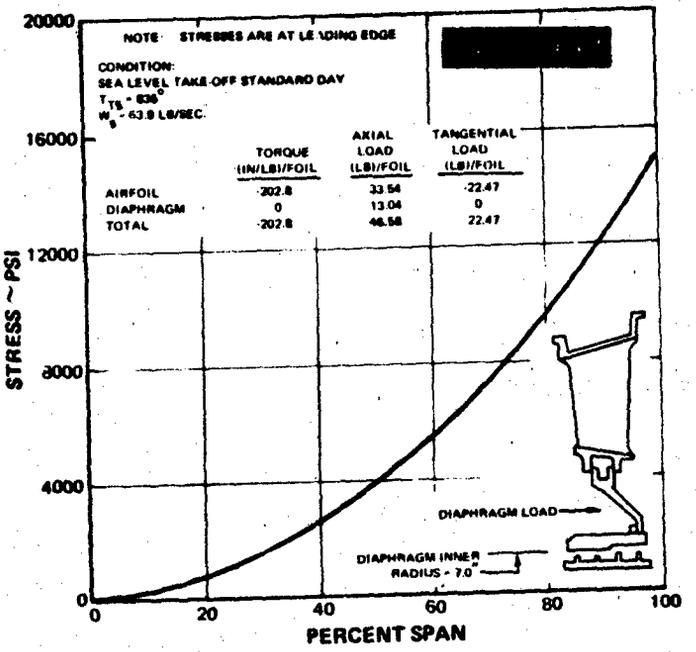

Figure 146 First-Stage Vane Gas Bending Stress versus Percent Span

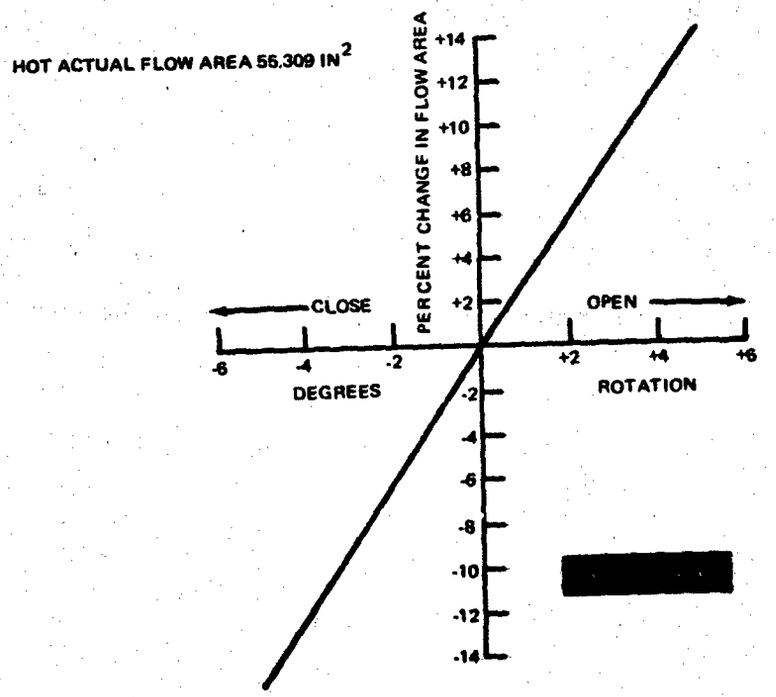

Figure 147 First-Stage Vane Flow Area versus Rotation

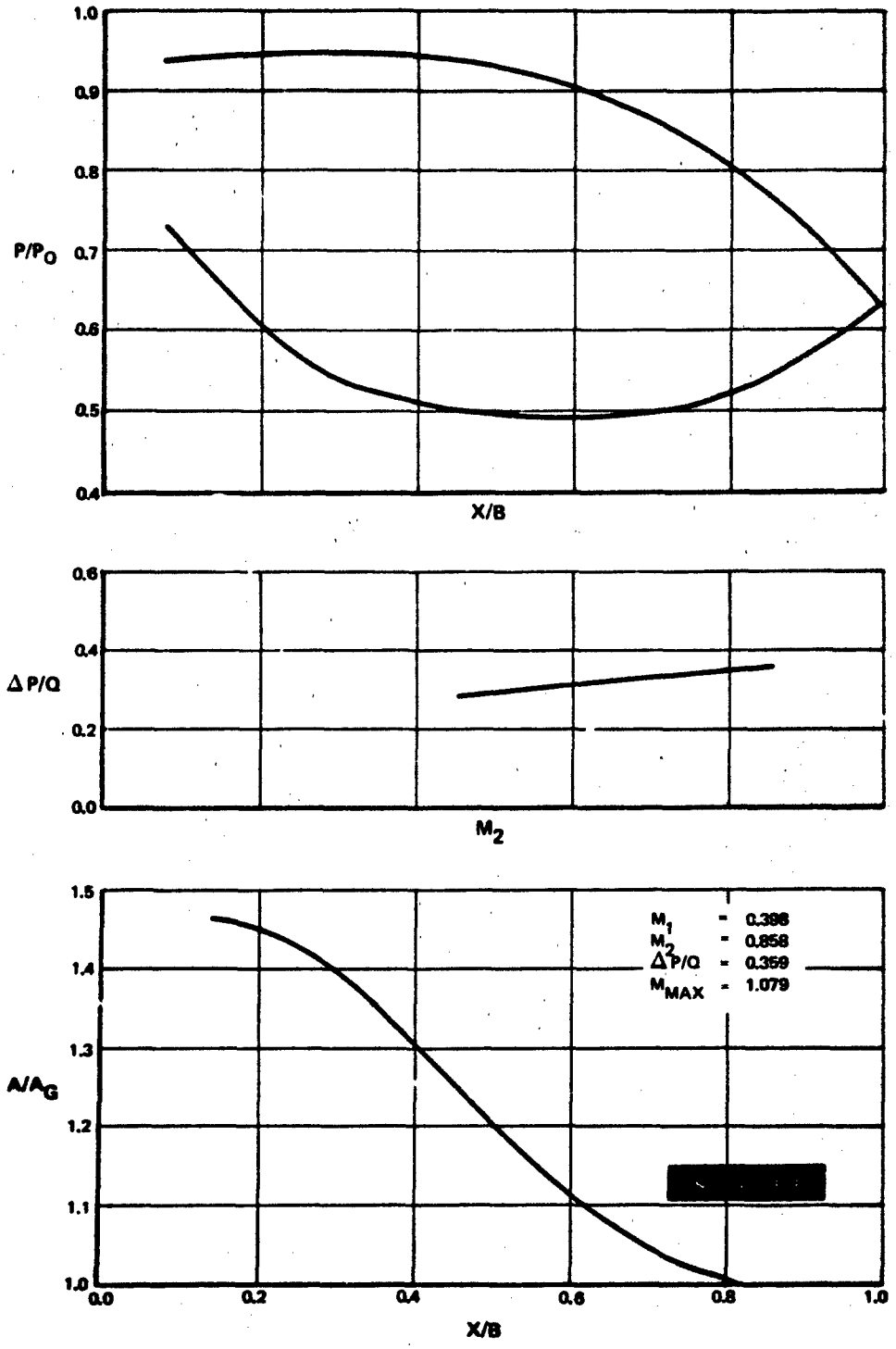

Figure 148 First-Stage Vane, Root Section

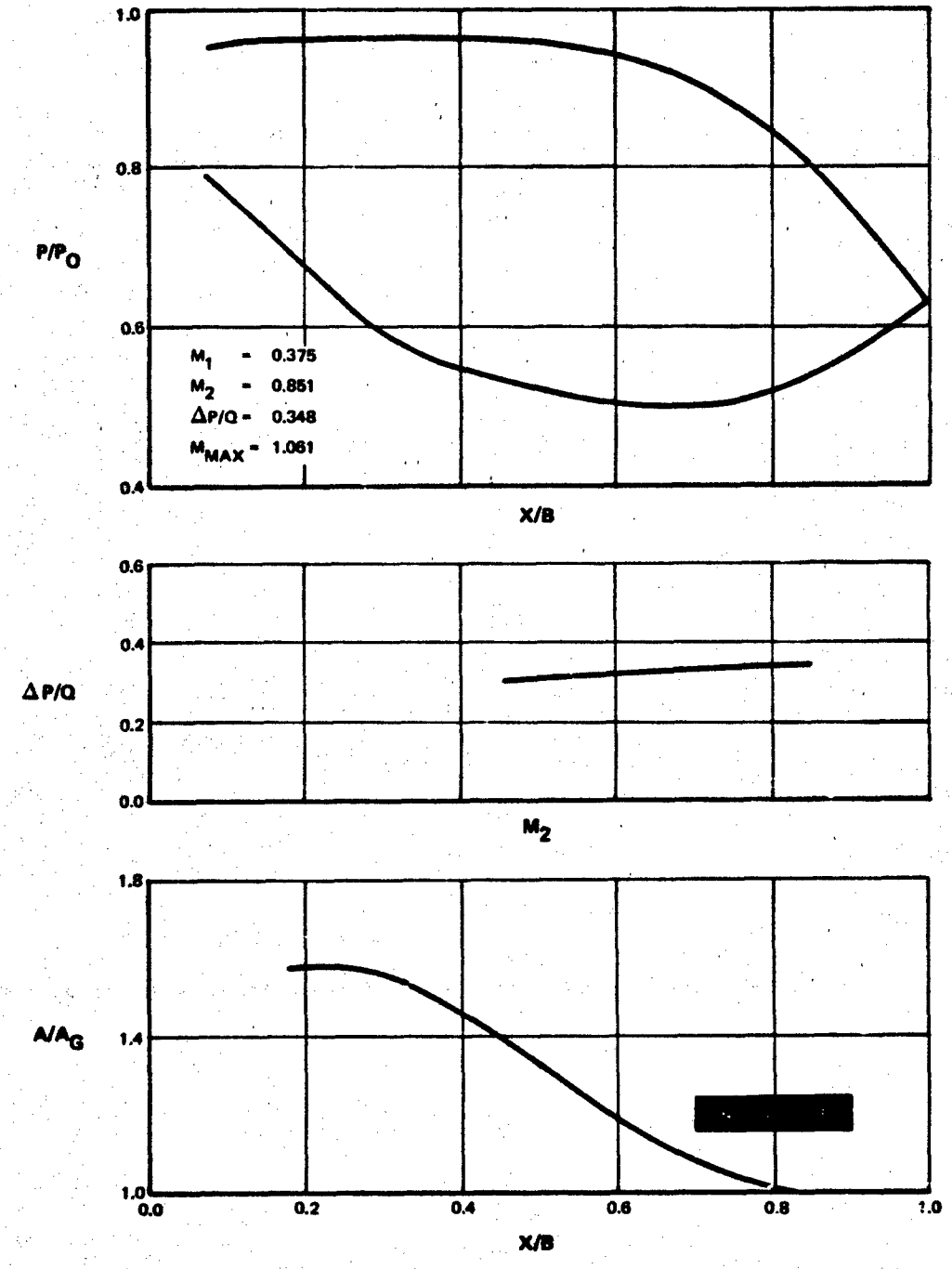

Figure 149 First-Stage Vane, ¼ Root Section

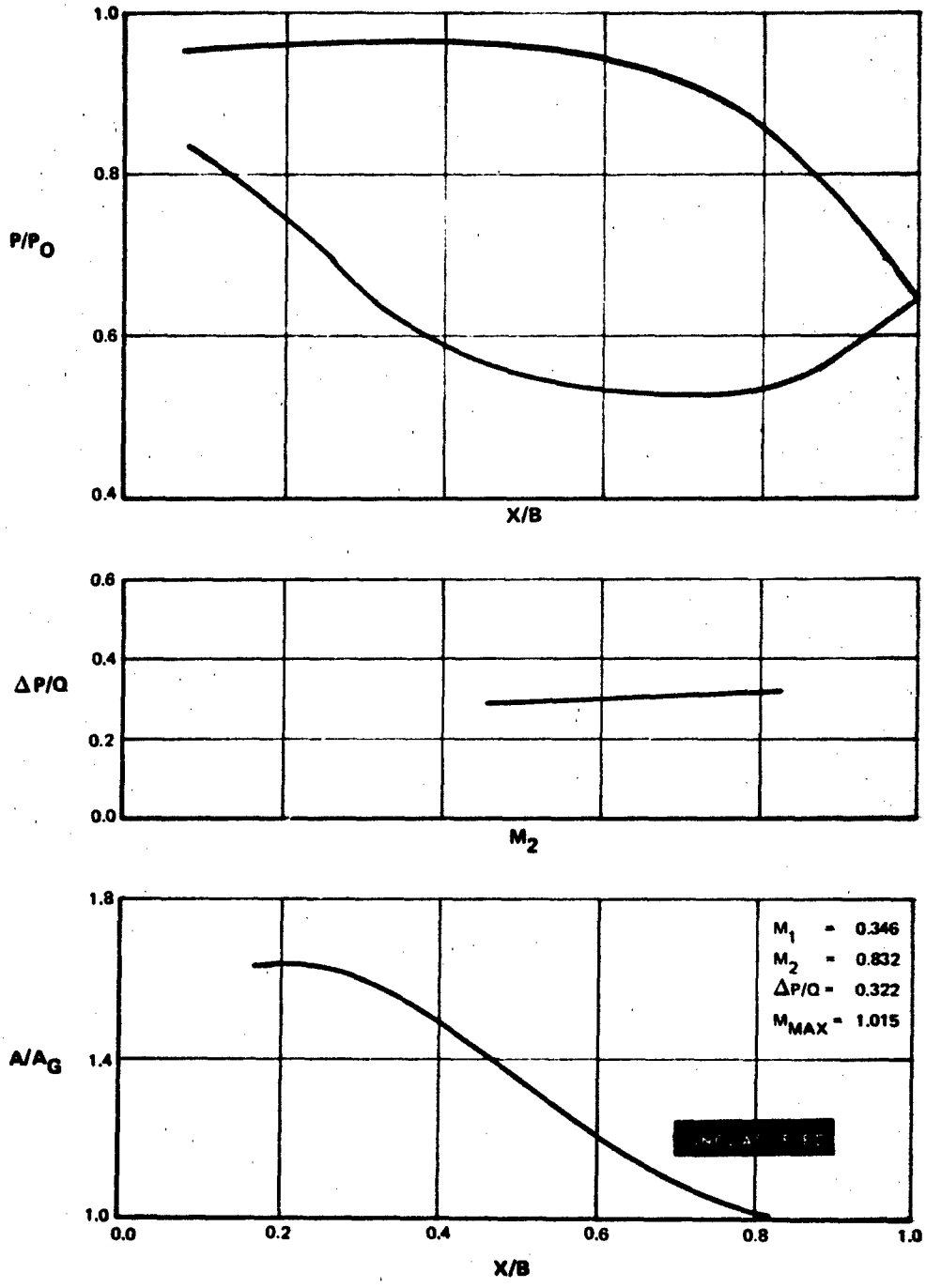

Figure 150 First-Stage Vane, Mean Section

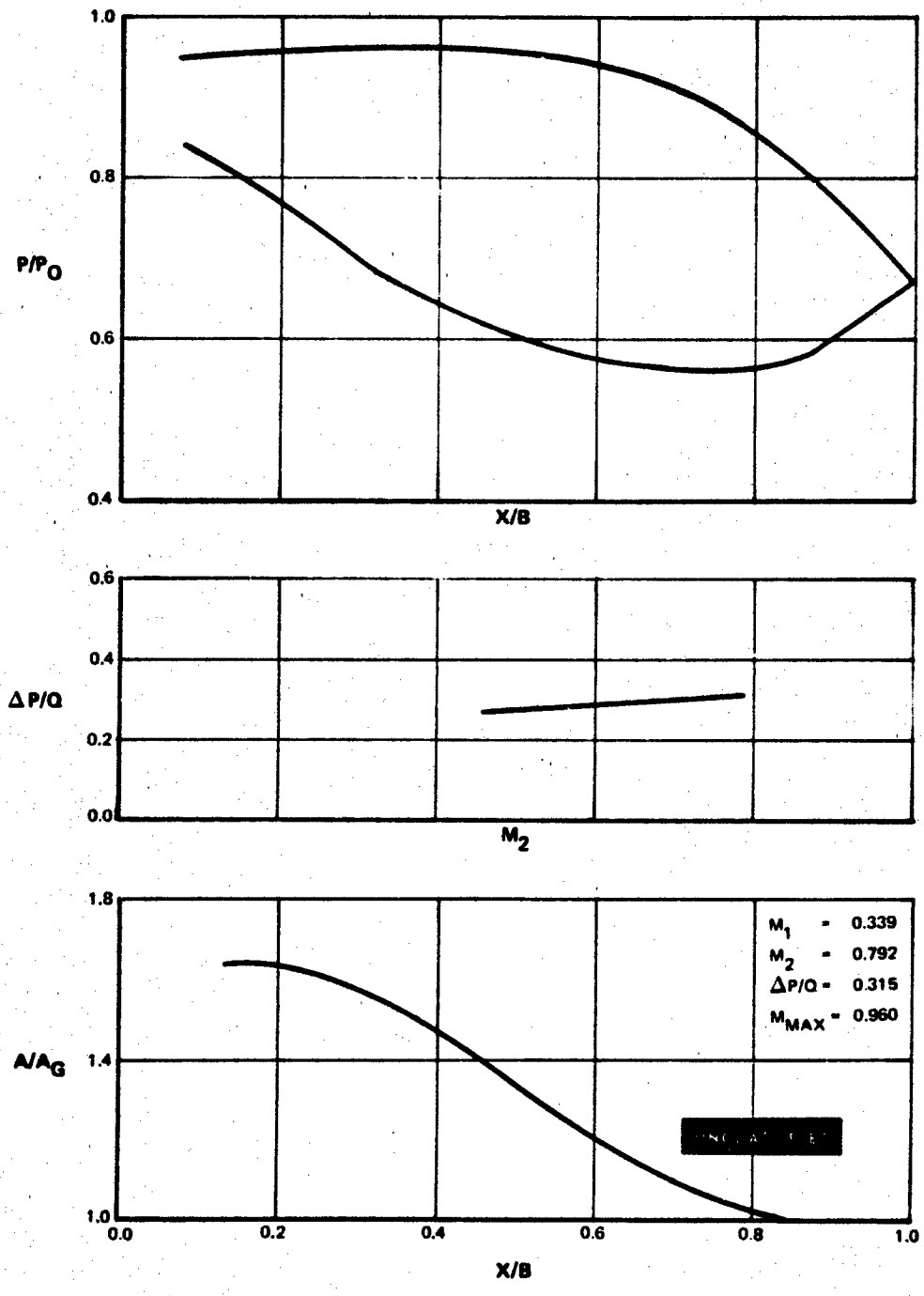

Figure 151 First-Stage Vane, ¼ Tip Section

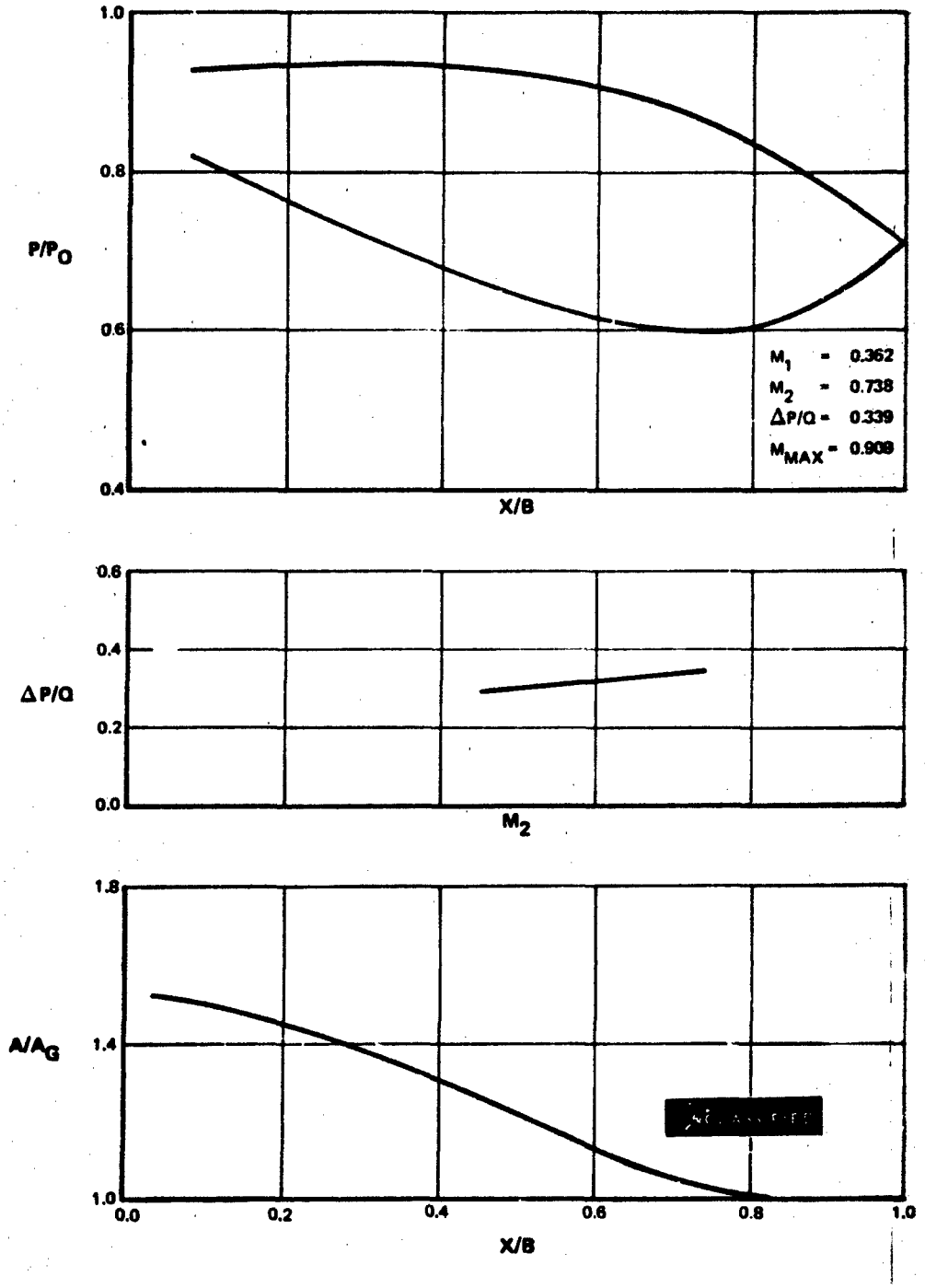

Figure 152 First-Stage Vane, Tip Section

APPENDIX II

FIRST-STAGE BLADE FINAL DESIGN

FOIL WEIGHT	0.0523 LB/FOIL
SHROUD WEIGHT	0.0110 LB/FOIL
TOTAL WEIGHT	0.0633 LB/FOIL
NO. OF FOILS	106
ρ	0.286 LB/IN^3
WEIGHT (ALL FOILS)	6.710 LBS

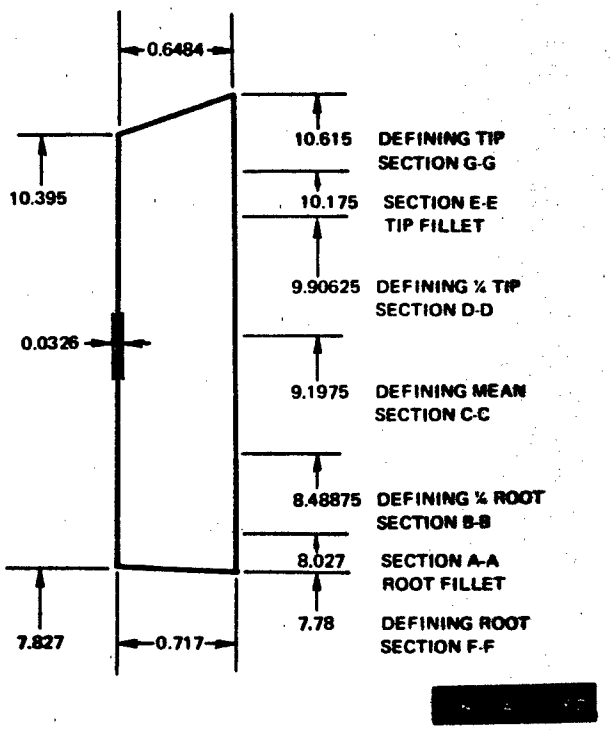

Figure 153 First-Stage Blade Elevation

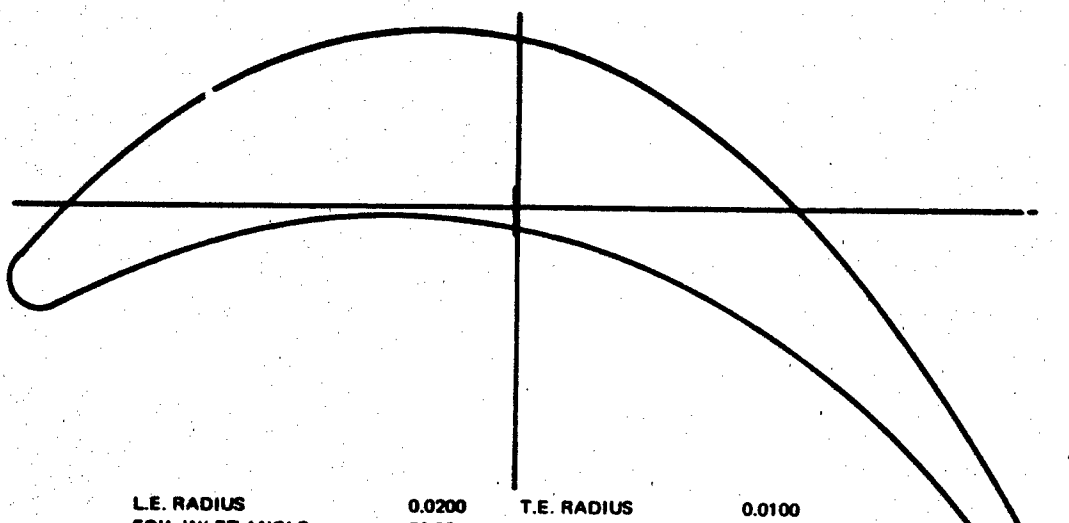

L.E. RADIUS	0.0200	T.E. RADIUS	0.0100
FOIL INLET ANGLE	50.06	FOIL EXIT ANGLE	31.99
L.E. WEDGE ANGLE	20.08	T.E. WEDGE ANGLE	4.96
UNCOVERED TURN	16.55	GAGING ANGLE	32.97
NUMBER OF FOILS	106	DIAMETER HOT	15.560
PITCH HOT	0.4612	GAGING HOT	0.2510
AXIAL WIDTH	0.7176	METAL AREA	0.0687
RAD. REF. POINT X	.03464	RAD. REF. POINT Y	0.2610
C.G. POINT X	.03464	C.G. POINT Y	0.2610

[redacted]

Figure 154 Section F-F, First Blade Root, Cylindrical

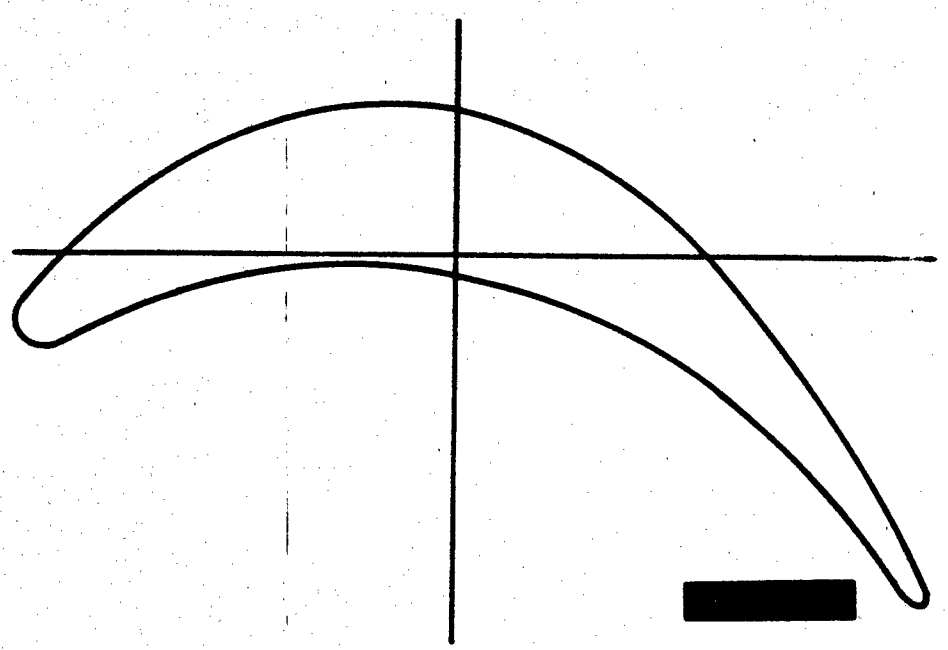

[redacted]

Figure 155 Section F-F, First Blade Root, Planar

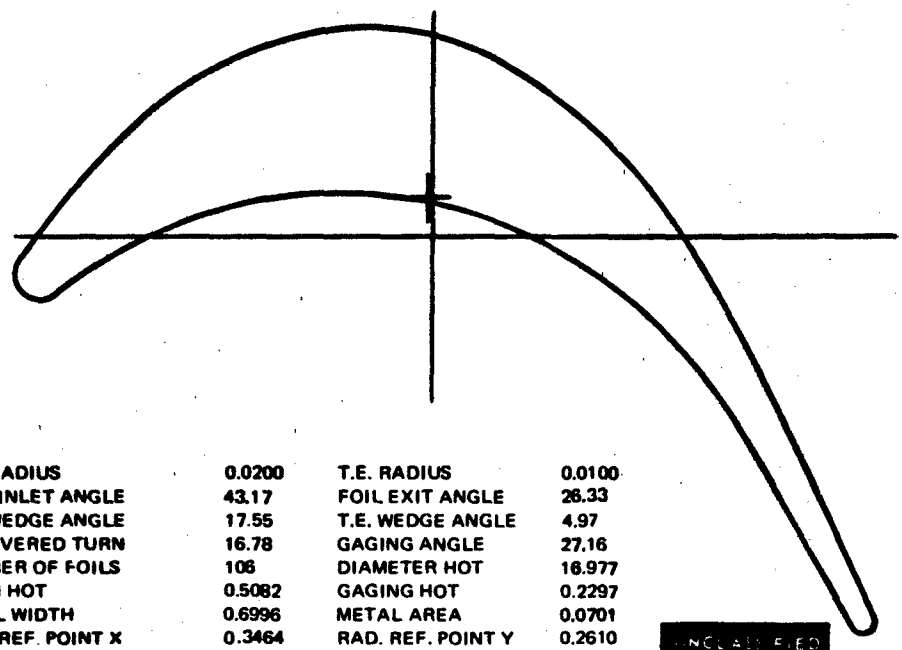

L.E. RADIUS	0.0200	T.E. RADIUS	0.0100
FOIL INLET ANGLE	43.17	FOIL EXIT ANGLE	26.33
L.E. WEDGE ANGLE	17.55	T.E. WEDGE ANGLE	4.97
UNCOVERED TURN	16.78	GAGING ANGLE	27.16
NUMBER OF FOILS	106	DIAMETER HOT	16.977
PITCH HOT	0.5082	GAGING HOT	0.2297
AXIAL WIDTH	0.6996	METAL AREA	0.0701
RAD. REF. POINT X	0.3464	RAD. REF. POINT Y	0.2610
C.G. POINT X	0.3447	C.G. POINT Y	0.2905

[redacted]

Figure 156 Section B-B, First Blade ¼ Root, Cylindrical

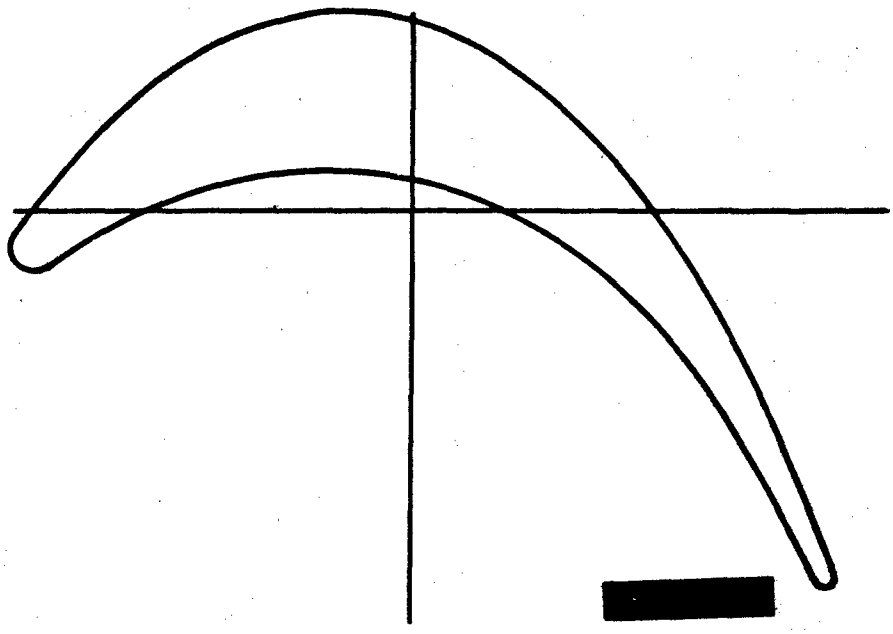

[redacted]

Figure 157 Section B-B, First Blade ¼ Root, Planar

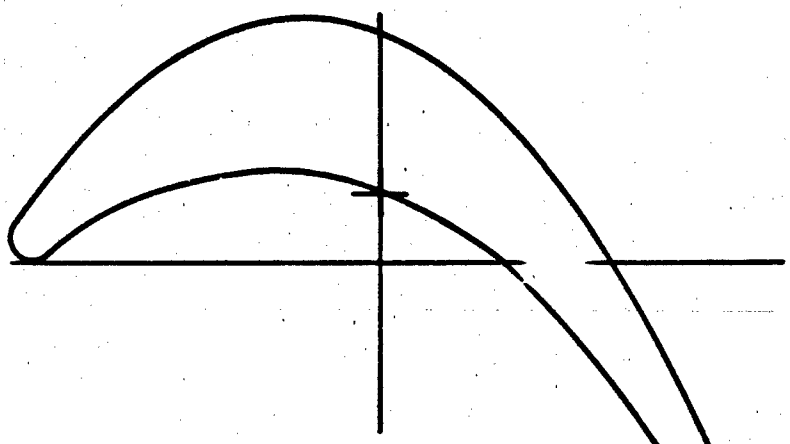

L.E. RADIUS	0.0200	T.E. RADIUS	0.0100
FOIL INLET ANGLE	42.57	FOIL EXIT ANGLE	25.96
L.E. WEDGE ANGLE	15.05	T.E. WEDGE ANGLE	4.97
UNCOVERED TURN	15.35	GAGING ANGLE	26.30
NUMBER OF FOILS	106	DIAMETER HOT	18.396
PITCH HOT	0.5452	GAGING HOT	0.2416
AXIAL WIDTH	0.6816	METAL AREA	0.0710
RAD. REF. POINT X	0.3464	RAD. REF. POINT Y	0.2610
C.G. POINT X	0.3524	C.G. POINT Y	0.3200

NCLASSIF ED

Figure 158 Section C-C, First Blade Mean, Cylindrical

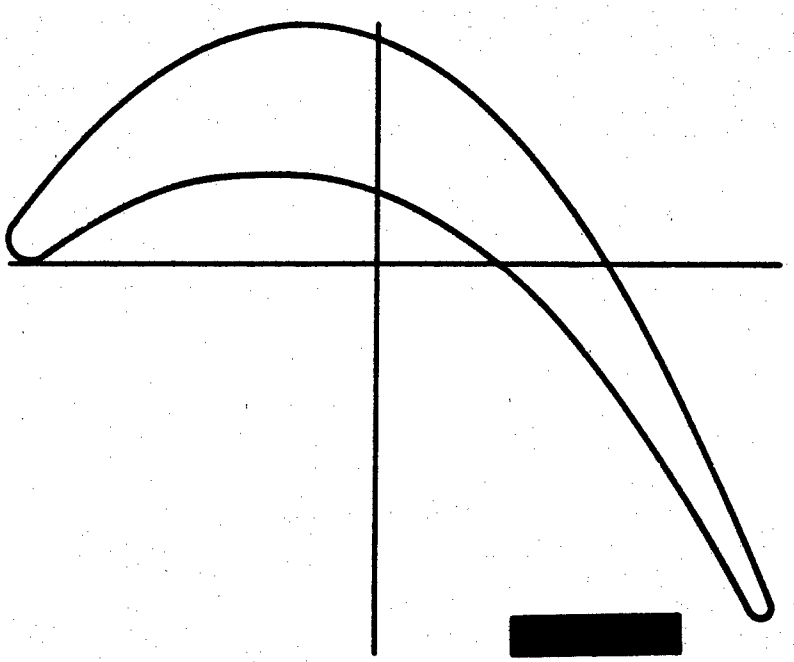

Figure 159 Section C-C, First Blade Mean, Planar

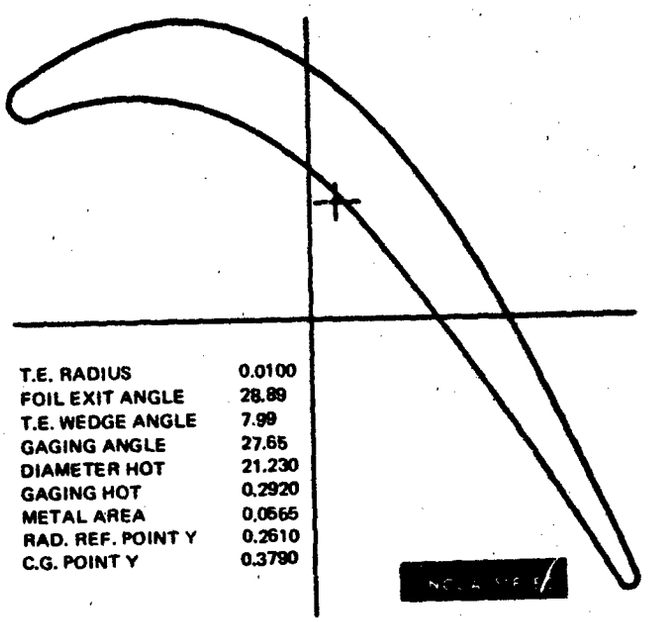

L.E. RADIUS	0.0200	T.E. RADIUS	0.0100
FOIL INLET ANGLE	60.49	FOIL EXIT ANGLE	28.89
L.E. WEDGE ANGLE	15.03	T.E. WEDGE ANGLE	7.99
UNCOVERED TURN	14.94	GAGING ANGLE	27.65
NUMBER OF FOILS	106	DIAMETER HOT	21.230
PITCH HOT	0.6292	GAGING HOT	0.2920
AXIAL WIDTH	0.6456	METAL AREA	0.0565
RAD. REF. POINT X	0.3464	RAD. REF. POINT Y	0.2610
C. G. POINT X	0.3765	C.G. POINT Y	0.3790

Figure 160 Section G-G, First Blade Tip, Cylindrical

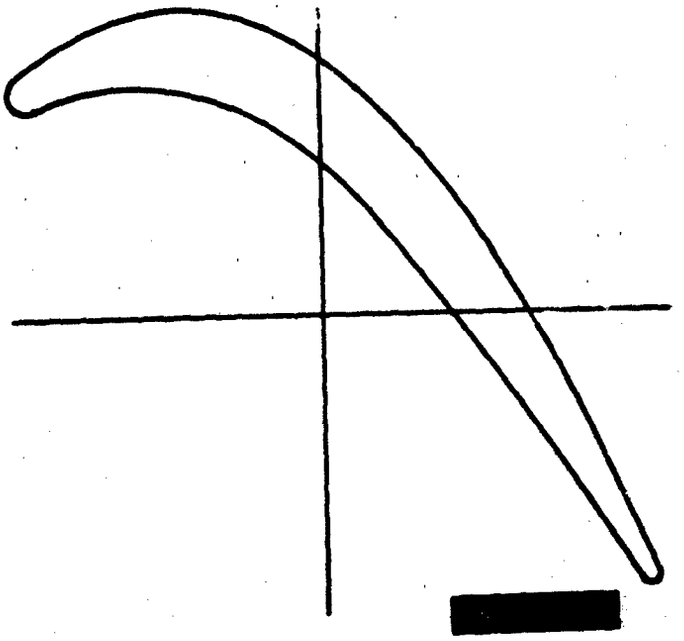

Figure 161 Section G-G, First Blade Tip, Planar

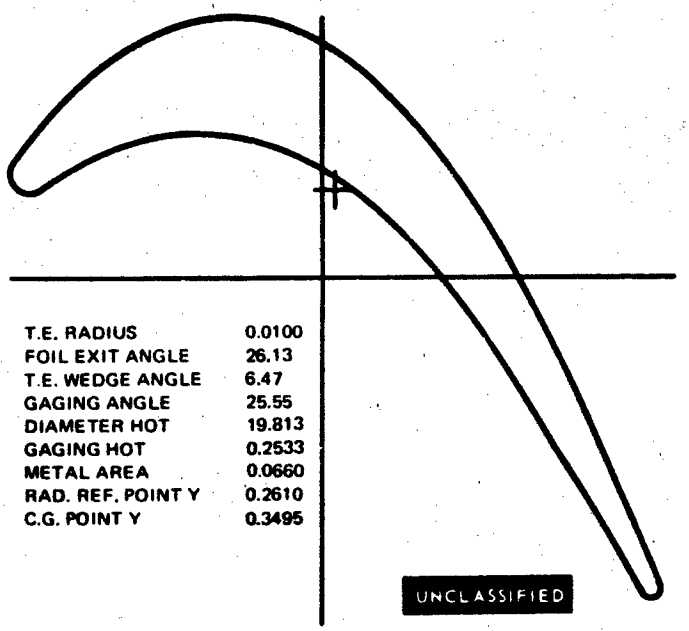

L.E. RADIUS	0.0200	T.E. RADIUS	0.0100
FOIL INLET ANGLE	44.56	FOIL EXIT ANGLE	26.13
L.E. WEDGE ANGLE	15.05	T.E. WEDGE ANGLE	6.47
UNCOVERED TURN	14.07	GAGING ANGLE	25.55
NUMBER OF FOILS	106	DIAMETER HOT	19.813
PITCH HOT	0.5872	GAGING HOT	0.2533
AXIAL WIDTH	0.6636	METAL AREA	0.0660
RAD. REF. POINT X	0.3464	RAD. REF. POINT Y	0.2610
C.G. POINT X	0.3590	C.G. POINT Y	0.3495

Figure 162 Section D-D, First Blade ¼ Tip, Cylindrical

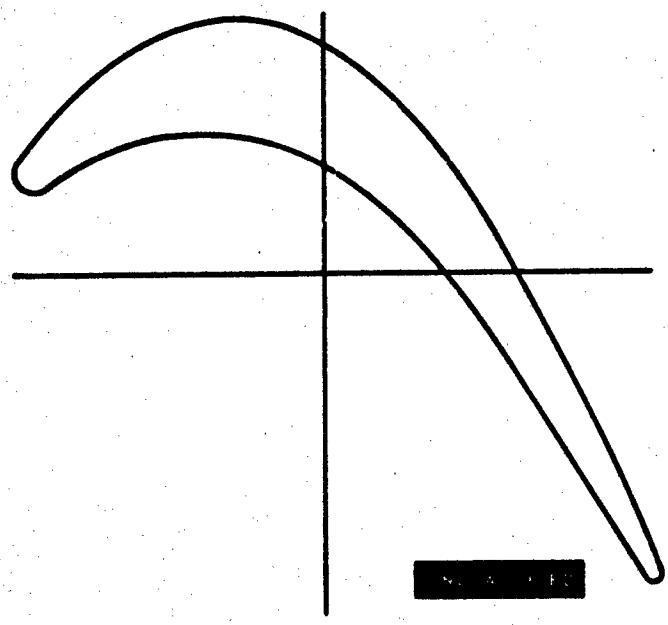

Figure 163 Section D-D, First Blade ¼ Tip, Planar

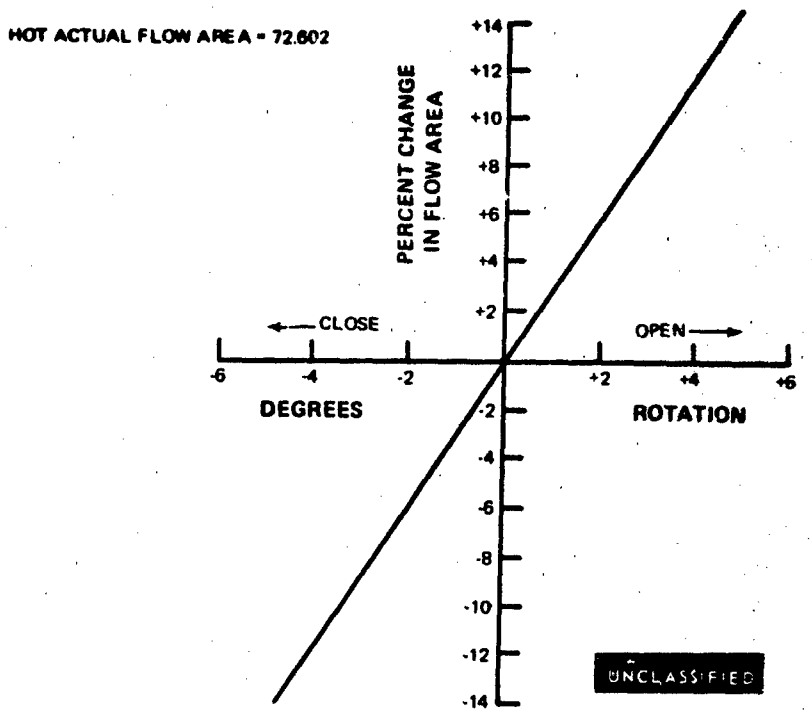

Figure 164 First-Stage Blade Flow Area Versus Rotation

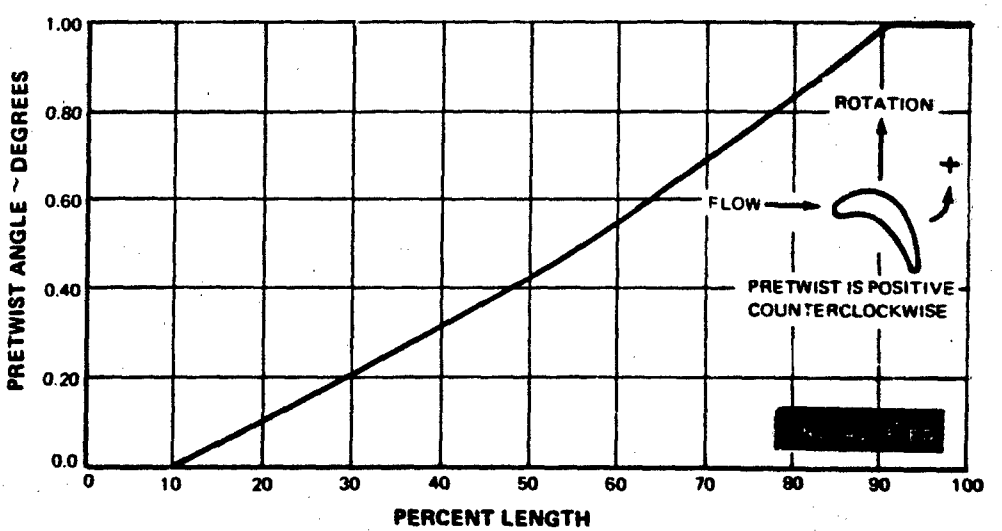

Figure 165 First-Stage Blade Pretwist Versus Percent Length

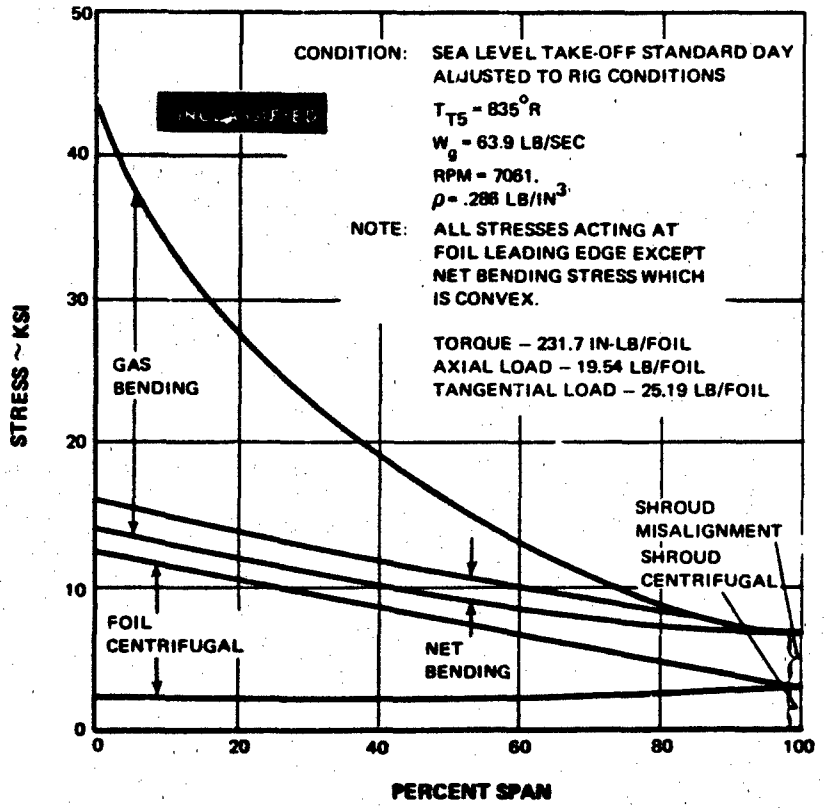

Figure 166 First-Stage Blade Stress

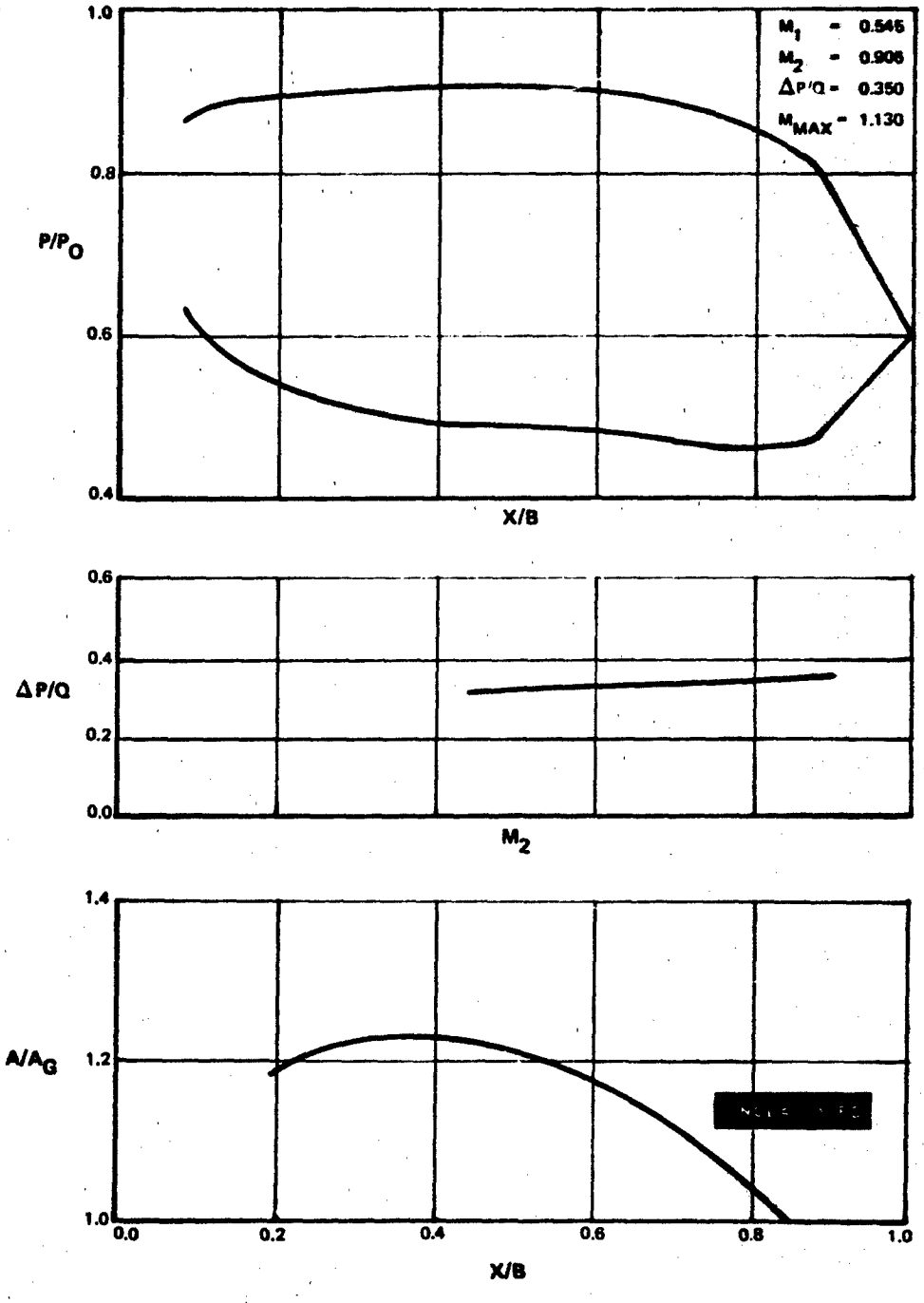

Figure 167 First-Stage Blade, Root Section

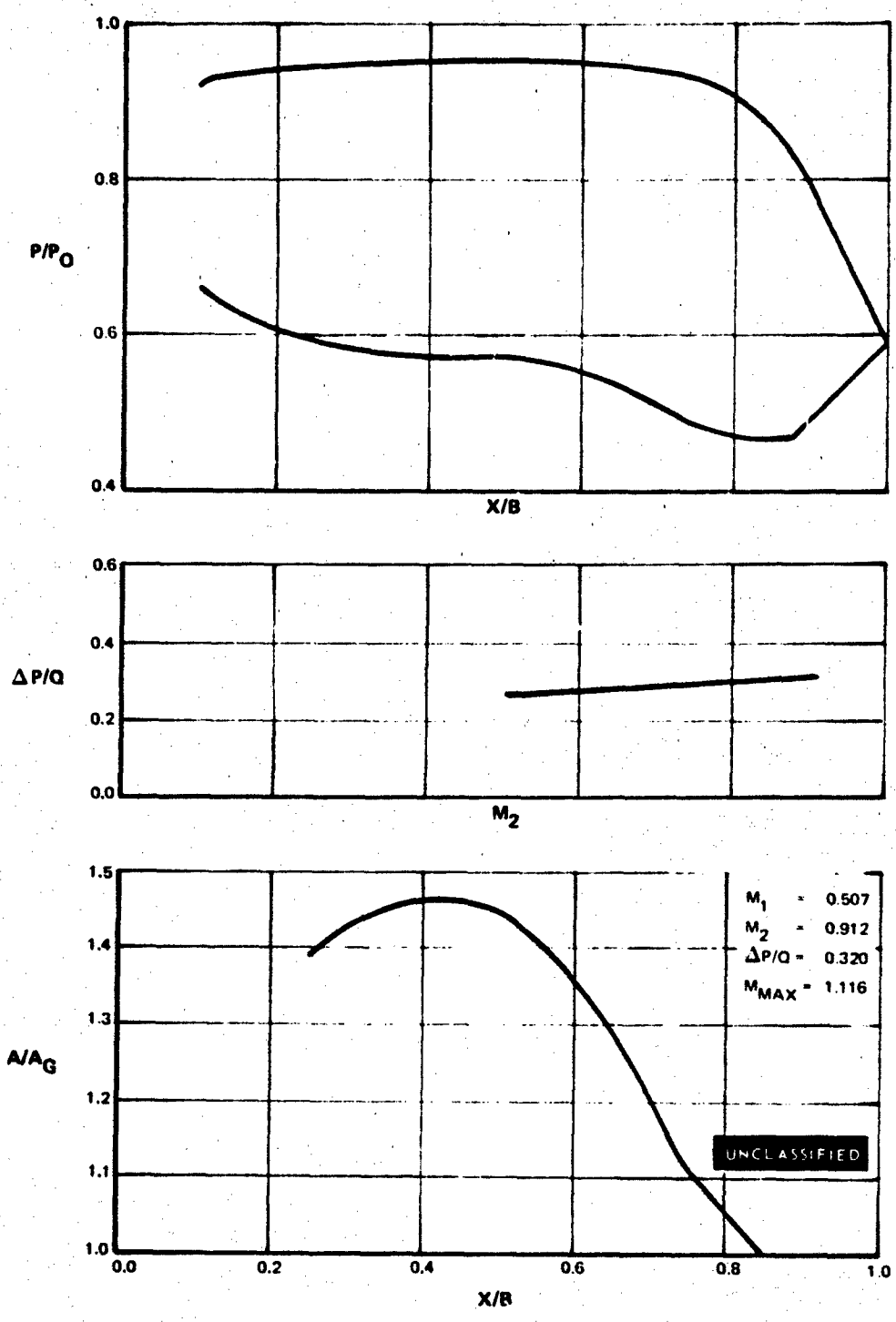

Figure 168 First-Stage Blade, ¼ Root Section

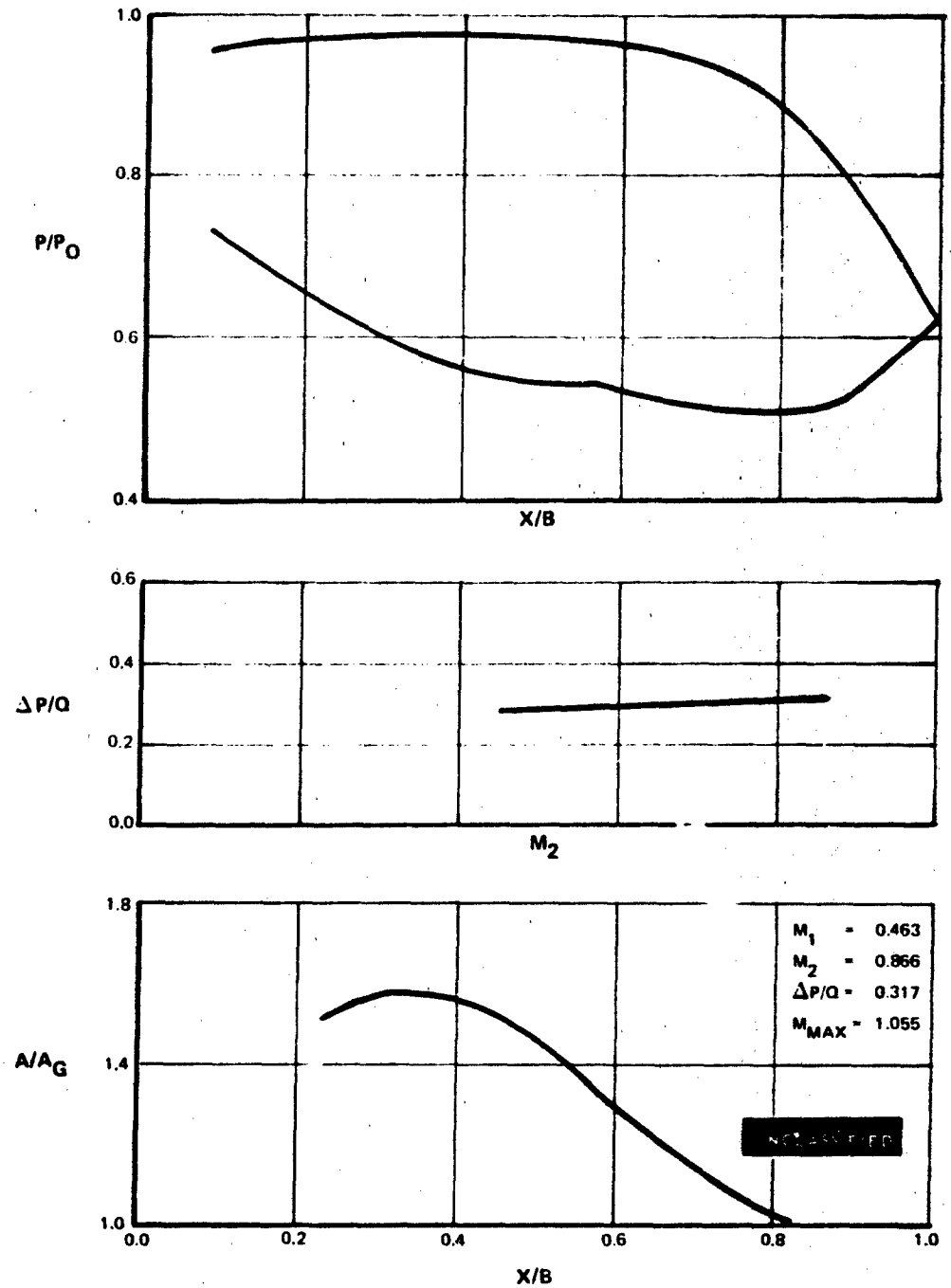

Figure 169 First-Stage Blade, Mean Section

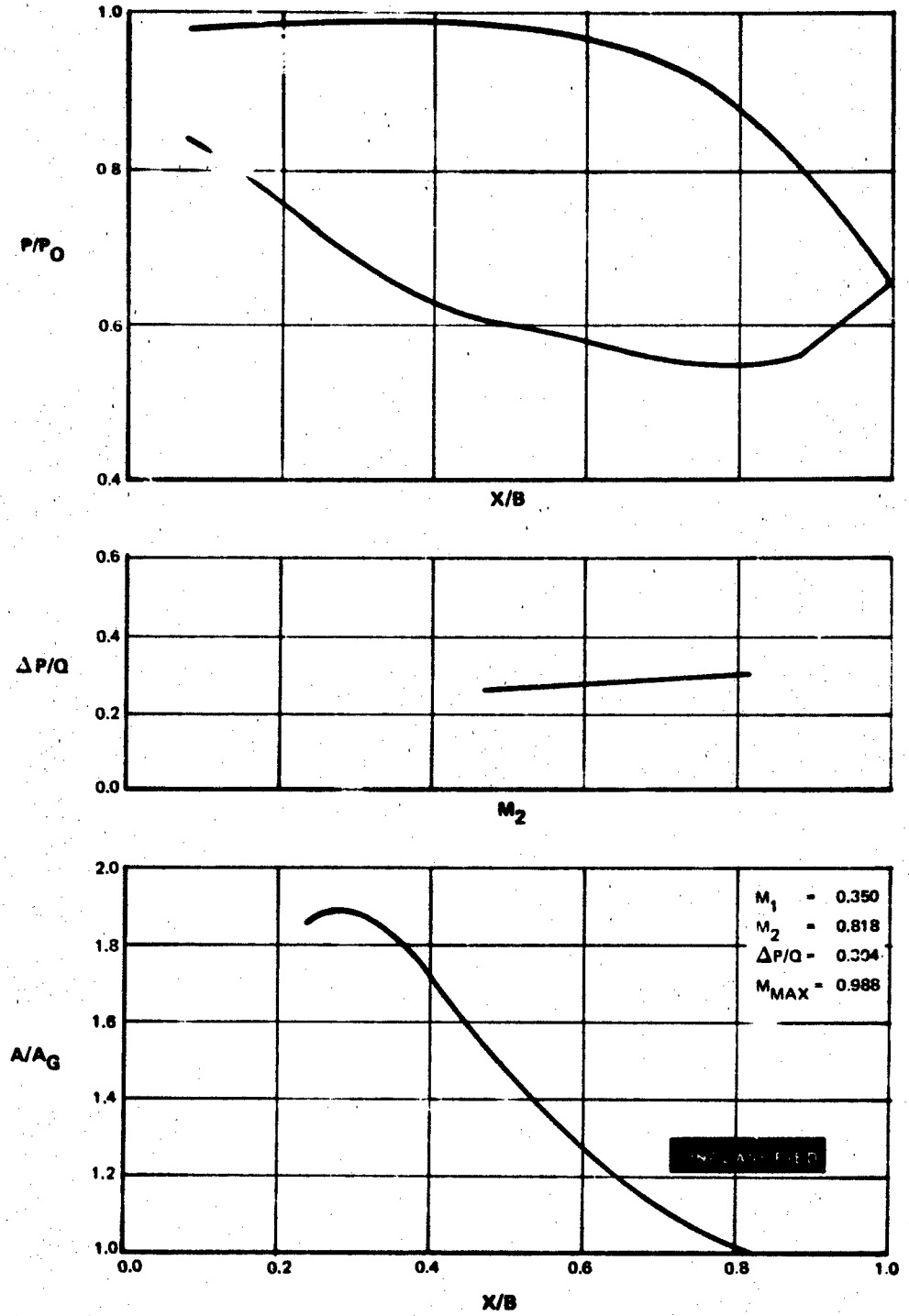

Figure 170 First-Stage Blade, ¼ Tip Section

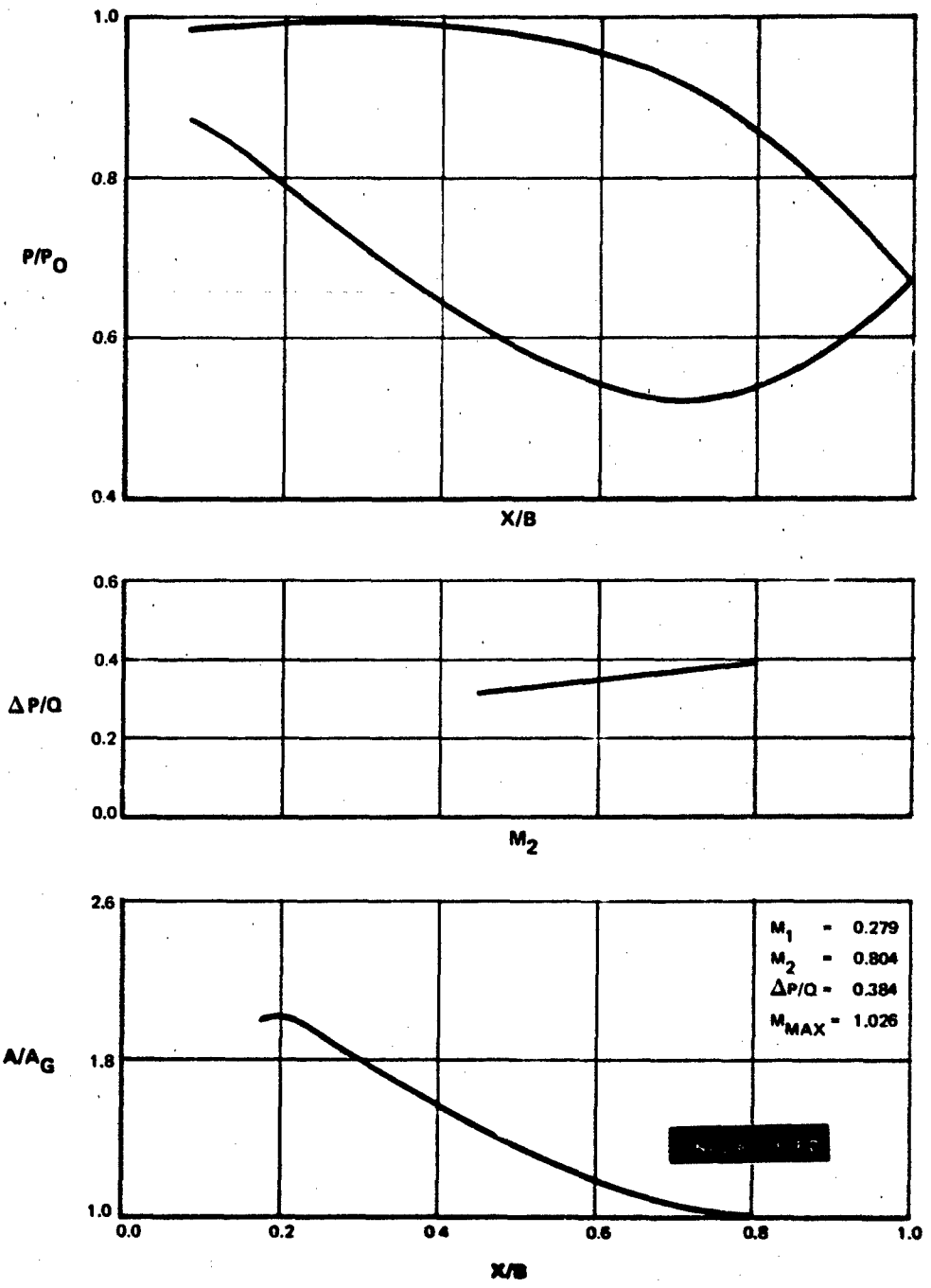

Figure 171 First-Stage Blade, Tip Section

(The reverse of this page is blank.)

APPENDIX III

SECOND-STAGE VANE FINAL DESIGN

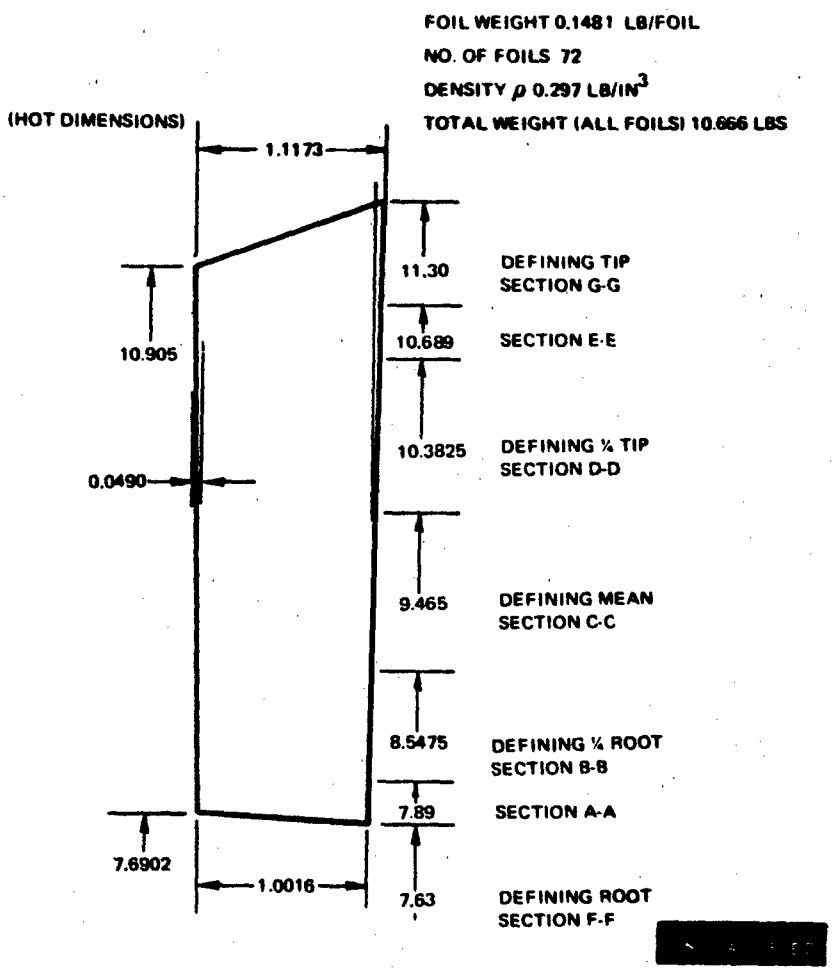

Figure 172 Second-Stage Vane Elevation (Hot Dimensions)

L.E. RADIUS	0.0200	T.E. RADIUS	0.0100
FOIL INLET ANGLE	46.89	FOIL EXIT ANGLE	36.50
L.E. WEDGE ANGLE	16.04	T.E. WEDGE ANGLE	4.98
UNCOVERED TURN	14.30	GAGING ANGLE	36.03
NUMBER OF FOILS	72	DIAMETER HOT	15.260
PITCH HOT	0.6658	GAGING HOT	0.3917
AXIAL WIDTH	0.9980	METAL AREA	0.1018
RAD. REF. POINT X	0.4700	RAD. REF. POINT Y	0.3703
C.G. POINT X	0.4700	C.G. POINT Y	0.3703

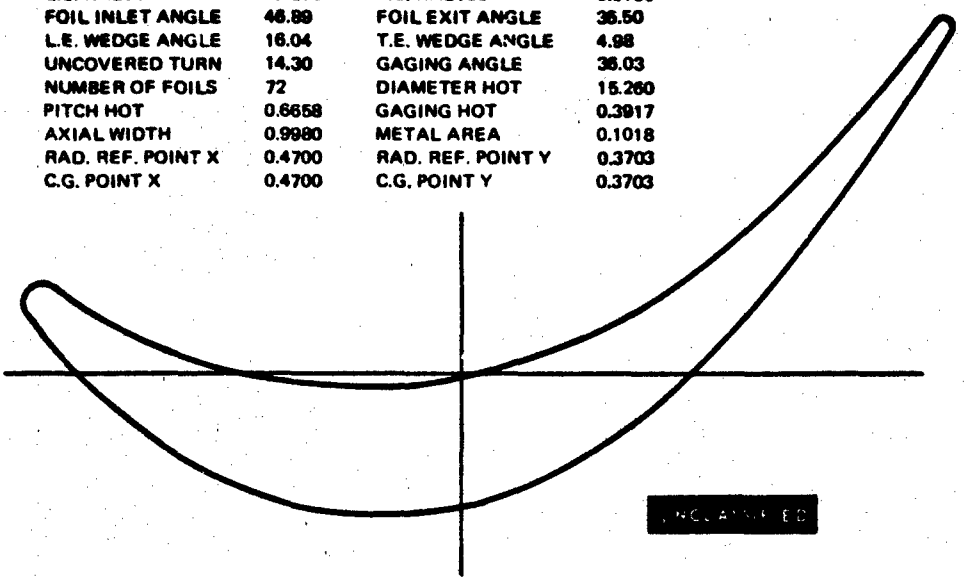

Figure 173 Section F-F, Second Vane Root, Cylindrical

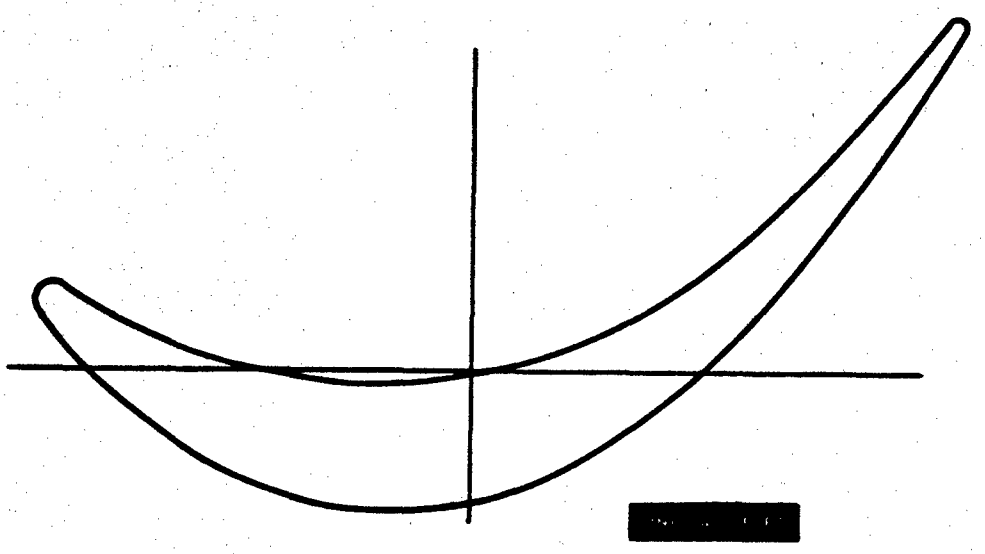

Figure 174 Section F-F, Second Vane Root, Planar

L.E. RADIUS	0.0200	L.E. RADIUS	0.0100
FOIL INLET ANGLE	37.96	FOIL EXIT ANGLE	28.15
L.E. WEDGE ANGLE	17.88	T.E. WEDGE ANGLE	5.91
UNCOVERED TURN	14.32	GAGING ANGLE	28.49
NUMBER OF FOILS	72	DIAMETER HOT	17.095
PITCH HOT	0.7459	GAGING HOT	0.3658
AXIAL WIDTH	1.0275	METAL AREA	0.1353
RAD. REF. POINT X	0.4700	RAD.REF.POINT Y	0.3703
C.G. POINT X	0.4765	C.G. POINT Y	0.4218

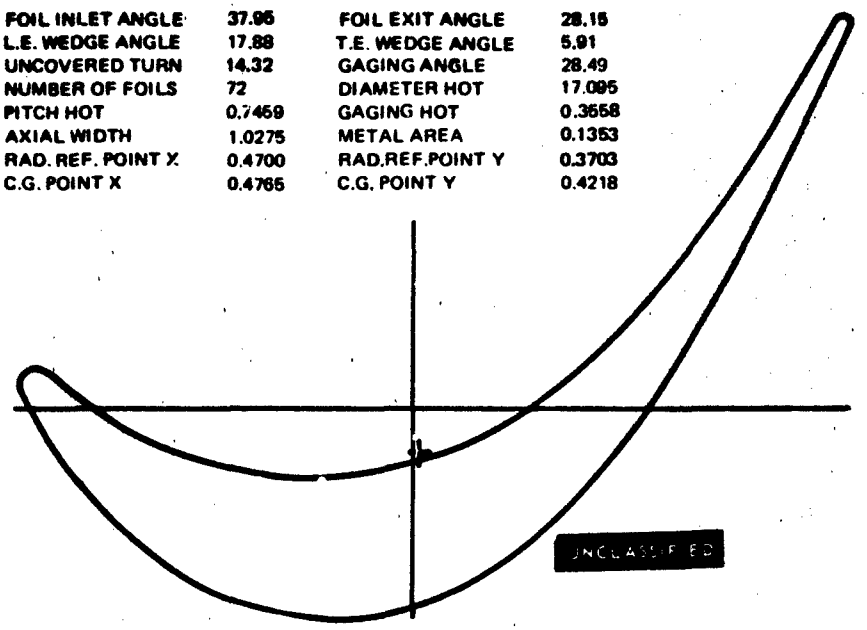

Figure 175 Section B-B, Second Vane ¼ Root, Cylindrical

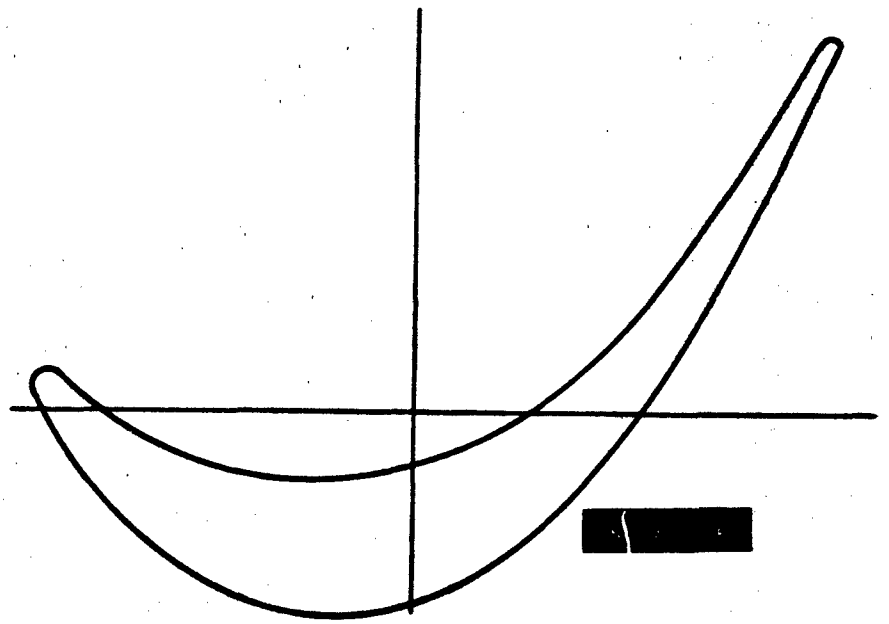

Figure 176 Section B-B, Second Vane ¼ Root, Planar

L.E. RADIUS	0.0200	T.E. RADIUS	0.0100
FOIL INLET ANGLE	44.21	FOIL EXIT ANGLE	25.50
L.E. WEDGE ANGLE	19.96	T.E. WEDGE ANGLE	6.94
UNCOVERED TURN	15.63	GAGING ANGLE	25.95
NUMBER OF FOILS	72	DIAMETER HOT	18.930
PITCH	0.8260	GAGING HOT	0.3614
AXIAL WIDTH	1.0570	METAL AREA	0.1590
RAD. REF. POINT X	0.4700	RAD. REF. POINT Y	0.3703
C.G. POINT X	0.4955	C.G. POINT Y	0.4212

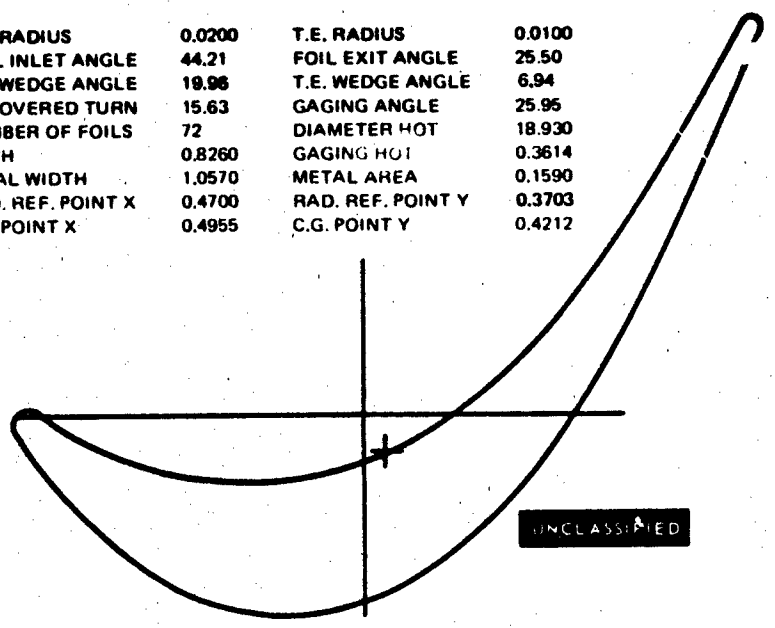

Figure 177 Section C-C, Second Vane Mean, Cylindrical

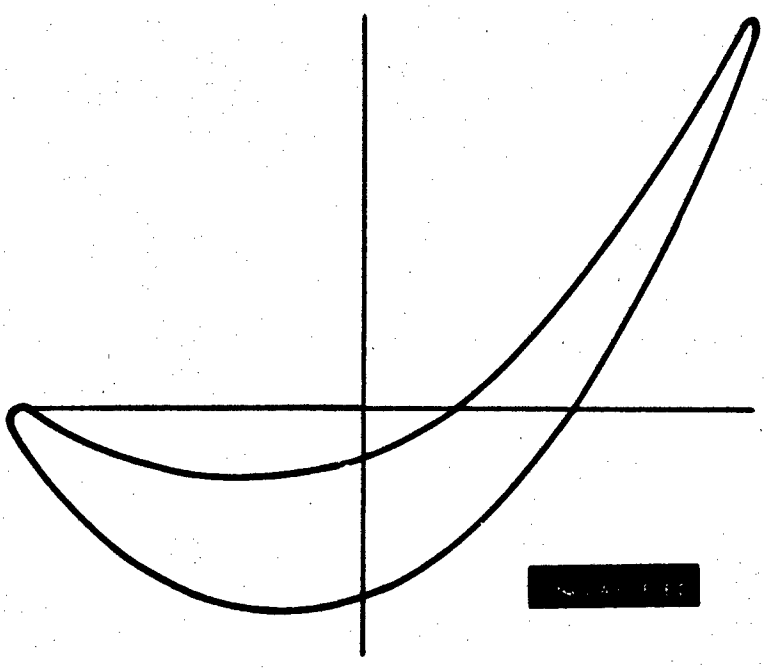

Figure 178 Section C-C, Second Vane Mean, Planar

L.E. RADIUS	0.0200	T.E. RADIUS	0.0100
FOIL INLET ANGLE	61.58	FOIL EXIT ANGLE	24.61
L.E. WEDGE ANGLE	20.01	T.E. WEDGE ANGLE	6.46
UNCOVERED TURN	14.02	GAGING ANGLE	24.88
NUMBER OF FOILS	72	DIAMETER HOT	20.765
PITCH HOT	0.9060	GAGING HOT	0.3306
AXIAL WIDTH	1.0885	METAL AREA	0.1556
RAD. REF. POINT X	0.4700	RAD. REF. POINT Y	0.3703
C.G. POINT X	0.5035	C.G. POINT Y	0.3910

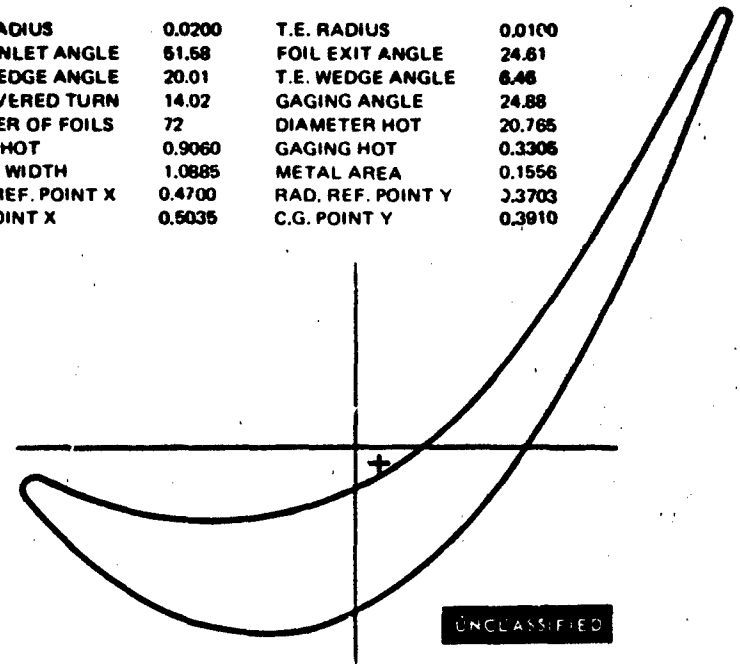

Figure 179 Section D-D, Second Vane ¼ Tip, Cylindrical

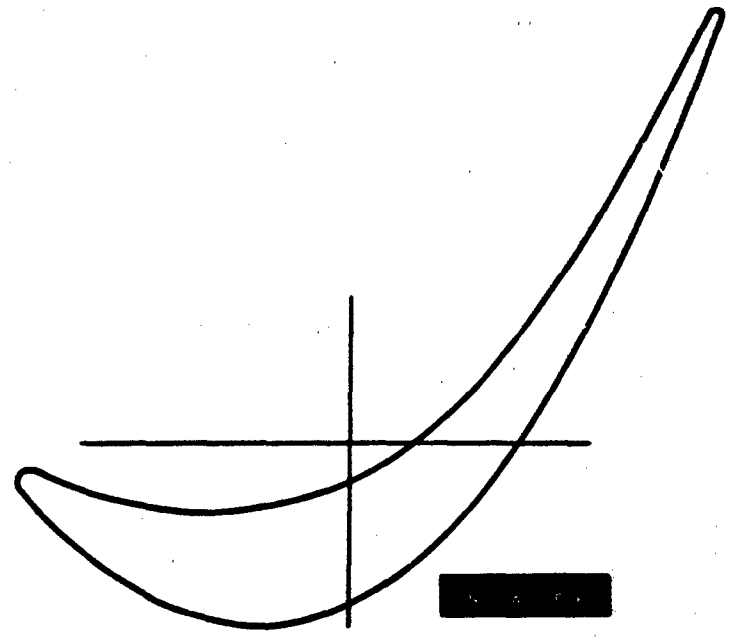

Figure 180 Section D-D, Second Vane ¼ Tip, Planar

L.E. RADIUS	0.0200	T.E. RADIUS	0.0100
FOIL INLET ANGLE	60.70	FOIL EXIT ANGLE	26.86
L.E. WEDGE ANGLE	20.08	T.E. WEDGE ANGLE	5.98
UNCOVERED TURN	13.60	GAGING ANGLE	26.85
NUMBER OF FOILS	72	DIAMETER HOT	22.600
PITCH HOT	0.9861	GAGING HOT	0.4454
AXIAL WIDTH	1.1160	METAL AREA	0.1525
RAD. REF. POINT X	0.4700	RAD. REF. POINT Y	0.3703
C.G. POINT X	0.5141	C.G. POINT Y	0.3551

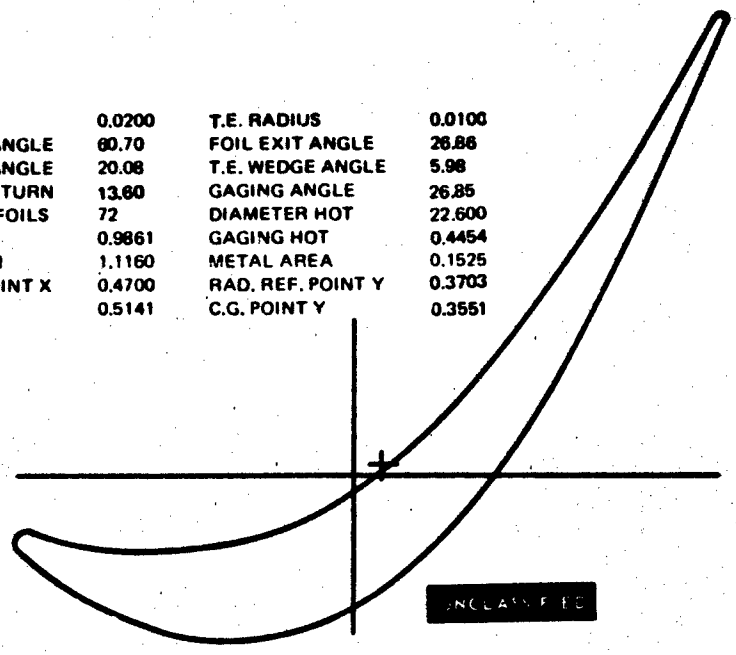

Figure 181 Section G-G, Second Vane Tip, Cylindrical

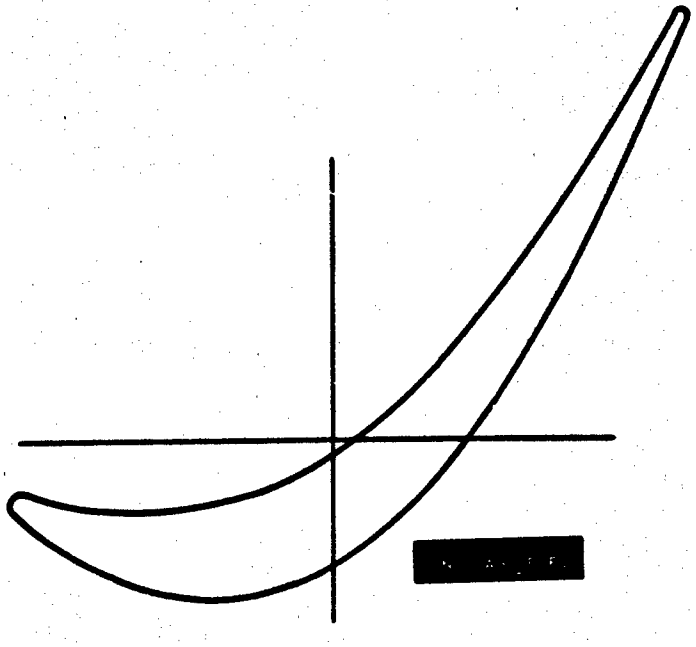

Figure 182 Section G-G, Second Vane Tip, Planar

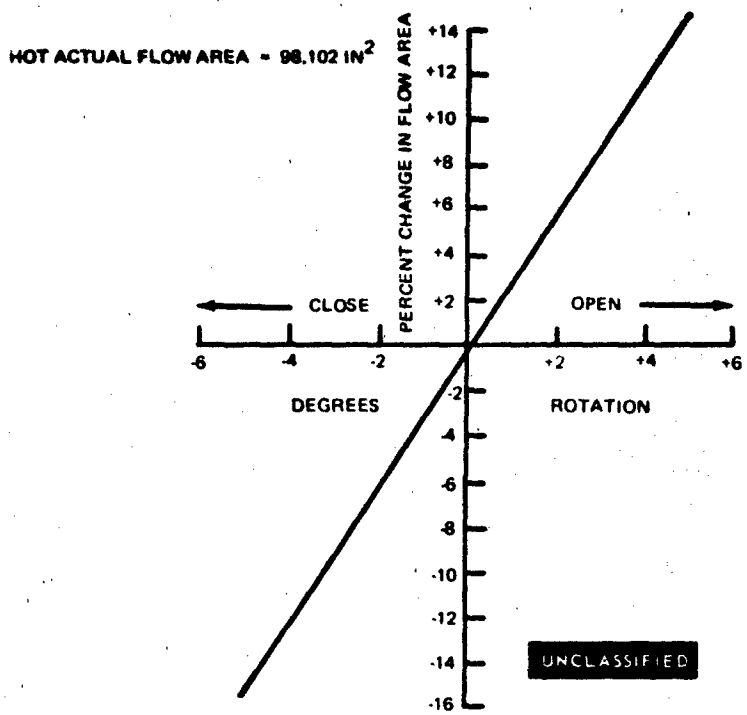

Figure 183 Second-Stage Vane Flow Area Versus Rotation

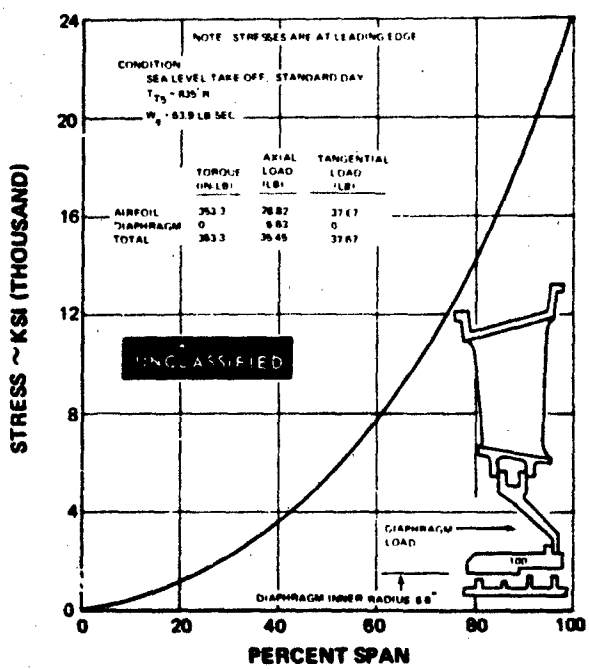

Figure 184 Second-Stage Vane, Gas Bending Stress Versus Percent Span

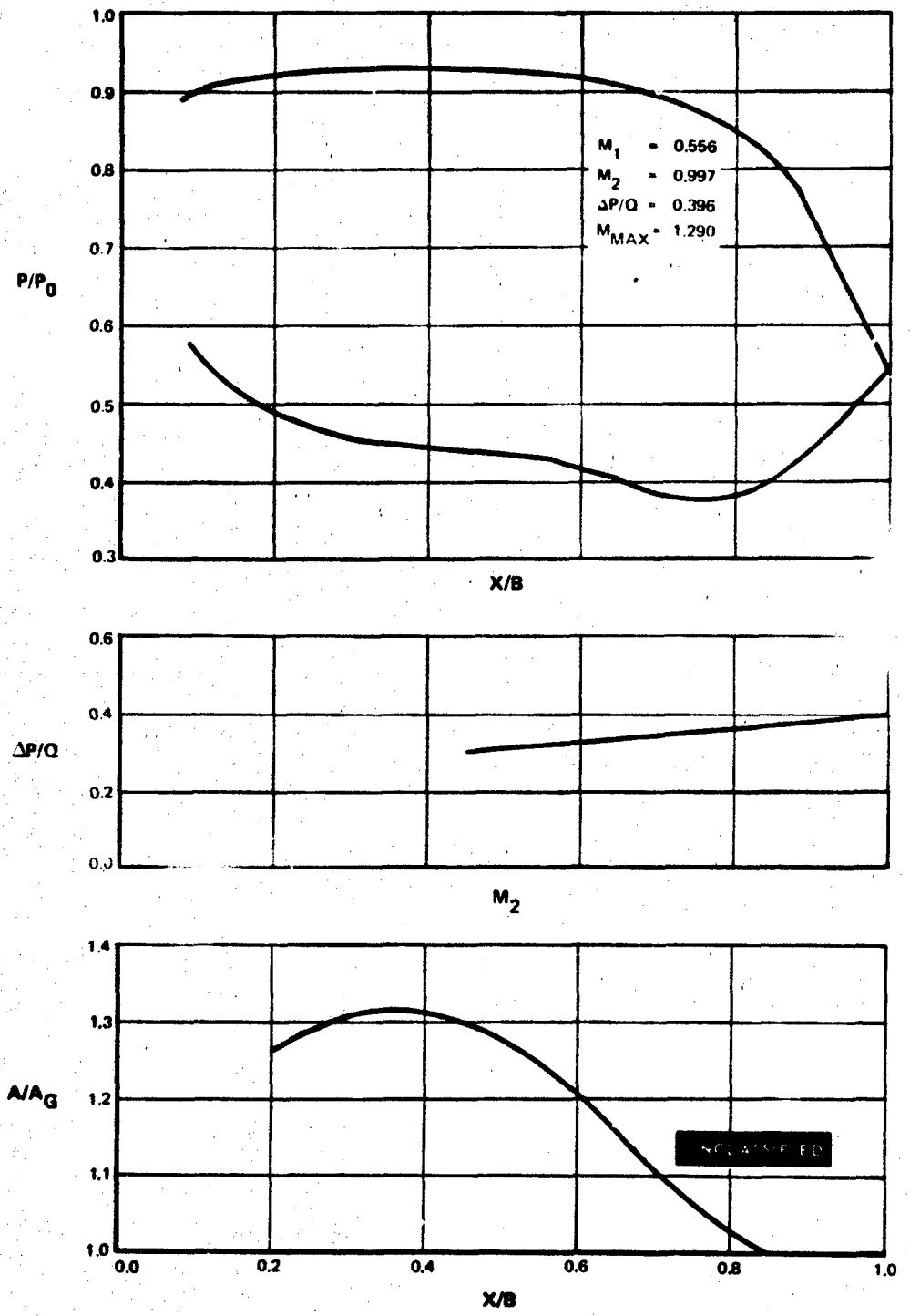

Figure 185 Second-Stage Vane, Root Section

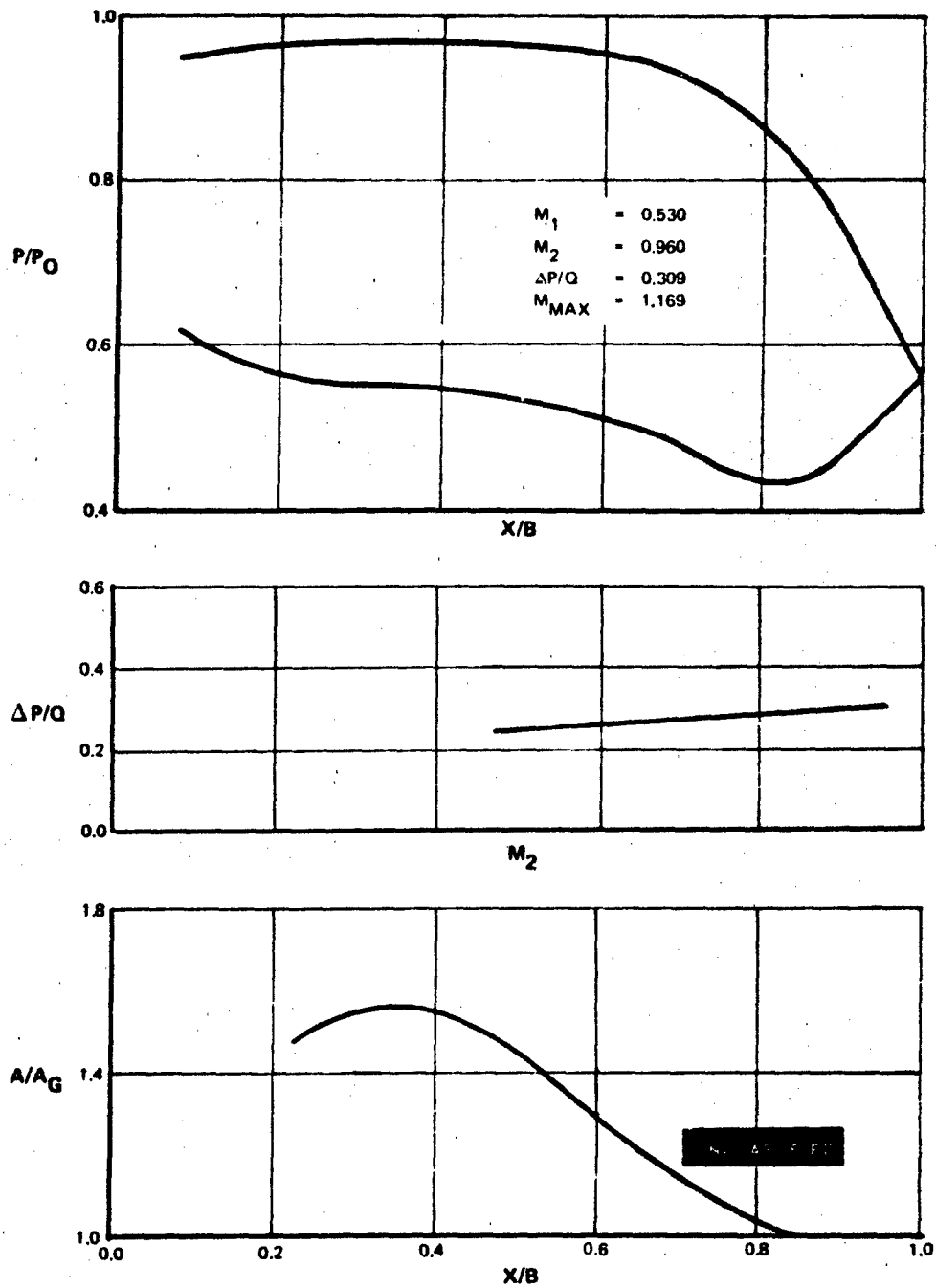

Figure 186 Second-Stage Vane, ¼ Root Section

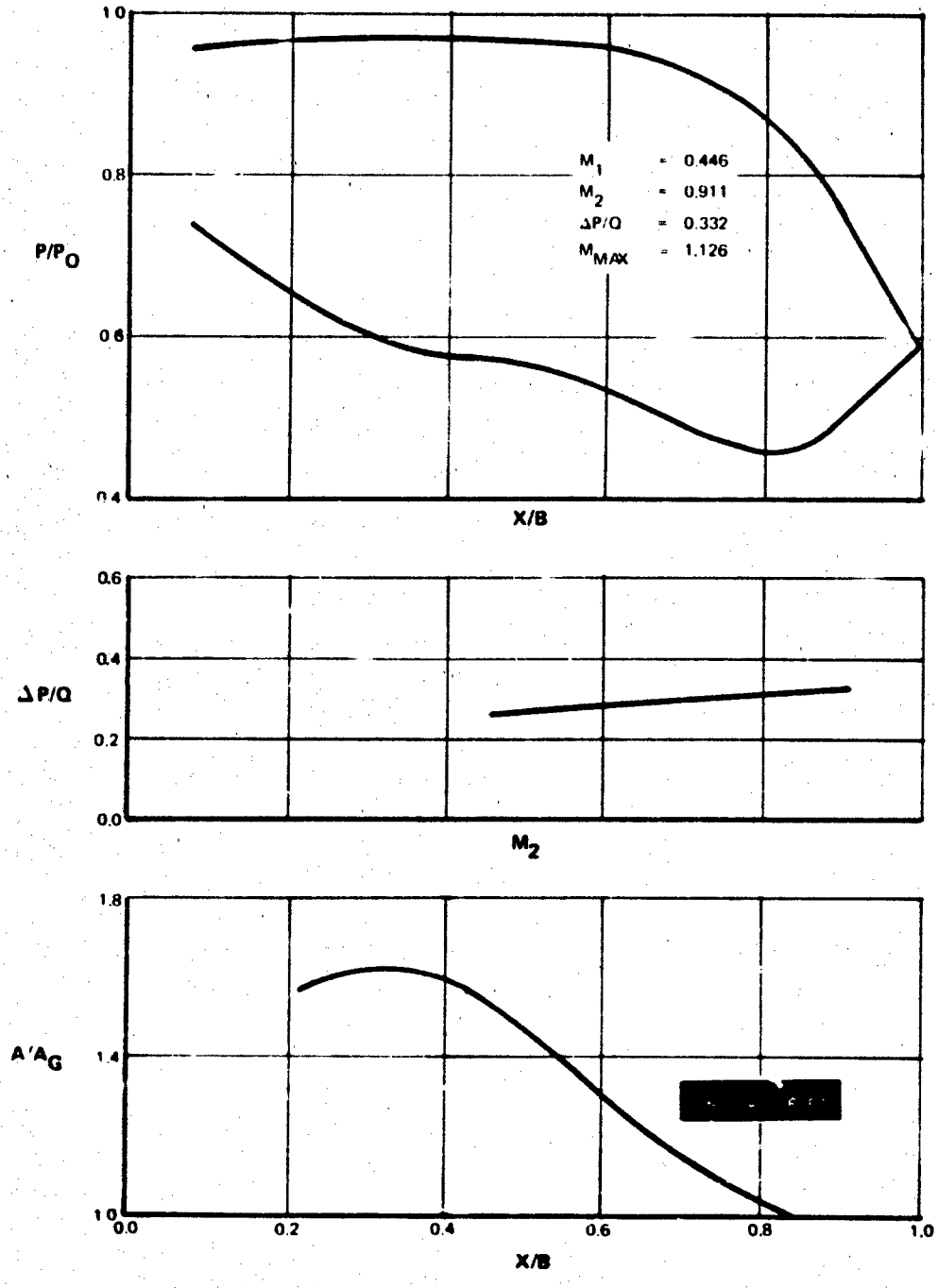

Figure 187 Second-Stage Vane, Mean Section

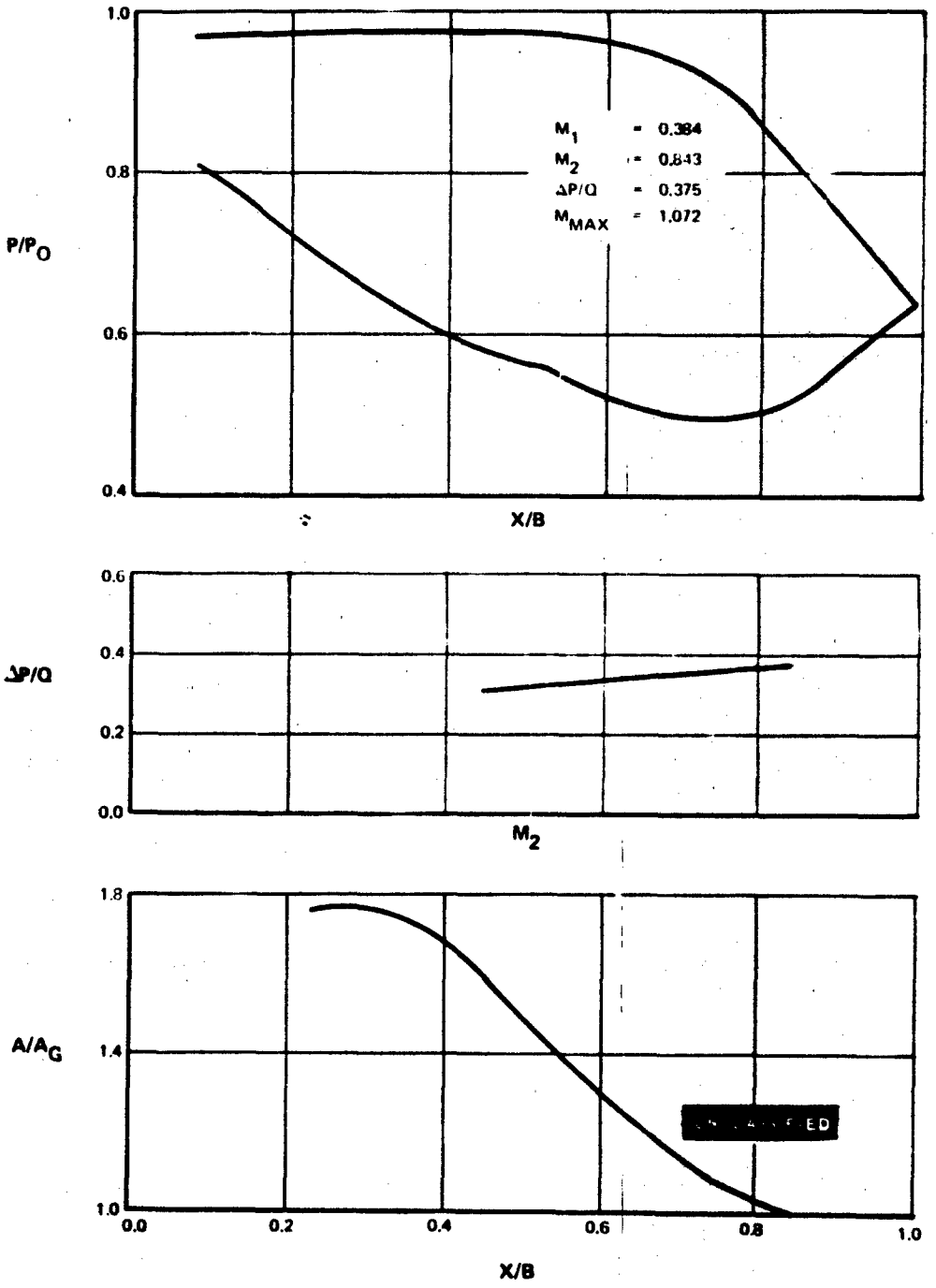

Figure 188 Second-Stage Vane, ¼ Tip Section

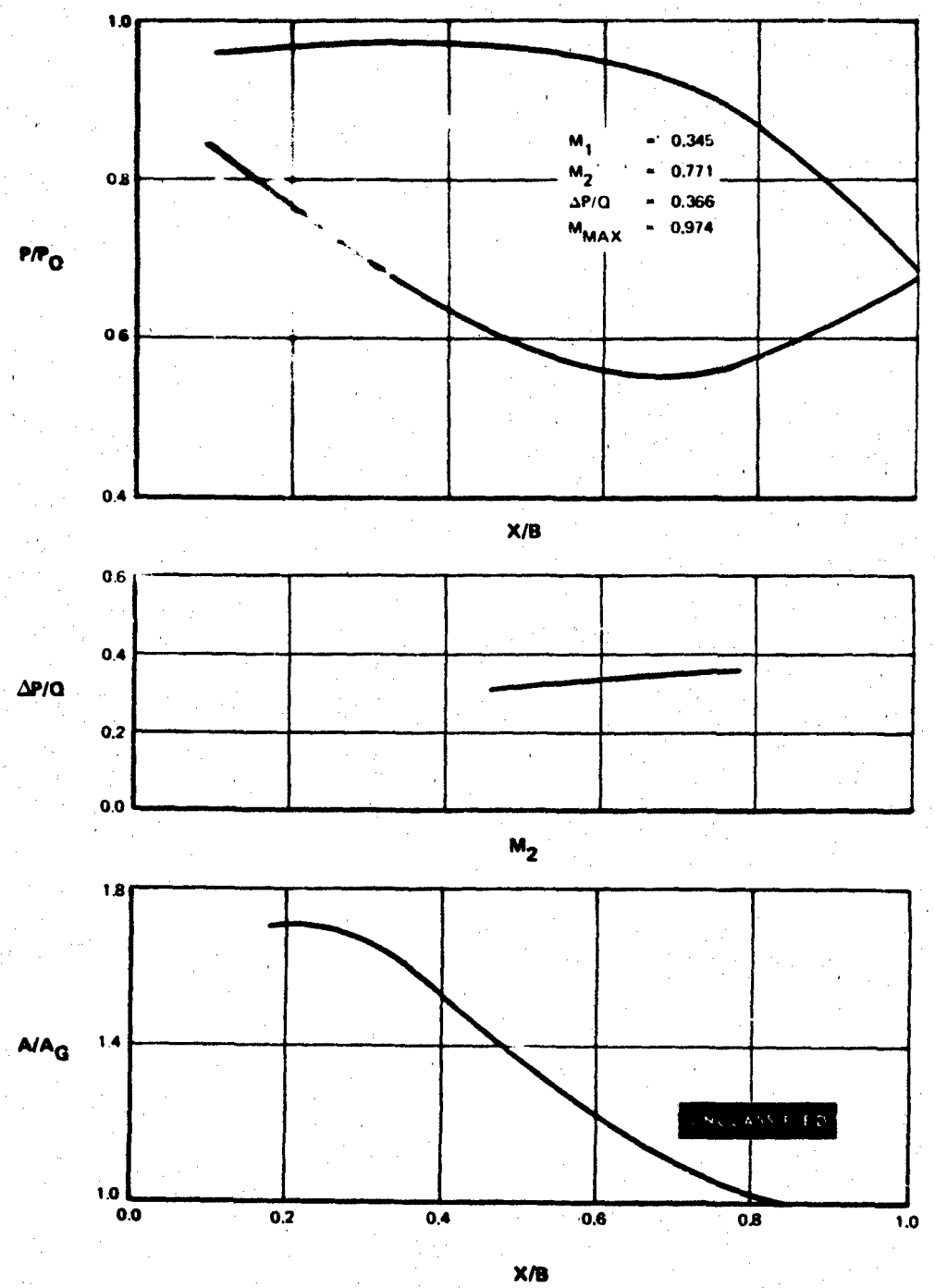

Figure 189 Second-Stage Vane, Tip Section

APPENDIX IV

SECOND-STAGE BLADE FINAL DESIGN

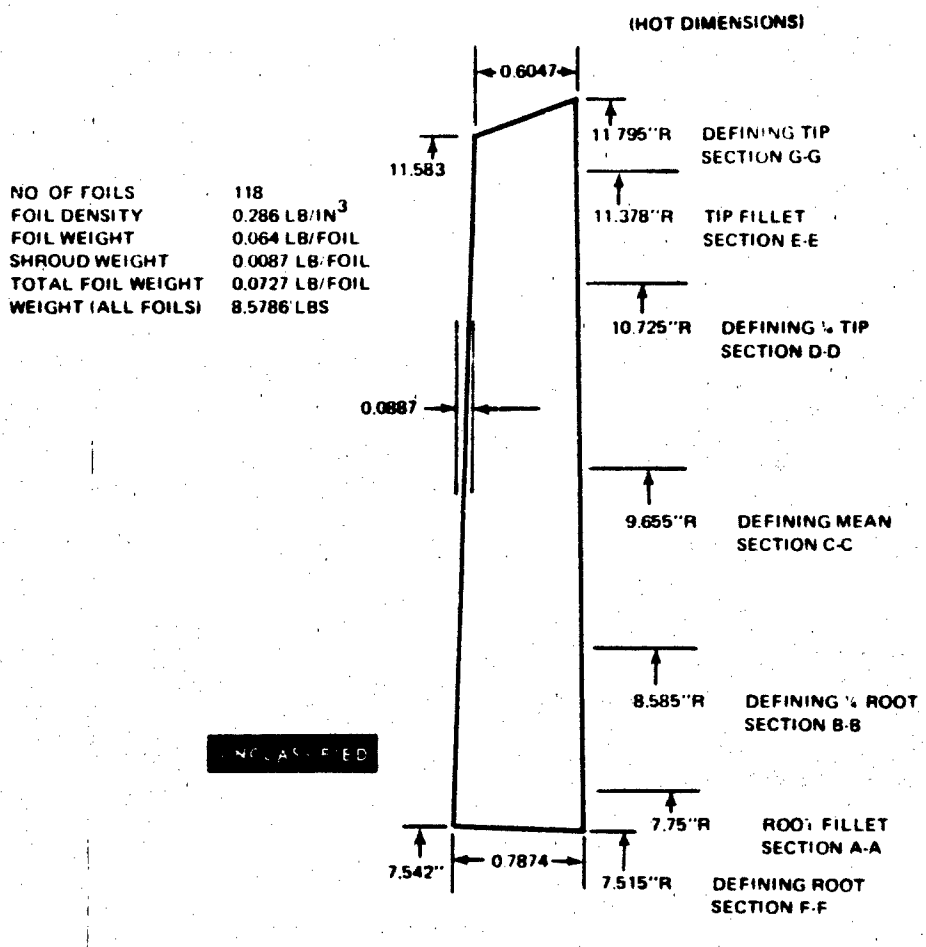

Figure 190 Second-Stage Blade Elevation (Hot Dimensions)

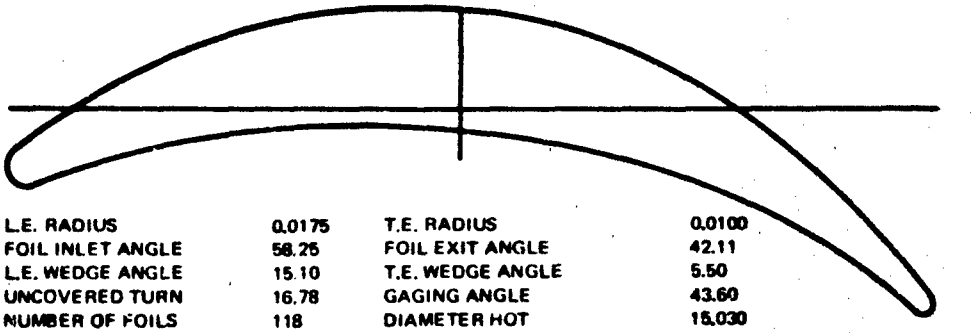

L.E. RADIUS	0.0175	T.E. RADIUS	0.0100
FOIL INLET ANGLE	58.25	FOIL EXIT ANGLE	42.11
L.E. WEDGE ANGLE	15.10	T.E. WEDGE ANGLE	5.50
UNCOVERED TURN	16.78	GAGING ANGLE	43.60
NUMBER OF FOILS	118	DIAMETER HOT	15.030
PITCH HOT	0.4002	GAGING HOT	0.2760
AXIAL WIDTH	0.7880	METAL AREA	0.0607
RAD. REF. POINT X	0.3845	RAD. REF. POINT Y	0.1620
C.G. POINT X	0.3846	C. G. POINT Y	0.1620

[redacted]

Figure 191 Section F-F, Second Blade Root, Cylindrical

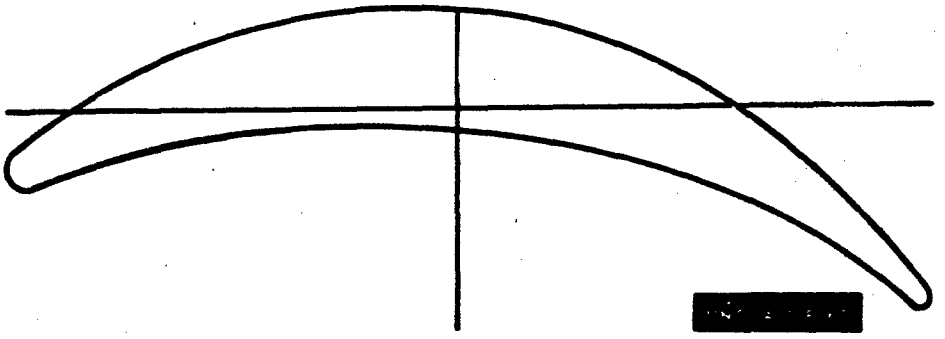

[redacted]

Figure 192 Section F-F, Second Blade Root, Planar

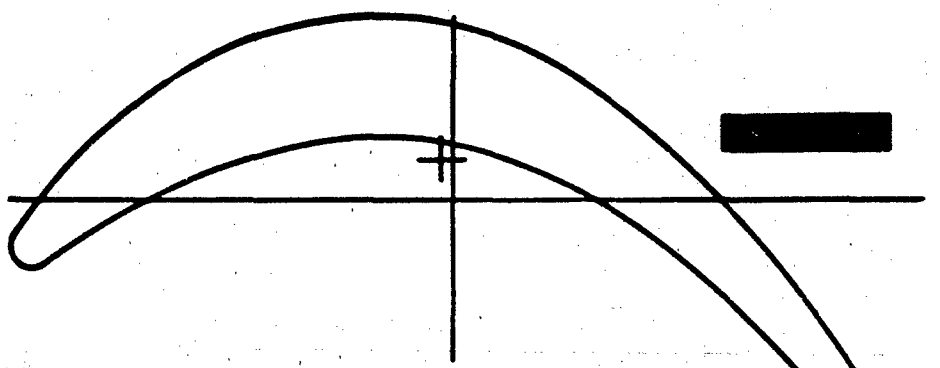

L.E. RADIUS	0.0170	T.E. RADIUS	0.0100
FOIL INLET ANGLE	45.29	FOIL EXIT ANGLE	34.32
L.E. WEDGE ANGLE	20.02	T.E. WEDGE ANGLE	5.97
UNCOVERED TURN	15.51	GAGING ANGLE	34.74
NUMBER OF FOILS	118	DIAMETER HOT	17.170
PITCH HOT	0.4571	GAGING HOT	[redacted]
AXIAL WIDTH	0.7410	METAL AREA	[redacted]
RAD. REF. POINT X	0.3845	RAD. REF. POINT Y	[redacted]
C.G. POINT X	0.3749	C. G. POINT Y	[redacted]

Figure 193 Section B-B, Second Blade ¼ Root, Cylindrical

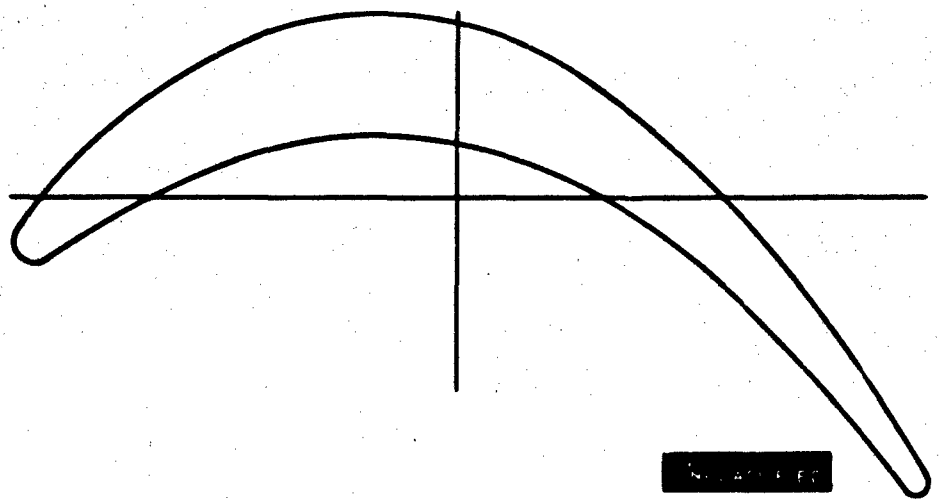

Figure 194 Section B-B, Second Blade ¼ Root, Planar

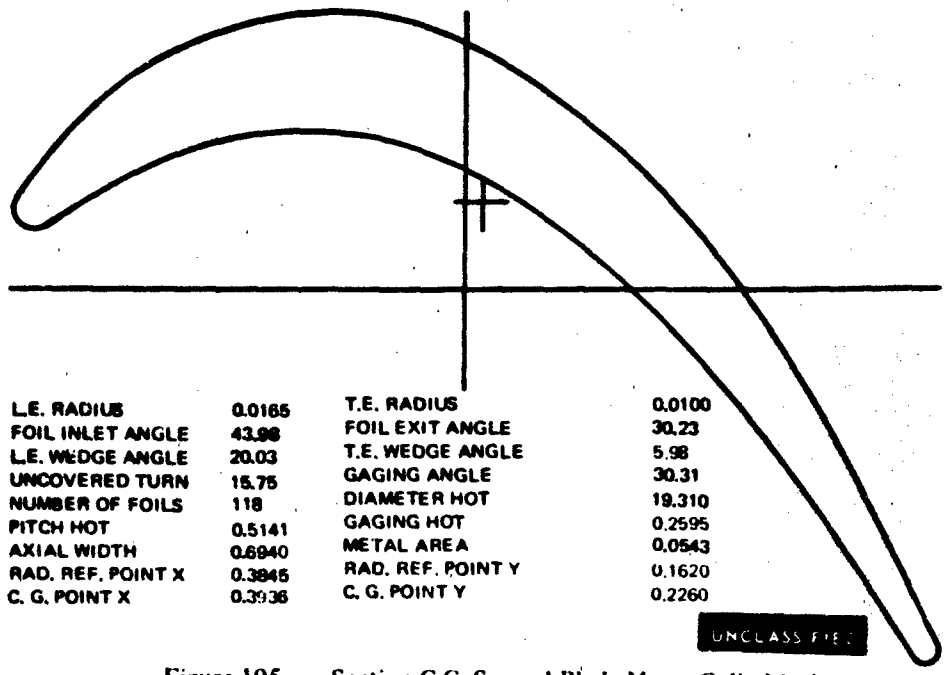

L.E. RADIUS	0.0165	T.E. RADIUS	0.0100
FOIL INLET ANGLE	43.98	FOIL EXIT ANGLE	30.23
L.E. WEDGE ANGLE	20.03	T.E. WEDGE ANGLE	5.98
UNCOVERED TURN	15.75	GAGING ANGLE	30.31
NUMBER OF FOILS	118	DIAMETER HOT	19.310
PITCH HOT	0.5141	GAGING HOT	0.2595
AXIAL WIDTH	0.6940	METAL AREA	0.0543
RAD. REF. POINT X	0.3845	RAD. REF. POINT Y	0.1620
C. G. POINT X	0.3936	C. G. POINT Y	0.2260

UNCLASSIFIED

Figure 195 Section C-C, Second Blade Mean, Cylindrical

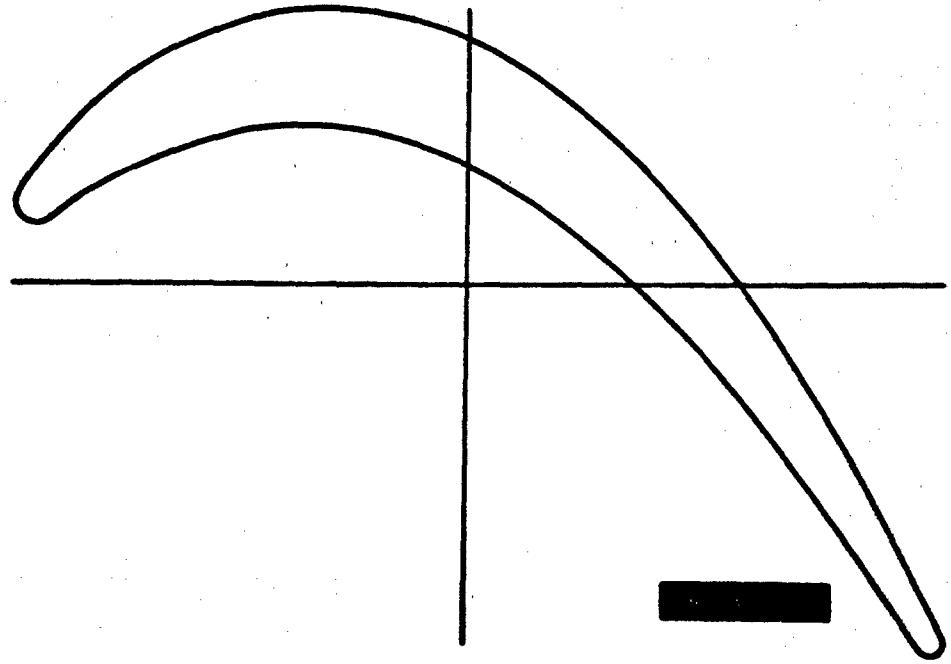

Figure 196 Section C-C, Second Blade Mean, Planar

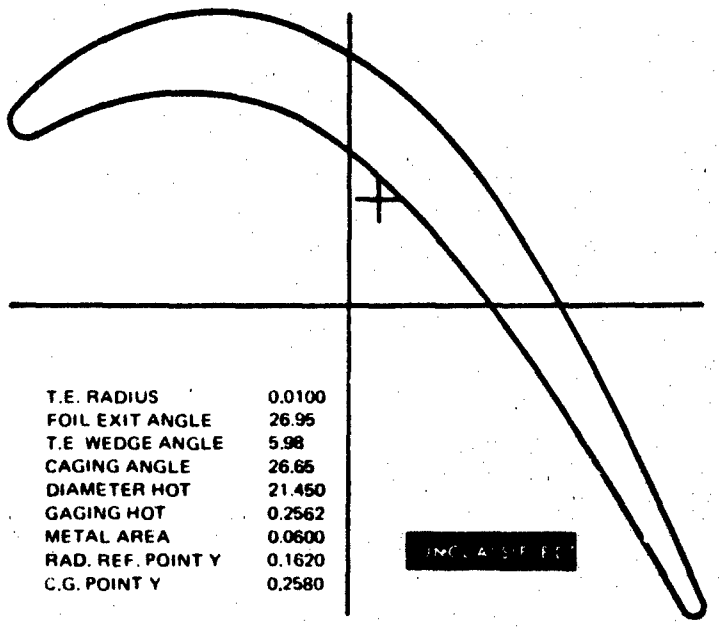

L.E. RADIUS	0.0160	T.E. RADIUS	0.0100
FOIL INLET ANGLE	52.62	FOIL EXIT ANGLE	26.95
L.E. WEDGE ANGLE	20.15	T.E WEDGE ANGLE	5.98
UNCOVERED TURN	15.27	CAGING ANGLE	26.65
NUMBER OF FOILS	118	DIAMETER HOT	21.450
PITCH HOT	0.5711	GAGING HOT	0.2562
AXIAL WIDTH	0.6470	METAL AREA	0.0600
RAD. REF. POINT X	0.3845	RAD. REF. POINT Y	0.1620
C.G. POINT X	0.4121	C.G. POINT Y	0.2580

Figure 197 Section D-D, Second Blade ¼ Tip, Cylindrical

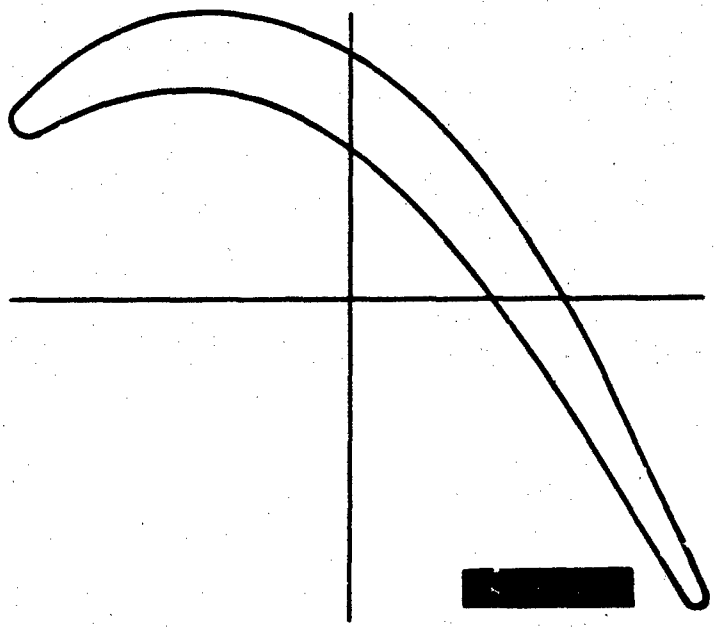

Figure 198 Section D-D, Second Blade ¼ Tip, Planar

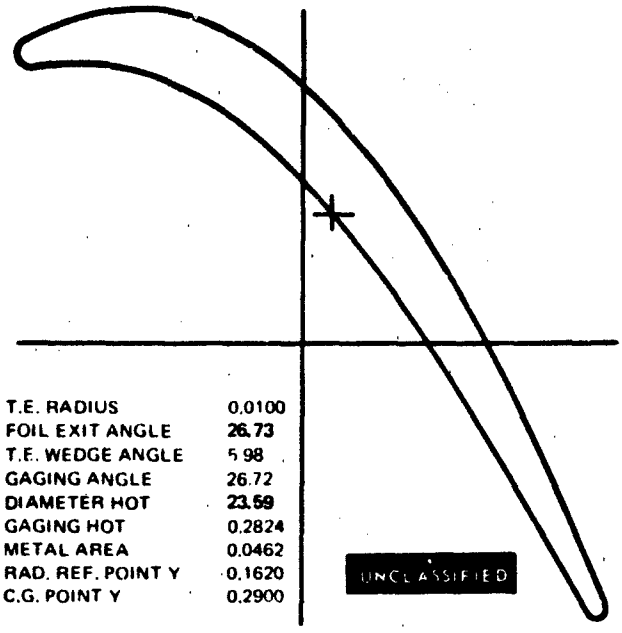

L.E. RADIUS	0.0155	T.E. RADIUS	0.0100
FOIL INLET ANGLE	71.60	FOIL EXIT ANGLE	26.73
L.E. WEDGE ANGLE	20.00	T.E. WEDGE ANGLE	5.98
UNCOVERED TURN	14.62	GAGING ANGLE	26.72
NUMBER OF FOILS	118	DIAMETER HOT	23.59
PITCH HOT	0.6281	GAGING HOT	0.2824
AXIAL WIDTH	0.6000	METAL AREA	0.0462
RAD.REF. POINT X	0.3845	RAD. REF. POINT Y	0.1620
C.G. POINT X	0.4141	C.G. POINT Y	0.2900

Figure 199 Section G-G, Second Blade Tip, Cylindrical

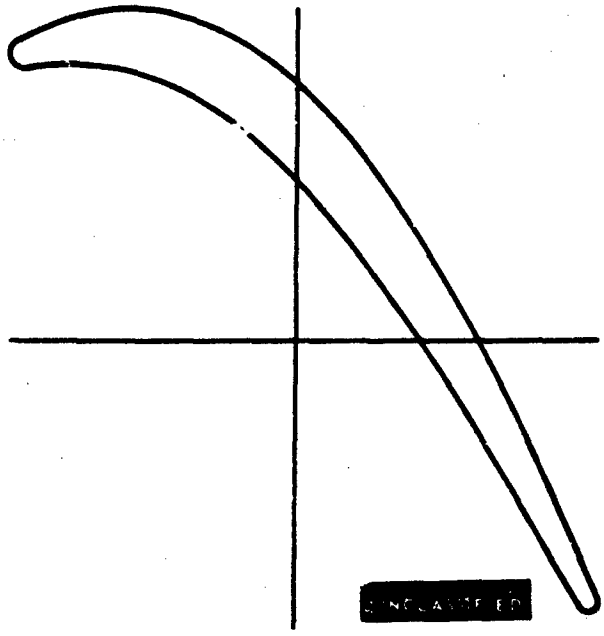

Figure 200 Section G-G, Second Blade Tip, Planar

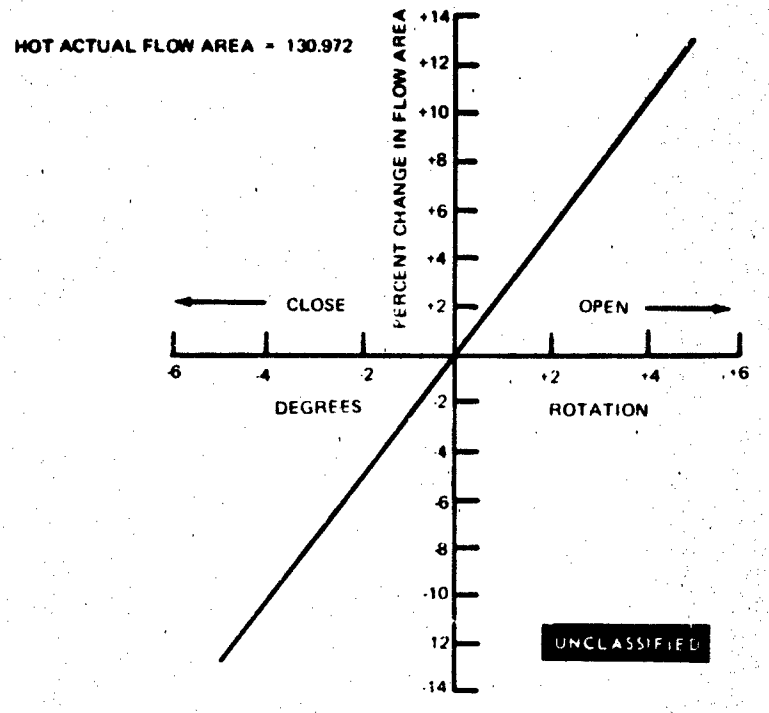

Figure 201 Second-Stage Blade, Flow Area Versus Rotation

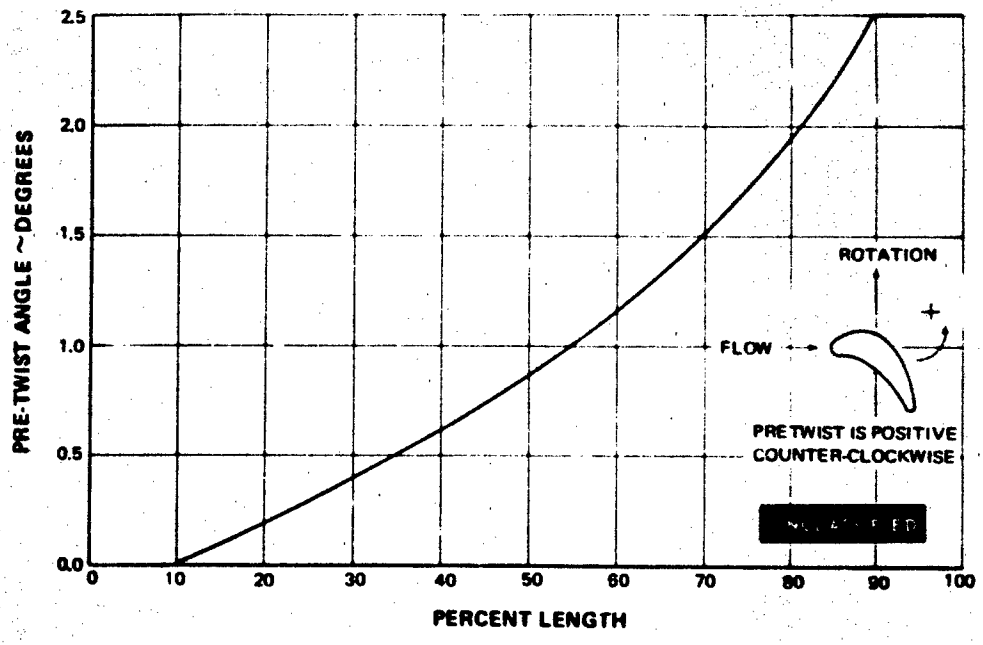

Figure 202 Second-Stage Blade, Pretwist Versus Percent Length

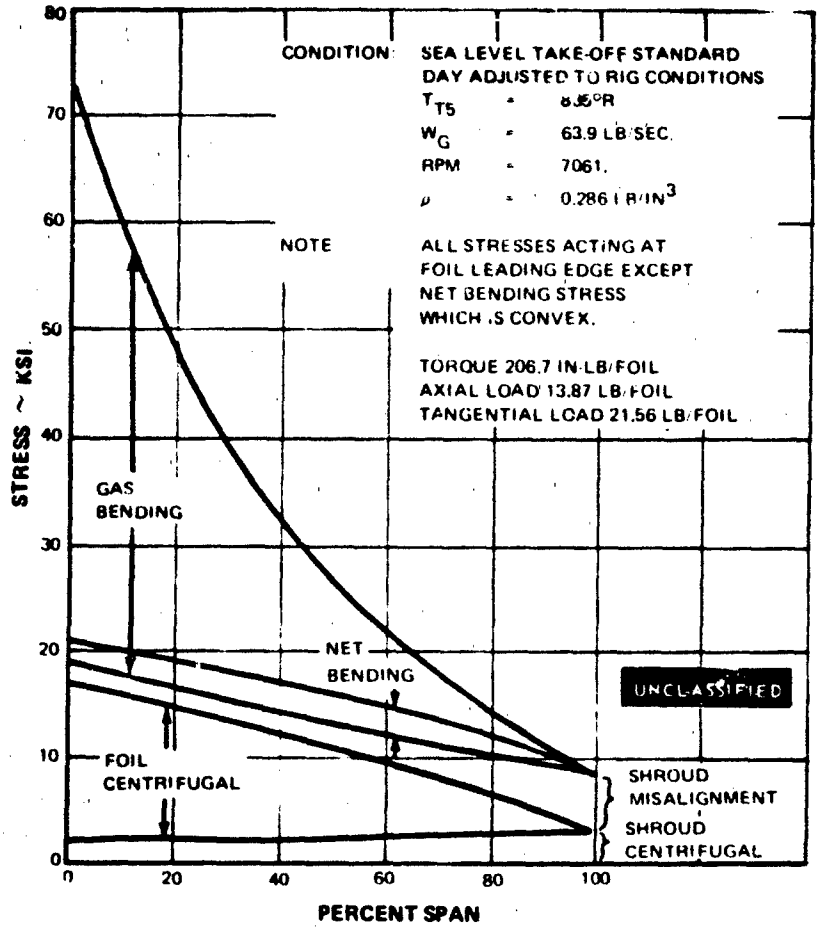

Figure 203 Second-Stage Blade Stress

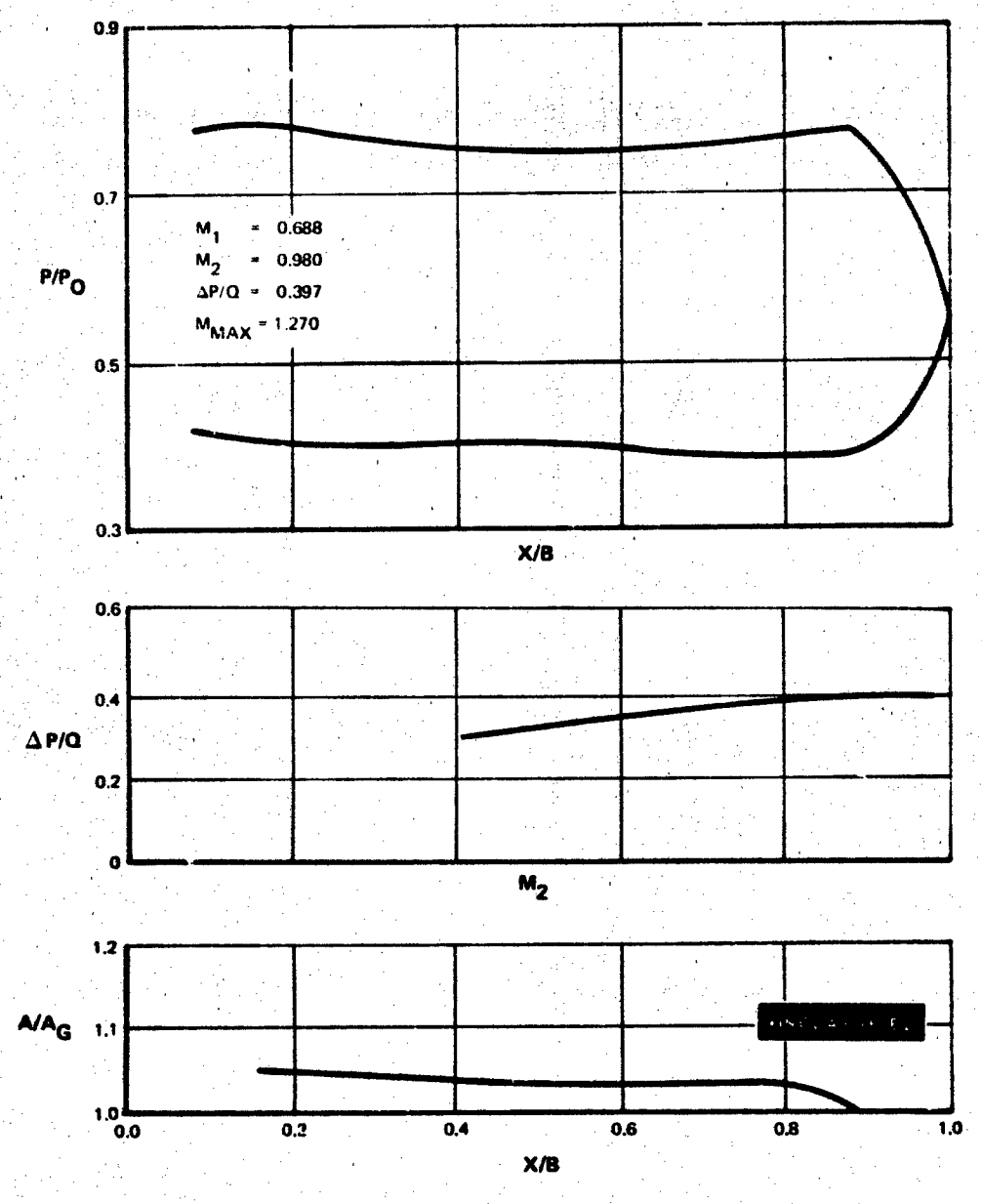

Figure 204 Second-Stage Blade, Root Section

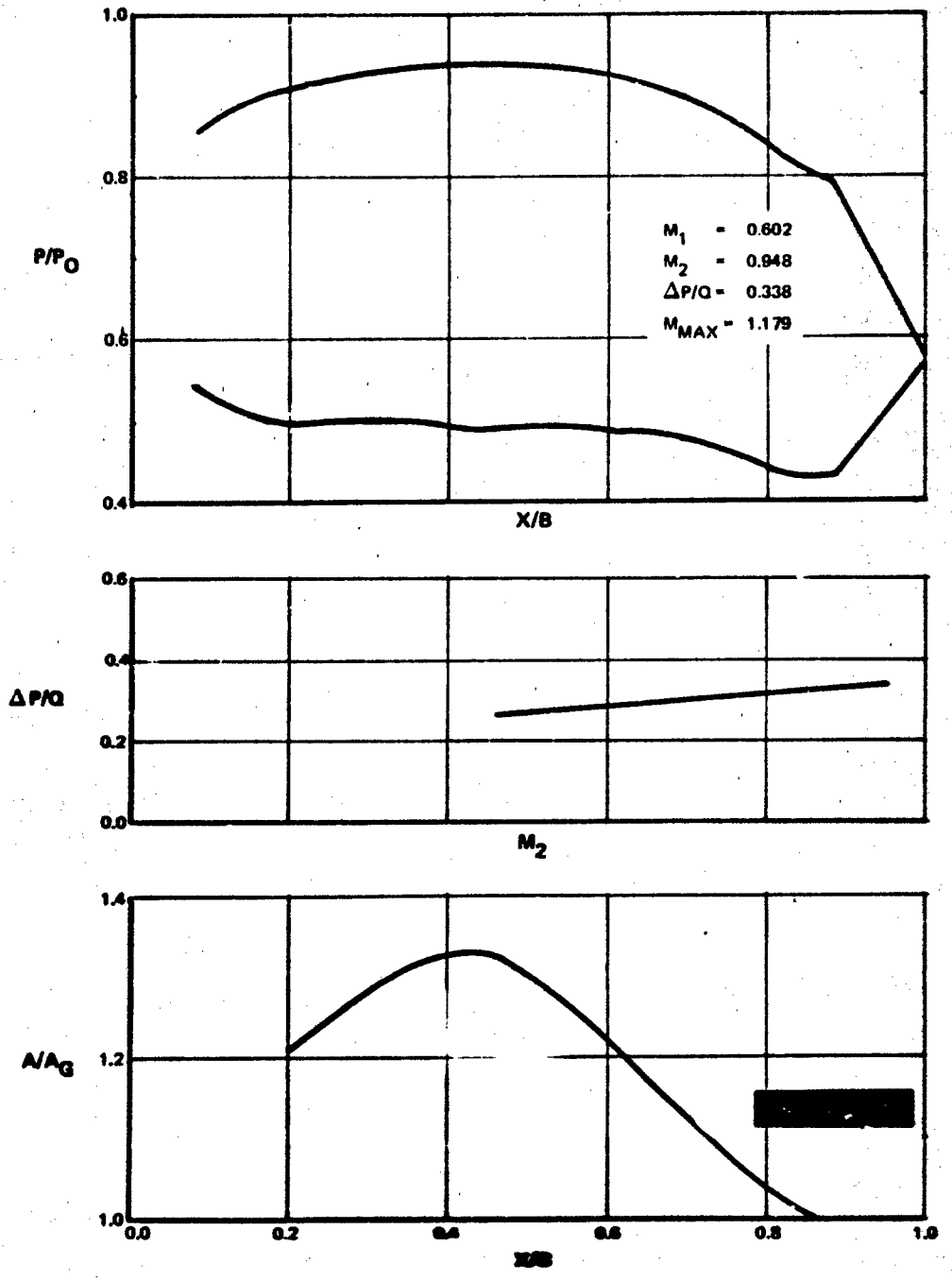

Figure 205 Second-Stage Blade, % Root Section

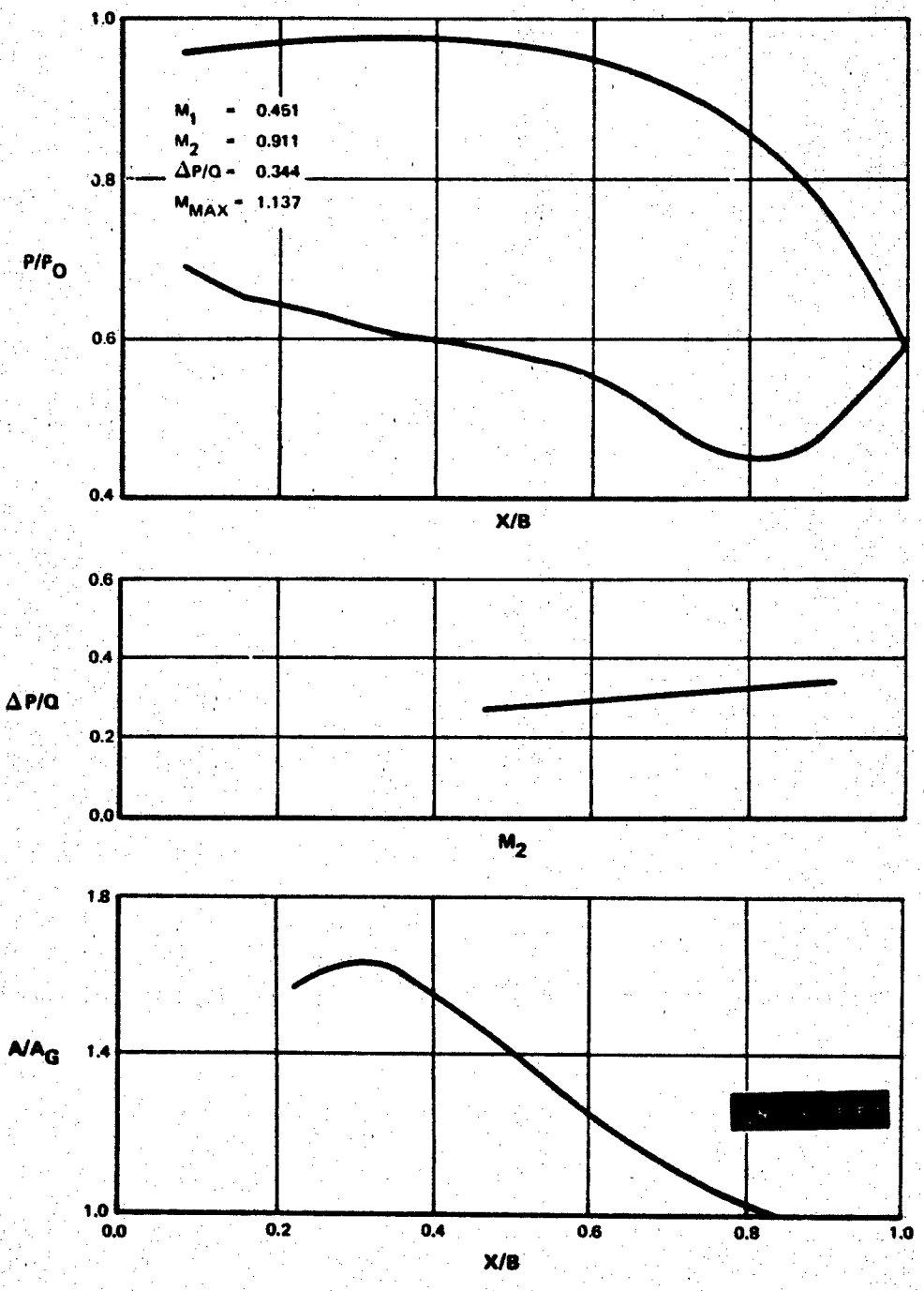

Figure 206 Second-Stage Blade, Mean Section

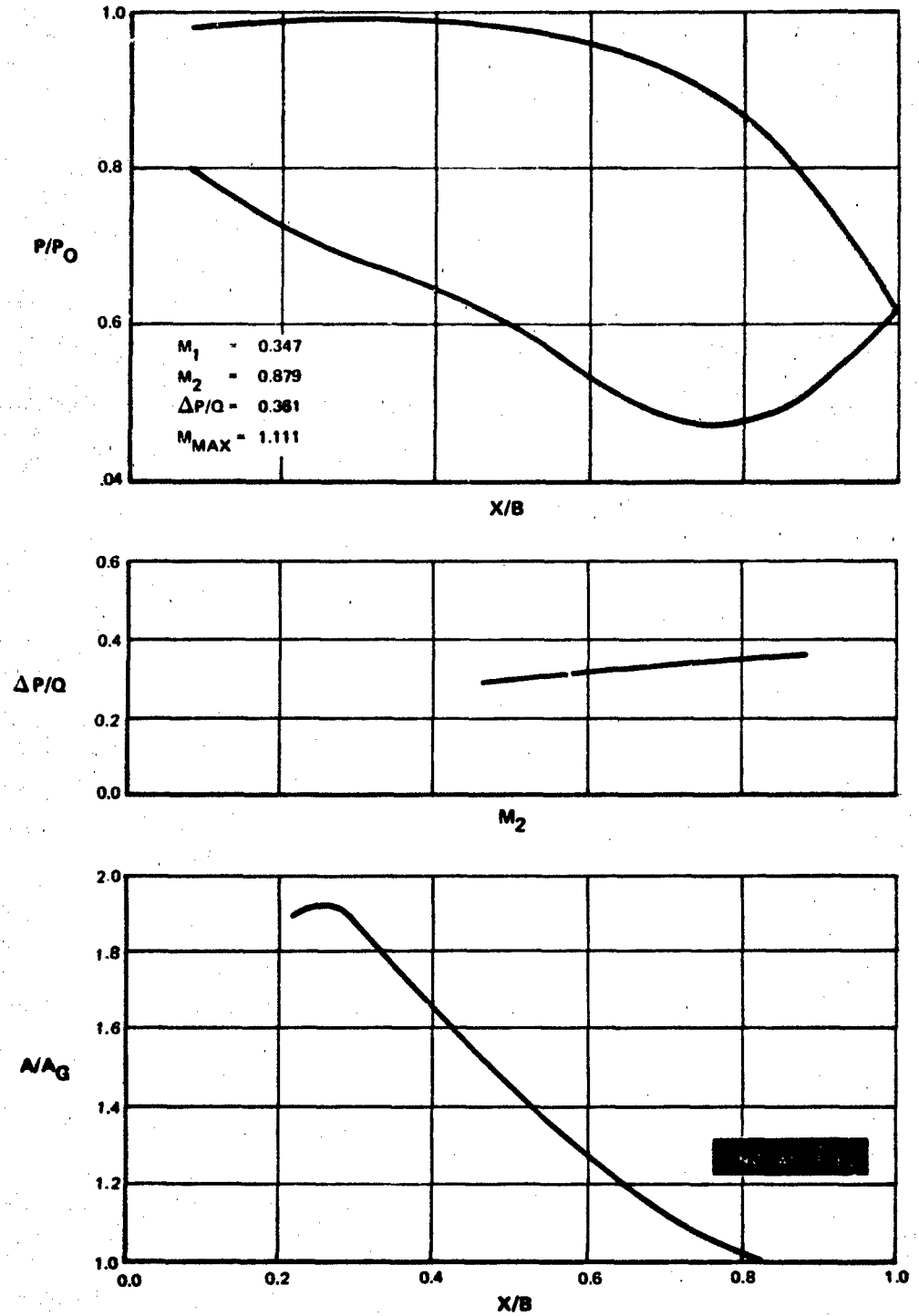

Figure 207 Second-Stage Blade, ¼ Tip Section

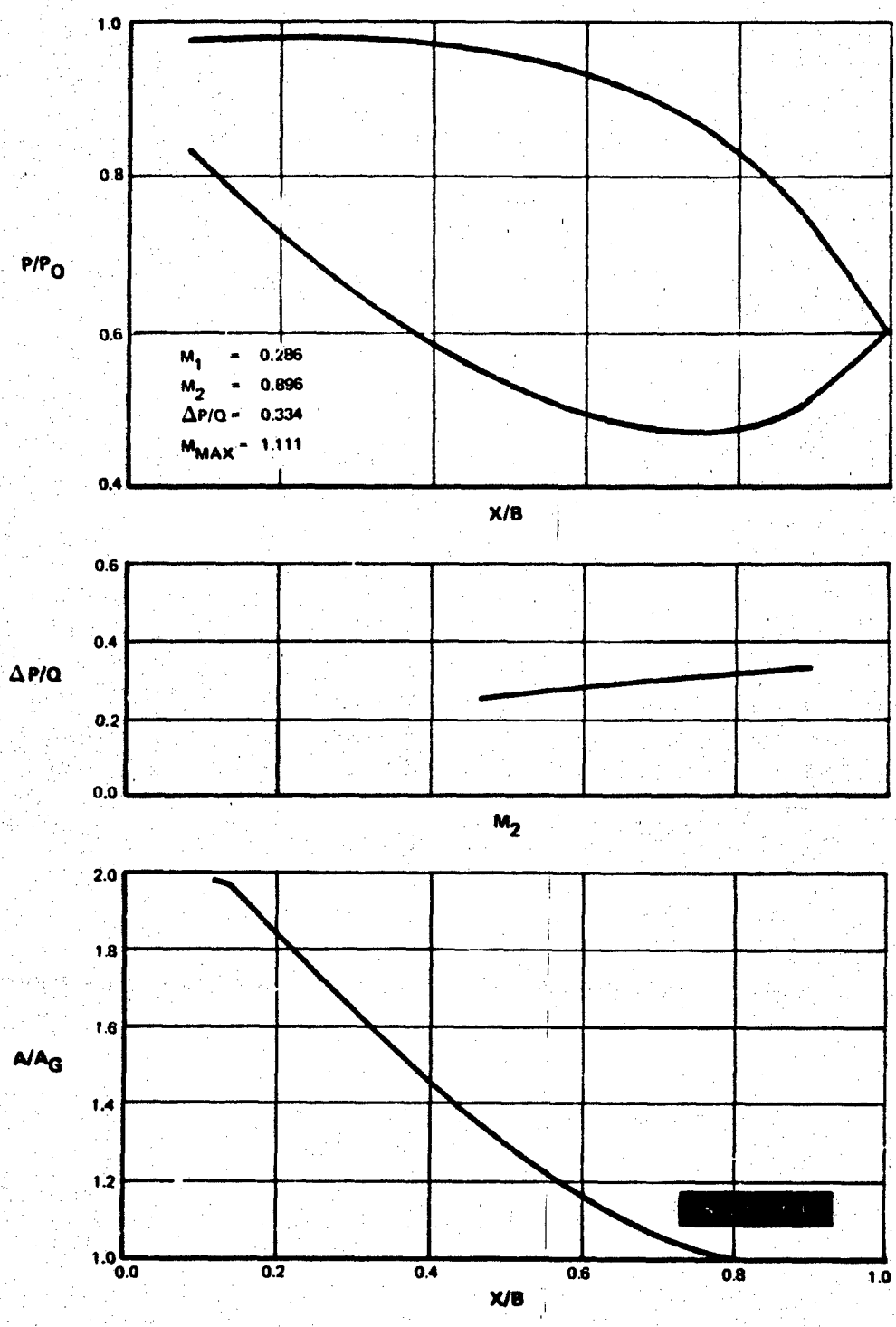

Figure 208 Second-Stage Blade, Tip Section

(The reverse of this page is blank.)

APPENDIX V

EXIT GUIDE VANE CALCULATIONS

APPENDIX V

EXIT GUIDE VANE CALCULATIONS

A. THE DETERMINATION OF THE EGV EXIT MACH NUMBER

(U) From the equation of conservation of mass, $\dot{m}_e = \dot{m}_i$, we find that

$$\rho_e V_e A_e \cos\beta_e = \rho_i V_i A_i \cos\beta_i \quad .$$

(U) Using the gas law, $p = \rho RT$, and noting that $\beta_e \equiv 0$, the above equation becomes

$$\frac{p_e}{T_e} V_e A_e = \frac{p_i}{T_i} V_i A_i \cos\beta_i \quad .$$

(U) From the definition of Mach number, $M = \dfrac{V}{\sqrt{gRT}}$, we find that

$$\frac{p_e}{\sqrt{T_e}} M_e A_e = \frac{p_i}{\sqrt{T_i}} M_i A_i \cos\beta_i \quad .$$

(U) Using the steady-flow energy equation,

$$\frac{T_o}{T} = 1 + \frac{k-1}{2} M^2 \quad ,$$

and the isentropic relationship,

$$\frac{p_o}{p} = \left(\frac{T_o}{T}\right)^{\frac{k}{k-1}} \quad ,$$

and by noting for an adiabatic cascade, $T_{oe} = T_{oi}$, we find that

$$\frac{p_{oe}}{\left(1+\frac{k-1}{2} M_e^2\right)^{\frac{k+1}{2(k-1)}}} M_e A_e = \frac{p_{oi}}{\left(1+\frac{k-1}{2} M_i^2\right)^{\frac{k+1}{2(k-1)}}} M_i A_i \cos\beta_i \quad .$$

(U) Setting $p_{oe} = p_{oi}$, which increases the exit density, thereby decreasing the exit velocity and consequently increasing diffusion, yields, finally,

$$M_e = M_i \frac{A_i}{A_e} \cos \beta_i \left[\frac{1 + \frac{k-1}{2} M_e^2}{1 + \frac{k-1}{2} M_i^2} \right]^{\frac{k+1}{2(k-1)}}$$

(U) For subsonic flow, M_e can be determined iteratively by setting a first guess at M_e equal to zero and by using the above equation and the method of successive substitutions.

B. THE RELATIONSHIP BETWEEN THE ACTUAL CHORD AND THE AXIAL CHORD FOR A CIRCULAR ARC AIRFOIL WITH AXIAL OUTFLOW

(U) The geometry necessary to solve the problem is shown in the following figure:

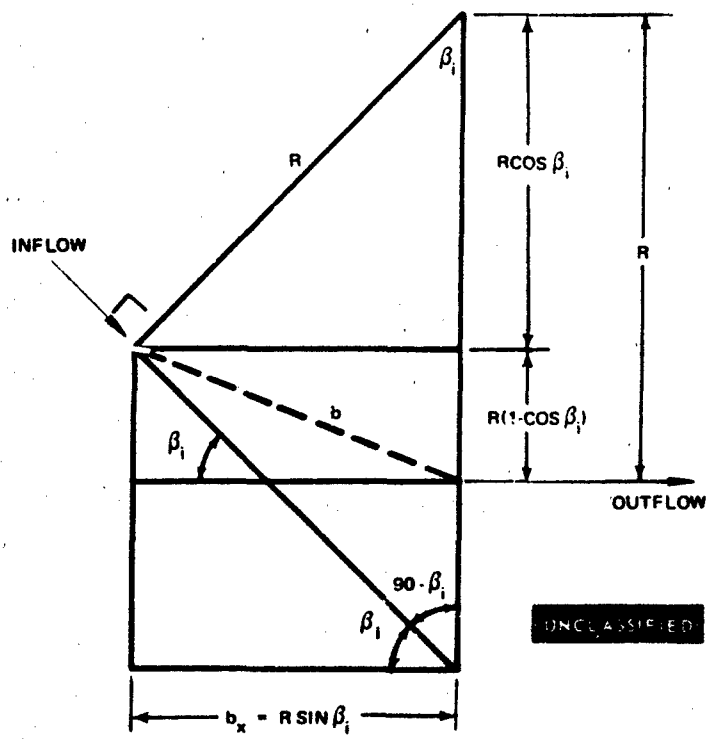

(U) b is found, from the Pythagorian theorem, to be

$$b^2 = R^2 (1 - \cos\beta_i)^2 + R^2 \sin^2\beta_i = R^2 (1 - 2\cos\beta_i + \cos^2\beta_i + \sin^2\beta_i)$$

$$= 2R^2 (1 - \cos\beta_i), \text{ therefore,}$$

$$b = R\sqrt{2(1 - \cos\beta_i)}.$$

(U) Since $b_x = R \sin\beta_i$, it follows that

$$\frac{b}{b_x} = \sqrt{\frac{2}{1 + \cos\beta_i}}$$

(U) This derivation is based on the assumptions that no incidence or deviation exist.

C. CURVE FIT OF Z_p VERSUS D_f

(U) Figure 149 (a), page 205 of Reference (6) gives compressor cascade loss (Z_p) versus diffusion factor (D_f). A simple, but accurate, fit for this data turns out to be three (3) linear segments. The end points for the three lines are,

Z_p (0) = 0.005

Z_p (0.4) = 0.010

Z_p (0.6) = 0.020

Z_p (0.7) = 0.060

(U) The general form of the equation is,

$$Z_p(D_f) = A + BD_f$$

(U) The necessary coefficients are given in the following table:

	B	Region
	0.0125	$0 \leq D_f < 0.4$
	0.0500	$0.4 \leq D_f < 0.6$
	0.4000	$0.6 \leq D_f \leq 0.7$

D. THE CALCULATION OF THE TOTAL PRESSURE PROFILE LOSS, $(\Delta p_o/p_o)_p$, FROM THE PROFILE–LOSS PARAMETER, Z_p

(U) Z_p is defined as

$$Z_p = \frac{\bar{\omega}_{pi} \cos \beta_e}{2\sigma} \left(\frac{\cos \beta_e}{\cos \beta_i} \right)^2 ,$$

which for axial outflow, reduces to

$$Z_p = \frac{\bar{\omega}_{pi}}{2\sigma \cos^2 \beta_i} ,$$

or

$$\bar{\omega}_{pi} = 2\sigma Z_p \cos^2 \beta_i ,$$

where

$$\bar{\omega}_{pi} \equiv \frac{P_{oi} - P_{oep}}{P_{oi} - P_i} = \frac{\dfrac{P_{oi} - P_{oep}}{P_{oi}}}{1 - \dfrac{P_i}{P_{oi}}} = \frac{\left(\dfrac{\Delta p_o}{p_o} \right)_p}{1 - \dfrac{p_i}{p_{oi}}} .$$

(U) Using the steady-flow energy equation,

$$\frac{T_{oi}}{T_i} = 1 + \frac{k-1}{2} M_i^2 ,$$

and the isentropic relationship,

$$\frac{p_{oi}}{p_i} = \left(\frac{T_{oi}}{T_i} \right)^{\frac{k}{k-1}}$$

we find that, after some rearrangement,

$$\left(\frac{\Delta p_o}{p_o}\right)_p = \bar{\omega}_{pi}\left[\frac{\left(1+\frac{k-1}{2}M_i^2\right)^{\frac{k}{k-1}}-1}{\left(1+\frac{k-1}{2}M_i^2\right)^{\frac{k}{k-1}}}\right]$$

(U) Substituting the expression for $\bar{\omega}_{pi}$, determined before, we finally find that

$$\left(\frac{\Delta p_o}{p_o}\right)_p = 2Z_p\,\sigma\cos^2\beta_i\left[\frac{\left(1+\frac{k-1}{2}M_i^2\right)^{\frac{k}{k-1}}-1}{\left(1+\frac{k-1}{2}M_i^2\right)^{\frac{k}{k-1}}}\right]$$

E. INCLUSION OF THE END WALL LOSSES

(U) The total loss may be looked upon as the sum of the profile and end losses, such that

$$\frac{\Delta p_o}{p_o} = \left(\frac{\Delta p_o}{p_o}\right)_p + \left(\frac{\Delta p_o}{p_o}\right)_{el}.$$

(U) Which may be rewritten as

$$\frac{\Delta p_o}{p_o} = \left(\frac{\Delta p_o}{p_o}\right)_p\left(1+\frac{\left(\frac{\Delta p_o}{p_o}\right)_{el}}{\left(\frac{\Delta p_o}{p_o}\right)_p}\right).$$

(U) Since the cascade is lightly loaded, we may assume that little channel crossflow will occur on the end walls and, to a good degree of accuracy, the loss mechanisms may be assumed the same on the end walls as on the average of the airfoil surfaces. This is the same as saying that the end wall-loss-to-profile-loss ratio is the same as the wetted-wall-surface-area-to-airfoil-surface-area-ratio. It follows then, that

$$\frac{\left(\frac{\Delta p_o}{p_o}\right)_{el}}{\left(\frac{\Delta p_o}{p_o}\right)_p} = \frac{A_{wall}}{A_{profile}} = \frac{2\tau b_x}{2hb} = \frac{1}{\left(\frac{h}{b_x}\right)\left(\frac{b}{\tau}\right)} = \frac{1}{\sigma\, AR} .$$

(U) Therefore,

$$\frac{\Delta p_o}{p_o} = \left(\frac{\Delta p_o}{p_o}\right)_p \left(1 + \frac{1}{\sigma\, AR}\right) .$$

F. EGV $\Delta p_o/p_o$ AS A STAGNATION EFFICIENCY PENALTY

(U) For the purposes of this Appendix, only, define the turbine first vane inlet as station one (1), the turbine second blade exit as station two (2), and the EGV exit as station three (3). The overall efficiency is

$$\eta_{T-T} = \frac{\frac{\Delta T_o}{T_o}}{1 - \left(\frac{p_{o3}}{p_{o1}}\right)^{\frac{k-1}{k}}} .$$

(U) The total pressure ratio in the denominator may be rearranged into a more useful form

$$\frac{p_{o3}}{p_{o1}} = \frac{p_{o2}}{p_{o1}} \frac{p_{o3}}{p_{o2}} = \frac{p_{o2}}{p_{o1}} \left(1 - \frac{\Delta p_o}{p_o}\right) .$$

where $\frac{\Delta p_o}{p_o} = \frac{p_{o2} - p_{o3}}{p_{o2}} \equiv \frac{p_{oi} - p_{oe}}{p_{oi}}$ is the EGV total pressure loss.

(U) These total pressures are defined as mass-averaged values, at their respective axial locations.

(U) Therefore,

$$\eta_{T-T} = \frac{\frac{\Delta T_o}{T_o}}{1-\left(\frac{p_{02}}{p_{01}}\right)^{\frac{k-1}{k}} \cdot \left(1-\frac{\Delta p_o}{p_o}\right)^{\frac{k-1}{k}}}$$

(U) The efficiency which will be measured in the test stand, $\eta_{T\text{-}T\ MEASURED}$, is

$$\eta_{T\text{-}T\ MEASURED} = \frac{\frac{\Delta T_o}{T_o}}{1-\left(\frac{p_{02}}{p_{01}}\right)^{\frac{k-1}{k}}} .$$

(U) Combining the expressions for $\eta_{T\text{-}T}$ and $\eta_{T\text{-}T\ MEASURED}$ we find,

$$\frac{\eta_{T\text{-}T}}{\eta_{T\text{-}T\ MEASURED}} = \frac{1-\left(\frac{p_{02}}{p_{01}}\right)^{\frac{k-1}{k}}}{1-\left(\frac{p_{02}}{p_{01}}\right)^{\frac{k-1}{k}} \left(1-\frac{\Delta p_o}{p_o}\right)^{\frac{k-1}{k}}} ,$$

where at the design point the pressure ratio is set at the design value so that the above expression may be evaluated for various $\Delta p_o/p_o$'s. Finally then,

$$\frac{\eta_{T\text{-}T}}{\eta_{T\text{-}T\ MEASURED}} = \frac{P_R^{\frac{k-1}{k}} - 1}{P_R^{\frac{k-1}{k}} - \left(1-\frac{\Delta p_o}{p_o}\right)^{\frac{k-1}{k}}} .$$

(The reverse of this page is blank.)

APPENDIX VI

LOW SOLIDITY AIRFOIL SECTIONS

UNCLASSIFIED

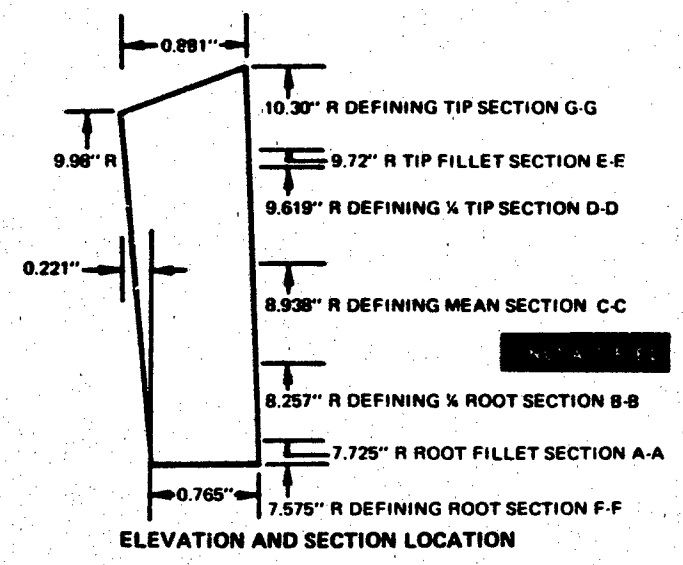

Figure 209 Medium Reaction, Low Solidity, First-Stage Vane

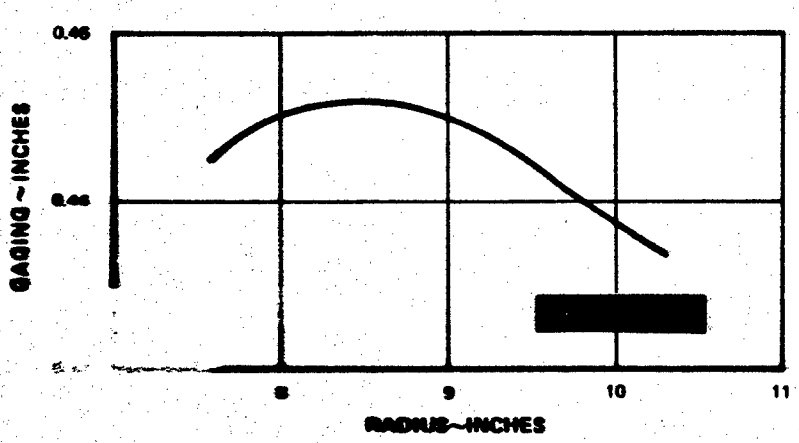

Figure 210 [redacted] Low Solidity, First-Stage Vane – Gaging Distribution

UNCLASSIFIED

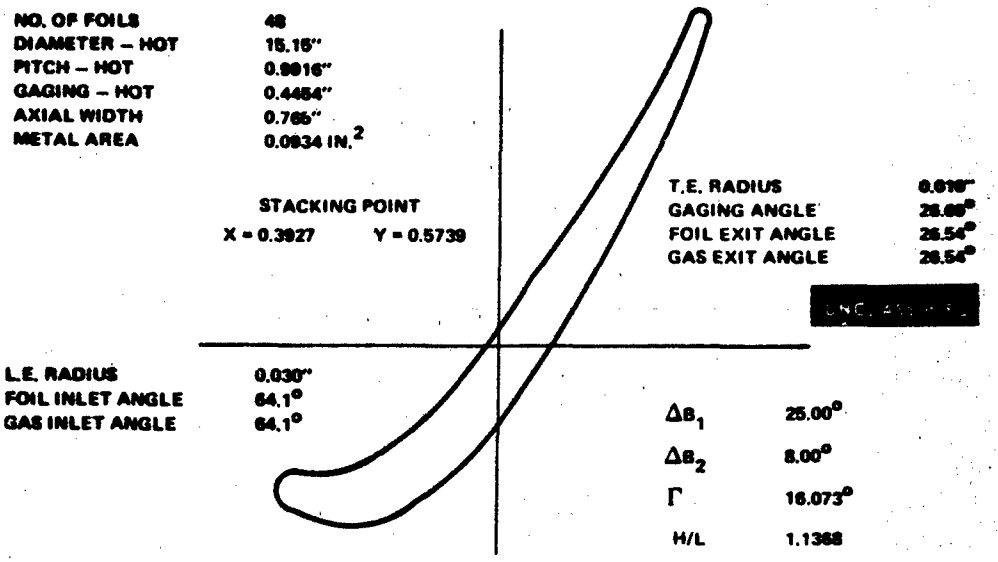

Figure 211 Medium Reaction, Low Solidity, First-Stage Vane, Root (F-F) Section

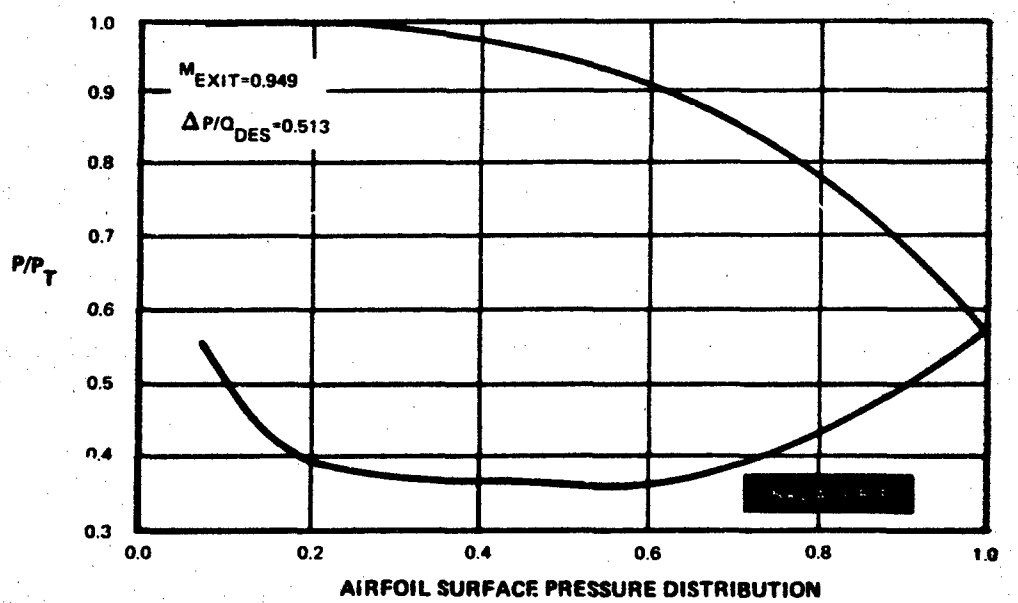

Figure 212 Medium Reaction, Low Solidity, First-Stage Vane Root

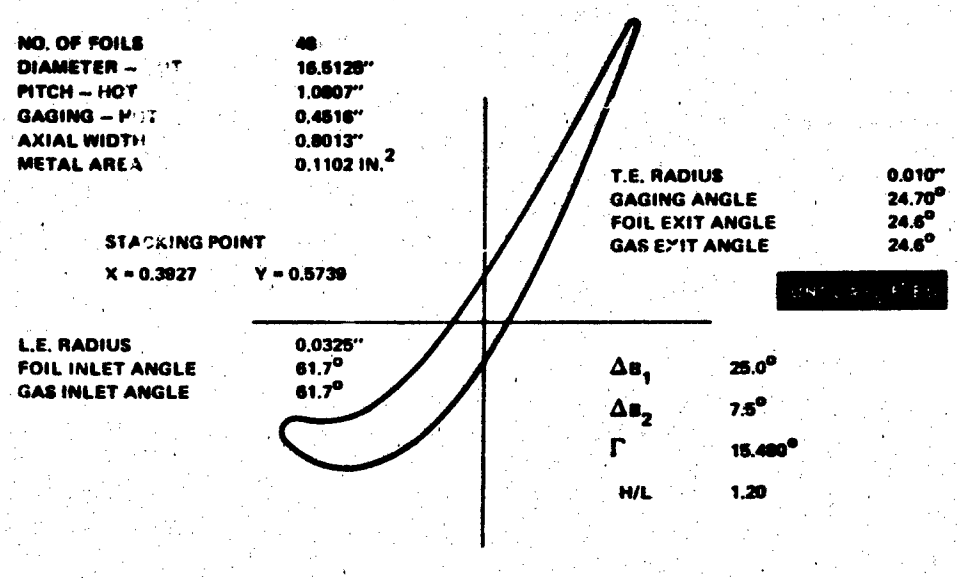

Figure 213 Medium Reaction, Low Solidity, First-Stage Vane ¼ Root (B-B) Section

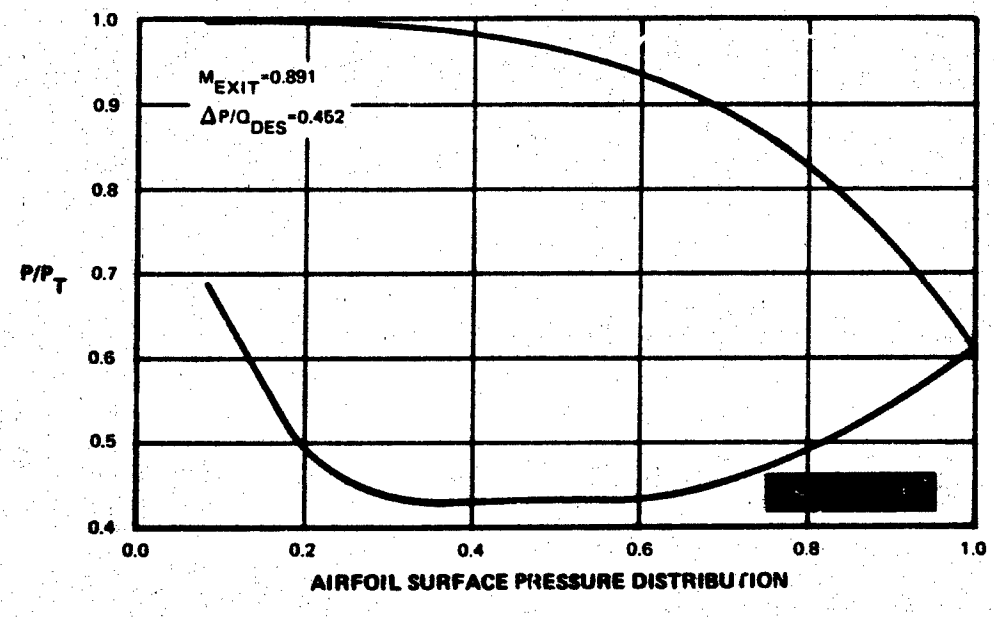

Figure 214 Medium Reaction, Low Solidity, First-Stage Vane ¼ Root

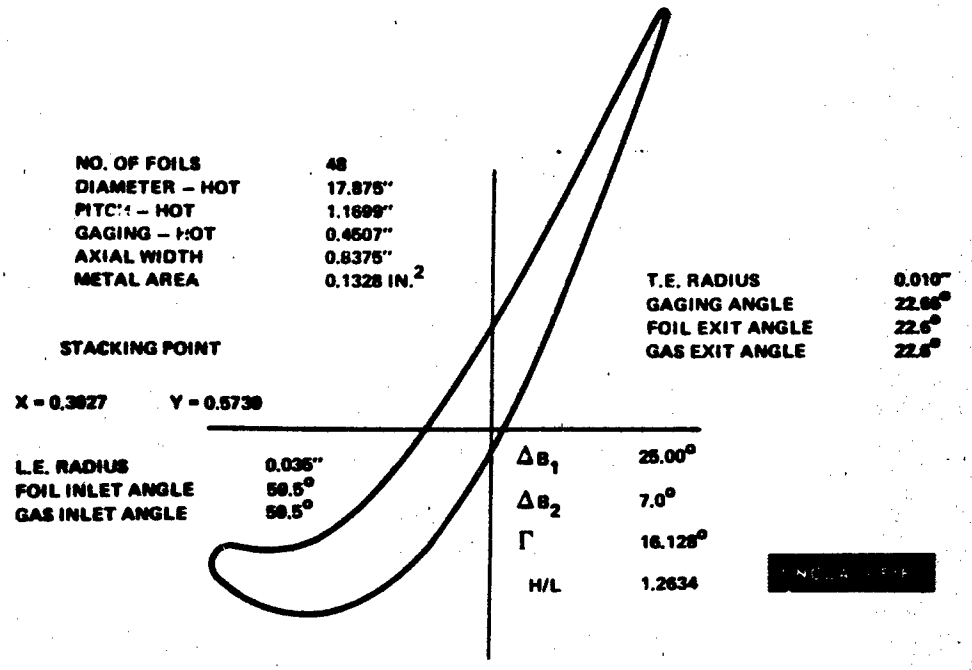

Figure 215 Medium Reaction, Low Solidity, First-Stage Vane Mean (C-C) Section

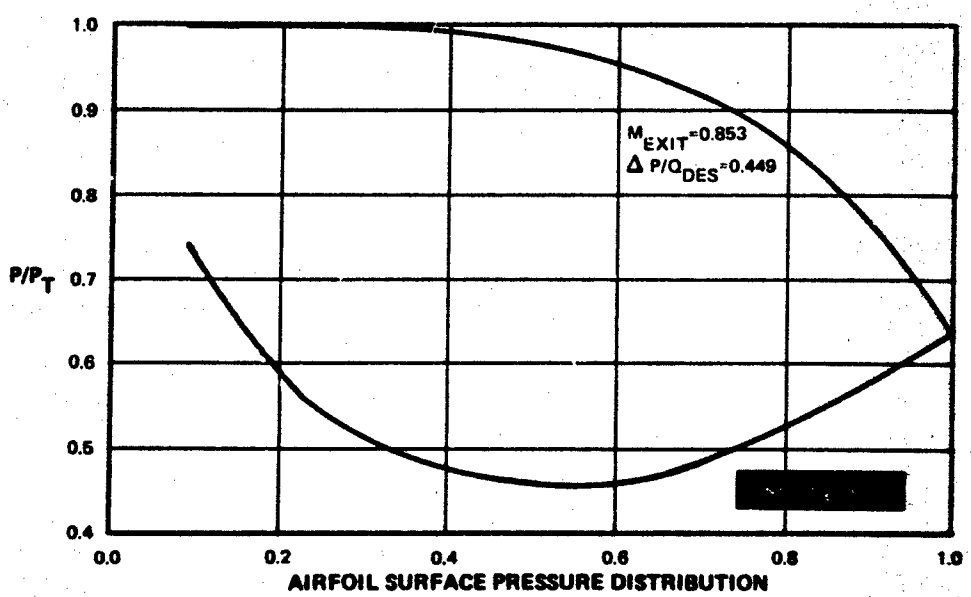

Figure 216 Medium Reaction, Low Solidity, First-Stage Vane Mean

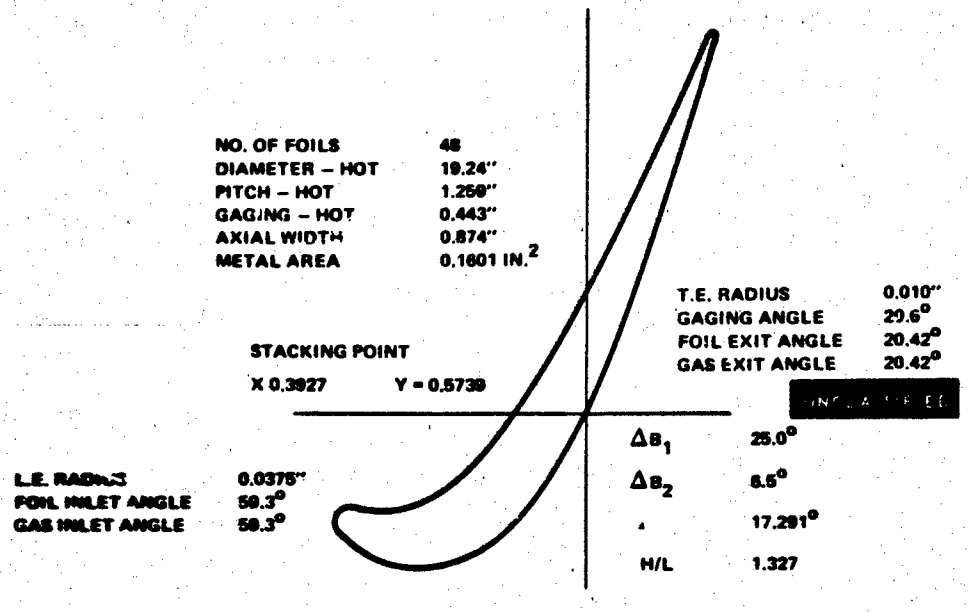

Figure 217 Medium Reaction, Low Solidity, First-Stage Vane ¼ Tip (D-D) Section

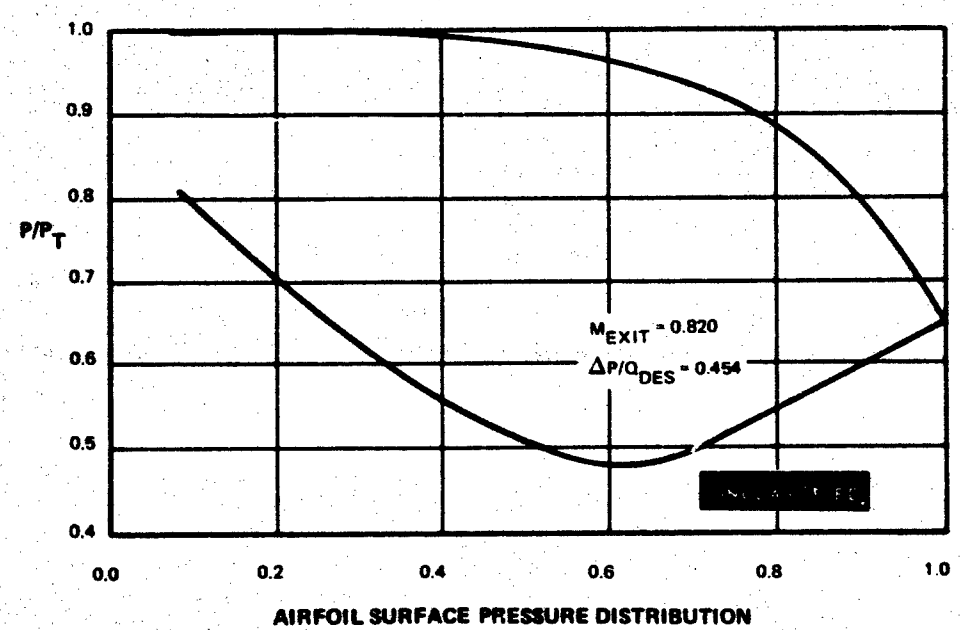

Figure 218 Medium Reaction, Low Solidity, First-Stage Vane ¼ Tip

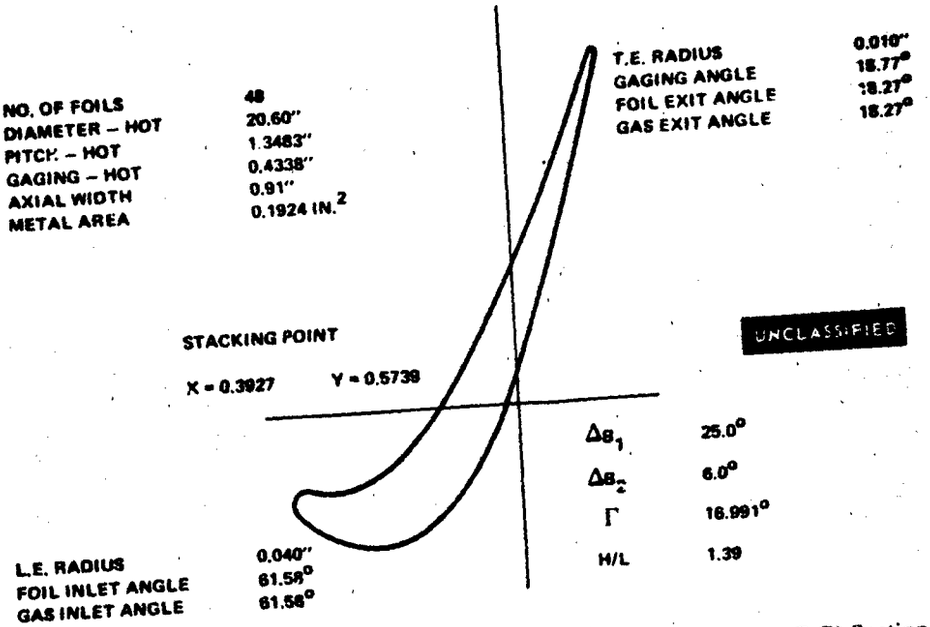

Figure 219 Medium Reaction, Low Solidity, First-Stage Vane Tip (G-G) Section

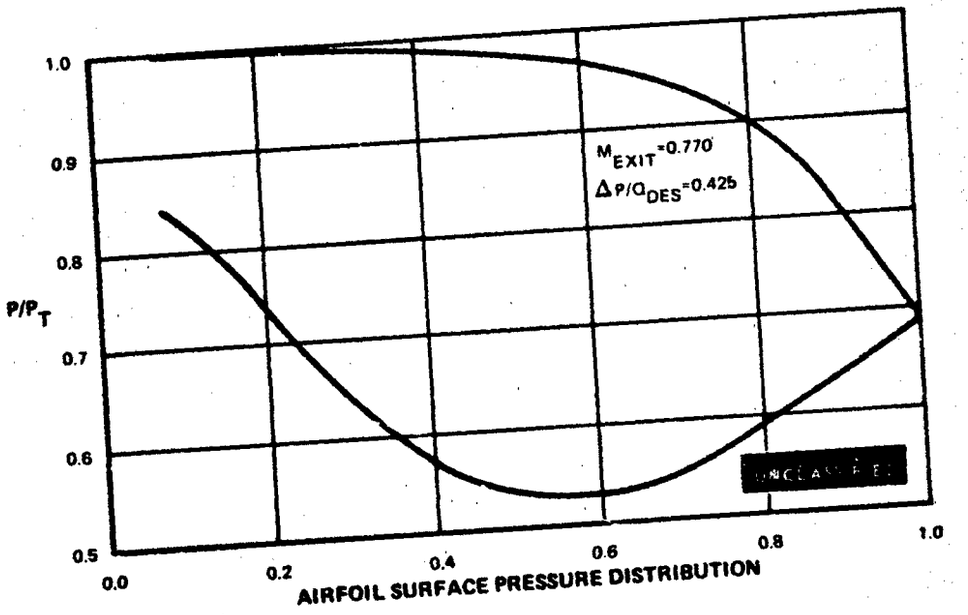

Figure 220 Medium Reaction, Low Solidity, First-Stage Vane Tip

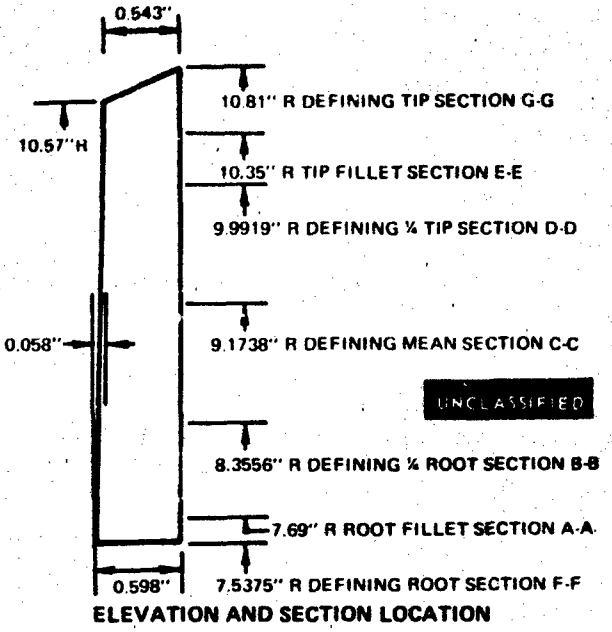

Figure 221 Medium Reaction, Low Solidity, First-Stage Blade

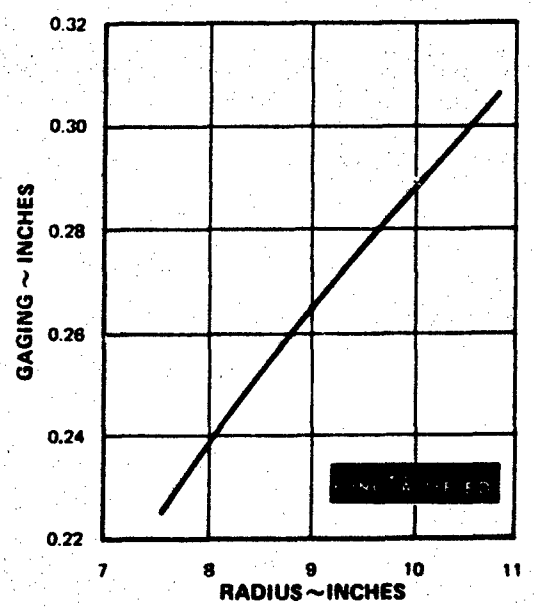

Figure 222 Medium Reaction, Low Solidity, First-Stage Blade – Gaging Distribution

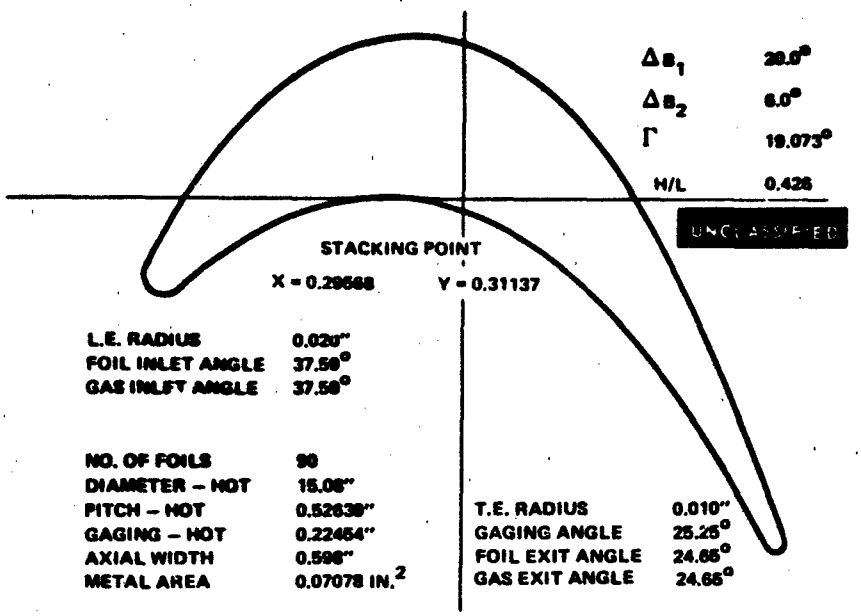

Figure 223 Medium Reaction, Low Solidity, First-Stage Blade Root (F-F) Section

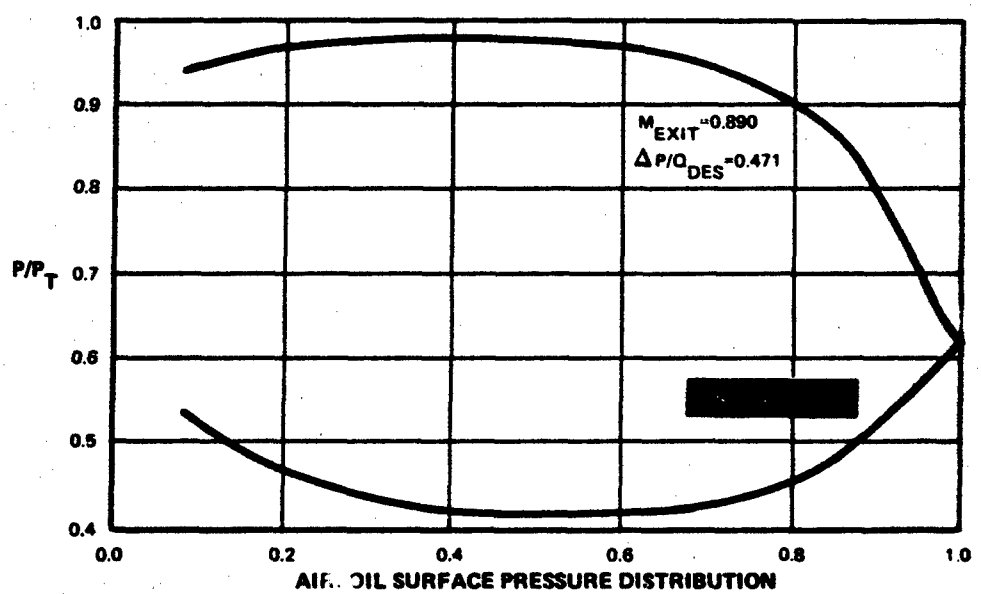

Figure 224 Medium Reaction, Low Solidity, First-Stage Blade Root

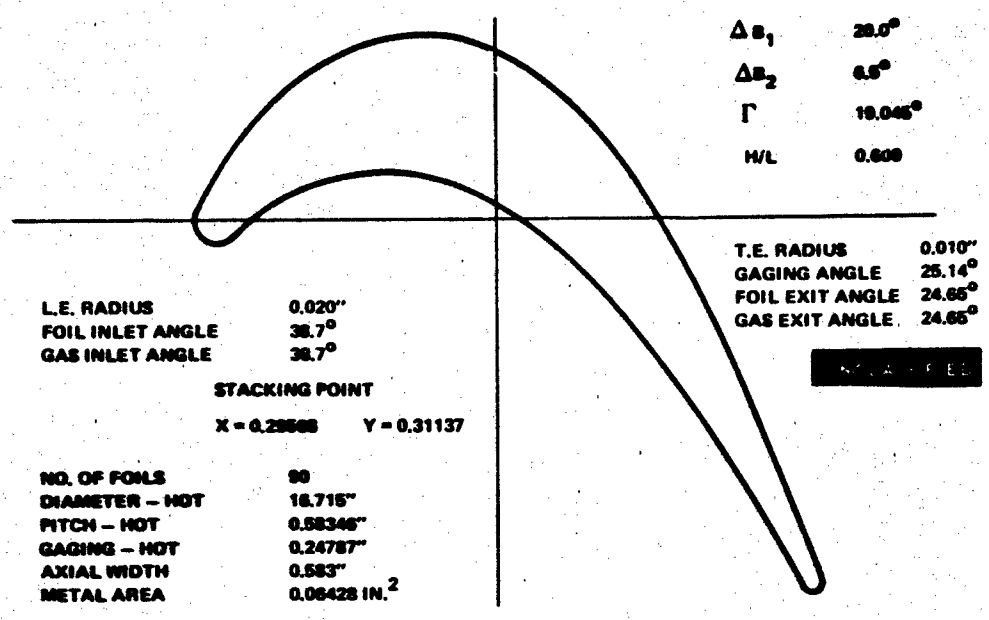

Figure 225 Medium Reaction, Low Solidity, First-Stage Blade ¼ Root (B-B) Section

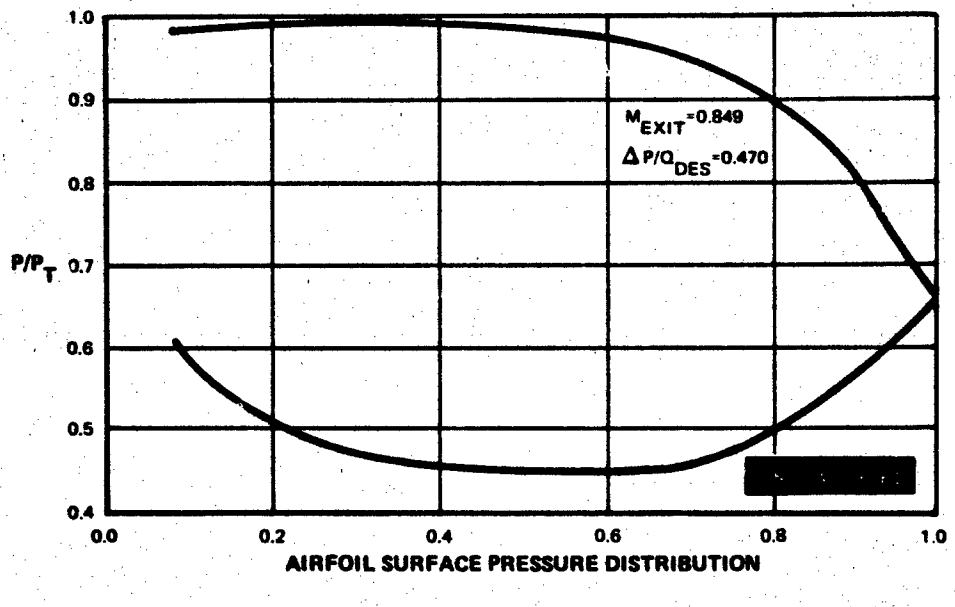

Figure 226 Medium Reaction, Low Solidity, First-Stage Blade ¼ Root

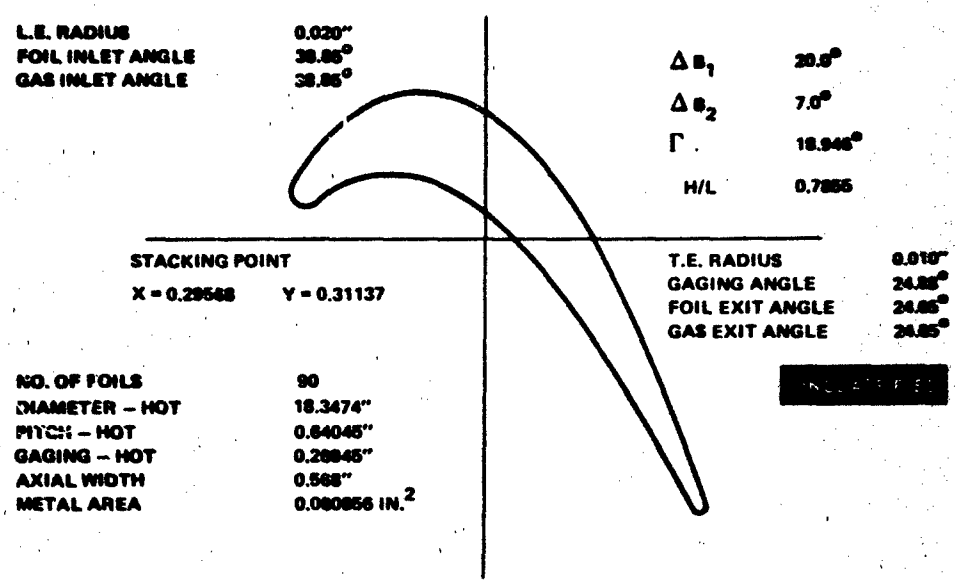

Figure 227 Medium Reaction, Low Solidity, First-Stage Blade Mean (C-C) Section

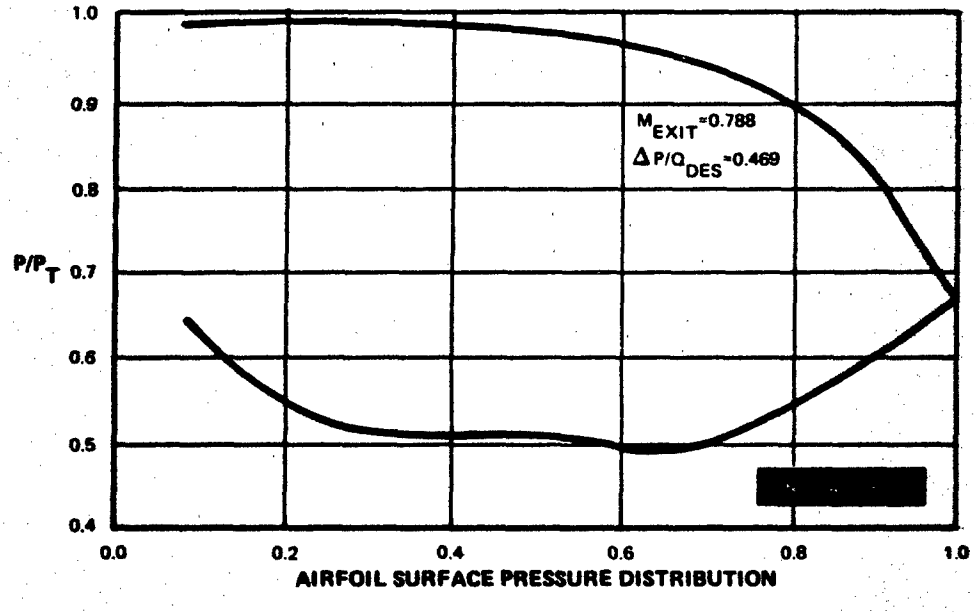

Figure 228 Medium Reaction, Low Solidity, First-Stage Blade Mean

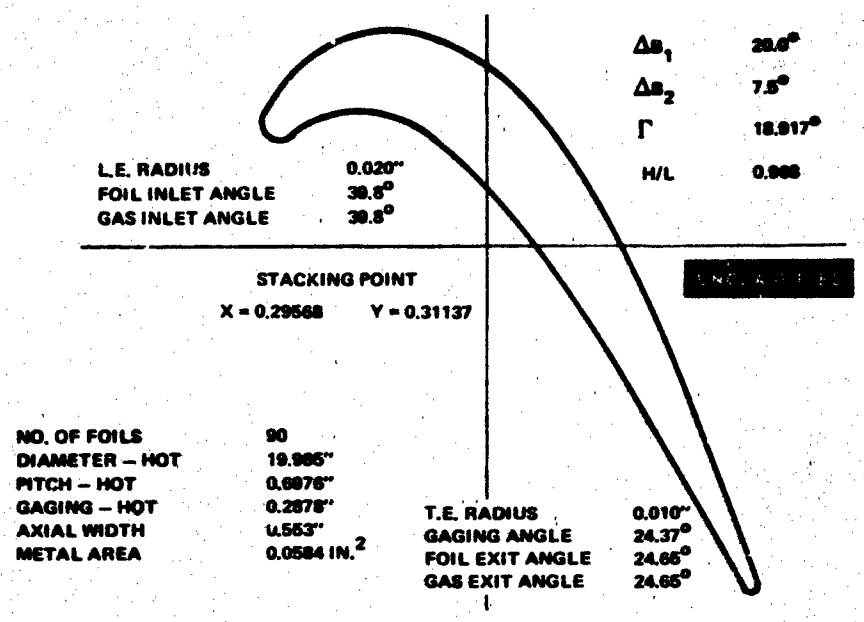

Figure 229 Medium Reaction, Low Solidity, First-Stage Blade ¼ Tip (D-D) Section

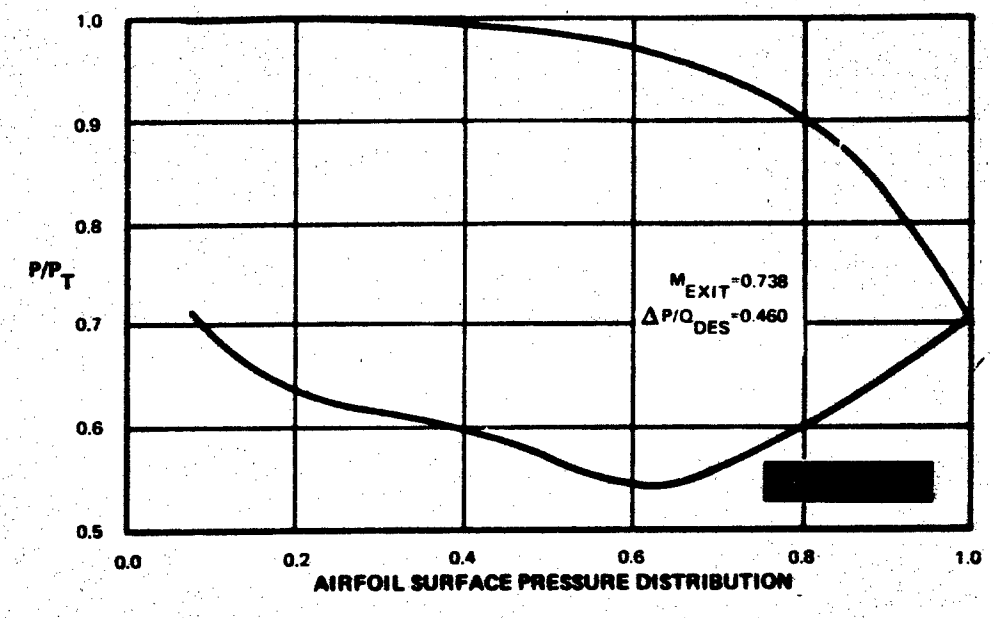

Figure 230 Medium Reaction, Low Solidity, First-Stage Blade ¼ Tip

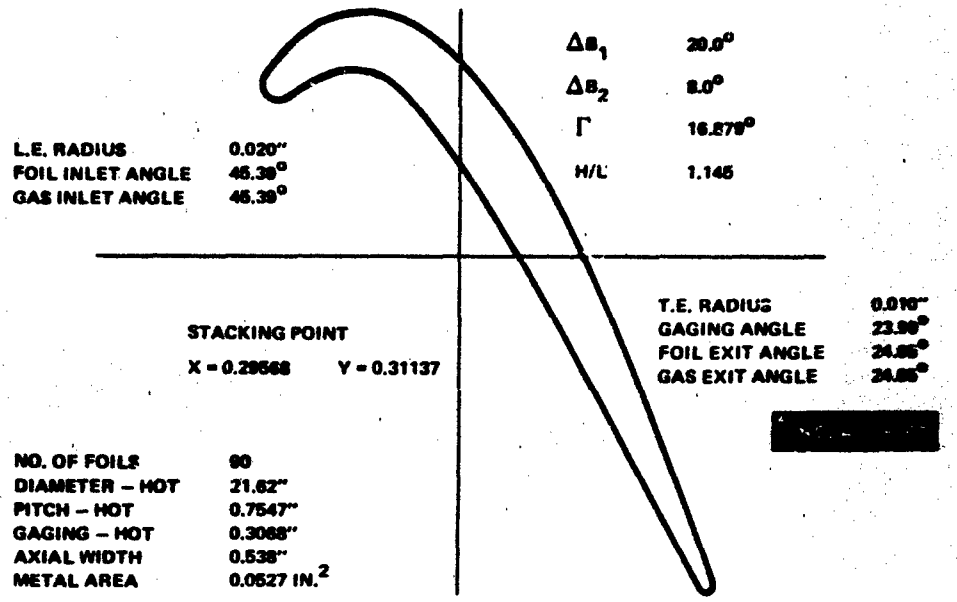

Figure 231 Medium Reaction, Low Solidity, First-Stage Blade Tip (G-G) Section

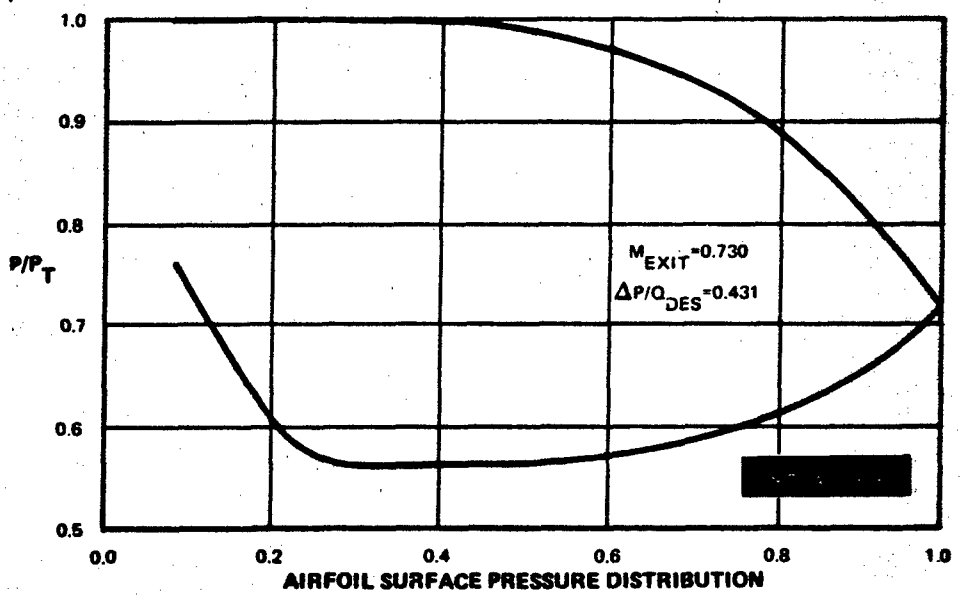

Figure 232 Medium Reaction, Low Solidity, First-Stage Blade Tip

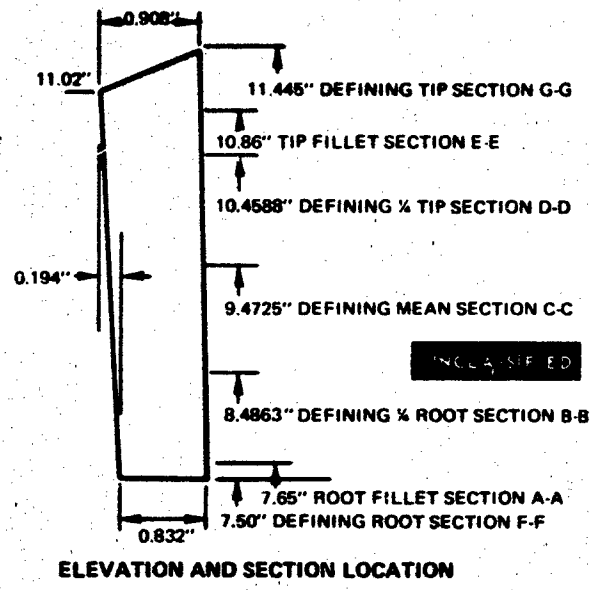

Figure 233 Medium Reaction, Low Solidity, Second-Stage Vane

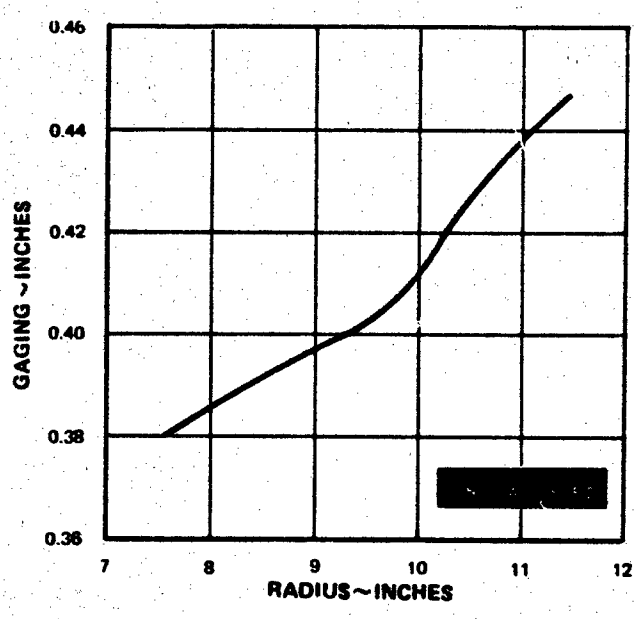

Figure 234 Medium Reaction, Low Solidity, Second-Stage Vane – Gaging Distribution

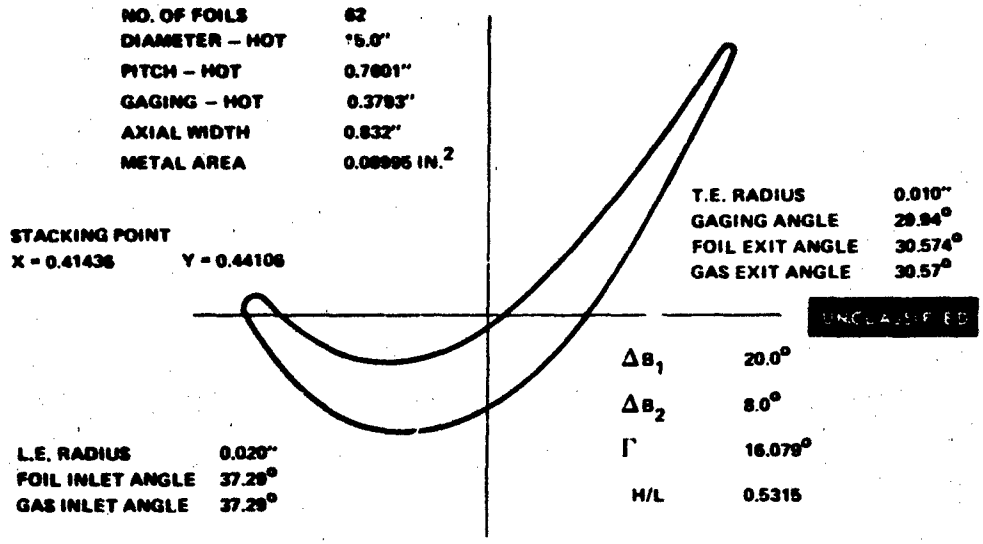

Figure 235 Medium Reaction, Low Solidity, Second-Stage Vane Root (F-F) Section

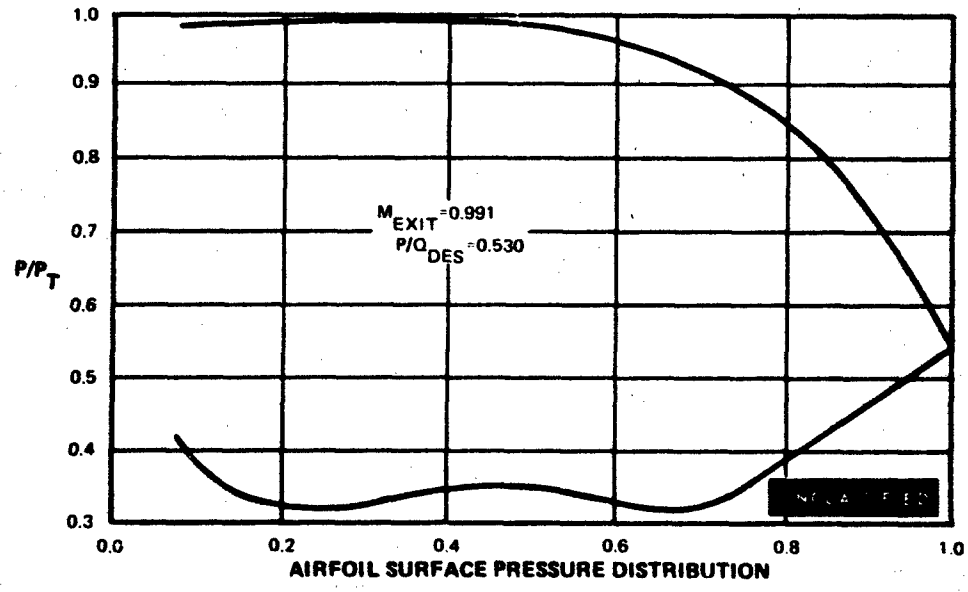

Figure 236 Medium Reaction, Low Solidity, Second-Stage Vane Root

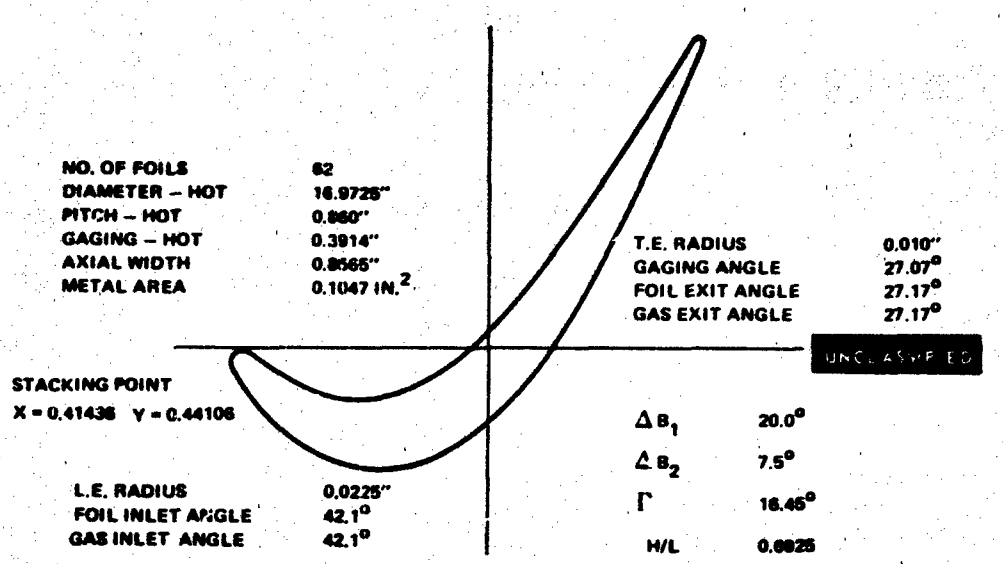

Figure 237 Medium Reaction, Low Solidity, Second-Stage Vane ¼ Root (B-B) Section

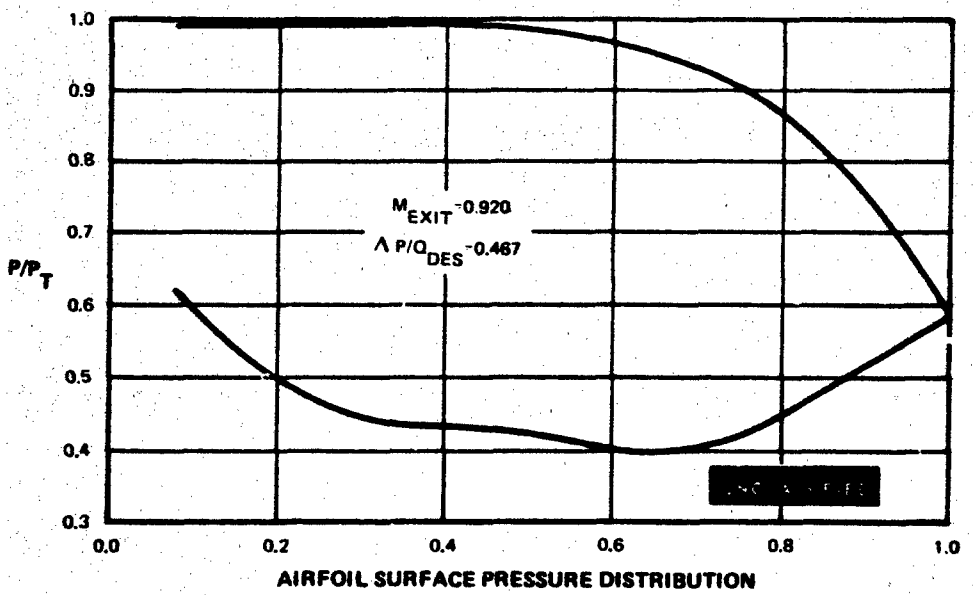

Figure 238 Medium Reaction, Low Solidity, Second-Stage Vane ½ Root

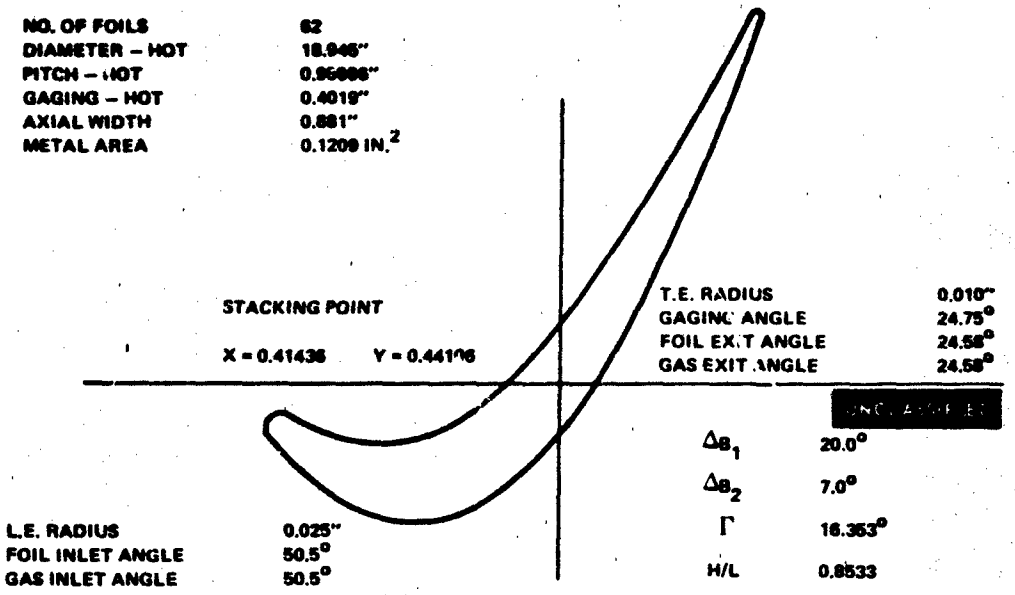

Figure 239 Medium Reaction, Low Solidity, Second-Stage Vane Mean (C-C) Section

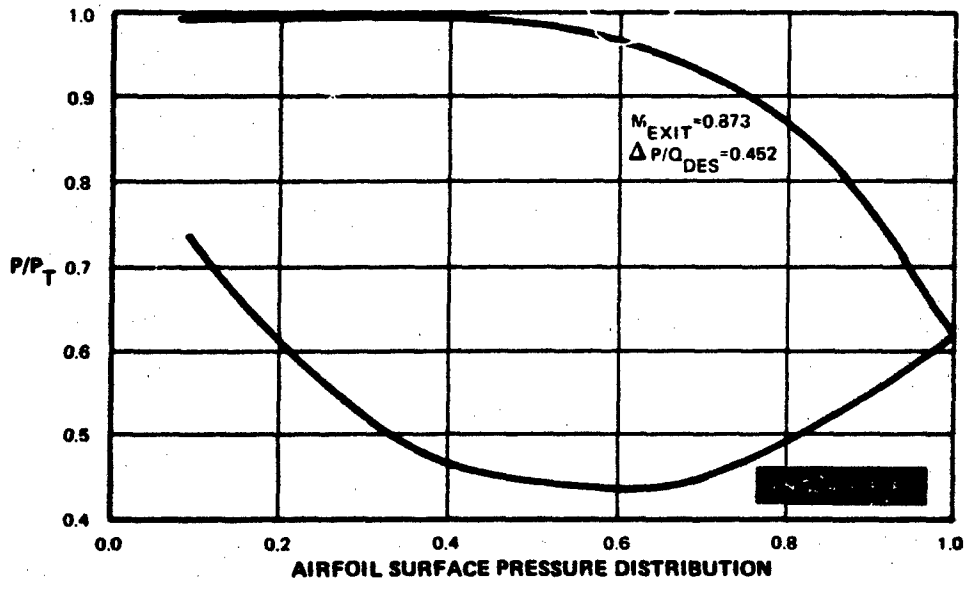

Figure 240 Medium Reaction, Low Solidity, Second-Stage Vane Mean

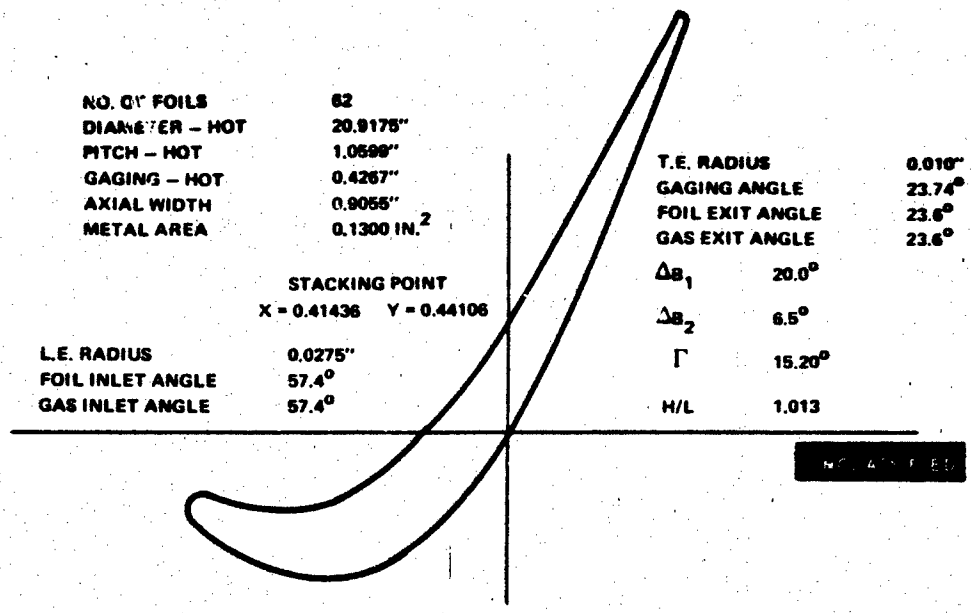

Figure 241 Medium Reaction, Low Solidity, Second-Stage Vane ¼ Tip (D-D) Section

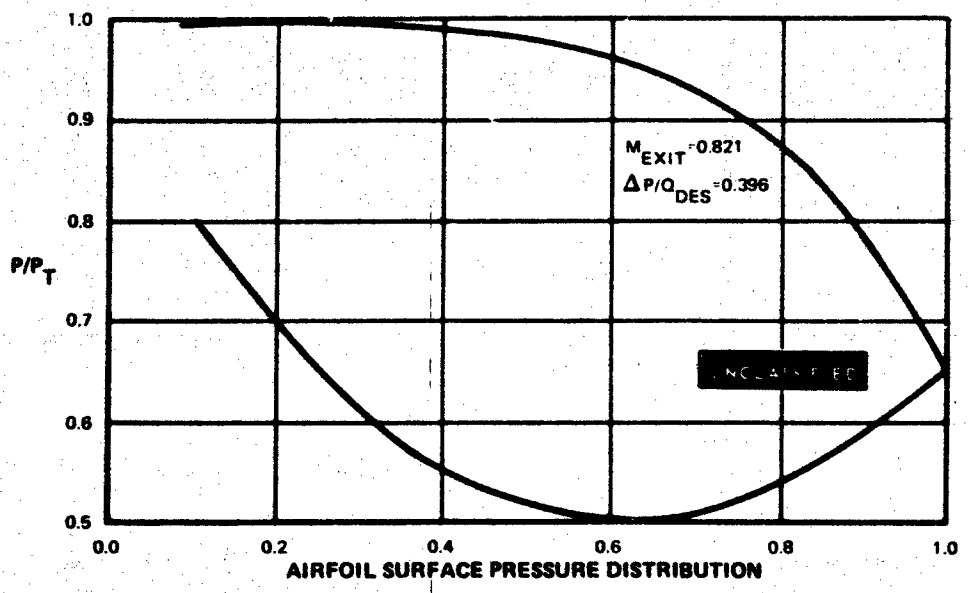

Figure 242 Medium Reaction, Low Solidity, Second-Stage Vane ¼ Tip

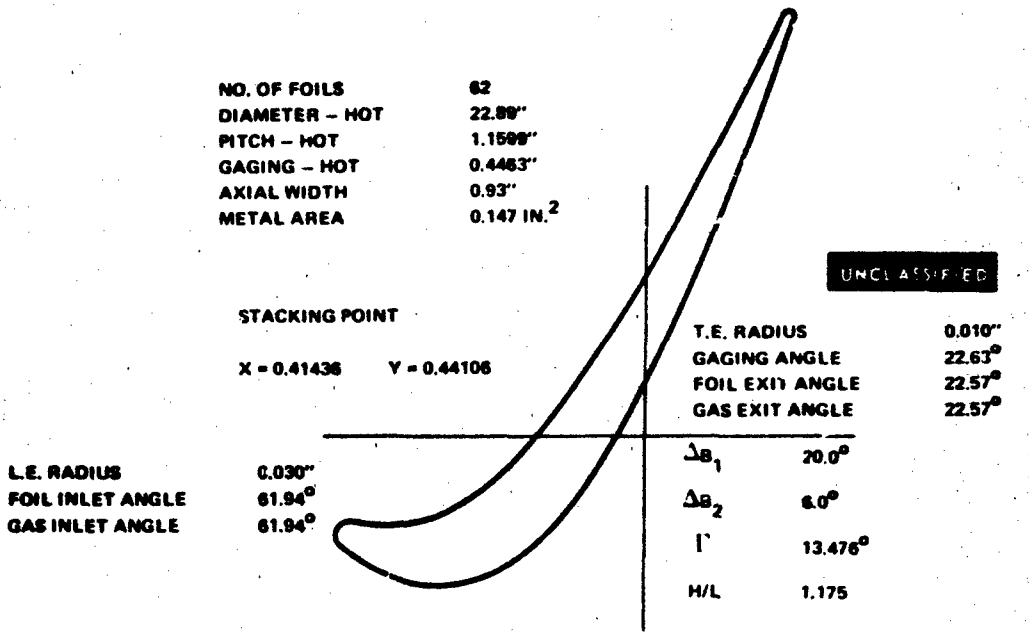

Figure 243 Medium Reaction, Low Solidity, Second-Stage Vane Tip (H-H) Section

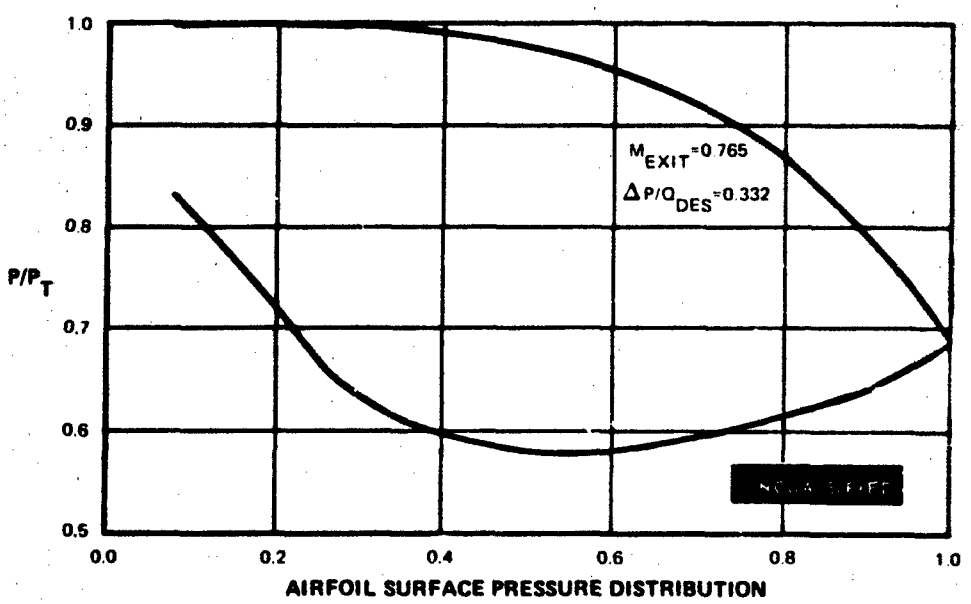

Figure 244 Medium Reaction, Low Solidity, Second-Stage Vane Tip

APPENDIX VII

LOW SOLIDITY AIRFOIL COOkDINATES

TABLE XVIII
FIRST STAGE VANE

Section F-F AT R = 7.57503

Percent X	X	Y (Top)	(Circle)		Y (Bot)	(Circle)
.00	.00000	.83806	.82424		.78218	.82424
.01	.00765	.84468	.84415		.78548	.80434
.02	.01530	.85074			.78845	.79825
.03	.02295	.85626			.79108	.79530
.04	.03060	.86128			.79336	.79453
.05	.03825	.86581			.79530	
.10	.07650	.88181			.79967	
.15	.11475	.88803			.79510	
.20	.15300	.88576			.78179	
.25	.19125	.87588			.76032	
.30	.22950	.85900			.73152	
.35	.26775	.83553			.69635	
.40	.30600	.80574			.65575	
.45	.34425	.76977			.61060	
.50	.38250	.72768			.56166	
.55	.42075	.67938			.50960	
.60	.45900	.62478			.45495	
.65	.49725	.56396			.39814	
.70	.53550	.49721			.33954	
.75	.57375	.42499			.27943	
.80	.61200	.34787			.21806	
.85	.65025	.26645			.15562	
.90	.68850	.18131			.09226	
.95	.72675	.09300			.02812	
.98	.74970	.03869			-.01070	-.00849
.99	.75735	.02039			-.02369	-.00973
1.00	.76500	.00199	-.00000		-.03670	-.00000

LE Center	(.02973,	.82424)	R = .02973			
TE Center	(.75500,	-.00000)	R = .01000			
Center of Gravity	(.39272,	.57391)				
Radial Reference	(.39272,	.57391)				
Gaging =	.44537					
Nose Point	(.00435,	.80877)				
Tail Point	(.75938,	-.00900)				
LE Tangency Points	Top	(.01127,	.84755)	Bottom	(.03310,	.79471)
TE Tangency Points	Top	(.76423,	.00384)	Bottom	(.74639,	-.00510)

Inlet Angle = 67.55274
Exit Angle = 26.58656

No. of Blades = 48
Pitch = .99157

Tolerance = -.00000
Gaging = .44537

Uncovered Turning = 16.10159
Gaging Angle = 26.68948

Area = .09348
Axial Chord = .76500

TABLE XIX
FIRST STAGE VANE

Section A-A AT R = 7.72500

Percent X	X	Y (Top)	(Circle)	Y (Bot)	(Circle)
.00	-.01376	.83678	.82278	.77986	.82278
.01	-.00603	.84352	.84301	.78317	.80254
.02	.00170	.84975		.78618	.79634
.03	.00943	.85547		.78886	.79329
.04	.01716	.86072		.79123	.79244
.05	.02489	.86551		.79327	
.10	.06354	.88300		.79842	
.15	.10219	.89074		.79484	
.20	.14083	.88974		.78246	
.25	.17948	.88073		.76164	
.30	.21813	.86423		.73305	
.35	.25678	.84064		.69760	
.40	.29543	.81022		.65628	
.45	.33408	.77317		.61003	
.50	.37273	.72958		.55972	
.55	.41138	.67950		.50607	
.60	.45003	.62294		.44968	
.65	.48868	.56008		.39104	
.70	.52733	.49123		.33054	
.75	.56597	.41686		.26851	
.80	.60462	.33754		.20519	
.85	.64327	.25383		.14079	
.90	.68192	.16631		.07547	
.95	.72057	.07551		.00938	
.98	.74376	.01965		-.03060	-.02846
.99	.75149	.00082		-.04398	-.02982
1.00	.75922	-.01811	-.02008	-.05738	-.02008

LE Center	(.01658,	.82278)	R = .03034		
TE Center	(.74922,	-.02008)	R = .01000		
Center of Gravity	(.38239,	.57138)			
Radial Reference	(.39272,	.57391)			
Gaging =	.44737				
Nose Point	(-.00930,	.80693)			
Tail Point	(.75354,	-.02910)			
LE Tangency Points	Top	(-.00245,	.84641)	Bottom	(.02058, .79270)
TE Tangency Points	Top	(.75848,	-.01629)	Bottom	(.74056, -.02509)

Inlet Angle = 66.78992
Exit Angle = 26.16331

[redacted]

No. of Blades = 48
Pitch = 1.01120

Tolerance = -.00000
Gaging = .44737

Uncovered Turning = 15.82365
Gaging Angle = 26.25784

Area = .09669
Axial Chord = .77298

TABLE XX
FIRST STAGE VANE

Section B-B AT R = 8.25700

Percent X	X	Y (Top)	(Circle)	Y (Bot)	(Circle)
.00	-.06257	.83410	.81962	.77278	.81962
.01	-.05456	.84142	.84098	.77639	.79826
.02	-.04654	.84830		.77972	.79162
.03	-0.3853	.85474		.78278	.78827
.04	-.03052	.86075		.78555	.78716
.05	-.02250	.86633		.78801	
.10	.01756	.88811		.79561	
.15	.05762	.90005		.79465	
.20	.09769	.90268		.78453	
.25	.13775	.89641		.76513	
.30	.17782	.88157		.73683	
.35	.21788	.85844		.70040	
.40	.25795	.82722		.65685	
.45	.29801	.78807		.60728	
.50	.33808	.74110		.55271	
.55	.37814	.68637		.49404	
.60	.41821	.62397		.43203	
.65	.45827	.55419		.36729	
.70	.49833	.47754		.30033	
.75	.53840	.39466		.23155	
.80	.57846	.30626		.16125	
.85	.61853	.21304		.08970	
.90	.65859	.11569		.01711	
.95	.69866	.01480		-.05637	
.98	.72270	-.04721		-.10083	-.09893
.99	.73071	-.06810		-.11571	-.10075
1.00	.73872	-.08910	-.09094	-.13061	-.09094

LE Center (-.03010, .81962) R = .03247
TE Center (.72872, -.09094) R = .01000

Center of Gravity (.34803, .56220)
Radial Reference (.39272, .57391)

Gaging = .45160

Nose Point (-.05742, .80207)
Tail Point (.73280, -.10008)

Le Tangency Points	Top	(-.05124,	.84426)	Bottom	(-.02405,	.78772)
TE Tangency Points	Top	(.73806,	-.08738)	Bottom	(.71992,	-.09570)

Inlet Angle = 64.31708
Exit Angle = 24.64504

No. of Blades = 48
Pitch = 1.08084

Tolerance = -.00000
Gaging = .45160

Uncovered Turning = 15.51388
Gaging Angle = 24.69737

Area = .11027
Axial Chord = .80129

TABLE XXI
FIRST STAGE VANE

Section C-C AT R = 8.93800

Percent X	X	Y (Top)	(Circle)	Y (Bot)	(Circle)
.00	-.12505	.83473	.81984	.76671	.81984
.01	-.11667	.84295	.84261	.77109	.79708
.02	-.10830	.85068		[illegible]	.78990
.03	-.09992	.85793		[illegible]	.78617
.04	-.09154	.86471		.78228	.78475
.05	-.08317	.87103		.78534	.78537
.10	-.04129	.89613		.79529	
.15	.00058	.91107		.79583	
.20	.04246	.91654		.78655	
.25	.08434	.91305		.76740	
.30	.12621	.90087		.73872	
.35	.16809	.88014		.70118	
.40	.20996	.85085		.65565	
.45	.25184	.81285		.60311	
.50	.29372	.76580		.54453	
.55	.33559	.70921		.48081	
.60	.37747	.64240		.41275	
.65	.41935	.56517		.34104	
.70	.46122	.47809		.26627	
.75	.50310	.38232		.18892	
.80	.54498	.27932		.10940	
.85	.58685	.17049		.02803	
.90	.62873	.05709		-.05491	
.95	.67060	-.05990		-.13918	
.98	.69573	-.13147		-.19032	-.18875
.99	.70411	-.15553		-.20745	-.19124
1.00	.71248	-.17968	-.18137	-.22462	-.18137

LE Center (-.08992, .81984) R = .03513
TE Center (.70248, -.18137) R = .01000

Center of Gravity (.30845, .55052)
Radial Reference (.39272, .57391)

Gaging = .45071

Nose Point (-.11867, .79965)
Tail Point (.70624, -.19064)

LE Tangency Points Top (-.11374, .84566) Bottom (-.08180, .78567)
TE Tangency Points Top (.71193, -.17809) Bottom (.69350, -.18578)

Inlet Angle = 61.97033
Exit Angle = 22.64833

No. of Blades = 48
Pitch = 1.16998

Tolerance = -.00000
Gaging = .45071

Uncovered Turning = 16.14165
Gaging Angle = 22.65807

Area = .13286
Axial Chord = .83753

TABLE XXII
FIRST STAGE VANE

Section D-D AT R = 9.61900

Percent X	X	Y (Top)	(Circle)	Y (Bot)	Circle
.00	-.18752	.83706	.82115	.76343	.82115
.01	-.17879	.84570	.84529	.76825	.79701
.02	-.17005	.85383		.77270	.78932
.03	-.16131	.86147		.77677	.78523
.04	-.15257	.86863		.78047	.78353
.05	-.14383	.87532		.78378	.78391
.10	-.10015	.90230		.79448	
.15	-.05646	.91933		.79522	
.20	-.01277	.92729		.78591	
.25	.03092	.92668		.76669	
.30	.07461	.91777		.73787	
.35	.11829	.90059		.69997	
.40	.16198	.87495		.65361	
.45	.20567	.84045		.59949	
.50	.24936	.79633		.53834	
.55	.29305	.74143		.47091	
.60	.33674	.67395		.39787	
.65	.38042	.59200		.31988	
.70	.42411	.49530		.23752	
.75	.46780	.38550		.15131	
.80	.51149	.26532		.06172	
.85	.55518	.13743		-.03085	
.90	.59886	.00400		-.12603	
.95	.64255	-.13340		-.22353	
.98	.66877	-.21726		-.28303	-.28183
.99	.67750	-.24542		-.30301	-.28510
1.00	.68624	-.27366	-.27517	-.32307	-.27517

LE Center	(-.14981,	.82115)	R = .03772			
TE Center	(.67624,	-.27517)	R = .01000			
Center of Gravity	(.27190,	.53883)				
Radial Reference	(.39272,	.57391)				
Gaging =	.44299					
Nose Point	(-.18052,	.79926)				
Tail Point	(.67964,	-.28458)				
LE Tangency Points	Top	(-.17550,	.84876)	Bottom	(-.14084,	.78451)
TE Tangency Points	Top	(.68579,	-.27222)	Bottom	(.66708,	-.27921)

Inlet Angle = 61.65043
Exit Angle = 20.48513

No. of Blades = 48
Pitch = 1.25912

Tolerance = -.00000
Gaging = .44299

Uncovered Turning = 17.31866
Gaging Angle = 20.59899

Area = .16024
Axial Chord = .87376

TABLE XXIII
FIRST STAGE VANE

Section E-E AT R = 9.72000

Percent X	X	Y (Top)	(Circle)	Y (Bot)	(Circle)
.00	-.19679	.83693	.82079	.76267	.82079
.01	-.18800	.84557	.84513	.76750	.79645
.02	-.17921	.85371		.77195	.78869
.03	-.17041	.86137		.77602	.78454
.04	-.16162	.86855		.77971	.78281
.05	-.15283	.87529		.78301	.78315
.10	-.10888	.90259		.79365	
.15	-.06492	.92011		.79432	
.20	-.02096	.92865		.78496	
.25	.02300	.92867		.76572	
.30	.06695	.92039		.73691	
.35	.11091	.90380		.69900	
.40	.15487	.87869		.65259	
.45	.19882	.84459		.59832	
.50	.24278	.80072		.53689	
.55	.28674	.74586		.46900	
.60	.33069	.67810		.39531	
.65	.37465	.59540		.31646	
.70	.41861	.49737		.23301	
.75	.46256	.38565		.14549	
.80	.50652	.26304		.05436	
.85	.55048	.13235		-.03996	
.90	.59443	-.00416		-.13711	
.95	.63839	-.14483		-.23677	
.98	.66477	-.23072		-.29765	-.29651
.99	.67356	-.25956		-.31811	-.29991
1.00	.68235	-.28849	-.28998	-.33866	-.28998

LE Center	(-.15869,	.82079)	R = .03809		
TE Center	(.67234,	-.28998)	R = .01000		
Center of Gravity	(.26614,	.53715)			
Radial Reference	(.39272,	.57391)			
Gaging =	.44156				
Nose Point	(-.18979,	.79879)			
Tail Point	(.67570,	-.29940)			
LE Tangency Points	Top	(-.18457,	.84874)	Bottom	(-.14974, .78376)
TE Tangency Points	Top	(.68192,	-.28707)	Bottom	(.66317, -.29395)
Inlet Angle =	61.80563				
Exit Angle =	20.16326				
No. of Blades =	48				
Pitch =	1.27234				
Tolerance =	-.00000				
Gaging =	.44156				
Uncovered Turning =	17.41389				
Gaging Angle =	28.30677				
. . =	.86471				
m0 =	.87914				

TABLE XXIV
FIRST STAGE VANE

Section G-G AT R = 10.30000

Percent X	X	Y (Top)	(Circle)	Y (Bot)	(Circle)
.00	-.25000	.83233	.81430	.75547	.81430
.01	-.24090	.84054	.83977	.76000	.78882
.02	-.23180	.84843		.76415	.78064
.03	-.22270	.85601		.76792	.77621
.04	-.21360	.86326		.77132	.77427
.05	-.20450	.87019		.77433	.77444
.10	-.15900	.90006		.78368	
.15	-.11350	.92184		.78341	
.20	-.06800	.93541		.77353	
.25	-.02250	.94053		.75414	
.30	.02300	.93689		.72543	
.35	.06850	.92405		.68767	
.40	.11400	.90145		.64120	
.45	.15950	.86836		.58642	
.50	.20500	.82383		.52377	
.55	.25050	.76657		.45371	
.60	.29600	.69488		.37672	
.65	.34150	.60683		.29328	
.70	.38700	.50162		.20385	
.75	.43250	.38032		.10890	
.80	.47800	.24532		.00885	
.85	.52350	.09948		-.09589	
.90	.56900	-.05459		-.20493	
.95	.61450	-.21482		-.31792	
.98	.64180	-.31324		-.38747	-.38671
.99	.65090	-.34636		-.41093	-.39094
1.00	.66000	-.37963	-.38097	-.43453	-.38097

LE Center	(-.20979,	.81430)	R = .04021			
TE Center	(.65000,	-.38097)	R = .01000			
Center of Gravity	(.23032,	.52714)				
Radial Reference	(.39272,	.57391)				
Gaging =	.43382					
Nose Point	(-.24356,	.79247)				
Tail Point	(.65305,	-.39050)				
LE Tangency Points	Top	(-.23614,	.84467)	Bottom	(-.20170,	.77491)
TE Tangency Points	Top	(.65965,	-.37833)	Bottom	(.64068,	-.38463)

Inlet Angle =	63.72772
Exit Angle =	18.36435
No. of Blades =	48
Pitch =	1.34827
Tolerance =	-.00000
Gaging =	.43382
Uncovered Turning =	17.01983
Gaging Angle =	18.76954
Area =	.19253
Axial Chord =	.91000

TABLE XXV
FIRST STAGE BLADE

Section F-F AT R = 7.53750

Percent X	X	Y (Top)	(Circle)	Y (Bot)	(Circle)
.00	.00000	.24684	.24190	.19366	.24190
.01	.00598	.25824		.20009	.22760
.02	.01196	.26918		.20632	.22354
.03	.01794	.27971		.21237	.22194
.04	.02392	.28983		.21822	.22220
.05	.02990	.29957		.22389	.22439
.10	.05980	.34289		.24946	
.15	.08970	.37825		.27052	
.20	.11960	.40661		.28719	
.25	.14950	.42859		.29957	
.30	.17940	.44461		.30771	
.35	.20930	.45493		.31165	
.40	.23920	.45969		.31143	
.45	.26910	.45890		.30703	
.50	.29900	.45246		.29844	
.55	.32890	.44016		.28561	
.60	.35880	.42162		.26847	
.65	.38870	.39629		.24693	
.70	.41860	.36334		.22087	
.75	.44850	.32168		.19013	
.80	.47840	.27094		.15454	
.85	.50830	.21196		.11385	
.90	.53820	.14639		.06779	
.95	.56810	.07591		.01601	
.98	.58604	.03186		-.01798	-.00990
.99	.59202	.01694		-.02981	-.00921
1.00	.59800	.00191	-.00002	-.04191	-.00002

LE Center	(.02007,	.24190)	R = .02007			
TE Center	(.58794,	-.00002)	R = .01006			
Center of Gravity	(.29568,	.31137)				
Radial Reference	(.29568,	.31137)				
Gaging =	.22431					
Nose Point	(.00868,	.22537)				
Tail Point	(.59204,	-.00920)				
LE Tangency Points	Top	(.00230,	.25123)	Bottom	(.03312,	.22664)
TE Tangency Points	Top	(.59729,	.00370)	Bottom	(.57904,	-.00471)

Inlet Angle = 38.58149
Exit Angle = 24.76439

No. of Blades = 90
Pitch = .52622

Tolerance = .00000
Gaging = .22431

Uncovered Turning = 19.20171
Gaging Angle = 25.23070

Area = .07079
Axial Chord = .59800

TABLE XXVI
FIRST STAGE BLADE

Section A-A AT R = 7.69000

Percent X	X	Y (Top)	(Circle)		Y (Bot)	(Circle)
.00	.00289	.25940	.25439		.20641	.25439
.01	.00884	.27060			.21277	.24013
.02	.01479	.28135			.21894	.23606
.03	.02075	.29167			.22492	.23444
.04	.02670	.30158			.23070	.23467
.05	.03265	.31110			.23630	.23681
.10	.06241	.35328			.26143	
.15	.09217	.38746			.28193	
.20	.12193	.41460			.29791	
.25	.15169	.43536			.30946	
.30	.18145	.45018			.31665	
.35	.21122	.45931			.31954	
.40	.24098	.46289			.31814	
.45	.27074	.46095			.31244	
.50	.30050	.45339			.30246	
.55	.33026	.43997			.28816	
.60	.36002	.42034			.26951	
.65	.38978	.39391			.24645	
.70	.41954	.35983			.21892	
.75	.44930	.31711			.18682	
.80	.47906	.26556			.15003	
.85	.50882	.20609			.10840	
.90	.53859	.14031			.06173	
.95	.56835	.06983			.00981	
.98	.58620	.02585			-.02398	-.01584
.99	.59216	.01096			-.03570	-.01513
1.00	.59811	-.00403	-.00595		-.04765	-.00595
LE Center	(.02296,	.25439)	R = .02008			
TE Center	(.58805,	-.00595)	R = .01006			
Center of Gravity	(.29803,	.31324)				
Radial Reference	(.29568,	.31137)				
Gaging =	.22875					
Nose Point	(.01149,	.23792)				
Tail Point	(.59216,	-.01513)				
LE Tangency Points	Top	(.00524,	.26381)	Bottom	(.03592,	.23906)
TE Tangency Points	Top	(.59740,	-.00224)	Bottom	(.57916,	-.01065)
Inlet Angle =	38.90183					
Exit Angle =	24.75265					
No. of Blades =	90					
Pitch =	.53686					
Tolerance =	.00000					
Gaging =	.22875					
Uncovered Turning =	19.09236					
Gaging Angle =	25.21931					
Area =	.06932					
Axial Chord =	.59522					

TABLE XXVII
FIRST STAGE BLADE

Section B-B AT R = 8.35560

Percent X	X	Y (Top)	(Circle)	Y (Bot)	(Circle)
.00	.01550	.31316	.30800	.26023	.30890
.01	.02133	.32377		.26653	.29384
.02	.02716	.33386		.27260	.28975
.03	.03299	.34348		.27845	.28806
.04	.03882	.35264		.28406	.28815
.05	.04465	.36136		.28945	.29004
.10	.07380	.39915		.31306	
.15	.10295	.42845		.33121	
.20	.13211	.45050		.34404	
.25	.16126	.46608		.35171	
.30	.19041	.47570		.35434	
.35	.21956	.47967		.35208	
.40	.24871	.47817		.34505	
.45	.27786	.47122		.33337	
.50	.30702	.45875		.31718	
.55	.33617	.44053		.29659	
.60	.36532	.41617		.27171	
.65	.39447	.38506		.24264	
.70	.42362	.34635		.20949	
.75	.45278	.29948		.17238	
.80	.48193	.24484		.13138	
.85	.51108	.18356		.08662	
.90	.54023	.11707		.03816	
.95	.56938	.04668		-.01390	
.98	.58687	.00301		-.04682	-.03839
.99	.59270	-.01175		-.05807	-.03760
1.00	.59853	-.02659	-.02849	-.06946	-.02849

LE Center	(.03560,	.30800)	R = .02010
TE Center	(.58850,	-.02849)	R = .01003
Center of Gravity	(.30834,	.32127)	
Radial Reference	(.29568,	.31137)	
Gaging =	.24775		
Nose Point	(.02392,	.29164)	
Tail Point	(.59260,	-.03765)	

LE Tangency Points	Top	(.01798,	.31768)	Bottom	(.04825,	[illegible]
TE Tangency Points	Top	(.59784,	-.02482)	Bottom	(.57964,	[illegible]

Inlet Angle =	39.89523
Exit Angle =	24.71229
No. of Blades =	90
Pitch =	.58333
Tolerance =	.00000
Gaging =	.24775
Uncovered Turning =	19.07593
Gaging Angle =	25.13289
Area =	.06429
Axial Chord =	.58303

TABLE XXVIII
FIRST STAGE BLADE

Section C-C AT R = 9.17380

Percent X	X	Y (Top)	(Circle)	Y (Bot)	(Circle)
.00	.03100	.37881	.37360	.32431	.37360
.01	.03668	.38908		.33097	.35957
.02	.04236	.39868		.33731	.35546
.03	.04804	.40767		.34333	.35367
.04	.05372	.41610		.34903	.35359
.05	.05940	.42401		.35441	.35518
.10	.08780	.45676		.37671	
.15	.11620	.48020		.39170	
.20	.14460	.49606		.39986	
.25	.17300	.50538		.40166	
.30	.20140	.50881		.39754	
.35	.22980	.50674		.38791	
.40	.25820	.49938		.37319	
.45	.28660	.48677		.35373	
.50	.31500	.46882		.32990	
.55	.34340	.44526		.30200	
.60	.37180	.41562		.27034	
.65	.40020	.37916		.23520	
.70	.42860	.33524		.19684	
.75	.45700	.28395		.15548	
.80	.48540	.22613		.11134	
.85	.51380	.16299		.06463	
.90	.54220	.09578		.01553	
.95	.57060	.02552		-.03580	
.98	.58764	-.01777		-.06760	-.05881
.99	.59332	-.03235		-.07836	-.05791
1.00	.59900	-.04701	-.04888	-.08920	-.04888

[illegible] Center	(.05118,	.37360)	R = .02018
[illegible] Center	(.58898,	-.04888)	R = .01002
Center of Gravity	(.32150,	.33117)	
Radial Reference	(.29568,	.31137)	
Gaging =	.26941		
Nose Point	(.03954,	.35712)	
Tail Point	(.59307,	-.05803)	

LE Tangency Points	Top	(.03352,	.38337)	Bottom	(.06364,	.35773)
TE Tangency Points	Top	(.59832,	-.04526)	Bottom	(.58105,	-.05361)

Inlet Angle =	40.40195
Exit Angle =	24.68435
No. of Blades =	90
Pitch =	.64045
Tolerance =	.00000
Gaging =	.26941
Uncovered Turning =	19.01534
Gaging Angle =	24.87597
Area =	.06084
Axial Chord =	.56800

TABLE XXIX
FIRST STAGE BLADE

Section D-D AT R = 9.0120

Percent X	X	Y (Top)	(Circle)	Y (Bot)	(Circle)
.00	.04650	.44895	.44355	.39364	.44355
.01	.05203	.45859		.40049	.42964
.02	.05756	.46736		.40693	.42551
.03	.06309	.47536		.41296	.42363
.04	.06862	.48269		.41860	.42339
.05	.07415	.48942		.42384	.42470
.10	.10180	.51564		.44425	
.15	.12945	.53232		.45548	
.20	.15710	.54165		.45826	
.25	.18475	.54484		.45341	
.30	.21240	.54260		.44176	
.35	.24005	.53431		.42413	
.40	.26770	.52312		.40127	
.45	.29535	.50603		.37386	
.50	.32300	.48382		.34249	
.55	.35066	.45604		.30771	
.60	.37831	.42191		.26995	
.65	.40596	.38049		.22962	
.70	.43361	.33157		.18703	
.75	.46126	.27590		.14249	
.80	.48891	.21479		.09623	
.85	.51656	.14960		.04846	
.90	.54421	.08146		-.00063	
.95	.57186	.01119		-.05090	
.98	.58845	-.03175		-.08157	-.07243
.99	.59398	-.04616		-.09187	-.07143
1.00	.59951	-.06063	-.06247	-.10221	-.06247

LE Center	(.06675,	.44355)	R = .02025		
TE Center	(.58950,	-.06247)	R = .01001		
Center of Gravity	(.33674,	.34107)			
Radial Reference	(.29568,	.31137)			
Gaging =	.28782				
Nose Point	(.05494,	.42710)			
Tail Point	(.59358,	-.07161)			
LE Tangency Points	Top	(.04918,	.45363)	Bottom	(.07878, .42726)
TE Tangency Points	Top	(.59885,	-.05890)	Bottom	(.58070, .06724)
Inlet Angle =	41.69758				
Exit Angle =	24.66691				
No. of Blades =	90				
Pitch =	.69757				
Tolerance =	.00000				
Gaging =	.28782				
Uncovered Turning =	19.08049				
Gaging Angle =	24.36859				
Area =	.05834				
Axial Chord =	.55301				

UNCLASSIFIED

TABLE XXX
FIRST STAGE BLADE

Section E-E AT R = 10.35000

Percent X	X	Y (Top)	(Circle)		Y (Bot)	(Circle)
.00	.05328	.47913	.47346		.42631	.47346
.01	.05875	.48811			.43244	.45963
.02	.06421	.49628			.43825	.45549
.03	.06968	.50375			.44373	.45359
.04	.07514	.51059			.44888	.45329
.05	.08061	.51685			.45371	.45451
.10	.10793	.54112			.47293	
.15	.13525	.55603			.48392	
.20	.16257	.56356			.48658	
.25	.18990	.56479			.48079	
.30	.21722	.56039			.46682	
.35	.24454	.55072			.44559	
.40	.27186	.53595			.41844	
.45	.29918	.51608			.38660	
.50	.32651	.49094			.35106	
.55	.35383	.46015			.31256	
.60	.38115	.42306			.27164	
.65	.40847	.37905			.22872	
.70	.43580	.32818			.18414	
.75	.46312	.27128			.13817	
.80	.49044	.20958			.09101	
.85	.51776	.14426			.04284	
.90	.54509	.07628			-.00619	
.95	.57241	.00635			-.05596	
.98	.58880	-.03634			-.08614	-.07684
.99	.59427	-.05066			-.09625	-.07579
1.00	.59973	-.06504	-.06688		-.10637	-.06688

LE Center	(.07352,	.47346)	R = .02023
TE Center	(.58972,	-.06688)	R = .01001
Center of Gravity	(.34318,	.34547)	
Radial Reference	(.29568,	.31137)	
Gaging =	.29638		
Nose Point	(.06119,	.45742)	
Tail Point	(.59380,	-.07601)	
LE Tangency Points	Top	(.05624,	.48398) Bottom (.08516, .45691)
TE Tangency Points	Top	(.59908,	-.06332) Bottom (.58093, -.07165)
Inlet Angle =	43.10744		
Exit Angle =	24.66352		
No. of Blades =	90		
Pitch =	.72257		
Tolerance =	.00000		
Gaging =	.29638		
Uncovered Turning =	18.50842		
Gaging Angle =	24.21622		
Area =	.05635		
Axial Chord =	.54645		

TABLE XXXI
FIRST STAGE BLADE

Section G-G AT R = 10.81000

Percent X	X	Y (Top)	(Circle)	Y (Bot)	(Circle)
.00	.06200	.51659	.51025	.47034	.51025
.01	.06738	.52426		.47461	.49657
.02	.07276	.53143		.47880	.49246
.03	.07814	.53814		.48288	.49055
.04	.08352	.54439		.48687	.49021
.05	.08890	.55020		.49075	.49135
.10	.11580	.57333		.50807	
.15	.14270	.58764		.52064	
.20	.16960	.59422		.52604	
.25	.19650	.59383		.52162	
.30	.22340	.58698		.50596	
.35	.25030	.57404		.48007	
.40	.27720	.55520		.44651	
.45	.30410	.53058		.40781	
.50	.33100	.50017		.36577	
.55	.35790	.46388		.32155	
.60	.38480	.42156		.27587	
.65	.41170	.37375		.22917	
.70	.43860	.32066		.18174	
.75	.46550	.26307		.13379	
.80	.49240	.20170		.08543	
.85	.51930	.13723		.03676	
.90	.54620	.07023		-.01216	
.9	.57310	.00118		-.06126	
.98	.58924	-.04106		-.09080	-.08131
.99	[illegible]	-.05525		-.10066	-.08020
1.00	.60[illegible]	-.06951	-.07133	-.11052	-.07133

LE Center (.08208, .51025) R = .02008
TE Center (.59000, -.07133) R = .01000

Center of Gravity [illegible] .35097)
Radial Reference (.2[illegible] .31137)

Gaging = .30683

Nose Point (.06847, .19548
Tail Point (.59407, [illegible]

LE Tangency Points Top (.06564, [illegible] 96, .49336)
TE Tangency Points Top (.59935, Bo[illegible] -.07613)

Inlet Angle = 46.13427
Exit Angle = 24.66373

[illegible]

No. of Blades = 90
Pitch = .75468

Tolerance = .00000
Gaging = .30683

Uncovered Turning = 17.00699
Gaging Angle = 23.98976

Area = .05266
Axial Chord = .53800

TABLE XXXII
SECOND STAGE VANE

Section F-F AT R = 7.5000

Percent X	X	Y (Top)	(Circle)	Y (Bot)	(Circle)
.00	.00000	.43107	.42615	.37900	.42616
.01	.00832	.44694		.38736	.40995
.02	.01664	.46171		.39553	.40648
.03	.02496	.47550		.40352	.40684
.04	.03328	.48840		.41130	.41120
.05	.04160	.50047		.41889	
.10	.08320	.55046		.45353	
.15	.12480	.58652		.48207	
.20	.16640	.61158		.50365	
.25	.20800	.62738		.51752	
.30	.24960	.63502		.52314	
.35	.29120	.63520		.52028	
.40	.33280	.62837		.50906	
.45	.37440	.61474		.48993	
.50	.41600	.59436		.46358	
.55	.45760	.56712		.43084	
.60	.49920	.53271		.39257	
.65	.54080	.49061		.34961	
.70	.58240	.44008		.30270	
.75	.62400	.38100		.25247	
.80	.66560	.31435		.19948	
.85	.70720	.24176		.14417	
.90	.74880	.16478		.08691	
.95	.79040	.08468		.02802	
.98	.81536	.03551		-.00799	-.00749
.99	.82368	.01897		-.02009	-.00986
1.00	.83200	.00236	-.00000	-.03225	-.00000

LE Center	(.01996,	.42616)	R = .01996			
TE Center	(.82200,	-.00000)	R = .01000			
Center of Gravity	(.41436,	.44106)				
Radial Reference	(.41436,	.44106)				
Gaging =	.37933					
Nose Point	(.00856,	.40977)				
Tail Point	(.82701,	-.00866)				
LE Tangency Points	Top	(.00228,	.43543)	Bottom	(.03340,	.41141)
TE Tangency Points	Top	(.83094,	.00448)	Bottom	(.81378,	-.00570)
Inlet Angle =	37.66198					
Exit Angle =	30.66686					
No. of Blades =	62					
Pitch =	.76006					
Tolerance =	-.00000					
Gaging =	.37933					
Uncovered Turning =	16.16284					
Gaging Angle =	29.93923					
Area =	.09004					
Axial Chord =	.83200					

TABLE XXXIII
SECOND STAGE VANE

Section A-A AT R = 7.6500

Percent X	X	Y (Top)	(Circle)	Y (Bot)	(Circle)
.00	-.00826	.43686	.43176	.38420	.43176
.01	.00009	.45247		.39249	.41533
.02	.00845	.46705		.40059	.41176
.03	.01681	.48060		.40849	.41199
.04	.02516	.49345		.41620	.41622
.05	.03352	.50542		.42371	
.10	.07531	.55508		.45789	
.15	.11709	.59092		.48588	
.20	.15888	.61573		.50683	
.25	.20067	.63120		.52000	
.30	.24245	.63841		.52484	
.35	.28424	.63806		.52113	
.40	.32603	.63057		.50898	
.45	.36781	.61618		.48883	
.50	.40960	.59493		.46139	
.55	.45138	.56668		.42748	
.60	.49317	.53113		.38798	
.65	.53496	.48772		.34370	
.70	.57674	.43572		.29541	
.75	.61853	.37502		.24376	
.80	.66032	.30664		.18929	
.85	.70210	.23217		.13246	
.90	.74389	.15320		.07366	
.95	.78568	.07099		.01319	
.98	.81075	.02050		-.02378	-.02327
.99	.81910	.00352		-.03621	-.02572
1.00	.82746	-.01354	-.01586	-.04869	-.01586

LE Center	(.01206,	.43176)	R = .02033		
TE Center	(.81746,	-.01586)	R = .01000		
Center of Gravity	(.40910,	.43863)			
Radial Reference	(.41436,	.44106)			
Gaging =	.38168				
Nose Point	(.00032,	.41517)			
Tail Point	(.82239,	-.02456)			
LE Tangency Points	Top	(-.00586,	.44136)	Bottom	(.02565, .41663)
TE Tangency Points	Top	(.82644,	-.01146)	Bottom	(.80918, -.02147)
Inlet Angle =	38.12138				
Exit Angle =	30.12342				
No. of Blades =	62				
Pitch =	.77526				
Tolerance =	-.00000				
Gaging =	.38168				
Uncovered Turning =	16.19122				
Gaging Angle =	29.49366				
Area =	.09198				
Axial Chord	.83573				

TABLE XXXIV
SECOND STAGE VANE

Section B-B AT R = 8.48630

Percent X	X	Y (Top)	(Circle)	Y (Bot)	(Circle)
.00	-.05434	.47259	.46606	.41826	.46606
.01	-.04578	.48[illegible]		.42569	.44841
.02	-.03721	[illegible]		.43292	.44424
.03	-.02865	.51114		.43996	.44383
.04	-.02008	.52261		.44678	.44694
.05	-.01152	.53353		.45339	
.10	.03131	.57954		.48302	
.15	.07413	.61339		.50633	
.20	.11696	.63682		.52253	
.25	.15978	.65098		.53093	
.30	.20261	.65664		.53100	
.35	.24543	.65428		.52248	
.40	.28826	.64418		.50543	
.45	.33108	.62646		.48019	
.50	.37391	.60105		.44735	
.55	.41673	.56773		.40765	
.60	.45956	.52610		.36188	
.65	.50238	.47547		.31087	
.70	.54521	.41513		.25534	
.75	.58803	.34512		.19598	
.80	.63086	.26653		.13337	
.85	.67368	.18098		.06800	
.90	.71651	.09012		.00030	
.95	.75933	-.00469		-.06940	
.98	.78503	-.06302		-.11204	-.11151
.99	.79359	-.08267		-.12638	-.11439
1.00	.80216	-.10241	-.10489	-.14078	-.10449

LE Center	(-.03187,	.46606)	R = .02247
TE Center	(.79216,	-.10449)	R = .01000
Center of Gravity	(.38080,	.42506)	
Radial Reference	(.41436,	.44106)	

Gaging = .39137

Nose Point	(-.04621,	.44876)
Tail Point	(.79665,	-.11342)

LE Tangency Points	Top	(-.05088,	.47805)	Bottom	(-.01814,	.44828)
TE Tangency Points	Top	(.80133,	-.10050)	Bottom	(.78359,	-.10965)

Inlet Angle = 42.28695
Exit Angle = 27.26412

No. of Blades = 62
Pitch = .86002

Tolerance = -.00000
Gaging = .39137

Uncovered Turning = 16.52136
Gaging Angle = 27.06930

Area = .10475
Axial Chord = .85650

TABLE XXXV
SECOND STAGE VANE

Section C-C At R = 9.47250

Percent X	X	Y (Top)	(Circle)	Y (Bot)	(Circle)
.00	-.10868	.52464	.51547	.47084	.51547
.01	-.09987	.53503		.47656	.49643
.02	-.09106	.54502		.48210	.49160
.03	-.08225	.55461		.48744	.49053
.04	-.07344	.56381		.49258	.49269
.05	-.06463	.57263		.49751	
.10	-.02058	.61110		.51883	
.15	.02347	.64056		.53411	
.20	.06752	.66135		.54264	
.25	.11157	.67373		.54381	
.30	.15562	.67781		.53711	
.35	.19967	.67363		.52224	
.40	.24372	.66111		.49911	
.45	.28777	.64009		.46790	
.50	.33182	.61030		.42898	
.55	.37587	.57132		.38292	
.60	.41992	.52259		.33036	
.65	.46397	.46336		.27202	
.70	.50802	.39298		.20859	
.75	.55207	.31178		.14073	
.80	.59612	.22102		.06903	
.85	.64017	.12242		-.00597	
.90	.68422	.01771		-.08383	
.95	.72827	-.09165		-.16413	
.98	.75470	-.15901		-.21334	-.21287
.99	.76351	-.18171		-.22990	-.21631
1.00	.77232	-.20452	-.20638	-.24654	-.20638

LE Center	(-.08369,	.51547)	R = .02499
TE Center	(.76232,	-.20638)	R = .01000
Center of Gravity	(.34749,	.40907)	
Radial Reference	(.41436,	.44106)	
Gaging =	.40189		
Nose Point	(-.10230,	.49879)	
Tail Point	(.76640,	-.21551)	

LE Tangency Points	Top	(-.10275,	.53164)	Bottom	(-.07149,	.49367)
TE Tangency Points	Top	(.77165,	-.20278)	Bottom	(.75351,	-.21112)

Inlet Angle =	50.54000
Exit Angle =	24.67797
No. of Blades =	62
Pitch =	.95996
Tolerance =	-.00000
Gaging =	.40189
Uncovered Turning =	16.38115
Gaging Angle =	24.74958
Area =	.12101
Axial Chord =	.88100

TABLE XXXVI
SECOND STAGE VANE

Section D-D AT R = 10.46000

Percent X	X	Y (Top)	(Circle)	Y (Bot)	(Circle)
.00	-.16309	.59157	.57965	.53641	.57965
.01	-.15403	.60006		.54101	.55925
.02	-.14498	.60821		.54540	.55379
.03	-.13592	.61603		.54956	.55214
.04	-.12687	.62353		.55349	.55355
.05	-.11781	.63069		.55719	
.10	-.07254	.66161		.57195	
.15	-.02726	.68436		.57997	
.20	.01802	.69894		.58059	
.25	.06329	.70529		.57324	
.30	.10857	.70331		.55755	
.35	.15385	.69281		.53336	
.40	.19912	.67357		.50077	
.45	.24440	.64530		.46010	
.50	.28968	.60760		.41188	
.55	.33495	.56001		.35675	
.60	.38023	.50192		.29543	
.65	.42551	.43265		.22865	
.70	.47078	.35203		.15708	
.75	.51606	.26087		.08138	
.80	.56134	.16069		.00209	
.85	.60661	.05324		-.08028	
.90	.65189	-.05987		-.16530	
.95	.69717	-.17730		-.25260	
.98	.72433	-.24940		-.30595	-.30569
.99	.73339	-.27367		-.32388	-.30979
1.00	.74244	-.29804	-.29984	-.34188	-.29984

LE Center	(-.13558,	.57965) R = .02751
TE Center	(.73244,	-.29984) R = .01000
Center of Gravity	(.30914,	.39305)
Radial Reference	(.41436,	.44106)
Gaging =	.42673	
Nose Point	(-.15809,	.56383)
Tail Point	(.73637,	-.30903)

LE Tangency Points	Top	(-.15439,	.59972)	Bottom	(-.12518,	.55418)
TE Tangency Points	Top	(.74182,	-.29635)	Bottom	(.72353,	-.30437)

Inlet Angle =	57.32598
Exit Angle =	23.68411
No. of Blades =	62
Pitch =	1.06003
Tolerance =	-.00000
Gaging =	.42673
Uncovered Turning =	15.36695
Gaging Angle =	23.73858
Area =	.13017
Axial Chord =	.90553

TABLE XXXVII
SECOND STAGE VANE

Section E-E AT R = 10.86000

Percent X	X	Y (Top)	(Circle)	Y (Bot)	(Circle)
.00	-.18513	.61763	.60465	.56120	.60465
.01	-.17597	.62564	.62559	.56561	.58372
.02	-.16682	.63332		.56975	.57802
.03	-.15766	.64068		.57363	.57615
.04	-.14851	.64772		.57725	.57731
.05	-.13935	.65444		.58059	
.10	-.09358	.68318		.59302	
.15	-.04781	.70380		.59792	
.20	-.00203	.71615		.59478	
.25	.04374	.72009		.58324	
.30	.08951	.71539		.56311	
.35	.13529	.70184		.53443	
.40	.18106	.67916		.49744	
.45	.22683	.64702		.45255	
.50	.27261	.60509		.40036	
.55	.31838	.55295		.34153	
.60	.36415	.49011		.27675	
.65	.40993	.41611		.20672	
.70	.45570	.33103		.13208	
.75	.50147	.23583		.05342	
.80	.54725	.13202		-.02873	
.85	.59302	.02123		-.11391	
.90	.63879	-.09503		-.20173	
.95	.68457	-.21555		-.29184	
.98	.71203	-.28950		-.34689	-.34671
.99	.72119	-.31438		-.36539	-.35111
1.00	.73034	-.33937	-.34114	-.38396	-.34114

LE Center	(-.15661,	.60465)
TE Center	(.72034,	-.34114)
	R = .02852	
	R = .01000	
Center of Gravity	(.29130,	.38652)
Radial Reference	(.41436,	.44106)
Gaging =	.43602	
Nose Point	(-.18049,	.58906)
Tail Point	(.72422,	-.35036)

LE Tangency Points	Top	(-.17494,	.62650)	Bottom	(-.14683,	.57786)
TE Tangency Points	Top	(.72973,	-.33770)	Bottom	(.71139,	-.34561)

Inlet Angle =	59.97635
Exit Angle =	23.31807
No. of Blades =	62
Pitch =	1.10057
Tolerance =	.00000
Gaging =	.43602
Uncovered Turning =	14.69557
Gaging Angle =	23.33963
Area =	.13553
Axial Chord =	.91547

TABLE XXXVIII
SECOND STAGE VANE

Section H-H AT R = 11.41000

Percent X	X	Y (Top)	(Circle)	Y (Bot)	(Circle)
.00	-.21543	.65025	.63591	.59147	.63591
.01	-.20614	.65777	.65758	.59584	.61424
.02	-.19685	.66499		.59985	.60823
.03	-.18756	.67192		.60352	.60607
.04	-.17827	.67854		.60683	.60689
.05	-.16898	.68486		.60978	
.10	-.12252	.71172		.61911	
.15	-.07606	.73043		.61925	
.20	-.02961	.74060		.61018	
.25	.01685	.74184		.59201	
.30	.06331	.73375		.56502	
.35	.10976	.71599		.52961	
.40	.15622	.68822		.48627	
.45	.20268	.65014		.43557	
.50	.24913	.60151		.37813	
.55	.29559	.54211		.31456	
.60	.34205	.47180		.24544	
.65	.38850	.39059		.17136	
.70	.43496	.29898		.09284	
.75	.48142	.19804		.01035	
.80	.52787	.08908		-.07566	
.85	.57433	-.02656		-.16482	
.90	.62079	-.14762		-.25677	
.95	.66724	-.27305		-.35121	
.98	.69512	-.35005		-.40896	-.40887
.99	.70441	-.37597		-.42838	-.41371
1.00	.71370	-.40200	-.40374	-.44788	-.40374

LE Center	(-.18552,	.63591)	R = .02991
TE Center	(.70370,	-.40374)	R = .01000
Center of Gravity	(.26463,	.37765)	
Radial Reference	(.41436,	.44106)	
Gaging =	.44578		
Nose Point	(-.21110,	.62041)	
Tail Point	(.70748,	-.41299)	

LE Tangency Points	Top	(-.20388,	.65953)	Bottom	(-.17646,	.60740)
TE Tangency Points	Top	(.71312,	-.40037)	Bottom	(.69469,	-.40808)

Inlet Angle =	62.25150
Exit Angle =	22.70245
No. of Blades =	62
Pitch =	1.15631
Tolerance -	-.00000
Gaging =	.44578
Uncovered Turning =	13.56141
Gaging Angle =	22.67599
Area =	.14634
Axial Chord =	.92913

TABLE XXXIX
SECOND STAGE VANE

Section G-G AT R = 11.44500

Percent X	X	Y (Top)	(Circle)	Y (Bot)	(Circle)
.00	-.21736	.65220	.63778	.59324	.63778
.01	-.20806	65969	.65950	.59762	.61607
.02	-.19876	.66690		.60164	.61003
.03	-.18946	.67380		.60530	.60785
.04	-.18016	68041		.60859	.60866
.05	-.17086	68670		.61152	
.10	-.12436	.71349		.62066	
.15	-.07786	.73212		.62048	
.20	-.03136	.74219		.61100	
.25	.01514	.74328		.59238	
.30	.06164	.73499		.56492	
.35	.10814	.71696		.52905	
.40	.15464	.68885		.48530	
.45	.20114	.65037		.43423	
.50	.24764	.60128		.37647	
.55	.29414	.54138		.31260	
.60	.34064	.47056		.24323	
.65	.38714	.38885		.16891	
.70	.43364	.29682		.09015	
.75	.48014	.19551		.00743	
.80	.52664	.08621		-.07883	
.85	.57314	-.02975		-.16824	
.90	.61964	-.15113		-.26047	
.95	.66614	-.27691		-.35520	
.98	.69404	-.35412		-.41314	-.41305
.99	.70334	-.38011		-.43262	-.41792
1.00	.71264	-.40622	-.40794	-.45218	-.40794

LE Center	(-.18736,	.63778)	R = .03000
TE Center	(.70264,	-.40794)	R = .01000
Center of Gravity	(.26284,	.37709)	
Radial Reference	(.41436,	.44106)	
Gaging -	.44628		
Nose Point	(-.21304,	.62227)	
Tail Point	(.70641,	-.41721)	

LE Tangency Points	Top	(-.20573,	.66150)	Bottom	(-.17834,	.60917)
TE Tangency Points	Top	(.71206,	-.40459)	Bottom	(.69363,	-.41228)

Inlet Angle =	62.37158
Exit Angle =	22.65937
No. of Blades =	62
Pitch =	1.15986
Tolerance =	-.00000
Gaging =	.44628
Uncovered Turning =	13.47667
Gaging Angle =	22.62978
Area =	.14717
Axial Chord	.93000

UNCLASSIFIED

APPENDIX VIII

DERIVATION OF EQUATION USED IN CALCULATING MASS FLOW INGESTION IN TURBINE ROOT CAVITIES

APPENDIX VIII

DERIVATION OF EQUATION USED IN CALCULATING MASS FLOW INGESTION IN TURBINE ROOT CAVITIES

(U) The following analysis is offered as a method to obtain a rough estimate of the amount of flow ingested into the root cavities. The assumptions used are:

1. Constant specific heats.
2. The ingested mass flow is the same at each of the four root cavities.
3. The total pressure of the ingested flow is reduced from the free stream value to the cavity static pressure at the point of ingestion.
4. The ingested flow, upon re-entering the mainstream, has no effect on the turbine performance.
5. The turbine is adiabatic.

(U) The appropriate T-S diagram is shown in the following figure:

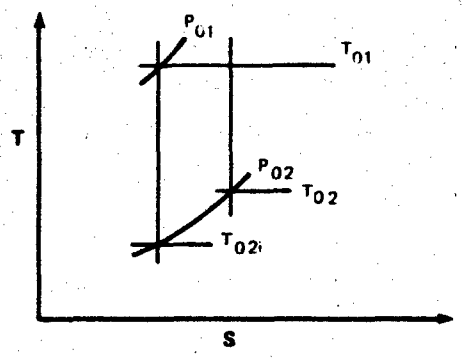

(U) It follows from this diagram that the turbine efficiency is:

$$\eta_T = \frac{1 - \frac{T_{o2}}{T_{o1}}}{1 - \left(\frac{P_{o2}}{P_{o1}}\right)^{\frac{k-1}{k}}}$$

The dimensionless stage entropy increase, $\frac{\Delta S}{C_p}$, is:

$$\frac{\Delta S}{C_p} = \ln\left(\frac{T_{o2}}{T_{o1}}\right) - \ln\left(\frac{P_{o2}}{P_{o1}}\right)^{\frac{k-1}{k}}$$

(U) Raising this expression to the e power and rearranging yields:

$$\frac{T_{o2}}{T_{o1}} = e^{\frac{\Delta S}{C_p}} \left(\frac{P_{o2}}{P_{o1}}\right)^{\frac{k-1}{k}}$$

(U) Substituting this expression into the efficiency equation and solving for the exponetial entropy finally reveals that:

$$e^{\frac{\Delta S}{C_p}} = \eta_T + (1 - \eta_T) P_R^{\frac{k-1}{k}} \qquad (1)$$

(U) The stage entropy increase can be computed by summing the individual entropy increases that occur from inlet to exit, i.e.,

$$\frac{\Delta S}{C_p} = \sum_{j=1}^{n} \frac{\Delta S_j}{C_p} \qquad (2)$$

(U) There are three basic types of terms to consider:

1) Row Losses
   - Profile
   - Secondary
2) Rotor Tip Leakage
3) Parasitic Loss, i.e., ingestion

(U) The effects of tip leakage will be taken into account by using the method of Egli. The ingestion loss will then be deduced from the difference of the loss computed by considering only the row losses and rotor tip losses, and the loss computed from the efficiency measured in the rig. Furthermore, the assumptions 2, 4, and 5 will be used to compute the ingested mass flow rate.

(U) The row loss terms arising in equation (2) are:

$$\sum\left(\frac{\Delta S}{C_p}\right)_{\substack{\text{row}\\\text{loss}}} = \left(\frac{\Delta S}{C_p}\right)_{1V} + \left(\frac{\Delta S}{C_p}\right)_{1B} + \left(\frac{\Delta S}{C_p}\right)_{2V} + \left(\frac{\Delta S}{C_p}\right)_{2B}$$

$$\sum\left(\frac{\Delta S}{C_p}\right)_{\substack{\text{row}\\\text{loss}}} = -\ln\left[1-\left(\frac{\Delta P_o}{P_o}\right)_{1V}\right]^{\eta_{L1B}\left(\frac{k-1}{k}\right)} - \ln\left[1-\left(\frac{\Delta P_o}{P_o}\right)_{1B}\right]^{\eta_{L1B}\left(\frac{k-1}{k}\right)}$$

$$-\ln\left[1-\left(\frac{\Delta P_o}{P_o}\right)_{2V}\right]^{\eta_{L2B}\left(\frac{k-1}{k}\right)} - \ln\left[1-\left(\frac{\Delta P_o}{P_o}\right)_{2B}\right]^{\eta_{L2B}\left(\frac{k-1}{k}\right)}$$

(U) The leakage efficiencies appear in the vane loss forms in the above equation because the losses due to rotor tip leakage flow are computed by assuming that this flow expands through the entire stage pressure ratio without doing any work, hence:

$$\sum\left(\frac{\Delta S}{C_p}\right)_{\substack{\text{rotor tip}\\\text{leakage}}} = \ln P_{R1S}^{\left(1-\eta_{L1B}\right)\left(\frac{k-1}{k}\right)} + \ln P_{R2S}^{\left(1-\eta_{L2B}\right)\left(\frac{k-1}{k}\right)}$$

Combining the preceeding equation with equation (3) and reducing the resulting equation to a simpler form yields,

$$\sum\left(\frac{\Delta S}{C_p}\right)_{\substack{\text{row}\\\text{loss}}} + \sum\left(\frac{\Delta S}{C_p}\right)_{\substack{\text{rotor tip}\\\text{leakage}}} =$$

$$\ln\left\{\frac{P_{R1S}^{\left(1-\eta_{L1B}\right)} P_{R2S}^{\left(1-\eta_{L2B}\right)}}{\left[\left(1-\left(\frac{\Delta P_o}{P_o}\right)_{1V}\right)\left(1-\left(\frac{\Delta P_o}{P_o}\right)_{1B}\right)\right]^{\eta_{L1B}}\left[\left(1-\left(\frac{\Delta P_o}{P_o}\right)_{2V}\right)\left(1-\left(\frac{\Delta P_o}{P_o}\right)_{2B}\right)\right]^{\eta_{L2B}}}\right\}^{\frac{k-1}{k}} \quad (4)$$

(U) For the four cavities, the entropy increase is,

$$\sum \left(\frac{\Delta S}{C_p}\right)_{\substack{\text{cavity}\\ \text{ingestion}}} = \ln\left[\prod_{i=1}^{4}\left(\frac{P_{o\ \text{mainstream}}}{P_{o\ \text{cavity}}}\right)_i\right]^{(1-\eta_1)\left(\frac{k-1}{k}\right)} \qquad (5)$$

(U) Combining equations (1), (4) and (5) gives the result:

$$\eta_T = \frac{1}{1-P_R^{\left(\frac{k-1}{k}\right)}}\left\{1-P_R^{\frac{k-1}{k}}+\left\{\left(\frac{P_{R1S}^{(1-\eta_{L1B})}\ P_{R2S}^{(1-\eta_{L2B})}}{\left[\left(1-\left(\frac{\Delta P_o}{P_o}\right)_{1V}\right)\left(1-\left(\frac{\Delta P_o}{P_o}\right)_{1B}\right)\right]^{\eta_{L1B}}}\right)\times\right.\right.$$

$$\left.\left.\left(\frac{\left[\prod_{i=1}^{4}\left(\frac{P_{o\ \text{mainstream}}}{P_{o\ \text{cavity}}}\right)_i\right]^{(1-\eta_1)}}{\left[\left(1-\left(\frac{\Delta P_o}{P_o}\right)_{2V}\right)\left(1-\left(\frac{\Delta P_o}{P_o}\right)_{2B}\right)\right]^{\eta_{L2B}}}\right)\right\}^{\frac{k-1}{k}}\right\}$$

Nomenclature

T	–	Absolute temperature
P	–	Absolute pressure
S	–	Mass specific entropy
e	–	Base of the natural log system
η_T	–	Turbine total-to-total efficiency
C_p	–	Specific heat at constant pressure
k	–	Specific heat ratio
ln	–	Natural logarithm
P_R	–	Turbine total-to-total pressure ratio
η_L	–	Rotor leakage efficiency, the ratio of mass flow passing through the blade to the turbine mass flow rate
η_I	–	Ingestion efficiency, the ratio of the mass flow not ingested into a cavity to the turbine mass flow rate

Subscripts

o	–	Stagnation condition
1	–	turbine inlet plane
2	–	Turbine exit plane
i	–	Ideal state
1V	–	First vane
1B	–	First blade
2V	–	Second vane
2B	–	Second blade
1S	–	First stage
2S	–	Second stage

REFERENCES

1. H. Welna, D. E. Dahlberg and W. H. Heiser; (Unclassified title) Investigation of a Highly Loaded Two-Stage Fan-Drive Turbine; Technical Report, AFAPL-TR-69-92 Volume I; Pratt & Whitney Aircraft Division of United Aircraft Corporation; June 1968; Confidential.

2. H. Welna, D. E. Dahlberg and W. H. Heiser; (Unclassified title) Investigation of a Highly Loaded Two-Stage Fan-Drive Turbine; Technical Report AFAPL-TR-69-92 Volume 2; Pratt & Whitney Aircraft Division of United Aircraft Corporation; December 1968; Confidential.

3. H. Welna, D. E. Dahlberg and W. H. Heiser; (Unclassified title) Investigation of a Highly Loaded Two-Stage Fan-Drive Turbine; Technical Report AFAPL-TR-69-92 Volume 3; Pratt & Whitney Aircraft Division of United Aircraft Corporation; June 1969; Confidential.

4. H. Welna, D. E. Dahlberg, W. H. Heiser; (Unclassified title) Investigation of a Highly Loaded Two-Stage Fan-Drive Turbine; Technical Report AFAPL-TR-69-92, Volume IV; Pratt & Whitney Aircraft Division of United Aircraft Corporation; December 1969; Confidential.

5. H. Welna, D.E. Dahlberg and W.H. Heiser; (Unclassified title) Investigation of a Highly Loaded Two-Stage Fan-Drive Turbine; Technical Report AFAPL-TR-69-92, Volume V; Pratt & Whitney Aircraft Division of United Aircraft Corporation; June 1970; Confidential.

6. Aerodynamic Design of Axial Flow Compressors, NASA SP-36, Washington, D. C., 1965, (pp. 201-207).

Unclassified

Security Classification

DOCUMENT CONTROL DATA - R & D

(Security classification of title, body of abstract and indexing annotation must be entered when the overall report is classified)

1. ORIGINATING ACTIVITY (Corporate author) Pratt & Whitney Aircraft Division United Aircraft Corporation East Hartford, Conn. 06108	2a. REPORT SECURITY CLASSIFICATION Confidential 2b. GROUP 4

3. REPORT TITLE

(U) Investigation of a highly loaded two-stage fan-drive turbine.
VOLUME VI. FINAL TECHNICAL REPORT

4. DESCRIPTIVE NOTES (Type of report and inclusive dates)

Final Technical Report (January 1, 1968 – November 1, 1971)

5. AUTHOR(S) (First name, middle initial, last name)

Welna, Henry; Dahlberg, Donald E.

6. REPORT DATE	7a. TOTAL NO. OF PAGES	7b. NO. OF REFS
November 1971	222	6

8a. CONTRACT OR GRANT NO.	9a. ORIGINATOR'S REPORT NUMBER(S)
F33615-68-C-1208 b. PROJECT NO. 3066 c. Task No. 306606 d.	PWA-4291 9b. OTHER REPORT NO(S) (Any other numbers that may be assigned this report) AFAPL-TR-69-92 Volume VI

10. DISTRIBUTION STATEMENT

11. SUPPLEMENTARY NOTES	12. SPONSORING MILITARY ACTIVITY
	Air Force Aero Propulsion Laboratory Wright-Patterson AFB, Ohio 45433

13. ABSTRACT

(U) An exploratory research program was conducted to develop turbine aerodynamic methods and design procedures for efficient high work, low pressure turbines. This program consisted of various phases, including analyses of promising increased loading concepts, and experimental cascade testing to verify and extend the turbine aerodynamic techniques and design procedures. Based on these findings, a two-stage turbine was designed and evaluated in a rotating cold flow rig in order to demonstrate the effectiveness of the techniques.

(U) The results of the efforts leading to the design and evaluation of the demonstrator turbine have been reported in detail in previously published Interim Technical Reports (AFAPL-TR-69-92, Volumes 1 through 5). This final Technical report (AFAPL-TR-69-92, Volume 6) summarizes that work and presents in its entirety the design and results of the investigation of the demonstrator turbine builds.

DD FORM 1 NOV 68 1473 REPLACES DD FORM 1473, 1 JAN 64, WHICH IS OBSOLETE FOR ARMY USE.

Unclassified

Security Classification

(This page is unclassified)

[redacted]

Unclassified
Security Classification

14. KEY WORDS	LINK A		LINK B		LINK C	
	ROLE	WT	ROLE	WT	ROLE	WT
Turbine Aerodynamic Design						
Boundary Layer Control Survey						

[redacted]

(This page is unclassified)

Unclassified
Security Classification